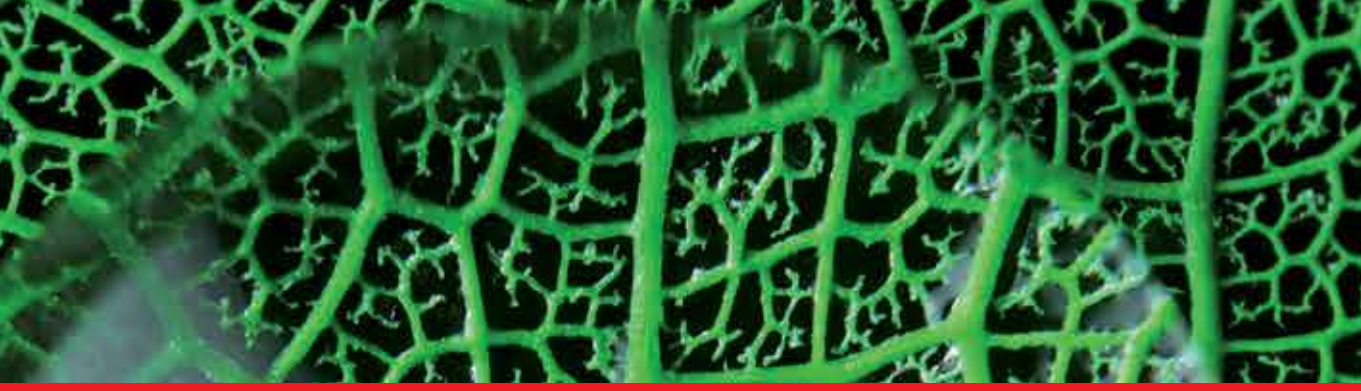

IntechOpen

Applied Photosynthesis

New Progress

Edited by Mohammad Mahdi Najafpour

APPLIED PHOTOSYNTHESIS - NEW PROGRESS

Edited by **Mohammad Mahdi Najafpour**

Applied Photosynthesis - New Progress
http://dx.doi.org/10.5772/61357
Edited by Mohammad Mahdi Najafpour

Contributors

Erkin Zakhidov, Sherzod Nematov, Vakhobjon Kuvondikov, Zhi-Gang Zhou, Yan-Hui Bi, Mingnan Qu, Saber Hamdani, James A. Bunce, Alexander Andreevich Ivlev, Yoav Evron, Roman Voloshin, Suleyman Allakhverdiev, Margarita Rodionova, Sergey Zharmukhamedov, Jian-Ren Shen, Markus Kärkäs, Björn Åkermark, Tanja Laine, Eric Johnston, Jorge Marques Da Silva, Jean-David Rochaix, Suzan Khayyat, Rosilda Selvin, L.Selva Roselin

Notice

First published in Croatia, 2016 by INTECH d.o.o.
eBook (PDF) Published by IN TECH d.o.o.
Place and year of publication of eBook (PDF): Rijeka, 2019.
IntechOpen is the global imprint of IN TECH d.o.o.
Printed in Croatia

Legal deposit, Croatia: National and University Library in Zagreb

Additional hard and PDF copies can be obtained from orders@intechopen.com

Applied Photosynthesis - New Progress
Edited by Mohammad Mahdi Najafpour
p. cm.
ISBN 978-953-51-2267-8
eBook (PDF) ISBN 978-953-51-5427-3

Meet the editor

Mohammad Mahdi Najafpour received his PhD in Inorganic Chemistry from the Sharif University of Technology, Tehran, Iran, in 2009. Mahdi is a recipient of several awards and fellowships, notably the gold medal of the National Chemistry Olympiad in 2004; he ranked first in the Khwarizmi Youth Festival in 2010, and he was selected for the TWAS young affiliateship (2014), the Al-Biruni award by the Academy of Sciences of Iran (2015), and he was selected among the best researchers in Iran by Ministry of Science of Iran (2015). Currently, he is a faculty member in Chemistry in the Institute for Advanced Studies in Basic Sciences (IASBS) (Zanjan, Iran). As a nano-bioinorganic chemist, Mahdi believes that with learning strategies from natural systems, design of modern catalysts for all reactions using only earth-abundant, low-cost and environment-friendly metal ions is possible. Mahdi and his research group explore transition metal compounds such as water-oxidizing catalysts for artificial photosynthesis. He is the author of over 160 publications in these and other areas.

Contents

Preface

Using the energy from sunlight, *Photosynthesis* usually converts carbon dioxide into organic compounds, which are important for all living creatures. In oxygenic photosynthesis process, water is also efficiently oxidized to oxygen, which is also necessary to sustain respiring organisms. Photosynthesis is one of the most important reactions on Earth, and it is a scientific field that is intrinsically interdisciplinary. Many research groups have considered photosynthesis. The advances in characterization techniques and their application to the field have improved our understanding of photosynthesis and, now, our knowledge of the process and of the structures of reaction components has been advancing so rapidly and revealing that photosynthesis is even more clearly an integrated biological process of continuing interest and of profound importance. However, now photosynthesis is considered by us to understand the secrets of Nature to efficiently capture and store sunlight.

The book is the result of the effort of many experts, and I would like to take this opportunity to thank all contributors for their chapters. I wish to express my gratitude to the staff at InTech for their kind assistances. I am grateful to the Institute for Advanced Studies in Basic Sciences (Zanjan, Iran) for their support. I also thank my wife, Mary, for her encouragement and infinite patience throughout the time that the book was being prepared.

Finally, I would like to dedicate the book to Mr. Abdourrahim Najafpour for all his kindness, help, support and encouragement in my life.

Dr. Mohammad Mahdi Najafpour
Department of Chemistry
Center for Research in Climate Change and Global Warming,
Institute for Advanced Studies in Basic Sciences
Zanjan, Iran

Chapter 1

Monitoring Photosynthesis by *In Vivo* Chlorophyll Fluorescence: Application to High-Throughput Plant Phenotyping

Jorge Marques da Silva

Additional information is available at the end of the chapter

http://dx.doi.org/10.5772/62391

Abstract

In spite of the decrease in the rate of population growth, world population is expected to rise from the current figure (slightly above to 7.2 billion) to reach 9.6 billion in 2050. There is therefore a pressing need to increase food production. Since most of the best arable lands are already under production, expanding the agricultural areas would have negative impacts on important natural areas. Thereby, increasing the productivity of the current agricultural areas is the chief objective of agronomical planners, and planting more productive and better adapted plant varieties is crucial to achieve it. In fact, plant breeding is at the forefront of concern of both agronomists and plant biologists. Plant breeding is a millenary activity that deeply changed our world. However, the use of molecular biology techniques jointly with informatics capabilities—giving rise to the omics techniques—deeply accelerated plant breeding, providing new and better plant varieties at an increased pace. The advances in genomics, though, far by-passed the advances in phenomics, and so there is a rising consensus among plant breeders that plant phenotyping is a bottleneck to advancing plant breeding. Therefore, a range of international initiatives in high-throughput plant phenotyping (HTPP) are at course, and new automated equipment is being developed. Phenotyping plants, however, is not a simple matter. To begin with, it has to be decided which parameters to measure in order to extrapolate to the desired goals, plant resistance and plant productivity. For this, as well as for plant breeding, an in-depth knowledge of plant physiology is required. Photosynthesis has been considered as a good indicator of overall plant performance. It is the only energy input in plants and thereby impacts all aspects of plant metabolism and physiology. The cumulative rate of photosynthesis over the growing season is the primary determinant of crop biomass. It largely determines the redox state of plant cells, and therefore, it is at the core of regulatory networks. Therefore, assessing photosynthesis and the photosynthetic apparatus plays a core role on plant phenotyping. Nevertheless, high-throughput phenotyping demands very rapid measurements, and consequently the most common method of photosynthesis measurement—the infra-red gas analysis—is not well suited for this

purpose. On the contrary, the techniques based on *in vivo* chlorophyll (Chl) a fluorescence measurements are perfectly fit. In this chapter, an historical perspective on the development of *in vivo* Chl a measurement is briefly addressed. Then, the state of the art of the fluorescence-based techniques of photosynthesis assessment is presented, and their potential use in HTPP is evaluated. Finally, the current use of these techniques in the main systems of phenotyping is surveyed.

Keywords: photosynthesis, photochemistry, chlorophyll fluorescence, optical techniques, plant phenomics, high-throughput plant phenotyping

1. Introduction: Food security, plant breeding, and high-throughput plant phenotyping

Albeit the rate on population rise is slowing down, world population is still increasing; from the current figure slightly above 7.2 billion, it is expected to reach 9.6 billion by 2050 [1]. Therefore, there is a pressing need to increase the global food production ([2] and references therein). Mostly, the population increase is expected to occur in developing countries ([3] and references therein), where the current productivity of farms is far below the one in the developed world. For instance, in India, where the population is expected to surpass China's, the current productivity of wheat farming is only one third than that of France, while rice productivity accounts for less than half of China's [4]. Increasing food production and ensuring availability of safe and nutritious food at affordable prices to the population of developing countries are, therefore, a pressing urgency. As most of the best arable lands are already under production, expanding the agricultural areas would have negative impacts on important natural areas. Thereby, increasing the productivity of the current agricultural areas is the chief objective [5], which requires more productive and better adapted plant varieties [6]. There is a long tradition of conventional plant breeding that deeply changed our world [7]. Moreover, being a cost-effective tool for increasing nutritional value of forage and crops, plant breeding still can contribute to global food security [4]. Therefore, it is at the forefront of concern of both agronomists and plant biologists. The use of molecular biology techniques jointly with informatics capabilities—giving rise to the omics techniques—deeply accelerated plant breeding, providing better plant varieties at an increased pace [8]. In fact, during the past 20 years, molecular profiling and classical sequencing technologies enabled significant advances toward the large-scale characterization of plant genomes [9], yielding valuable tools for plant breeding such as marker-assisted selection [10]. However, integrating approaches across all scales, from molecular to field applications, are necessary to develop sustainable plant production with higher yield. Regrettably, the advances in genomics far by-passed the advances in phenomics, and therefore, there is a rising consensus among plant biologists that plant phenotyping is a bottleneck to advancing both fundamental research and plant breeding [11]. Therefore, a range of international initiatives in high-throughput plant phenotyping (HTPP) are at course, and new automated equipment is being developed [12]. Plant phenotyping is "the application of a set of methodologies and protocols used to measure plant growth, architecture, and composi-

http://dx.doi.org/10.5772/62391

tion with a certain accuracy and precision at different scales of organization, from organs to canopies" [11]. Phenotyping, being a paradigm of the interdisciplinary character of modern plant physiology [13], is not a simple matter. To begin with, it has to be decided which parameters to measure to extrapolate to the desired plant traits (resistance and productivity). That is, researchers need sound and robust knowledge about the traits that are indicative of the intended performance. Here, mechanistic understanding of plant physiology plays a role in identifying useful parameters and proxies to measure [11]. In any case, it seems plausible that effective HTPP platforms will involve the measurement of multiple parameters. Two classes of parameters are of major importance: structural parameters and photosynthetic parameters. The structure of both the shoots [14] and the roots has been primarily phenotyped using a broad range of cameras sensitive in the visible spectral range. Conversely, photosynthetic activity has been phenotyped mainly by using *in vivo* chlorophyll (Chl) fluorescence techniques.

2. Photosynthesis: a proxy of plant performance

An in-depth knowledge of plant physiology is required for successful plant breeding [15], as most of plant stresses are under the control of complex traits [16]. In particular, as accumulating data did not fit into conventional theories, it becomes clear that metabolic engineering is in need of a better understanding of metabolic regulation and plasticity [8]. Photosynthesis has been considered as a good indicator of overall plant performance. It is the only significant energy input in plants and thereby impacts all aspects of plant metabolism and physiology. The cumulative rate of photosynthesis over the growing season is the primary determinant of crop biomass [17]. Photosynthesis largely determines the redox state of plant cells and therefore is at the core of regulatory networks [18]. Therefore, assessing photosynthesis and the photosynthetic apparatus plays a core role on plant phenotyping. Nevertheless, high-throughput phenotyping demands very rapid measurements, and consequently, the most common methods of photosynthesis measurement—the infra-red gas analysis and the polarographic measurement of oxygen evolution—are not well suited for this purpose. On the contrary, optical methods present considerable advantages for *in vivo* and *in vitro* assessment of the physiological condition of live tissues, as compared to chemical and physicochemical methods, because they are much faster, non-invasive, and non-destructive (e.g. [19, 20]). Among these, *in vivo* Chl fluorescence measurements are best suited for this purpose. Albeit the use of optical methods in plant phenotyping has been recently reviewed [21], to our knowledge, a review specifically addressing the use of Chl fluorescence techniques in HTPP is missing in the literature. In the following sections, an historical perspective on the development of *in vivo* Chl fluorescence measurement, from the seminal work of Kautsky and Hirsch [22] to the ground-breaking invention of pulse amplitude modulation (PAM) [23], is briefly addressed. Then, the current state of the art of the Chl fluorescence measurement techniques is presented, and their potential use in HTPP is evaluated.

3. Chlorophyll fluorescence

The emission of photons from excited molecules was named fluorescence by the Irish physicist George Gabriel Stokes [24], after fluorspar or fluoride, the mineral from calcium fluorite where he studied the phenomenon. When a molecule of Chl a from the antenna complex of a photosynthetic organism is hit by a photon, it absorbs its energy and an electron is raised to a higher energy level S1 (singlet 1, corresponding to the absorption of one red photon) or S3 (singlet 3, corresponding to the absorption of one blue photon; **Figure 1**).

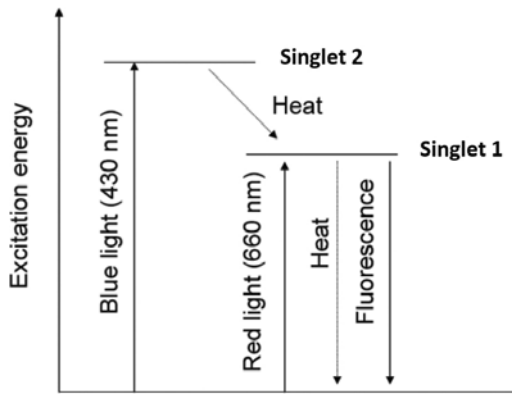

Figure 1. Simplified diagram of the energy levels of the singlet excitation states of chlorophyll a molecules. *Source*: Adapted from Ref. [25].

The excited molecule is very unstable, and its excess energy is promptly released. There are three different competing ways of de-excitation: (1) heat dissipation; (2) photochemical utilization of energy; and (3) fluorescence emission. The relative contribution of each process is dependent on the physiological status of the photosynthetic systems [25]. In the last few decades, the measurement of Chl fluorescence has become a universal technique in the study of virtually all types of photosynthetic entities, including fruits [26–28], corals [29], seagrasses [30], macroalgae [31], microphytobenthos [32–34], and many types of higher plants, such as tobacco [35], maize [36], and tomato [37]. The use of Chl fluorescence has been recently proposed for detecting early responses to abiotic and biotic stresses, before a decline in growth can be observed [38–40]. Likewise, there are numerous applications of Chl fluorescence in the horticultural sectors (reviewed in [41]). With the advent of different instrumental techniques, Chl fluorometry developed into various types, with different timescales of signal capturing [42]. It is useful, however, to divide the currently available techniques for *in vivo* Chl fluorescence measurements into passive and active [43]. While passive techniques measure fluorescence emission under actinic light, active techniques stimulate fluorescence emission using dedicated light sources.

3.1. Passive fluorescence

Albeit it has been known for a long time that Chl, like many other molecules, emits fluorescence after excitation, it was not until 1931 that Kautsky and Hirsch observed that the *in vivo* emission of fluorescence during a dark–light transition showed a typical variation [22], usually known as the Kautsky induction curve or simply Kautsky effect. Even though these authors have speculated on a possible relation between the observed fluorescence emission and carbon fixation, the molecular basis of photosynthesis was, at the time, poorly understood,[1] and therefore, their observations did not significantly impact photosynthesis research. As the understanding of the molecular mechanisms progressed, however, prototypes of continuous fluorescence recording fluorometers were built and used in photosynthesis research [45]. These simple devices had limited use in stress physiology, but Lichtenthaler and Rinderle [46] developed the Vitality Index (Rfd = $F_v'/(F_m–F_v')$) and successfully used it to detect low temperature stress in higher plants. However, continuous fluorescence recording fluorometers acquired increase potential in photosynthesis research only when equipped with high-time resolution capacities. This allowed to explore the kinetics of the fast phase of fluorescence signal rise in a dark–light transition. Although the exploration of these signals begun earlier with experimental prototypes, it was the commercial availability of the Plant Efficiency Analyzer by the UK-based manufacturer Hansatech that made this technique widely available to plant physiologists and plant breeders. In Switzerland, Reto Strasser provided the theoretical basis for the interpretation of these signals [47]. His group at the University of Genève have developed the JIP test (termed after the main inflections in the fast fluorescence rise, called J, I, and P) to analyze the photosystem II (PS II) behavior [48] (**Figure 2**).

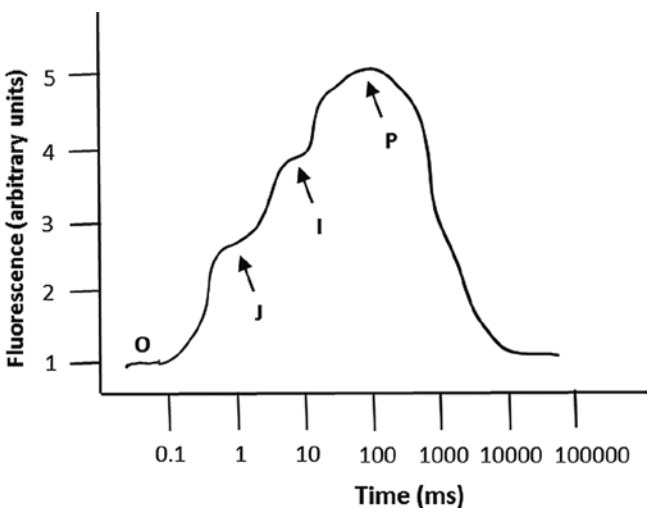

Figure 2. Chlorophyll fluorescence induction curve (OJIP transient).

[1] Please note that the very concept of photosynthesis as being a redox process was only to be demonstrated 6 years later [44].

Based on the Chl a fast fluorescence transient measurement [49], numerous indexes and parameters quantifying the energy flow related to the different phases in the PS II photochemical reactions can be calculated. The JIP transient rise reflects the successive but overlapping reduction of the electron acceptor pool of PS II [50] and can be used to obtain information on the redox state of the photosynthetic electron transport chain, on the stoichiometry of its components and on the relative PS II antenna size [51]. This transient has been found to be very sensitive to stress caused by changes in different biotic and abiotic conditions, presenting alterations even before visible symptoms could be detected on the plants [52–57]. Albeit some information may be obtained from the application of the JIP test to pre-illuminated leaves, the most used protocols require a dark-adaptation period [58]. This may be achieved for many leaves simultaneously by using the leaf clips provided by the manufacturer Hansatech. Individual measurements are rapid as usually a 1-second light (saturating) pulse is applied, and the kinetics of fluorescence rise is immediately recorded. Therefore, the main hindrance to the use of the JIP test on high-throughput automated plant phenotyping is the need to previously dark-adapt the samples (**Table 1**). Albeit this technique has been proved useful in manual low-throughput plant phenotyping [57, 59], none of the commercial phenotyping platforms makes use of it. It is possible to envisage, however, a system where whole plants would be pre-adapted for dark conditions, and non-contact measurements of the fluorescence induction curve would be made. In fact, imaging of the JIP parameters is already possible and has been used to screen wild barley genotypes under heat stress [60]. Passive fluorescence spectra of leaves may also be obtained and provide information on the status of the photosynthetic apparatus [61]. However, fluorescence emission spectra have been studied mainly with active fluorescence techniques, mostly with laser-induced fluorescence (LIF) [62] which is discussed in the next section.

3.2. Active fluorescence

3.2.1. ***Laser-induced fluorescence***

Since LIF measurements can be carried out remotely, allowing, for example, to inspect difficult-to-access canopies, this technique is particularly interesting for HTPP in the field. In fact, large crop areas can be efficiently surveyed by scanning an instrument placed at a high viewpoint or by mounting it in an airplane or a drone [63]. LIF was applied for estimating the overall metabolic activity of plants during a defined period of time [64, 65]; differentiating plant species [66–68]; assessing potassium deficiency [69]; estimating the maturity of lettuce [70]; detecting mildew and rust fungal [71] and bacterial [72] infections; and studying the influence of water stress [73, 74], ambient light [68], UV radiation [75], atmospheric [76], and soil pollutants [76, 77] and excess of ammonium nitrate [78] and nickel [79] on plant physiology. In addition, LIF has been used to assess the productive biomass of benthic diatoms [62, 80] and to differentiate between groups of macroalgae [81]. LIF spectra of plant leaves present a local Chl emission maximum in the red region of the spectrum at 685 nm (F685) and an absolute maximum at the far-red region, circa 740 nm (F740) [65, 75]. The relative intensity, shape, and wavelength of these peaks are dependent on the physiological status of the photosynthetic apparatus. Changes in the Fr/Ffr ratio were suggested to be well correlated to Chl a concen-

tration [69, 82, 83], which is altered, in most plant species by stress [84]. In addition to changes in the Chl concentration, other factors, related to membrane lipid composition and protein environment [85] as well as leaf ultrastructure and the accumulation of specific light absorbing metabolites, such as anthocyanins, are likely to affect Fr/Ffr ratios. It is known that water stress significantly impacts leaf lipid composition of thylakoid membranes, causing a decrease in the contents of polar lipids, namely chloroplast-specific glycolipids as well as changes in their fatty acid composition, likely to affect membrane fluidity [86]. In forest species subjected to severe drought, Lavrov and coworkers [73] showed that the red/far-red emission fluorescence ratio (Fr/Ffr) is very well correlated with the maximum potential photochemical efficiency of PS II estimated with a Plant Efficiency Analyzer (Hansatech, U.K.). Also, simultaneous measurement of Chl fluorescence in maize (*Zea mays*), sugar beet (*Beta vulgaris*), and kalanchoë (*Kalanchoë* sp.) by LIF and PAM indicated that the steady state of fluorescence is useful for water stress detection [87]. Albeit LIF has been extensively used in applied research, its possibilities have not been thoroughly explored in fundamental research. In fact, even though *Arabidopsis thaliana* had become the main model organism in plant biology, applications of LIF to this species are almost absent, the exceptions being a study on npq mutants, altered in the expression of the PS II PsbS protein [88] and, more recently, a study on the water stress effect on photosynthesis [74]. Advanced variations of this technique as is the case of laser-induced fluorescence transients (LIFT) allow the calculation of quantum efficiency [89], leading values in line with the ones obtained by the more established technique of PAM fluorometry (see below).

3.2.2. *Conventional pulse amplitude modulated fluorescence*

Active fluorescence protocols exploiting PAM [23] can measure the potential and effective quantum efficiency of photosystem II, the electron transport rate, and the extent of non-photochemical quenching. Based on the concepts used in the light-doubling technique [90], PAM fluorometry enables to distinguish between the photochemical (qP) and non-photochemical (i.e., dissipative; qN and NPQ) use of light energy. Notably, the quantum efficiency of photosystem II can be measured much more easily than the other parameters [91]. Kitajima and Butler [92] showed that the maximum potential quantum yield of PS II is characterized by the dimensionless parameter F_v/F_m (the ratio of variable and maximum fluorescence measured after saturating light pulses). A very constant value of 0.832 ± 0.004 was found for healthy leaves of a very wide variety of species [93] while stress due to disease or environmental conditions is indicated by lower values. The basal fluorescence (F_o) is dependent on the tissues' Chl concentration [33], which, in turn, depends on the physiological condition of the photosynthetic system. However, severe stress may change the basal fluorescence yield, affecting the relation between F_o and Chl concentration. In fact, a significant increase of F_o due to heat stress, independent of the Chl concentration was reported by Havaux and Strasser [94]. The heat-induced increase of the basal fluorescence intensity probably reflects a disturbance on the organization of thylakoid membranes [95]. The F_v/F_m parameter appears to be relatively insensitive to severe water limitation but could be used to differentiate between responses during cold. On the basis of the calculation of the fluorescence index $\Delta F/F_m'$ (where ΔF is the difference between the maximal fluorescence [F_m'] and the steady-state fluorescence [F] of

light-adapted samples), which measures the effective quantum yield of PS II [96], PAM fluorometry allows the construction of rapid light curves (RLCs) relating the rate of photosynthetic electron transport and incident photon irradiance [97, 98]. PAM was successfully applied to a wide range of plants, such as the olive tree, rosemary, and lavender [99]; *Paspalum dilatatum* [100], *Phillyrea angustifolia* [101], and other Mediterranean shrubs [102]; the tropical grass *Setaria sphacelata* [84] and several C4 turfgrasses [103]; maize [36, 104]; and *Arabidopsis thaliana* [105], among others.

3.2.3. ***Imaging pulse amplitude modulated fluorescence***

The development of Chl fluorescence imaging systems by numerous research groups [106–108] together with the emergence of commercially available models by PSI (Brno, Czech Republic), Walz Systems (Effeltrich, Germany), and Technologica Ltd. (Colchester, UK) has greatly increased the versatility of Chl fluorometry techniques (reviewed in [109]). Systems that image at the microscopic level allow to measure PS II photochemical efficiencies from chloroplasts within intact leaves and from individual cells within mixed populations [107, 110]. On the other hand, lower resolution imaging systems allow the mapping of fluorescence parameters over large areas, making it a unique technique to study the spatial heterogeneity of the photosynthetic activity across an autotrophic surface [111–113]. Conventional and imaging techniques use different technologies, namely in the detection processes of the fluorescence signal: a photodiode or phototube in conventional PAM fluorometry and a charge-coupled device (CCD) camera in imaging-PAM fluorometry. Consequently, caution is needed when comparing results from conventional and imaging fluorescence techniques [114]. Nevertheless, imaging-PAM fluorometry has proven to be a powerful technique and new technological developments, as the use of semi-automated systems equipped with fluorescence cameras continuously assessing the photochemical activity of leaves [115] are in course.

4. High-throughput plant phenotyping platforms and chlorophyll fluorescence techniques

The advancement of plant phenotyping is a key factor for the success of modern plant breeding and basic plant research. Since the recognition of the phenotyping bottleneck to plant breeding [12], a global effort to provide HTPP platforms was set on. Currently, most platforms are user-built, but some commercial platforms are already available, as is the case of the German platform from the manufacturer LemnaTec and the Czech platform from the manufacturer Photon System Instruments (PSI). The Canadian-based firm Qubit Systems offers a modified version of the PSI platform. To provide high-throughput phenotyping capabilities to plant breeders, numerous user-built phenotyping facilities are organized in networks, the most prominent being the European Plant Phenotyping Network, which offers access to 23 different plant phenotyping facilities to the user community [116]. Some countries organized national networks, as is the case of the German Plant Phenotyping Network [117] and the UK Plant Phenomics Network [118]. The Jülich Plant Phenotyping Centre [119] is a leading EPPN

member. Jülich's platform makes use of LIFT to perform middle-range remote sensing of crops [119]. The commercial phenotyping platforms do not use LIF technologies. A simplified JIP test (restricted to the calculation of F_v/F_m) is used in the commercial platform from LemnaTech; a LemnaTech module with this feature is incorporated in the Leibniz Institute of Plant Genetics and Crop Plant Research (IPK) HTPP Platform [120]. PlantScreen, the commercial platform from PSI, uses conventional PAM fluorometry to perform quenching analysis. This platform has been used to phenotype cold-tolerant pea (*Pisum sativum*) plants [121]. Kjaer and Ottosen [122] used six independent PAM fluorometers in a HTPP experiment to assess daily growth of field-grown *Brassica napus*. In this case, however, the PAM system was exclusively used to show that the near infra-red laser beam of a 3D laser scanning, used for phenotyping, had not a deleterious effect over the photosynthetic metabolism of the plants. Bellasio and coworkers [123] have used an imaging-PAM system based on a FluorCam camera (PSI) inserted in a user-developed setting to phenotype common bean (*Phaseolus vulgaris*). The French platforms based at Montpellier [124] use an imaging-PAM system based on Walz's devices. An important advantage of Chl fluorescence imaging is that it can be used to screen a large number of small plants simultaneously [125]. A recent advance introduced by Serôdio and coworkers [126] allows the rapid generation of light curves from non-sequential, temporally independent fluorescence measurements. This technique has the potential to bring the valuable information provided by fluorescence RLCs into the realm of HTPP. David Kramer's group, at the Michigan State University, is currently developing a multi-instrument platform entitled Dynamic Environmental Photosynthetic Imaging (DEPI) [127], with the aim of reproducing in phytotrons the dynamics of field conditions, while continuously recording multiple parameters related with them photosynthetic performance.

Technique	**Potential**	**Limitations**	**Current use**	
			User-developed	**Commercial**
JIP test	Very fast measurements; well-established technique; successfully used in low-throughput plant phenotyping, including in field conditions	Need of a dark-adaptation period; signal interpretation not always straight forward; plant contact required	IPK (LemnaTech module)	LemnaTech (limited to F_v/F_m)
LIF	Middle-distance remote sensing; suitable for field phenotyping; LIFT allows the calculation of quantum efficiency	Fluorescence spectra less informative than variable fluorescence Very limited use in model plants	JPPC	Unreported
Conventional PAM	Very informative, physiological interpretation well established	Most protocols need a dark-adaptation period; measurements possible only at close range	Unreported	PlantScreen (Photon System Instruments) [121]

Technique	Potential	Limitations	Current use	
			User-developed	Commercial
Imaging PAM	Allows mapping of the photosynthetic heterogeneity over an autotrophic surface; facilitates replication.	Most protocols need a dark-adaptation period; measurements possible only at close range Expensive and sensitive equipment	JPPC [123]; M3P	PlantScreen (Photon System Instruments)

Note: JPPC: Jülich Plant Phenotyping Centre [119]; IPK: Leibniz Institute of Plant Genetics and Crop Plant Research [120]; M3P: INRA—Montpellier Plant Phenotyping Platforms [124].

Table 1. Applications of chlorophyll a fluorescence techniques in high-throughput plant phenotyping.

5. Prospective

Chl fluorescence techniques will continue to play a major role on HTPP. Among these, imaging-PAM techniques will play a pivotal role, although specific cases will require different technological solutions. Moreover, field HTPP, which is expected to be fostered in the forthcoming years, will require technologies not dependent on sample dark adaptations and able to operate at medium-range distance, where the family of techniques based on LIF may play a role. Finally, the development of low-cost HTPP platforms [128], required to improve plant breeding in developing countries, is expected to make use of the less expensive Chl measurement techniques, namely passive fluorescence. On the other hand, high-technology in-house HTPP platforms are expected to make simultaneously use of different Chl fluorescence techniques, integrated in a systems approach to plant phenomics.

Author details

Jorge Marques da Silva

Department of Plant Biology, Biosystems and Integrative Sciences Institute, University of Lisbon, Lisbon, Portugal

References

[1] United Nations (2014) Concise Report on the World Population Situation in 2014. Department of Economic and Social Affairs, Population Division, United Nations, New York.

[2] Godfray HCJ, Beddington JR, Crute JI, Haddad L, Lawrence D, Muir JF, Pretty J, Robinson S, Thomas S, Toulmin C (2010) Food security: the challenge of feeding 9 billion people. Science 327: 812–818.

[3] Gore A (2013) The Future: Six Drivers of Global Change. Random House, New York.

[4] Neethu F, Namitha E (2015) Plant breeding as a means to achieve food security. International Journal of Applied Research 1 (8): 123–125.

[5] Phalan B, Balmford A, Green RE, Scharlemann JPW (2011) Minimising harm to biodiversity of producing more food globally. Food Policy 36: S62–S71.

[6] Husenov B, Makhkamov M, Garkava-Gustavsson L, Muminjanov H, Johansson E (2015) Breeding for wheat quality to assure food security of a staple crop: the case study of Tajikistan. Agriculture & Food Security 4: 9.

[7] Hallauer AR (2011) Evolution of plant breeding. Crop Breeding and Applied Biotechnology 11: 197–206.

[8] Morandini P, Salamini F (2003) Plant biotechnology and breeding: allied for years to come. Tends in Plant Science 8 (2): 70–75.

[9] Yano M, Tuberosa R (2009) Genome studies and molecular genetics—from sequence to crops: genomics comes of age. Current Opinion in Plant Biology 12: 103–106.

[10] Francia E, Tacconi G, Crosatti C, Barabaschi D, Bulgarelli D, Dall'Aglio E, Vale G (2005) Marker assisted selection in crop plants. Plant Cell, Tissue and Organ Culture 82: 317–342.

[11] Fiorani F, Schurr U (2013) Future scenarios for plant phenotyping. Annual Review of Plant Biology 64: 267–291.

[12] Furbank R, Tester M (2011) Phenomics – technologies to relieve the phenotyping bottleneck. Trends in Plant Science 16 (12): 635–644.

[13] Marques da Silva J, Casetta E (2015) The evolutionary stages of plant physiology and a plea for transdisciplinarity. Axiomathes 25: 205–215.

[14] Lièvre M, Wuyts N, Cookson SJ, Bresson J, Dapp M, Vasseur F, Massonnet C, Tisné Bettembourg M, Balsera C, Bédiée A, Bouvery F, Dauzat M, Rolland G, Vile D, Granier C (2013) Phenotyping the kinematics of leaf development in flowering plants: recommendations and pitfalls. WIREs Developmental Biology 2: 809–821.

[15] Jackson P, Robertson M, Cooper M, Hammer G (1996) The role of physiological understanding in plant breeding; from a breeding perspective. Field Crops Research 49: 1–37.

[16] Duque S, Almeida AM, Bernardes da Silva A, MarquesdaSilva J, Farinha AP, Santos D, Fevereiro P, Araújo SS (2013) Abiotic stress responses in plants: unravelling the complexity of genes and networks to survive. In: Abiotic Stress – Plant Responses and Applications in Agriculture, pp. 49–101 (Vahdati K, Leslie C eds.), InTech, Rijeka.

[17] Parry MA, Hawkesford MJ (2012) An integrated approach to crop genetic improvement. Journal of Integrative Plant Biology 54 (4): 250–259.

[18] Scheibe R, Backhausen JE, Emmerlich V, Holtgrefe S (2005) Strategies to maintain redox homeostasis during photosynthesis under changing conditions. Journal of Experimental Botany 56 (416): 1481–1489.

[19] Berberan-Santos MN, Bodunov EN, Valeur B (2005) Mathematical functions for the analysis of luminescence decays with underlying distributions 1. Kohlrausch decay function (stretched exponential). Chemical Physics 315: 171–182.

[20] Berberan-Santos MN, Bodunov EN, Valeur B (2008) Luminescence decays with underlying distributions of rate constants: general properties and selected cases. In: Fluorescence of Supermolecules, Polymers and Nano-systems, pp. 67–103 (Berberan-Santos MN ed.), Springer, Berlin.

[21] Li L, Zhang Q, Huang D (2014) A review of imaging techniques for plant phenotyping. Sensors 14: 20078–20111.

[22] Kautsky H, Hirsch A (1931) Neue Versuche zur Kohlensäureassimilation (New experiments on carbonic acid assimilation). Naturwissenschaften 19: 48.

[23] Schreiber U, Schliwa U, Bilger W (1986) Continuous recording of photochemical and non-photochemical chlorophyll fluorescence quenching with a new type of modulation fluorometer. Photosynthesis Research 10: 51–62.

[24] Stokes GG (1852) On the change of refrangibility of light. Philosophical Transactions of the Royal Society of London 142: 463–562.

[25] Marques da Silva J, Bernardes da Silva A, Pádua M (2007) Modulated chlorophyll a fluorescence: a tool for teaching photosynthesis. Journal of Biological Education 41: 178–183.

[26] Cavaco AM, Antunes MDC, Marques da Silva J, Antunes R, Guerra R (2009) Preliminary results on the non-invasive diagnosis of superficial scald in 'Rocha' pear by fluorescence imaging. In: Proceedings of the 1st International Workshop in Computer Image Analysis in Agriculture, pp. 121–127, Potsdam.

[27] Guerra R, Gardé I, Antunes M, Marques da Silva J, Antunes R, Cavaco AM (2012) A possibility for non-invasive diagnosis of superficial scald in 'Rocha' pear based on chlorophyll a fluorescence, colorimetry, and the relation between alpha-farnesene and conjugated trienols. Scientia Horticulturae 134: 127–138.

[28] Breia R, Vieira S, Marques da Silva J, Gerós H, Cunha A (2013) Mapping grape berry photosynthesis by chlorophyll fluorescence imaging: the effect of saturating pulse intensity in different tissues. Photochemistry & Photobiology 89: 579–585.

[29] Ralph PJ, Schreiber U, Gademann R, Kühl M, Larkum AWD (2005) Coral photobiology studied with a new imaging pulse amplitude modulated fluorometer. Journal of Phycology 41: 335–342.

[30] Ralph PJ, Gademann R, Dennison WC (1998) In situ seagrass photosynthesis measured using a submersible, pulse-amplitude modulated fluorometer. Marine Biology 132: 367–373.

[31] Beer S, Larsson C, Poryan O, Axelsson L (2000) Photosynthetic rates of Ulva (Chlorophyta) measured by pulse amplitude modulated (PAM) fluorometry. European Journal of Phycology 35: 69–74.

[32] Serôdio J, Marques da Silva J, Catarino F (1997) Nondestructive tracing of migratory rhythms of intertidal benthic microalgae using in vivo chlorophyll a fluorescence. Journal of Phycology 33: 542–553.

[33] Serôdio J, Marques da Silva J, Catarino F (2001) Use of in vivo chlorophyll a fluorescence to quantify short-term variations in the productive biomass of intertidal microphytobenthos. Marine Ecology Progress Series 218: 45–61.

[34] Cartaxana P, Vieira S, Ribeiro L, Rocha R, Cruz S, Calado R, Marques da Silva J (2015) Effects of elevated temperature and CO_2 on intertidal microphytobenthos. BMC Ecology 15: 10.

[35] Almeida AM, Bernardes da Silva A, Araújo S, Cardoso L, Santos D, Tomé J, Marques da Silva J, Paul M, Fevereiro P (2007) Responses to water withdrawal of tobacco plants genetically engineered with the AtTPS1 gene: a special reference to photosynthetic parameters. Euphytica 154: 113–126.

[36] Cruz de Carvalho R, Cunha A, Marques da Silva J (2011) Photosynthesis by six Portuguese maize cultivars during drought stress and recovery. Acta Physiologiae Plantarum 33: 359–374.

[37] Willits DH, Peet MM (2001) Measurement of chlorophyll fluorescence as a heat stress indicator in tomato: laboratory and greenhouse comparisons. Journal of the American Society of Horticultural Sciences 126 (2): 188–194.

[38] Chaerle L, Lenk S, Leinonen I, Jones HG, Van Der Straeten D, Buschmann C (2009) Multi-sensor plant imaging: towards the development of a stress-catalogue. Biotechnology Journal 4: 1152–1156.

[39] Jansen M, Gilmer F, Biskup B, Nagel KA, Rascher U, Fischbach A, Briem S, Dreissen G, Tittmann S, Braun S, De Jaeger I, Metzlaff M, Schurr U, Scharr H, Walter A (2009) Simultaneous phenotyping of leaf growth and chlorophyll fluorescence via GROWSCREEN FLUORO allows detection of stress tolerance in *Arabidopsis thaliana* and other rosette plants. Functional Plant Biology 36 (11): 902–914.

[40] Munns R, James RA, Sirault XRR, Furbank RT, Jones HG (2010) New phenotyping methods for screening wheat and barley for beneficial responses to water deficit. Journal of Experimental Botany 61 (13): 3499–3507.

[41] Gorbe E, Calatayud A (2012) Applications of chlorophyll fluorescence imaging technique in horticultural research: a review. Scientia Horticulturae 138: 24–35.

[42] Misra AN, Misra M, Singh R (2012) Chlorophyll fluorescence in plant biology. In: Biophysics, pp. 171–192 (Misra AN ed.), InTech, Rijeka.

[43] Cendrero-Mateo MP, Moran MS, Papuga SA, Thorp KR, Alonso L, Moreno J, Ponce-Campos G, Rascher U, Wang G (2015) Plant chlorophyll fluorescence: active and passive measurements at canopy and leaf scales with different nitrogen treatments. Journal of Experimental Botany 67 (1): 275–286.

[44] Hill R (1937) Oxygen evolved by isolated chloroplasts. Nature 139: 881–882.

[45] Malkin S, Kok B (1966) Fluorescence induction studies in isolated chloroplasts. I. Number of components involved in the reaction and quantum yields. Biochimica Biophysica Acta 126: 413–432.

[46] Lichtenthaler H, Rinderle U (1988) The role of chlorophyll fluorescence in the detection of stress conditions in plants. Critical Reviews in Analytical Chemistry 19: 29–85.

[47] Strasser RJ (1986) Mono-bi-tri-and polypartite models in photosynthesis. Photosynthesis Research 10: 255–276.

[48] Strasser BJ, Strasser RJ (1995) Measuring fast fluorescence transients to address environmental questions: the JIP-test. In: Photosynthesis: From Light to Biosphere, pp. 977–980 (Mathis P ed.), Kluwer Academic Publishers, Dordrecht.

[49] Strasser BJ (1997) Donor side capacity of photosystem II probed by chlorophyll a fluorescence transients. Photosynthesis Research 52: 147–155.

[50] Govindjee (1995) Sixty-three years since Kautsky: chlorophyll a fluorescence. Australian Journal of Plant Physiology 22: 131–160.

[51] Kalaji HM, Schansker G, Ladle RJ, Goltsev V, Bosa K, Allakhverdiev SI, Brestic M, Bussotti F, Calatayud A, Dabrowski P, Elsheery NI, Ferroni L, Guidi L, Hogewoning SW, Jajoo A, Misra AN, Nebauer SG, Pancaldi S, Penella C, Poli D, Pollastrini M, Romanowska-Duda ZB, Rutkowska B, Serôdio J, Suresh K, Szulc W, Tambussi E, Yanniccari M, Zivcak M (2014) Frequently asked questions about in vivo chlorophyll fluorescence: practical issues. Photosynthesis Research 122: 121–158.

[52] Srivastava A, Guissé B, Greppin H, Strasser RJ (1997) Regulation of antenna structure and electron transport in photosystem II of *Pisum sativum* under elevated temperature probed by the fast polyphasic chlorophyll a fluorescence transient: OKJIP. Biochimica et Biophysica Acta 1320: 95–106.

[53] Tsimilli-Michael M, Eggenberg P, Biro B, Köves-Pechy K, Vörös I, Strasser RJ (2000) Synergistic and antagonistic effects of arbuscular mycorrhizal fungi and *Azospirillum* and *Rizhobium* nitrogen-fixers on the photosynthetic activity of alfalfa probed by the polyphasic chlorophyll a fluorescence transient O-J-I-P. Applied Soil Ecology 15: 169–182.

[54] Demetriou G, Neonaki C, Navakoudis E, Kotzabasis K (2007) Salt stress impact on the molecular structure and function of the photosynthetic apparatus—the protective role of polyamines. Biochimica et Biophysica Acta 1767: 272–280.

[55] Zivcák M, Brestic M, Olsovská K, Slamka P (2008) Performance index as a sensitive indicator of water stress in *Triticum aestivum* L. Plant, Soil and Environment 54: 133–139.

[56] Mathur S, Mehta P, Jajoo A (2013) Effects of dual stress (high salt and high temperature) on the photochemical efficiency of wheat leaves (*Triticum aestivum*). Physiology and Molecular Biology of Plants 19 (2): 179–188.

[57] Silvestre S, Araújo SS, Vaz Patto MC, Marques da Silva J (2014) Performance index: an expeditious tool to screen for improved drought resistance in the *Lathyrus* genus. Journal of Integrative Plant Biology 56 (7): 610–621.

[58] Zivcák M, Brestic M, Kalaji HM, Govindjee (2014) Photosynthetic responses of sun- and shade-grown barley leaves to high light: is the lower PSII connectivity in shade leaves associated with protection against excess of light? Photosynthesis Research 119: 339–354.

[59] Öz MT, Turan Ö, Kayihan C, Eyidoğan F, Ekmekçi Y, Yücel M, Öktem HA (2014) Evaluation of photosynthetic performance of wheat cultivars exposed to boron toxicity by the JIP fluorescence test. Photosynthetica 52 (4): 555–563.

[60] Jedmowski C, Brüggemann W (2015) Imaging of fast chlorophyll fluorescence induction curve (OJIP) parameters, applied in a screening study with wild barley (*Hordeum spontaneum*) genotypes under heat stress. Journal of Photochemistry and Photobiology B: Biology 151: 153–160.

[61] Van Wittenberghe S, Alonso L, Verrelst J, Hermans I, Delegido J, Veroustraete F, Valcke R, Moreno J, Samson R (2013) Upward and downward solar-induced chlorophyll fluorescence yield indices of four tree species as indicators of traffic pollution in Valencia. Environmental Pollution 173: 29–37.

[62] Vieira S, Lavrov A, Utkin A, Santos A, Vilar R, Marques da Silva J, Cartaxana P (2011) Effects of migration on intertidal microphytobenthos biomass measured by laser-induced fluorescence (LIF). Marine Ecology Progress Series 432: 45–52.

[63] Zarco-Tejada PJ, Gonzalez-Dugo V, Berni JAJ (2012) Fluorescence, temperature and narrow-band indices acquired from a UAV platform for water stress detection using a micro-hyperspectral imager and a thermal camera. Remote Sensing of Environment 117: 322–337.

[64] Astafurova TP, Grishin AI, Zotikova AP, Klimkin VM, Matvienko GG, Romanovskii OA, Sokovikov VG, Timofeev VI, Kharchenko OV (2001) Remote probing of plant photosynthetic apparatus by measuring laser-induced fluorescence. Russian Journal of Plant Physiology 48: 518–522.

[65] Zuev VV, Zueva NE, Grishaev MV (2009) Seasonal variations of fluorescence of Scotch pine according to data of measurements at Siberian Lidar Station. Atmospheric and Oceanic Optics 22 (1): 42–48.

[66] Saito Y, Saito R, Kawahara TD, Nomura A, Takeda S (2000) Development and performance characteristics of laser-induced fluorescence imaging lidar for forestry applications. Forest Ecology and Management 128: 129–137.

[67] Saito Y, Kurihara K, Takahashi H, Kobayashi F, Kawahara T, Nomura A, Takeda S (2002) Remote estimation of the chlorophyll concentration of living trees using laser-induced fluorescence imaging lidar. Optical Review 9 (2): 37–39.

[68] Richards TJ, Schuerger AC, Capelle G, Guikema JA (2003) Laser-induced fluorescence spectroscopy of dark- and light-adapted bean (*Phaseolus vulgaris* L.) and wheat (*Triticum aestivum* L.) plants grown under three irradiance levels and subjected to fluctuating lighting conditions. Remote Sensing of Environment 84: 323–341.

[69] Chappelle EW, Wood Jr. FM, McMurtrey III JE, Newcomb W (1984) Laser-induced fluorescence of green plants. 1: A technique for the remote detection of plant stress and species identification. Applied Optics 23 (1): 134.

[70] Brach EJ, Molnar JM, Jasmin JJ (1977) Detection of lettuce maturity and variety by remote sensing techniques. Journal of Agricultural Engineering Research 22: 45–54.

[71] Lüdeker W Dahn H-G, Günther HP (1996) Detection of fungal infection of plants by laser-induced fluorescence: an attempt to use remote sensing. Journal of Plant Physiology 148: 579–585.

[72] Pereira FMV, Milori DMBP, Pereira-Filho ER, Venâncio AL, Russo MST, Cardinali MCB, Martins PK, Freitas-Astúa J (2011) Laser-induced fluorescence imaging method to monitor citrus greening disease. Computers and Electronics in Agriculture 79: 90–93.

[73] Lavrov A, Utkin AB, Marques da Silva J, Vilar R, Santos NM, Alves B (2012) Water stress assessment of cork oak leaves and maritime pine needles based on LIF spectra. Optics and Spectroscopy 112: 271–279.

[74] Gameiro C, Utkin AB, Cartaxana P, Marques da Silva J, Matos AR (2015) The use of laser induced chlorophyll fluorescence (LIF) as a fast and non-destructive method to investigate water deficit in Arabidopsis. Agricultural Water Management 164 (1): 127–136.

[75] Edner H, Johansson J, Svanberg S, Wallinder E (1994) Fluorescence lidar multicolor imaging of vegetation. Applied Optics 33: 2471–2479.

[76] Grishin AI, Krekov GM, Krekova MM, Matvienko GG, Sukhanov AY, Timofeev VI, Fateyeva NL, Lisenko AA (2007) Investigation of organic aerosol of plants with fluorescence lidar. Atmospheric and Ocean Optics 20: 328–337.

[77] Fateyeva NL, Matvienko GG (2004) Application of the method of laser-induced fluorescence. In: SPIE Proceedings 5232 "Remote Sensing for Agriculture, Ecosystems,

and Hydrology V", pp. 652–657 (Owe M, D'Urso G, Moreno JF, Calera A eds.), SPIE Press, Bellingham.

[78] Fateyeva NL, Klimkin AV, Bender OV, Zotikova AP, Yamburov MS (2006) Analysis of laser-induced fluorescence in wood plants under nitrogen soil pollution. Atmospheric and Oceanic Optics 19: 189–192.

[79] Gopal R, Mishra KB, Zeeshan M, Prasad SM, Joshi MM (2002) Laser-induced chlorophyll fluorescence spectra of mug plants growing under nickel stress. Current Science 83 (7): 880–884.

[80] Utkin AB, Vieira S, Marques da Silva J, Lavrov A, Leite E, Cartaxana P (2013) Compact low-cost detector for in vivo assessment of microphytobenthos using laser induced fluorescence. Optics and Spectroscopy 114: 471–474.

[81] Gameiro C, Utkin AB, Cartaxana P (2015) Characterisation of estuarine intertidal macroalgae by laser-induced fluorescence. Estuarine, Coastal and Shelf Science 167: 119–124.

[82] Hák R, Lichtenthaler HK, Rinderle U (1990) Decrease of the chlorophyll fluorescence ratio F690/F730 during greening and development of leaves. Radiation and Environmental Biophysics 29: 329–336.

[83] Lichtenthaler HK, Hák R, Rinderle U (1990) The chlorophyll fluorescence ratio F690/F730 in leaves of different chlorophyll contents. Photosynthesis Research 25: 295–298.

[84] Marques da Silva J, Arrabaça MC (2004) Photosynthesis in the water stressed C_4 grass *Setaria sphacelata* is mainly limited by stomata with both rapidly and slowly imposed water deficits. Physiologia Plantarum 121: 409–420.

[85] Buschmann C (2007) Variability and application of the chlorophyll fluorescence emission ratio red/far red of leaves. Photosynthesis Research 92: 261–271.

[86] Gigon A, Matos AR, Laffray D, Zuily-Fodil Y, Pham-Thi AT (2004) Effect of drought stress on lipid metabolism in the leaves of *Arabidopsis thaliana* (ecotype Columbia). Annals of Botany 94: 345–351.

[87] Cerovic ZG, Goulas Y, Gorbunov M, Briantais J-M, Camenen L, Moya I (1996) Fluorosensing of water stress in plants: diurnal changes of the mean lifetime and yield of chlorophyll fluorescence, measured simultaneously and at distance with a τ-LIDAR and a modified PAM-fluorimeter, in maize, sugar beet, and kalanchoë. Remote Sensing of Environment 58 (3): 311–321.

[88] Kolber Z, Klimov D, Ananyev G, Rascher U, Berry J, Osmond B (2005) Measuring photosynthetic parameters at a distance: laser induced fluorescence transient (LIFT) method for remote measurements of photosynthesis in terrestrial vegetation. Photosynthesis Research 84: 121–129.

[89] Raesch AR, Muller O, Pieruschka R, Rascher U (2014) Field observations with laser-induced fluorescence transient (LIFT) method in barley and sugar beet. Agriculture 4: 159–169.

[90] Baker N, Bradbury M (1981) Possible applications of chlorophyll fluorescence techniques for studying photosynthesis in vivo. In: Plants and the Daylight Spectrum, pp. 355–372 (Smith H ed.), Academic Press, London.

[91] Maxwell K, Johnson GN (2000) Chlorophyll fluorescence—a practical guide. Journal of Experimental Botany 51: 659–668.

[92] Kitajima M, Butler WL (1975) Quenching of chlorophyll fluorescence and primary photochemistry in chloroplasts by dibromothymoquinone. Biochimica et Biophysica Acta 376: 105–115.

[93] Björkman O, Demmig B (1987) Photon yield of O_2 evolution and chlorophyll fluorescence characteristics at 77 K among vascular plants of diverse origins. Planta 170: 489–504.

[94] Havaux M, Strasser R (1992) Plasticity of the stress tolerance of the photosystem II in vivo. In: Research in Photosynthesis, vol. IV, pp. 149–152 (Murata N ed.), Kluwer Academic Publishers, Dordrecht.

[95] Kovács L, Damkjaer J, Kereiche S, Ilioaia C, Ruban AV, Boekema EJ, Jansson S, Horton P (2006) Lack of the light-harvesting complex CP24 affects the structure and function of the grana membranes of higher plant chloroplasts. The Plant Cell 18 (11): 3106–3120.

[96] Genty B, Briantais JM, Baker NR (1989) The relationship between the quantum yield of photosynthetic electron transport and quenching of chlorophyll fluorescence. Biochimica et Biophysica Acta 990: 87–92.

[97] Serôdio J, Vieira S, Cruz S, Barroso F (2005) Short-term variability in the photosynthetic activity of microphytobenthos as detected by measuring rapid light curves using variable fluorescence. Marine Biology 146: 903–914.

[98] Perkins RG, Mouget JL, Lefebvre S, Lavaud J (2006) Light response curve methodology and possible implications in the application of chlorophyll fluorescence to benthic diatoms. Marine Biology 149: 703–712.

[99] Nogués S, Baker NR (2000) Effects of drought on photosynthesis in Mediterranean plants grown under enhanced UV-B radiation. Journal of Experimental Botany 51: 1309–1317.

[100] Marques da Silva J, Arrabaça MC (l992). Characteristics of fluorescence emission by leaves of nitrogen starved *Paspalum dilatatum* POIR. Photosynthetica 26 (2): 253–256.

[101] Munne-Bosch S, Penuelas J (2003) Photo- and antioxidative protection, and a role for salicylic acid during drought and recovery in field-grown *Phillyrea angustifolia* plants. Planta 217: 758–766.

[102] Marques da Silva J (2007) Chlorophyll fluorescence parameters of three Mediterranean shrubs in a summer-autumn period in central Portugal. Biologia Plantarum 51: 741–745.

[103] Carmo-Silva A, Soares A, Marques da Silva J, Bernardes da Silva A, Keys A, Arrabaça MC (2007) Photosynthetic responses of three C4 grasses of different metabolic subtypes to water deficit. Functional Plant Biology 34: 204–213.

[104] Xu ZZ, Zhou GS, Wang YL, Han GX, Li YJ (2008) Changes in chlorophyll fluorescence in maize plants with imposed rapid dehydration at different leaf ages. Journal of Plant Growth Regulation 27: 83–92.

[105] Woo NS, Badger MR, Pogson BJ (2008) A rapid, non-invasive procedure for quantitative assessment of drought survival using chlorophyll fluorescence. Plant Methods 4: 27.

[106] Omasa K, Shimazaki KL, Aiga I, Larcher W, Onoe M (1987) Image analysis of chlorophyll fluorescence transients for diagnosing the photosynthetic system of attached leaves. Plant Physiology 84: 748–752.

[107] Oxborough K, Baker NR (1997) An instrument capable of imaging chlorophyll a fluorescence from intact leaves at very low irradiance and at cellular and subcellular levels of organization. Plant, Cell and Environment 20: 1473–1483.

[108] Nedbal L, Soukupova J, Kaftan D, Whitmarsh J, Trilek M (2000) Kinetic imaging of chlorophyll fluorescence using modulated light. Photosynthesis Research 66: 25–34.

[109] Oxborough K (2004) Imaging of chlorophyll a fluorescence: theoretical and practical aspects of an emerging technique for the monitoring of photosynthetic performance. Journal of Experimental Botany 55: 1195–1205.

[110] Oxborough K, Hanlon ARM, Underwood GJC, Baker NR (2000) In vivo estimation of the Photosystem II photochemical efficiency of individual microphytobenthic cells using high-resolution imaging of chlorophyll a fluorescence. Limnology and Oceanography 45: 1420–1425.

[111] Scholes JD, Rolfe SA (1996) Photosynthesis in localized regions of oat leaves infected with crown rust (*Puccinia coronata*): quantitative imaging of chlorophyll fluorescence. Planta 199: 573–582.

[112] Meng Q, Siebke K, Lippert P, Baur B, Mukherjee U, Weis E (2001) Sink-source transition in tobacco leaves visualized using chlorophyll fluorescence imaging. New Phytologist 151: 585–596.

[113] Hill R, Schreiber U, Gademann R, Larkum AWD, Kühl M, Ralph PJ (2004) Spatial heterogeneity of photosynthesis and the effect of temperature-induced bleaching conditions in three species of corals. Marine Biology 144: 633–640.

[114] Vieira S, Ribeiro L, Jesus B, Cartaxana P, Marques da Silva J (2013) Photosynthesis assessment in microphytobenthos with conventional and imaging pulse amplitude modulation fluorometry. Photochemistry and Photobiology 89: 97–102.

[115] Chaerle L, Hulsen K, Hermans C, Strasser RJ, Valcke R, Höfte M, Van Der Straeten D (2003) Robotized time-lapse imaging to assess in-planta uptake of phenylurea herbicides and their microbial degradation. Physiologia Plantarum 118: 613–619.

[116] EPPN (2016) http://www.plant-phenotyping-network.eu/eppn/home, downloaded January 14, 2016.

[117] DPPN (2016) http://www.dppn.de/dppn/EN/Home/home_node.html;jsessionid=EEB2F474C83047B82BA1B1DF745BCCCE, downloaded January 14, 2016.

[118] UKPPN (2016) http://www.ukppn.org.uk/, downloaded January 14, 2016.

[119] JPPC (2016) http://www.fz-juelich.de/portal/DE/Home/home_node.html, downloaded January 14, 2016.

[120] IPK (2016) http://www.ipk-gatersleben.de/en/institute/portrait/, downloaded January 14, 2016.

[121] Humplík JF, Lazár D, Fürst T, Husičková A, Hýbl M, Spíchal L (2015) Automated integrative high-throughput phenotyping of plant shoots: a case study of the cold-tolerance of pea (*Pisum sativum* L.). Plant Methods 11: 20.

[122] Kjaer KH, Ottosen C-O (2015) 3D laser triangulation for plant phenotyping in challenging environments. Sensors 15: 13533–13547.

[123] Bellasio C, Olejníčková J, Tesař R, Šebela D, Nedbal L (2012) 3D computer reconstruction of plant growth and chlorophyll fluorescence emission in three spatial dimension. Sensors 12: 1052–1071.

[124] M3P (2016) https://www6.montpellier.inra.fr/m3p/Infrastructure/Phenopsis-platform/Equipments

[125] Brestic M, Zivcak M (2013) PSII fluorescence techniques for measurement of drought and high temperature stress signal in crop plants: protocols and applications. In: Molecular Stress Physiology of Plants, pp. 87–131 (Rout GR, Das AB eds.), Springer, Dordrecht.

[126] Serôdio J, Ezequiel J, Frommlet J, Laviale M, Lavaud J (2013) A method for the rapid generation of nonsequential light-response curves of chlorophyll fluorescence. Plant Physiology 163: 1089–1102.

[127] Xu L, Cruz JA, Savage LJ, Kramer DM, Chen J (2015) Plant photosynthesis phenomics data quality control. Bioinformatics 31 (11): 1796–1804.

[128] Cessna S, Demmig-Adams B, Adams III WW (2010) Exploring photosynthesis and plant stress using inexpensive chlorophyll fluorometers. Journal of Natural Resources and Life Sciences Education 39: 22–30.

Chapter 2

The Dynamics of the Photosynthetic Apparatus in Algae

Jean-David Rochaix

Additional information is available at the end of the chapter

http://dx.doi.org/10.5772/62261

Abstract

Plants and algae are subjected to changes in light quality and quantity and in nutrient availability in their natural habitat. To adapt to these changing environmental conditions, these organisms have developed efficient means to adjust their photosynthetic apparatus so as to preserve photosynthetic efficiency and appropriate photoprotection. Under limiting light, this system optimizes light capture and photosynthetic yield through a reorganization of its light-harvesting system. In contrast, under high light, when the absorption capacity of the system is exceeded, the excess absorbed light energy is dissipated as heat to prevent oxidative damage. One of the key photosynthetic complexes, photosystem II, is prone to photodamage but is efficiently repaired. The photosynthetic machinery is also able to adjust when specific micronutrients such as copper, iron or sulfur become limiting by remodeling some of the photosynthetic complexes and metabolic pathways. While some of these responses occur in the short term, others occur in the long term and involve an intricate signaling system within chloroplasts and between the chloroplast and the nucleus accompanied with changes in gene expression. These signals involve the tetrapyrrole pathway, plastid protein synthesis, the redox state of the photosynthetic electron transport chain, reactive oxygen species and several metabolites.

Keywords: photosynthesis, thylakoid membrane, acclimation, retrograde signaling, *Chlamydomonas*

1. Introduction

Photosynthetic organisms are constantly subjected to changes in light quality and quantity and have to adapt to this changing environment. On the one hand they need light energy and have to collect it efficiently especially when light is limiting; on the other hand, they have to be able to dissipate the excess absorbed light energy when the capacity of the photosynthetic apparatus is exceeded. The primary events of photosynthesis occur in the thylakoids, a complex network

of membranes localized within chloroplasts. These primary reactions are mediated by three major protein–pigment complexes, photosystem II (PSII), the cytochrome b_6f complex (Cytb_6f) and photosystem I (PSI) embedded in the thylakoid membrane and which act in series. Both PSII and PSI are associated with their light-harvesting complex systems, LHCII and LHCI, respectively, which collect and transfer the light excitation energy to the reaction centers of the two photosystems. In both cases, a chlorophyll dimer is oxidized and a charge transfer occurs across the thylakoid membrane. PSII creates thereby a strong oxidant capable of splitting water on its donor side with concomitant evolution of molecular oxygen and the release of protons in the lumen side while electrons are transferred along the photosynthetic electron transport chain through PSII to the plastoquinone pool and Cytb_6f. This complex pumps protons from the stromal to the lumen side of the thylakoid membrane while transferring electrons to plastocyanin and PSI. Ultimately the electrons are transferred to ferredoxin and NADP(H), the final acceptor. A fourth complex, the ATP synthase, is functionally linked to the other three by using the proton gradient generated by the photosynthetic electron flow across the thylakoid membrane to produce ATP (**Figure 1**). Both ATP and NADPH fuel the Calvin–Benson cycle (CBC) for CO_2 assimilation. Besides linear electron flow (LEF), cyclic electron flow (CEF) occurs in which electrons are transferred from the PSI acceptor ferredoxin to the plastoquinone pool through either a type I/II thylakoid-bound NADH dehydrogenase [1] or the antimycin-sensitive pathway involving Pgr5 and Pgrl1 [2,3]. Analysis of a *pgr5* mutant of *Chlamydomonas* revealed that the loss of Pgr5 leads to a reduced proton gradient across the thylakoid membrane and to diminished CEF activity [4]. Pgrl1 has been proposed to act as a ferredoxin–plastoquinone reductase [3]. In contrast to linear electron flow, which generates both reducing power and ATP, CEF produces exclusively ATP. The NADPH/ATP ratio can thus be modulated through regulation of CEF versus LEF.

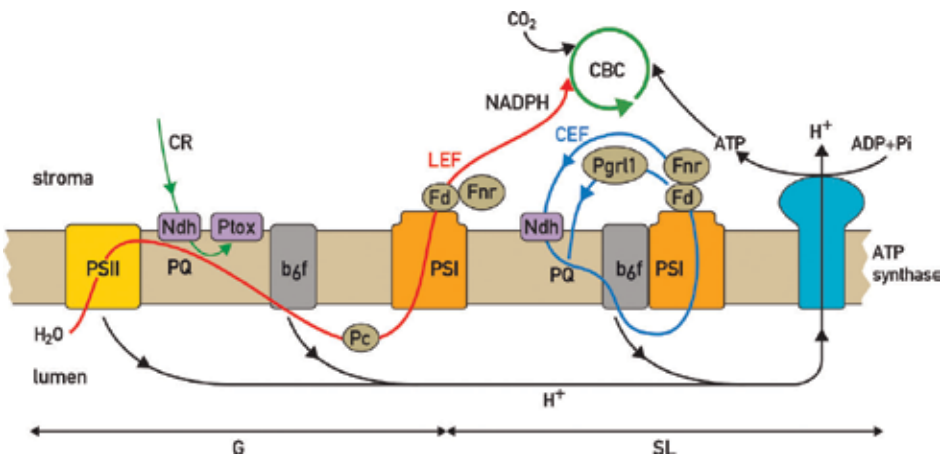

Figure 1. Scheme of the photosynthetic electron transport chain with PSII, Cytb_6f, PSI and ATP synthase.

Linear electron flow (LEF) and cyclic electron flow (CEF) are shown in red and blue, respectively, with arrows indicating the direction of electron flow. The LEF pathway is driven by the

http://dx.doi.org/10.5772/62261

two photochemical reactions of PSII and PSI: electrons are extracted by PSII from water and transferred subsequently to the PQ pool, Cytb_6f, plastocyanin (Pc), PSI and ferredoxin (Fd). Ferredoxin–NADPH reductase (Fnr) catalyzes the formation of NADPH at the expense of reduced Fd. The CEF pathway is driven by PSI in the stroma lamellae. In *C. reinhardtii*, PSI forms a supercomplex with Cytb_6f, Fnr, Pgrl1, Pgr5 and additional factors. Upon reduction of Fd, electrons are returned to the PQ pool either through the NADH complex (Ndh) or via Pgrl1 which acts as a Fd-PQ oxidoreductase. Both LEF and CEF are associated with proton pumping into the lumen. The resulting proton gradient is used by ATP synthase to produce ATP which together with NADPH drives CO_2 assimilation by the Calvin–Benson cycle (CBC). G, grana; SL, stroma lamellae. Reproduced from Ref. 5 with permission.

A striking feature of the thylakoid membrane is its lateral heterogeneity with two distinct domains consisting of appressed membranes, called grana, and stromal lamellae, which connect the grana regions with each other [6,7]. Whereas PSII is mainly localized in the grana regions, PSI and the ATP synthase are found in the stromal lamellae and in the margins of the grana [8]. This is because these two complexes have large domains protruding in the stromal phase which do not fit into the narrow membrane space between the grana lamellae. The organization of thylakoid membranes in the grana and stromal regions is determined to a large extent by the resident photosystem complexes. As an example, mutants deficient in PSI contain mostly grana with few stromal lamellae [9,10]. In contrast to the photosystems, the Cytb_6f complex is equally distributed between the grana and stromal thylakoid regions. Grana formation appears to be mediated by van der Waals attractive forces and electrostatic interactions in which LHCII plays an important role [11].

The LHCII and LHCI genes form a large family with each member encoding a protein with three transmembrane domains and up to eight chlorophyll *a*, six chlorophyll *b* and four xanthophyll molecules. In *Chlamydomonas*, there are nine major and three minor LHCII and nine LHCI genes [12]. The LHCII antenna comprises LHCII trimers connected to the PSII core through the CP26 and CP29 LHCII monomers. The LHCII trimers bind PSII at three sites named S (strong), M (medium) and L (loose). In vivo, PSII assembles as dimers associated with two S and M LHCII trimers to form the $C_2S_2M_2$ PSII-LHCII supercomplex in land plants [8]. Supercomplexes with one to three LHCII trimers per monomeric PSII core have also been detected in *Chlamydomonas* [13–15]. In eukaryotic algae the PSI complex is monomeric with a core consisting of the PsaA/PsaB heterodimer and additional subunits as well as up to 9 LHCI proteins in *Chlamydomonas.* It is noticeable that in contrast to the conserved core photosynthetic complexes, the antenna systems are considerably more diverse with hydrophobic membrane-embedded LHCs in plants, green and red algae and extrinsic hydrophilic phycobilisomes in red algae and cyanobacteria. Moreover, in most green algae, thylakoid membranes are not differentiated in the grana and stroma regions [16].

The aim of this chapter is to provide a description of the remarkable dynamics and flexibility of the photosynthetic apparatus of algae in response to changes in environmental conditions and to compare these responses with those of land plants. They include changes in light quality and quantity and in nutrient availability. These responses involve a reorganization of some of the photosynthetic complexes often mediated by posttranslational modifications of their

subunits through an extensive signaling network in chloroplasts and between chloroplasts and nucleus which modulates nuclear and plastid gene expression.

2. Adaptation to changes in light conditions

A distinctive feature of photosynthetic organisms is the presence of light-harvesting systems that funnel the absorbed light energy to the corresponding reaction centers and thereby considerably increase their absorption cross-section. Several regulatory mechanisms operate on these antenna systems for controlling the energy flux to the reaction centers. This is particularly important under changing environmental conditions when the photosynthetic apparatus needs to adapt quickly. Under limiting light, it optimizes its light absorption efficiency by adjusting the relative size of its antenna systems through the reversible allocation of a portion of LHCII between PSII and PSI, a process referred to as state transitions which occurs in algae, plants and cyanobacteria (for reviews see Refs. [17,18]). In contrast, when the absorbed light energy exceeds the capacity of the photosynthetic apparatus, it dissipates the excess excitation energy through nonphotochemical quenching (NPQ) as heat thereby avoiding photodamage (for reviews see Refs. [19,20]).

2.1. State transitions

Because the antenna systems of PSII and PSI have a different pigment composition, their relative light absorption properties change when the light quality varies. This is especially important for aquatic algae because the penetration of light in water changes depending on its wavelength; in particular, red light is more absorbed than blue light. Another example is provided by photosynthetic organisms growing under a canopy where far red light is enriched. These changes in light quality can result in an unequal excitation of PSII and PSI and thereby perturb the redox poise of the plastoquinone pool. Over excitation of PSII relative to PSI leads to increased reduction of the plastoquinone pool and favors thereby docking of plastoquinol to the Qo site of the Cytb_6f complex [21,22]. This process leads to activation of the chloroplast protein kinase Stt7/STN7 and to the phosphorylation of several proteins from LHCII [23,24]. Although the direct phosphorylation of LHCII by the St7/STN7 kinase has not yet been demonstrated, this kinase is the best candidate for the LHCII kinase because it is firmly associated with the Cytb_6f complex, and in its absence, state transitions no longer occur [25]. Furthermore, it is widely conserved in land plants, mosses and algae. As a result of this phosphorylation, a part of the LHCII antenna is detached from PSII and moves and binds to PSI thereby rebalancing the light excitation of PSII and PSI and enhancing photosynthetic yield. This process is reversible as overexcitation of PSI leads to the inactivation of the kinase and to dephosphorylation of LHCII by the PPH1/TAP38 protein phosphatase and its return to PSI [26,27]. Thus two different states can be defined, state 1 and state 2 corresponding to the association of the mobile LHCII antenna to PSII and PSI, respectively. However, a strict causal link between LHCII phosphorylation and its migration from PSII to PSI has been questioned recently by the finding that some phosphorylated LHCII remains associated with PSII supercomplexes and that LHCII serves as antenna for both photosystems under most natural

light conditions [13,28,29]. In plants, the LHCII S trimers comprise Lhcb1 and Lhcb2, whereas the M trimers contain Lhcb1 and Lhcb3 [30]. Both the S and M trimers are most likely not involved in state transitions because the PSII-LHCII supercomplex is unchanged upon phosphorylation [29] and PSI does not bind Lhcb3 in state 2 [30]. Thus LHCII phosphorylation is not sufficient to dissociate all LHCII trimers from PSII. It has therefore been proposed that the peripherally bound L trimers associate with PSI in state 2 [30]. Moreover, although Lhcb1 and Lhcb2 display similar phosphorylation kinetics during a state 1 to state 2 transition, only phosphorylated Lhcb2 but not Lhcb1 is part of the PSI-LHCII supercomplex [31]. A PSI supercomplex has been isolated and characterized in *Chlamydomonas*. It consists of PSI, Cytb_6f, LHCII, FNR (ferredoxin–NADPH reductase), PGRL1, a protein involved in CEF [3] and additional factors (**Figure 1**). The correlation between the occurrence of state transitions and CEF raised the possibility that state transitions may act as a switch between LEF and CEF in *Chlamydomonas* [32]. This interpretation is however not compatible with recent studies which indicate that CEF is activated in the *stt7* mutant when the metabolic demand for ATP increases during the induction of the carbon concentrating mechanism when CO_2 is limiting [33]. Also, analysis of the *stt7* and *ptox2* mutants, locked in state 1 and state 2, respectively, independent of the redox conditions led to similar conclusions [34]. The *ptox2* mutant is deficient in the plastid terminal oxidase which controls the redox state of the PQ pool in the dark [35]. Whereas the accumulation of reducing power and transition to state 2 correlated well with the enhancement of CEF in the wild type, this was not the case for *ptox2*. In this mutant, CEF was not enhanced under aerobic conditions in the dark even though it is locked in state 2 with phosphorylated LHCII. Moreover, CEF enhancement and formation of the PSI-Cytb_6f supercomplex were still observed in the *stt7* mutant when the PQ pool was reduced. It can be concluded that both of these processes occur under reducing conditions with no correlation with state transitions and their associated LHCII reorganization and that it is the redox state of the photosynthetic electron transport rather than state transitions that control CEF [34].

State transitions do not occur under high light because the LHCII kinase is inactivated [36]. The current view is that inactivation of the kinase is mediated by the ferredoxin–thioredoxin system and that a disulfide bond in the kinase rather than in the substrate may be the target site of thioredoxin [37,38]. In this respect, the N-terminal region of the kinase contains indeed two Cys residues, which are conserved in all species examined [23,24]. Both of these Cys are essential for the kinase activity because changes of either Cys through site-directed mutagenesis abolish the kinase activity [25]. It is noticeable that these Cys are located on the lumen side of the thylakoid membrane whereas the kinase catalytic domain is on the stromal side where the substrate sites of the LHCII proteins are located [23,25] (**Figure 2**). Although the conserved Cys residues in the lumen are on the opposite side of the stromal thioredoxin according to this model, one possibility is that thiol-reducing equivalents are transferred across the thylakoid membrane through the CcdA and Hcf164 proteins, which operate in this way during heme and Cytb_6f assembly [39,40]. Alternatively, transfer of thiol-reducing equivalents across the thylakoid membrane could also be mediated by Lto1 (lumen thiol oxidoreductase 1) which catalyzes the formation of disulfide bonds in the thylakoid lumen and is required for PSII assembly [41,42] (**Figure 2**). Its sulfhydryl oxidizing activity is linked to the reduction of phylloquinone, a redox component of PSI. It is not clear whether phylloquinone is involved

in other electron transfer processes besides those in PSI. Although the two lumenal Cys are prime candidates for the redox control of the activity of the Stt7/STN7 kinase, high light treatment did not change the redox state of these Cys [43]. Another possibility is that high light affects the folding of the kinase in the thylakoid membrane, in particular through reactive oxygen species (ROS) generated by the high light treatment.

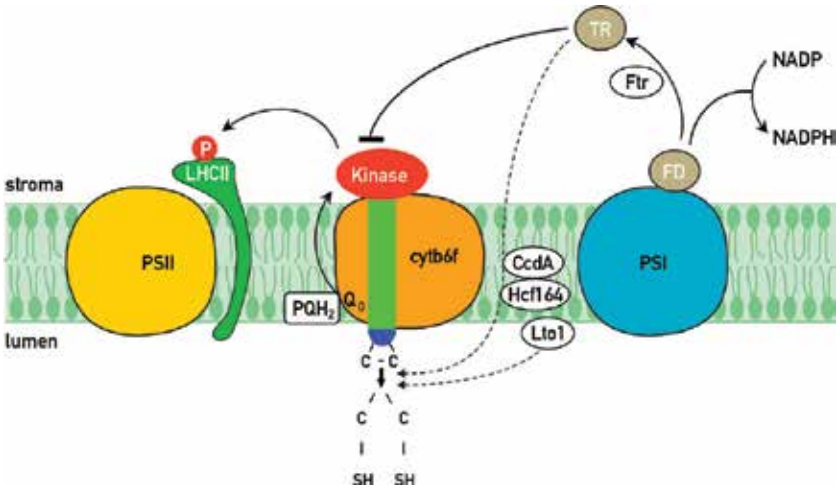

Figure 2. Regulation of the Stt7/STN7 kinase.

The Stt7/STN7 kinase is associated with the Cytb_6f complex. This kinase contains a transmembrane domain connecting its N-terminus on the lumen side with two conserved Cys residues to the catalytic domain on the stromal side of the thylakoid membrane. The major substrates of this kinase are the LHCII proteins of the PSII antenna. The LHCII kinase is known to be inactivated by high light through the Fd/Trx system. This system could modulate the redox state of the two lumenal Cys through two proteins, CcdA and Hcf164, known to mediate the transfer of thiol-reducing equivalents across the thylakoid membrane. Another possibility is that this process is catalyzed by Lto1, the lumenal thiol oxidoreductase 1.

It is known that the activation of the kinase is intimately connected to the docking of plastoquinone to the Qo site of the Cytb_6f complex [21,22] (**Figure 2**). Electron transfer from plastoquinol to Cyt *f* is mediated by the Rieske protein and involves the movement of this protein from the proximal to distal position within the Cytb_6f complex [44,45]. Recent studies have revealed that the two conserved Cys residues of the Stt7/STN7 kinase form an intramolecular disulfide bridge which appears to be essential for kinase activity [43]. However, no change in the redox state of these Cys could be detected during state transitions. It is only under prolonged anaerobic conditions that this disulfide bridge was reduced but at a significantly slower pace than transition from state 1 to state 2 which occurs under anaerobiosis in *Chlamydomonas* [46]. In wild-type *Arabidopsis* plants, the STN7 kinase is only observed as a monomer under both state 1 and state 2 conditions although the dimer could be detected in plants overexpressing STN7 or in mutants with changes in either of the two luminal Cys of

STN7 [47]. However, these results do not exclude the possibility of rapid and transient changes in the redox state of these two Cys. In fact, such changes were proposed to occur to accommodate all the known features of the Stt7/STN7 kinase [43]. A transient change from an intra- to intermolecular disulfide bond may occur which would activate the kinase and be coupled to the movement of the Rieske protein during electron transfer from plastoquinol to Cyt *f*. Moreover, it is interesting to note that the interaction site between the kinase and the Cytb_6f complex has been located close to the flexible glycine-rich hinge connecting the membrane anchor to the large head of the Rieske protein in the lumen [43]. A single chlorophyll *a* molecule with its phytyl tail close to the Qo site exists in Cytb_6f [48]. It is also possible that the kinase senses PQH_2 binding to the Qo site through the single chlorophyll *a* molecule of the Cytb_6f complex whose phytyl tail is close to the Qo site [48,49]. It was proposed that this molecule may play a role in the activation of the Stt7/STN7 kinase based on site-directed mutagenesis of the chlorophyll *a* binding site [50]. The activation of the kinase would be triggered through the transient formation of a STN7 dimer with two intermolecular disulfide bridges which would transduce the signal to the catalytic domain on the stromal side of the thylakoid membrane [43].

Another proposal for the mechanism of activation of the Stt7/STN7 kinase is that hydrogen peroxide may be involved by oxidizing the luminal C1 and C2 to form intra- and/or intermolecular disulfide bridges. It is based on the observation that singlet oxygen generated by PSII can oxidize plastoquinol with concomitant production of hydrogen peroxide in the thylakoid membranes [51]. However, this proposal is difficult to reconcile with the observation that these Cys exist mostly in the oxidized form and the conversion from intra- to intermolecular disulfide bridges appears to be only transient [43].

State transitions involve remodeling of the antenna system of PSII within the thylakoid membranes. This poses a challenging problem especially considering the fact that among biological membranes, the thylakoid membrane is very crowded with 70% of the surface area of grana membranes occupied by proteins and 30% by lipids [11]. Light-induced architectural changes in the folding of the thylakoid membrane are induced at least partly by changes in phosphorylation of thylakoid proteins catalyzed by the protein kinases Stt7/STN7 and Stl1/STN8, which most likely facilitate mobility of proteins in these membranes [52,53]. These two kinases appear to play an important role in chloroplast signaling in response to changing environmental conditions (**Figure 3**). Light irradiance, ambient CO_2 level and the cellular ATP/ADP ratio modulate the redox state of the plastoquinone pool of the electron transport chain which is sensed by the Stt7/STN7 kinase. Together with the Stl1/STN8 kinase and the two corresponding protein phosphatases PPH1/TAP38 and PBCP, Stt7/STN7 forms a central quartet which orchestrates the phosphorylation of the LHCII and the PSII core proteins (**Figure 3**). PTK is another chloroplast Ser/Thr kinase of the casein kinase II family which is associated with the plastid RNA polymerase and acts as a global regulator of chloroplast transcription [54,55]. The CSK kinase shares structural features with cyanobacterial sensor histidine kinases and is conserved in all major plant and algal lineages except *Chlamydomonas reinhardtii* [56]. Upon oxidation of the PQ pool, autophosphorylation of CSK occurs, an event which correlates with phosphorylation of the chloroplast σ factor Sig1 and the decrease of

psaAB gene expression. Furthermore, CSK interacts with PTK and SIG1 in yeast two-hybrid assays. Based on these results, it was proposed that CSK is regulated by the redox state of the PQ pool through the STN7 kinase (**Figure 3**) [56]. However, how the different kinases are linked within this chloroplast signaling network shown in **Figure 3** is still unclear.

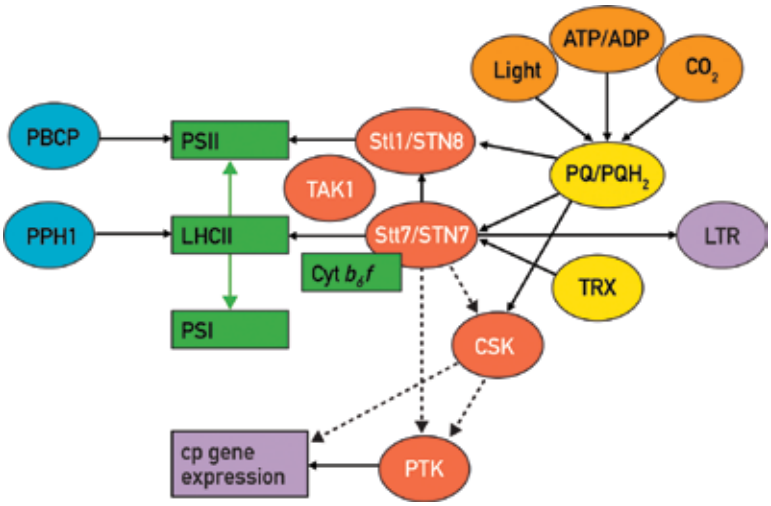

Figure 3. Chloroplast signaling.

The redox state of the PQ pool is modulated by the light irradiance, ATP/ADP ratio and ambient CO_2 level. The protein kinases Stl1/STN8, Stt7/STN7, CSK, PTK and TAK1 [57] are shown with their targets indicated by arrows. *Broken arrows* indicate putative targets. *LTR* long-term response involving retrograde signaling is mediated through Stt7/STN7. Reproduced from Ref. 58 with permission.

2.2. Non photochemical quenching

While state transitions are mainly involved in low light responses through an extensive reorganization of the antenna systems, other mechanisms for the regulation of light-harvesting operate when oxygenic photosynthetic organisms are suddenly exposed to large and sudden changes in light intensity in their natural habitat. In the case of aquatic algae, even moderate water mixing can bring algae from full darkness to high light within minutes [59,60]. Under these conditions, increased electron flow along the electron transport chain generates a large proton gradient. The resulting acidification of the thylakoid lumen leads to the de-excitation of singlet excited light-harvesting pigments and is measured as non-photochemical quenching (NPQ of chlorophyll fluorescence). NPQ comprises several components; the major one is the high energy state quenching qE, which leads to the harmless heat dissipation of the absorbed excess light energy [20,61]. The other components which also contribute to fluorescence quenching are the photoinhibitory quenching qI and state transitions qT although qT is not associated with thermal dissipation of excitation energy. The qE mechanism occurs in all major

algal taxa and land plants. However, the underlying molecular mechanisms of heat dissipation of excess excitation energy differ. The qE process involves both the xanthophyll cycle and the PsbS protein in plants. Another protein, LhcsR, has been shown to mediate qE in algae [19,62].

The proton gradient acts as a sensor of the state of the photosynthetic electron transport chain. The magnitude of this gradient is low under low light illumination and high under illumination with high light especially when it exceeds the capacity of the photosynthetic apparatus. The resulting acidification of the thylakoid lumen activates the xanthophyll cycle in which violaxanthin is de-epoxidized to zeaxanthin, a reaction catalyzed by violaxanthin de-epoxidase (VDE) which has an acidic pH optimum [63]. The reverse reaction is catalyzed by zeaxanthin epoxidase with a broad pH optimum and which in contrast to VDE is active both in the dark and in the light. Because the turnover of this enzyme is considerably lower than that of VDE, zeaxanthin accumulates rapidly during high light illumination. The zeaxanthin-dependent NPQ depends greatly on the grana structure as unstacking of the membranes abolishes qE. It was proposed that the organization of LHCII in an aggregated state within the stacked grana region is essential for efficient qE [64]. Both high proton concentration in the lumen and accumulation of zeaxanthin promote not only aggregation of LHCII but also that of the minor PSII antenna proteins CP29, CP26 and CP24 [65,66]. In plants, qE occurs in the LHC proteins at multiple sites of the antenna system [67]. These proteins have the ability to switch from an efficient light-harvesting mode to a light energy dissipating state [68]. Several mechanisms have been proposed including excitonic coupling, charge transfer and energy transfer between carotenoids and chlorophylls as well as chlorophyll–chlorophyll charge transfer states (for review see Ref. 20).

Another important player involved in NPQ is PsbS, a four-helix member of the LHC protein family [69]. However, this protein does not appear to bind pigments although a chlorophyll molecule was detected at the dimer interface in the PsbS crystals [70]. This protein appears to act as a sensor of the lumen pH most likely through protonation of its acidic lumen residues which in turn induces a rearrangement of the light-harvesting system required for induction of NPQ [71–73]. In this sense, PsbS would act as an antenna organizer, a view which is further supported by the fact that it is mobile in the thylakoid membrane [74], and it is able to associate with both the PSII core complex and LHCII [75]. Moreover, qE can be switched on without the PsbS protein if the lumen pH is very low [76]. It thus appears that protonated PsbS allows for a fast and efficient rearrangement of the PSII antenna which is still possible in its absence but requires a longer time.

In *Chlamydomonas reinhardtii* and *Phaeodactylum tricornutum*, two representatives of green algae and diatoms, respectively, qE is mediated by Lhcsr, another three helix member of the LHC protein family [62]. In high light, most Lhcsr genes are up-regulated in contrast to the light-harvesting genes which are down-regulated. Recent studies reveal that Lhcsr binds chlorophylls and xanthophylls *in vitro* and that it has a basal quenching activity associated with chlorophyll–xanthophyll charge transfer [77]. Its chlorophyll fluorescence lifetime is remarkably short and even shorter at low pH suggesting that this protein has some quenching activity even in low light which is enhanced at low pH. It was proposed that these properties could explain the low expression of Lhcsr under low light when constitutive quenching would be

wasteful [20]. The *Chlamydomonas* Lhcsr is bound to PSII where it may interact with the LHC proteins, especially Lhcbm1 which is known to be involved in thermal dissipation [78–80]. Interestingly, as several other LHC proteins, Lhcsr is phosphorylated by the Stt7 kinase and moves from PSII to PSI during a state 1 to state 2 transition [78]. This observation is particularly interesting with regard to chlorophyll fluorescence lifetime measurements which reveal two different kinetic components suggesting the existence of two underlying mechanisms [81]. It is noteworthy that although PsbS is also present in green algae, there is no evidence that it is involved in qE in these organisms. This is in contrast to the moss *Physcomitrella patens* that has both Lhcsr- and PsbS-dependent NPQ which operate independently and additively [82,83]. The maintenance of these two mechanisms in mosses may be linked to a greater need for inducible NPQ in these organisms [84].

NPQ has also been investigated in diatoms, a ubiquitous group of unicellular marine algae which make an important contribution to the global carbon assimilation [85]. Diatoms acquired their chloroplast through secondary endosymbiosis from a red algal ancestor [86]. In these organisms, similar to plants and green algae, qE relies on three interacting components, the light-induced proton gradient across the thylakoid membrane, the conversion of the xanthophyll diadinoxanthin (Dd) to diatoxanthin (Dt) catalyzed by the enzyme Dd-de-epoxidase which depends on a transthylakoid proton gradient and the Lhcx antenna proteins (for review see Ref. 87). Among these, Lhcx1 appears to play a major role in qE as changes in its level are directly related to the quenching of light energy [88]. Lhcx1 also plays an important general role in light responses in diatoms as it accumulates in different amounts in ecotypes originating from different latitudes. In contrast to land plants, the proton gradient is unable to induce NPQ on its own in diatoms. It is only required to activate the de-epoxidation of Dd. The qE process represents an important photoprotective mechanism and involves a reorganization of the antenna complexes of diatoms [87]. However, the quenching sites within the antenna systems of these organisms have not yet been precisely determined.

Another original feature of diatoms is the way they adjust the ATP/NADPH ratio which is important for proper carbon assimilation by the CBC and for optimal growth. In plants and green algae, this ratio is mainly set by the relative contributions of LEF and CEF and by the water-to-water cycles [89], whereas in diatoms this ratio relies principally on energetic exchanges between plastids and mitochondria [90]. These bidirectional organellar interactions involve the rerouting of reducing power generated by photosynthesis in the plastids to mitochondria and the import of ATP produced in the mitochondria to the plastids.

2.3. PSII repair cycle

Water splitting by PSII is one of the strongest oxidizing reactions which occurs in living organisms. As a result, photodamage to PSII is unavoidable. A remarkable feature of this system is that it is efficiently repaired [91]. PSII exists as a dimer in which each monomer consists of 28 subunits generally associated with two LHCII trimers in a supercomplex [8]. The PSII core consists of the two reaction center polypeptides D1 and D2 which form a central heterodimer which acts as ligand for the chlorophyll dimer P680 and the other redox components including the quinones Q_A and Q_B, the primary and secondary electron acceptors. Among

http://dx.doi.org/10.5772/62261

all PSII subunits, D1 is the major target of photodamage and needs to be specifically replaced. This process, called PSII repair cycle, involves the partial disassembly of the PSII supercomplex, the removal and degradation of the damaged D1 protein, its replacement by a newly synthesized copy and the reassembly of the PSII complex (**Figure 4**) [92]. An important feature of this repair cycle is that it is compartmentalized within the crowded thylakoid membrane [93]. Whereas damage of D1 occurs in the stacked grana region where most of PSII is located, the replacement of this protein takes place in the stroma lamellae. Although the exact role of phosphorylation is not fully understood, the current view is that the PSII repair cycle starts with phosphorylation of the PSII core subunits D1, D2, CP43 and PsbH mediated by the STN8 kinase [94,95] which leads to the disassembly of the PSII-LHCII supercomplex thereby allowing PSII to move to the grana margins and stroma lamellae [96,97]. Dephosphorylation by the PSII core phosphatase Pbcp [53] and by other unknown phosphatases is followed by the degradation of D1 by the FtsH and Deg proteases and a newly synthesized D1 is cotranslationally inserted into the PSII complex [98]. Finally, the reassembled PSII complex moves back to the grana and reforms a supercomplex with LHCII. To make this cycle efficient, it is essential that the enzymes involved are confined to distinct thylakoid membrane subcompartments. Thus, protein degradation occurs on the grana margins and protein synthesis on the stroma lamellae. Additionally, partial conversion of grana stacks to grana margins allows the proteases to access PSII [93].

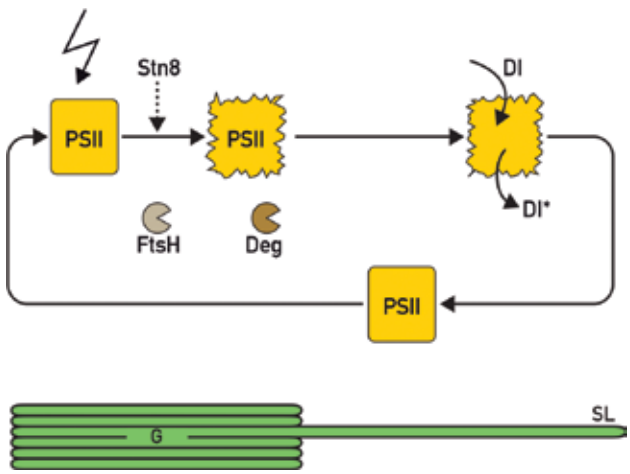

Figure 4. PSII repair cycle.

High light illumination leads to photooxidative damage of the PSII reaction center, especially the D1 protein. The PSII core proteins are phosphorylated and the damaged complex migrates from the grana (G) to the stromal lamellae (SL). The D1 protein is degraded by the FtsH and Deg proteases and upon its removal from the PSII reaction center a newly synthesized D1 protein is inserted cotranslationally into the complex which moves back to the grana and thereby completes the repair cycle. Reproduced from Ref. 5 with permission.

D1 degradation is significantly retarded in the *stn8* and *stn7 stn8* mutants of *Arabidopsis* in which the thylakoid membrane architecture is affected [52]. In the absence of STN8, grana diameter is increased and there are fewer grana stacks. This observation is particularly intriguing as it suggests that PSII core phosphorylation is important for maintaining grana size, a parameter which is highly conserved in land plants and algae [11]. Loss of STN8 also affects partitioning of FtsH between grana and stromal membranes and limits its access to the grana, and migration of D1 from the grana to the stroma lamellae is slowed down during the PSII repair cycle [52]. These observations are thus compatible with the view that PSII core phosphorylation has a strong impact on thylakoid membrane folding and architecture mediated most likely by electrostatic repulsion between membrane layers as proposed earlier [99].

3. Response of the photosynthetic apparatus to micronutrient depletion

The photosynthetic machinery comprises several protein–pigment complexes with specific cofactors including iron, copper, manganese and iron–sulfur centers. Under conditions of limitation of one of these micronutrients, the photosynthetic machinery displays a remarkable plasticity and ability to adapt to its new environment.

3.1. Copper deficiency

When *Chlamydomonas* cells face copper deficiency, the copper-binding protein plastocyanin that acts as an essential electron carrier between the Cytb_6f complex and PSI is degraded and replaced with Cyt *c6* [100]. In this way, the cells can maintain photosynthetic electron flow. Besides Cyt *c6*, Cpx (coproporphyrinogen oxidase) is also induced by copper deficiency at the transcriptional level [101]. The increase of Cpx1 expression may meet the demand for heme, the cofactor of Cyt *c6*. Crd1, another target besides Cyt *c6* and Cpx1 of this signal transduction pathway responsive to copper depletion, was identified through a genetic screen for a copper-conditional phenotype. Crd1 is a thylakoid diiron membrane protein which is required for the maintenance of PSI and LHCI in copper-deficient cells. It has an isoform, Cth1, which accumulates in copper-sufficient oxygenated cells whereas Crd1 accumulates in a reciprocal manner in copper-deficient cells or under anaerobiosis [101]. Crd1 and Cth1 are two isoforms of a subunit of the aerobic cyclase in chlorophyll biosynthesis with overlapping functions in the biosynthesis of Chl proteins [102].

3.2. Iron deficiency

Iron deficiency occurs often in nature and poses a challenge for photosynthetic organisms because of the abundance and importance of iron in the primary photosynthetic reactions. With its three 4Fe-4S centers, PSI is a prime target under these conditions. Under conditions of iron limitation, the level of PSI decreases when *Chlamydomonas* cells are grown in the presence of a carbon source such as acetate. Eventually, these Fe-deficient cells become chlorotic because of proteolytically-induced loss of both photosystems and Cytb_6f [103]. Before

chlorosis occurs, a graded response is induced, in which the LHCI antenna is dissociated from PSI. This dissociation appears to be caused by the decrease of the amount of the peripheral chlorophyll-binding PsaK subunit of PSI which is required for the functional connection of LHCI to PSI. Interestingly, loss of Crd1, the Fe-requiring aerobic oxidative cyclase in copper-sufficient cells, also leads to a lower accumulation of PsaK and to uncoupling of LHCI from PSI. It was proposed that a change in plastid iron content is sensed by the diiron enzyme Crd1 through the occupancy of its Fe-containing active site which determines its activity [103]. In turn, this would affect the flux through the chlorophyll biosynthetic pathway and PsaK stability. This response to Fe deficiency and also to light quantity and quality further involves a remodeling of the antenna complexes with the degradation of specific subunits and the synthesis of new ones leading to a new state of the photosynthetic apparatus which allows for optimal photosynthetic function and minimal photooxidative damage. The protective value of this antenna remodeling is further confirmed by the observation that the light sensitivity of a PsaF-deficient mutant [104] is alleviated in a *psaF-crd1* double mutant [101]. The proposed mechanism can be placed within a general frame for explaining the causal link between chlorosis induced by iron deficiency and loss of photosynthetic function.

Marine organisms can face iron limitation in the oceans. A deep-sea/ low light strain of the marine green alga *Ostreococcus* has lower photosynthetic activity due to the limited accumulation of PSI [105]. Interestingly, in this strain, electron flow from PSII is shuttled to a plastid plastoquinol terminal oxidase thereby bypassing electron transfer through the Cytb_6f complex. This water-to-water cycle allows for the pumping of additional protons to the lumen thylakoid space and thus facilitates ATP production and enhances qE in the case of absorption of excess light excitation energy.

Micronutrient limitation can also act at the level of the biosynthesis of the photosynthetic apparatus which is mediated by the concerted action of the nuclear and chloroplast genetic systems. It is well established that subunits of the photosynthetic complexes originate from these two systems. In addition, a large number of nucleus-encoded factors are required for chloroplast gene expression that act at various plastid posttranscriptional steps comprising RNA processing and stability, translation and assembly of the photosynthetic complexes. Many of these factors have unique gene targets in the plastid and often interact directly or indirectly with specific 5′-untranslated RNA sequences [106]. One of these factors, Taa1 is specifically required for the translation of the PsaA PSI reaction center subunit in *C. reinhardtii* [107]. Under iron limitation, this protein is down-regulated through a posttranscriptional process and it reaccumulates upon restoration of iron. Another recently identified factor is Mac1 which is necessary for stabilization of the *psaC* mRNA [108]. Under iron limitation, both Mac1 protein and *psaC* mRNA are reduced 2-fold and PsaC and PSI are destabilized. Thus, PSI abundance appears to be regulated by iron availability through at least two of these nucleus-encoded plastid factors specifically involved in PSI biosynthesis. Another intriguing observation is that Mac1 is differentially phosphorylated in response to changes in the redox state of the electron transport chain raising questions to what extent posttranslational protein changes modulate the assembly of photosynthetic complexes.

Similar findings have been reported for Mca1 and Tca1, two nucleus-encoded proteins that are required for the stability and translation of the *petA* mRNA encoding the Cyt *f* subunit in *C. reinhardtii*. Nitrogen deprivation leads to the proteolytic degradation of these factors and in turn to the loss of the Cytb_6f complex [109,110]. The response to nitrogen starvation also involves other factors required for the assembly of the Cytb_6f complex and its hemes [111].

3.3. Sulfur deprivation and hydrogen production

Many soil-dwelling algae like *Chlamydomonas* experience anoxic conditions especially during the night and are able to rapidly acclimate to anaerobiosis by shifting from aerobic to fermentative metabolism and can thus sustain energy production in the absence of photosynthesis [112–114]. These anaerobic conditions lead to the expression of the oxygen-sensitive hydrogenase which catalyzes the production of hydrogen from protons and electrons derived from the photosynthetic electron transport chain. Sulfur deprivation of *Chlamydomonas* cells leads to a significant decline in photosynthetic activity within 24 h although there is no proportional concomitant decline in the levels of the major photosynthetic complexes [115,116]. This decline in electron transport activity is due to the conversion of PSII centers from the Q_B-reducing to a Q_B nonreducing center [117]. This system has been used for improving hydrogen production in *Chlamydomonas* cells [118]. These cells as well other microalgal species possess a chloroplast (FeFe)-hydrogenase which acts as an additional sink when the photosynthetic electron transport chain is overreduced under anaerobic conditions. Upon sulfur deprivation, photosynthetic oxygen evolution decreases whereas respiration is maintained resulting in an anaerobic environment in a closed culture system. Although the exact physiological role of algal hydrogenases is not known, they are likely to play a significant role in redox poise, photoprotection and fermentative energy production [114].

4. Long-term response: changes in nuclear and chloroplast gene expression

While short-term responses of the photosynthetic apparatus involve mostly posttranslational mechanisms such as phosphorylation or changes in pH and ion levels, long-term responses are mediated through changes in the expression of specific chloroplast and nuclear genes and their products. Environmental changes such as changes in light quantity and quality lead to changes in the state of the chloroplast which are perceived by the nucleus through a signaling chain referred to as retrograde signaling. The components of this signaling chain are still largely unknown although a few potential retrograde signals have been identified [119]. Among these, tetrapyrroles appear to play a significant role. These compounds are involved in the chlorophyll biosynthetic pathway which needs to be tightly regulated to avoid photooxidative damage. Mg-protoporphyrin IX (Mg-Proto) was first shown to be involved in the repression of the LHCII genes in retrograde signaling in *Chlamydomonas* [120]. However, such a role for this tetrapyrrole in land plants gave rise to contradictory results and has been questioned [121–123]. In contrast, feeding experiments with Mg-Proto and hemin in *Chlamy-*

domonas induce increased expression of the gene of HemA (glutamyl-tRNA reductase) and of the heat shock proteins Hsp70A, Hsp70B and Hsp70E [124–126]. In this alga, both Mg-Proto and hemin are exclusively synthesized in the chloroplast. Genome-wide transcriptional profiling revealed that their exogenous addition to *Chlamydomonas* cells elicits transient changes in the expression of almost 1000 genes [127]. They include only few genes of photosynthetic proteins but several genes of enzymes of the tricarboxylic acid cycle, heme-binding proteins, stress-responsive proteins and proteins involved in protein folding and degradation. Because these tetrapyrroles are not present in the natural environment of the algae, it is likely that these two tetrapyrroles act as secondary messengers for adaptive responses affecting not only organellar proteins but also the entire cell. It is noticeable that these large changes in mRNA levels are not matched by similar changes in protein amount [127].

The synthesis of tetrapyrroles needs to be tightly controlled because some of these chlorophyll or heme precursors are very photodynamic and can cause serious photooxidative damage. In land plants, the conversion of protochlorophyllide (PChlide) to chlorophyllide (Chlide) is light dependent. In the dark, overaccumulation of PChlide is prevented through a negative feedback mediated by the Flu protein which inhibits glutamyl-tRNA reductase at an early step of the tetrapyrrole pathway (**Figure 5**) [128]. Although *Chlamydomonas* is able to synthesize chlorophyll in the dark, it also contains a Flu-like gene called Flp, which gives rise to two transcripts by alternative splicing [129]. The relative levels of the two corresponding Flp proteins correlate with the accumulation of specific porphyrin intermediates some of which have been implicated in a signaling chain from the chloroplast to the nucleus. Moreover, decreased levels of the Flp proteins lead to the accumulation of several porphyrin intermediates and to photobleaching when *Chlamydomonas* cells are transferred from the dark to the light. These Flp proteins therefore appear to act as regulators of chlorophyll synthesis and their expression is controlled by both light and plastid signals.

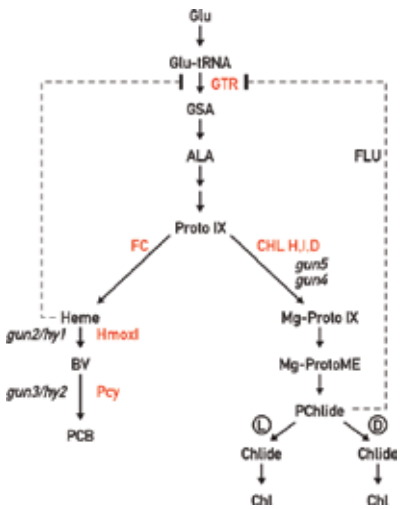

Figure 5. Tetrapyrrole pathway.

The heme and chlorophyll biosynthetic pathways branch at protoporphyrin IX (Prot IX). GTR, glutamine tRNA reductase, is subjected to feedback inhibition by heme and FLU. In most land plants, conversion of PChlide (protochlorophyllide) to Chlide is light-dependent (L, in *Chlamydomonas* this conversion also occurs in the dark, *D*). Through its negative feedback on GTR, FLU prevents overaccumulation of PChlide in the dark. The steps affected by the *gun* and *hy* mutations which affect retrograde signaling are indicated. GSA, glutamate 1-semialdehyde; ALA, 5-aminolevulinic acid; Chl, chlorophyll; Fc, ferrochelatase, Hmox1, heme oxygenase; BV, biliverdin; Pcy, bilin reductase; PCB, phytocyanobilin, CHLH, CHLI and CHLD are subunits of Mg-chelatase. Reproduced from Ref. 126 with permission.

Additional evidence for the involvement of tetrapyrroles in retrograde signaling comes from the identification of a functional bilin biosynthesis pathway in *Chlamydomonas* [130,131]. In this pathway, protoporphyrin IX is converted to protoheme and Mg-Proto by Fe- and Mg-chelatase, respectively. While heme is used as prosthetic group for many hemoproteins, a portion of heme is converted to biliverdin IXa by heme oxygenase (Hmox1) and in the next step by a ferredoxin-dependent phytochromobilin synthase (PcyA) to phytochromobilin which serves as chromophore of phytochromes (**Figure 5**). However, *Chlamydomonas* as well as other chlorophytes do not produce phytochromes, raising questions on the role of this pathway in these algae. Some clues came from the analysis of a mutant of *Chlamydomonas* deficient in Hmox1 whose phototrophic growth is compromised and in which the increase of chlorophyll upon a dark-to-light transition no longer occurs [131]. Comparative transcriptomic studies of wild-type and *hmox1* cells revealed a set of nuclear genes that are up-regulated by bilins and that comprise several oxygen-dependent redox enzymes such as mono-and dioxygenases, proteins with redox cofactors and enzymes of oxidative amino acid metabolism. These results raise the possibility that bilins operate within a retrograde signaling pathway that evolved in chlorophytes for the detoxification of ROS generated during sudden dark to light shifts. It remains to be seen whether bilins assume additional roles in chlorophytes besides ensuring smooth daily transitions from dark to light with minimal photooxidative damage.

A further striking example of the action of tetrapyrroles as mediators for plastid-to-nucleus-communication is the identification of a tetrapyrrole-regulated ubiquitin ligase for cell cycle coordination from organelle to nuclear DNA replication in the red alga *Cyanidioschyzon merolae* [132–134].

Redox changes within the photosynthetic electron transport chain occur upon changes in light quality and quantity, CO_2 levels, nutrient availability and elevated temperature. As a result of unequal excitation of PSI and PSII or of insufficient electron acceptor capacity on the PSI acceptor side, the redox state of the plastoquinone pool is altered. In this case, chloroplast gene expression is affected in land plants [135] although the evidence is less convincing in algae. However, in these organisms, there is unambiguous evidence that nuclear gene expression is affected [136]. A possible candidate for sensing the redox state of the plastoquinone pool is the chloroplast protein kinase Stt7/STN7 which is known to be activated when plastoquinol occupies the Qo site of the Cytb_6f complex [21,22]. During experiments in which plants were shifted from light preferentially absorbed by PSI to light preferentially absorbed by PSII, the

expression levels of 937 genes changed significantly in *Arabidopsis* [137]. 800 of these changes were dependent on STN7, indicating that most of these genes are under redox control.

In all situations in which the redox poise of the plastoquinone pool is affected, the relative sizes of the PSII and PSI antenna sizes play an important role. Several factors involved in antenna size were identified through a genetic screen in *Chlamydomonas* [138]. One of these factors, Tla1 functions as a regulator of chlorophyll content and antenna size and is localized in the chloroplast envelope. In the *tla1* mutant, thylakoid membranes were disorganized, appressed grana membranes were lost and accumulation of the PSII core proteins was reduced [138]. The second identified factor Tla2 corresponds to FtsY required for insertion of proteins into thylakoid membranes [139] and the third, Tla3 corresponds to SRP43, a component of chloroplast SRP, known to be essential for the integration of LHCII proteins into the thylakoid membrane [140].

Another protein regulating antenna size in *Chlamydomonas* is Nab1, a cytoplasmic repressor of translation of specific Lcbm isoforms [141]. By binding selectively to the mRNAs of these proteins with Lhcm6 mRNA as its principal target, it sequesters the RNA in translationally silent nucleoprotein complexes. The activity of Nab1 is regulated through a cysteine-based redox control and also by arginine methylation [141,142]. This protein apparently senses the increased or decreased demand for LHCII protein synthesis through changes in the cytosolic redox state although the underlying molecular mechanisms are still unknown.

5. Conclusions and perspectives

The photosynthetic apparatus is a complex machinery consisting of several large protein–pigment complexes whose components are encoded by both nuclear and chloroplast genes. Thus, the biosynthesis of this system involves two distinct genetic systems which act in a coordinate manner. In nature, photosynthetic organisms are subjected to continuous environmental changes and need to adapt so as to maintain optimal photosynthetic activity and to protect themselves from photooxidative damage. These processes can be grouped in short-term and long-term responses. The first occurs in the second-to-minute range and involves light-induced protein conformational changes, posttranslational protein modifications, cell compartment–specific pH changes and ion fluxes across the chloroplast and thylakoid membranes. The second occurs in the minute-to-hour range and involves changes in gene expression and protein accumulation, which depend on an intricate bilateral communication system between chloroplasts and nucleus. Many nuclear genes encoding chloroplast proteins have been identified which are required for chloroplast gene expression and act mainly at posttranscriptional steps. Some of these factors appear to act constitutively while others assume a regulatory role because they have short half-lives and their level varies greatly upon changes in environmental cues including light, temperature and nutrient availability. However, the molecular mechanisms underlying the intercompartmental communication between chloroplast, mitochondria and nucleus are still largely unknown although several retrograde signals have been identified. They involve specific compounds such as tetrapyrroles and

isoprenoids as well as plastid protein synthesis, the redox state of the photosynthetic electron transport chain and ROS generated under specific stress conditions. Moreover, a complex signaling network is operating within chloroplasts comprising several protein kinases and phosphatases, ion channels, and specific metabolites which act as signals and for the communication between chloroplast and nucleus. However, the signaling chains connecting these different components are still largely unknown and their identification remains an important challenge for future research.

The flexibility of the thylakoid membrane is truly remarkable. Although it is crowded with proteins, it still allows for efficient remodeling of the photosynthetic complexes within the thylakoid membrane especially in response to changes in the quality and quantity of light. Among these responses, state transitions and NPQ have been studied extensively and some of the underlying molecular mechanisms have been elucidated. However, many questions remain open. We still do not fully understand how the Stt7/STN7 kinase that plays a central role in state transitions and chloroplast signaling is activated and inactivated as a result of perturbations of the chloroplast redox poise. From an evolutionary point of view, it is particularly interesting to compare these adaptive responses in different photosynthetic organisms such as plants, fresh water and marine algae and cyanobacteria. In this respect, NPQ, the dissipation of excess excitation energy as heat in the light-harvesting systems of the photosystems, is of great importance and it is widely used in the plant kingdom. Recent studies on NPQ in different photosynthetic organisms raise several questions regarding the evolution of this essential photoprotective mechanism. For example, it is not clear why the Lhcsr proteins were lost during the transition from aquatic to land plants. Moreover, the qE process in most algae derived by secondary endosymbiosis from a red algal ancestor differs from that in extant red algae. All of these derived algae possess a xanthophyll cycle and Lhcsr-related proteins which are apparently absent in red algae [87] and which have been suggested to be derived from green algae [143,144]. It will clearly be important and challenging to elucidate these evolutionary puzzles.

Acknowledgment

I thank Nicolas Roggli for preparing the figures and Michel Goldschmidt-Clermont for critical reading of the manuscript. Work in the author's laboratory was supported by grants from the Swiss National Science Foundation.

Author details

Jean-David Rochaix*

Address all correspondence to: Jean-David.Rochaix@unige.ch

Departments of Molecular Biology and Plant Biology, University of Geneva University,

Geneva, Switzerland

References

[1] Burrows PA, Sazanov LA, Svab Z, Maliga P, Nixon PJ. Identification of a functional respiratory complex in chloroplasts through analysis of tobacco mutants containing disrupted plastid ndh genes. EMBO J. 1998;17(4):868–876.

[2] Munekage Y, Hojo M, Meurer J, Endo T, Tasaka M, Shikanai T. PGR5 is involved in cyclic electron flow around photosystem I and is essential for photoprotection in Arabidopsis. Cell. 2002;110(3):361–371.

[3] Hertle AP, Blunder T, Wunder T, Pesaresi P, Pribil M, Armbruster U, et al. PGRL1 is the elusive ferredoxin-plastoquinone reductase in photosynthetic cyclic electron flow. Mol Cell. 2013;49(3):511–523.

[4] Johnson X, Steinbeck J, Dent RM, Takahashi H, Richaud P, Ozawa S, et al. Proton gradient regulation 5-mediated cyclic electron flow under ATP- or redox-limited conditions: a study of DeltaATpase pgr5 and DeltarbcL pgr5 mutants in the green alga Chlamydomonas reinhardtii. Plant Physiol. 2014;165(1):438–452.

[5] Rochaix JD. Regulation and dynamics of the light-harvesting system. Annu Rev Plant Biol. 2014;65:287–309.

[6] Andersson B, Andersson J. Lateral heterogeneity in the distribution of chlorophyll-protein complexes of the thylakoid membranes of spinach chloroplasts. Biochem Biophys Acta. 1980;593(2):427–440.

[7] Albertsson P. A quantitative model of the domain structure of the photosynthetic membrane. Trends Plant Sci. 2001;6(8):349–358.

[8] Dekker JP, Boekema EJ. Supramolecular organization of thylakoid membrane proteins in green plants. Biochim Biophys Acta. 2005;1706(1–2):12–39.

[9] Lezhneva L, Meurer J. The nuclear factor HCF145 affects chloroplast psaA-psaB-rps14 transcript abundance in Arabidopsis thaliana. Plant J. 2004;38(5):740–753.

[10] Barneche F, Winter V, Crevecoeur M, Rochaix JD. ATAB2 is a novel factor in the signalling pathway of light-controlled synthesis of photosystem proteins. EMBO J. 2006;25(24):5907–5918. Epub 2006 Nov 30.

[11] Kirchhoff H, Haferkamp S, Allen JF, Epstein DB, Mullineaux CW. Protein diffusion and macromolecular crowding in thylakoid membranes. Plant Physiol. 2008;146(4):1571–1578.

[12] Minagawa J, Takahashi Y. Structure, function and assembly of Photosystem II and its light-harvesting proteins. Photosynth Res. 2004;82(3):241–263.

[13] Drop B, Webber-Birungi M, Yadav SK, Filipowicz-Szymanska A, Fusetti F, Boekema EJ, et al. Light-harvesting complex II (LHCII) and its supramolecular organization in Chlamydomonas reinhardtii. Biochim Biophys Acta. 2014;1837(1):63–72.

[14] Nield J, Kruse O, Ruprecht J, da Fonseca P, Buchel C, Barber J. Three-dimensional structure of Chlamydomonas reinhardtii and Synechococcus elongatus photosystem II complexes allows for comparison of their oxygen-evolving complex organization. J Biol Chem. 2000;275(36):27940–27946.

[15] Tokutsu R, Kato N, Bui KH, Ishikawa T, Minagawa J. Revisiting the supramolecular organization of photosystem II in Chlamydomonas reinhardtii. J Biol Chem. 2012;287(37):31574–31581.

[16] Gunning BES, Schwartz OM. Confocal microscopy of thylakoid autofluorescence in relation to origin of grana and phylogeny in the green algae. Aust J Plant Physiol 1999;26:695–708.

[17] Lemeille S, Rochaix JD. State transitions at the crossroad of thylakoid signalling pathways. Photosynth Res. 2010;106:33-46.

[18] Wollman FA. State transitions reveal the dynamics and flexibility of the photosynthetic apparatus. Embo J. 2001;20(14):3623–3630.

[19] Niyogi KK. PHOTOPROTECTION REVISITED: Genetic and Molecular Approaches. Annu Rev Plant Physiol Plant Mol Biol. 1999;50:333–359.

[20] Niyogi KK, Truong TB. Evolution of flexible non-photochemical quenching mechanisms that regulate light harvesting in oxygenic photosynthesis. Curr Opin Plant Biol. 2013;16(3):307–314.

[21] Vener AV, van Kan PJ, Rich PR, Ohad II, Andersson B. Plastoquinol at the quinol oxidation site of reduced cytochrome bf mediates signal transduction between light and protein phosphorylation: thylakoid protein kinase deactivation by a single-turnover flash. Proc Natl Acad Sci U S A. 1997;94(4):1585–1590.

[22] Zito F, Finazzi G, Delosme R, Nitschke W, Picot D, Wollman FA. The Qo site of cytochrome b6f complexes controls the activation of the LHCII kinase. Embo J. 1999;18(11):2961–2969.

[23] Depège N, Bellafiore S, Rochaix JD. Role of chloroplast protein kinase Stt7 in LHCII phosphorylation and state transition in Chlamydomonas. Science. 2003;299:1572–1575.

[24] Bellafiore S, Barneche F, Peltier G, Rochaix JD. State transitions and light adaptation require chloroplast thylakoid protein kinase STN7. Nature. 2005;433:892–895.

[25] Lemeille S, Willig A, Depège-Fargeix N, Delessert C, Bassi R, Rochaix JD. Analysis of the chloroplast protein kinase Stt7 during state transitions. PLoS Biol. 2009;7(3):e45.

[26] Pribil M, Pesaresi P, Hertle A, Barbato R, Leister D. Role of plastid protein phosphatase TAP38 in LHCII dephosphorylation and thylakoid electron flow. PLoS Biol. 2010;8(1):e1000288.

[27] Shapiguzov A, Ingelsson B, Samol I, Andres C, Kessler F, Rochaix JD, et al. The PPH1 phosphatase is specifically involved in LHCII dephosphorylation and state transitions in Arabidopsis. Proc Natl Acad Sci U S A. 2010;107(10):4782–4787.

[28] Wientjes E, Drp B, Kouril R, Boekema EJ, Croce R. Photosystem II supercomplex organization does not change during state transitions in Arabidopsis thaliana. New Phytologist. 2013a;in press.

[29] Wientjes E, Drop B, Kouril R, Boekema EJ, Croce R. During state 1 to state 2 transition in Arabidopsis thaliana, the photosystem II supercomplex gets phosphorylated but does not disassemble. J Biol Chem. 2013b;288(46):32821–32826.

[30] Galka P, Santabarbara S, Khuong TT, Degand H, Morsomme P, Jennings RC, et al. Functional analyses of the plant photosystem I-light-harvesting complex II supercomplex reveal that light-harvesting complex II loosely bound to photosystem II is a very efficient antenna for photosystem I in state II. Plant Cell. 2012;24(7):2963–2978.

[31] Longoni P, Douchi D, Cariti F, Fucile G, Goldschmidt-Clermont M. Phosphorylation of the Lhcb2 isoform of Light Harvesting Complex II is central to state transitions. Plant Physiol. 2015;169:2874-2883.

[32] Finazzi G, Rappaport F, Furia A, Fleischmann M, Rochaix JD, Zito F, Forti G. Involvement of state transitions in the switch between linear and cyclic electron flow in *Chlamydomonas reinhardtii*. EMBO Rep. 2002; 3: 280-285.

[33] Lucker B, Kramer DM. Regulation of cyclic electron flow in Chlamydomonas reinhardtii under fluctuating carbon availability. Photosynth Res. 2013;117(1–3):449–459.

[34] Takahashi H, Clowez S, Wollman FA, Vallon O, Rappaport F. Cyclic electron flow is redox-controlled but independent of state transition. Nat Commun. 2013;4:1954.

[35] Houille-Vernes L, Rappaport F, Wollman FA, Alric J, Johnson X. Plastid terminal oxidase 2 (PTOX2) is the major oxidase involved in chlororespiration in Chlamydomonas. Proc Natl Acad Sci U S A. 2011;108(51):20820–20825.

[36] Schuster G, Dewit M, Staehelin LA, Ohad I. Transient inactivation of the thylakoid photosystem II light-harvesting protein kinase system and concomitant changes in intramembrane particle size during photoinhibition of Chlamydomonas reinhardtii. J Cell Biol. 1986;103(1):71–80.

[37] Rintamaki E, Martinsuo P, Pursiheimo S, Aro EM. Cooperative regulation of light-harvesting complex II phosphorylation via the plastoquinol and ferredoxin-thioredoxin system in chloroplasts. Proc Natl Acad Sci U S A. 2000;97(21):11644–11649.

[38] Rintamaki E, Salonen M, Suoranta UM, Carlberg I, Andersson B, Aro EM. Phosphorylation of light-harvesting complex II and photosystem II core proteins shows different

irradiance-dependent regulation in vivo. Application of phosphothreonine antibodies to analysis of thylakoid phosphoproteins. J Biol Chem. 1997;272(48):30476–30482.

[39] Page ML, Hamel PP, Gabilly ST, Zegzouti H, Perea JV, Alonso JM, et al. A homolog of prokaryotic thiol disulfide transporter CcdA is required for the assembly of the cytochrome b6f complex in Arabidopsis chloroplasts. J Biol Chem. 2004;279(31):32474–32482. Epub 2004 May 24.

[40] Lennartz K, Plucken H, Seidler A, Westhoff P, Bechtold N, Meierhoff K. HCF164 encodes a thioredoxin-like protein involved in the biogenesis of the cytochrome b(6)f complex in Arabidopsis. Plant Cell. 2001;13(11):2539–2551.

[41] Karamoko M, Cline S, Redding K, Ruiz N, Hamel PP. Lumen Thiol Oxidoreductase1, a disulfide bond-forming catalyst, is required for the assembly of photosystem II in Arabidopsis. Plant Cell. 2011;23(12):4462–4475.

[42] Du JJ, Zhan CY, LuY, Cui HR, Wang XY. The conservative cysteines in transmembrane domain of AtVKOR/LTO1 are critical for photosynthetic growth and photosystem II activity in Arabidopsis. Frontiers in plant science. 2015;6:238.

[43] Darrouzet E, Moser CC, Dutton PL, Daldal F. Large scale domain movement in cytochrome bc(1): a new device for electron transfer in proteins. Trends Biochem Sci. 2001;26(7):445–451.

[44] Shapiguzov, A, Chai X, Fucile G, Longoni P, Zhang L, Rochaix JD. Activation of the Stt7/STN7 kinase through dynamic interactions with the cytochrome b_6f complex. Plant Physiol. 2016; Mar 3. pii: pp.01893.2015. [Epub ahead of print]

[45] Breyton C. Conformational changes in the cytochrome b6f complex induced by inhibitor binding. J Biol Chem. 2000;275(18):13195–13201.

[46] BultéL, Gans P, Rebeille F, Wollman FA. ATP control on state transitions in Chlamydomonas. Biochim Biophys Acta. 1990;1020:72–80.

[47] Wunder T, Liu Q, Aseeva E, Bonardi V, Leister D, Pribil M. Control of STN7 transcript abundance and transient STN7 dimerisation are involved in the regulation of STN7 activity. Planta. 2013;237(2):541–558.

[48] Stroebel D, Choquet Y, Popot JL, Picot D. An atypical haem in the cytochrome b(6)f complex. Nature. 2003;426(6965):413–418.

[49] Kurisu G, Zhang H, Smith JL, Cramer WA. Structure of the cytochrome b6f complex of oxygenic photosynthesis: tuning the cavity. Science. 2003;302(5647):1009–1014. Epub 2003 Oct 2.

[50] de Lacroix de Lavalette A, Finazzi G, Zito F. b6f-Associated chlorophyll: structural and dynamic contribution to the different cytochrome functions. Biochemistry. 2008;47:5259–5265.

[51] Khorobrykh SA, Karonen M, Tyystjarvi E. Experimental evidence suggesting that H2O2 is produced within the thylakoid membrane in a reaction between plastoquinol and singlet oxygen. FEBS Lett. 2015;589(6):779–786.

[52] Fristedt R, Willig A, Granath P, Crèvecoeur M, Rochaix JD, Vener A. Phosphorylation of photosystem II controls functional macroscopic folding of plant photosynthetic membranes. Plant Cell. 2009; 21:3950-3964.

[53] Samol I, Shapiguzov A, Ingelsson B, Fucile G, Crevecoeur M, Vener AV, et al. Identification of a photosystem II phosphatase involved in light acclimation in Arabidopsis. Plant Cell. 2012;24(6):2596–2609.

[54] Link G. Redox regulation of chloroplast transcription. Antioxid Redox Signal. 2003;5:79–87.

[55] Ogrzewalla K, Piotrowski M, Reinbothe S, Link G. The plastid transcription kinase from mustard (Sinapis alba L.). A nuclear-encoded CK2-type chloroplast enzyme with redox-sensitive function. Eur J Biochem. 2002;269(13):3329–3337.

[56] Puthiyaveetil S, Kavanagh TA, Cain P, Sullivan JA, Newell CA, Gray JC, et al. The ancestral symbiont sensor kinase CSK links photosynthesis with gene expression in chloroplasts. Proc Natl Acad Sci U S A. 2008;105(29):10061–10066.

[57] Snyders S, Kohorn BD. TAKs, thylakoid membrane protein kinases associated with energy transduction. J Biol Chem. 1999;274(14):9137–9140.

[58] Rochaix JD. Redox regulation of thylakoid protein kinases and photosynthetic gene expression. Antioxid Redox Signal. 2013;18(16):2184–2201.

[59] MacIntyre HL, Kana TM, Geider RJ. The effect of water motion on short-term rates of photosynthesis by marine phytoplankton. Trends Plant Sci. 2000;5(1):12–17.

[60] Schubert H, Forster RM. Sources of variability in the factors used for modellingprimary productivityin eutrophic waters. Hydrobiologia. 1997;349:75–85.

[61] Ruban AV, Johnson MP, Duffy CD. The photoprotective molecular switch in the photosystem II antenna. Biochim Biophys Acta. 2012;1817(1):167–181.

[62] Peers G, Truong TB, Ostendorf E, Busch A, Elrad D, Grossman AR, et al. An ancient light-harvesting protein is critical for the regulation of algal photosynthesis. Nature. 2009;462(7272):518–521.

[63] Demmig-Adams B, AdamsW-W. Photoprotection and other responses of plants to high light stress. Annu Rev Plant Physiol Plant Mol Biol. 1992;43:599–626.

[64] Horton P, Wentworth M, Ruban A. Control of the light harvesting function of chloroplast membranes: The LHCII-aggregation model for nonphotochemical quenching. FEBS Lett. 2005 ; 579 : 4201-4206.

[65] Phillip D, Ruban AV, Horton P, Asato A, Young AJ. Quenching of chlorophyll fluorescence in the major light-harvesting complex of photosystem II: a systematic study of the effect of carotenoid structure. Proc Natl Acad Sci U S A. 1996;93(4):1492–1497.

[66] Wentworth M, Ruban AV, Horton P. Kinetic analysis of nonphotochemical quenching of chlorophyll fluorescence. 2. Isolated light-harvesting complexes. Biochemistry. 2001;40(33):9902–9908.

[67] Holwarth AR, Miloslavina Y, Nilkens M, Jahns P. Identification of two quenching sites active in the regulation of photosynthetic light-harvesting studies by time-resolved fluorescence. Chem Phys Lett. 2009;483:262–267.

[68] Kruger TP, Ilioaia C, Johnson MP, Ruban AV, Papagiannakis E, Horton P, et al. Controlled disorder in plant light-harvesting complex II explains its photoprotective role. Biophys J. 2012;102(11):2669–2676.

[69] Li XP, Bjorkman O, Shih C, Grossman AR, Rosenquist M, Jansson S, et al. A pigment-binding protein essential for regulation of photosynthetic light harvesting. Nature. 2000;403(6768):391–395.

[70] Fan M, Li M, Liu Z, Cao P, Pan X, Zhang H, et al. Crystal structures of the PsbS protein essential for photoprotection in plants. Nat Struct Mol Biol. 2015;22(9):729–735.

[71] Li XP, Gilmore AM, Caffarri S, Bassi R, Golan T, Kramer D, et al. Regulation of photosynthetic light harvesting involves intrathylakoid lumen pH sensing by the PsbS protein. J Biol Chem. 2004;279(22):22866–22874.

[72] Betterle N, Ballottari M, Zorzan S, de Bianchi S, Cazzaniga S, Dall'osto L, et al. Light-induced dissociation of an antenna hetero-oligomer is needed for non-photochemical quenching induction. J Biol Chem. 2009;284(22):15255–15266.

[73] Goral TK, Johnson MP, Duffy CD, Brain AP, Ruban AV, Mullineaux CW. Light-harvesting antenna composition controls the macrostructure and dynamics of thylakoid membranes in Arabidopsis. Plant J. 2012;69(2):289–301.

[74] Teardo E, de Laureto PP, Bergantino E, Dalla Vecchia F, Rigoni F, Szabo I, et al. Evidences for interaction of PsbS with photosynthetic complexes in maize thylakoids. Biochim Biophys Acta. 2007;1767(6):703–711.

[75] Bergantino E, Segalla A, Brunetta A, Teardo E, Rigoni F, Giacometti GM, et al. Light- and pH-dependent structural changes in the PsbS subunit of photosystem II. Proc Natl Acad Sci U S A. 2003;100(25):15265–15270.

[76] Johnson MP, Ruban AV. Restoration of rapidly reversible photoprotective energy dissipation in the absence of PsbS protein by enhanced Deltap H. J Biol Chem. 2011;286(22):19973–19981.

[77] Bonente G, Ballottari M, Truong TB, Morosinotto T, Ahn TK, Fleming GR, et al. Analysis of LhcSR3, a protein essential for feedback de-excitation in the green alga Chlamydomonas reinhardtii. PLoS Biol. 2011;9(1):e1000577.

[78] Allorent G, Tokutsu R, Roach T, Peers G, Cardol P, Girard-Bascou J, et al. A dual strategy to cope with high light in Chlamydomonas reinhardtii. Plant Cell. 2013;25(2): 545–557.

[79] Elrad D, Niyogi KK, Grossman AR. A major light-harvesting polypeptide of photosystem II functions in thermal dissipation. Plant Cell. 2002;14(8):1801–1816.

[80] Ferrante P, Ballottari M, Bonente G, Giuliano G, Bassi R. LHCBM1 and LHCBM2/7 polypeptides, components of major LHCII complex, have distinct functional roles in photosynthetic antenna system of Chlamydomonas reinhardtii. J Biol Chem. 2012;287(20):16276–16288.

[81] Amarnath K, Zaks J, Park SD, Niyogi KK, Fleming GR. Fluorescence lifetime snapshots reveal two rapidly reversible mechanisms of photoprotection in live cells of Chlamydomonas reinhardtii. Proc Natl Acad Sci U S A. 2012;109(22):8405–8410.

[82] Alboresi A, Gerotto C, Giacometti GM, Bassi R, Morosinotto T. Physcomitrella patens mutants affected on heat dissipation clarify the evolution of photoprotection mechanisms upon land colonization. Proc Natl Acad Sci U S A. 2010;107(24):11128–11133.

[83] Gerotto C, Alboresi A, Giacometti GM, Bassi R, Morosinotto T. Coexistence of plant and algal energy dissipation mechanisms in the moss Physcomitrella patens. New Phytol. 2012;196(3):763–773.

[84] Gerotto C, Alboresi A, Giacometti GM, Bassi R, Morosinotto T. Role of PSBS and LHCSR in Physcomitrella patens acclimation to high light and low temperature. Plant Cell Environ. 2011;34(6):922–932.

[85] Geider RJ, Delucia EH, Falkowski PG, Finzi J. Primary productivity of planet earth: biological determinants and physical constraints in terrestrial and aquatic habitats. Global Change Biol. 2001;7:849–882.

[86] Keeling PJ. The number, speed, and impact of plastid endosymbioses in eukaryotic evolution. Annu Rev Plant Biol. 2013;64:583–607.

[87] Goss R, Lepetit B. Biodiversity of NPQ. J Plant Physiol. 2015;172:13–32.

[88] Bailleul B, Rogato A, de Martino A, Coesel S, Cardol P, Bowler C, et al. An atypical member of the light-harvesting complex stress-related protein family modulates diatom responses to light. Proc Natl Acad Sci U S A. 2010;107(42):18214–18219.

[89] Allen JF. Cyclic, pseudocyclic and noncyclic photophosphoryaltion: new links in the chain. Trends Plant Sci. 2003;8:15–19.

[90] Bailleul B, Berne N, Murik O, Petroutsos D, Prihoda J, Tanaka A, et al. Energetic coupling between plastids and mitochondria drives CO2 assimilation in diatoms. Nature. 2015;524(7565):366–369.

[91] Nixon PJ, Michoux F, Yu J, Boehm M, Komenda J. Recent advances in understanding the assembly and repair of photosystem II. Ann Bot. 2010;106(1):1–16.

[92] Aro EM, Virgin I, Andersson B. Photoinhibition of photosystem II. Inactivation, protein damage and turnover. Biochim Biophys Acta. 1993;1143(2):113–134.

[93] Puthiyaveetil S, Tsabari O, Lowry T, Lenhert S, Lewis RR, Reich Z, et al. Compartmentalization of the protein repair machinery in photosynthetic membranes. Proc Natl Acad Sci U S A. 2014;111(44):15839–15844.

[94] Vainonen JP, Hansson M, Vener AV. STN8 protein kinase in Arabidopsis thaliana is specific in phosphorylation of photosystem II core proteins. J Biol Chem. 2005;280(39): 33679–33686. Epub 2005 Jul 22.

[95] Bonardi V, Pesaresi P, Becker T, Schleiff E, Wagner R, Pfannschmidt T, et al. Photosystem II core phosphorylation and photosynthetic acclimation require two different protein kinases. Nature. 2005;437(7062):1179–1182.

[96] Tikkanen M, Nurmi M, Kangasjarvi S, Aro EM. Core protein phosphorylation facilitates the repair of photodamaged photosystem II at high light. Biochim Biophys Acta. 2008;1777(11):1432–1437.

[97] Herbstova M, Tietz S, Kinzel C, Turkina MV, Kirchhoff H. Architectural switch in plant photosynthetic membranes induced by light stress. Proc Natl Acad Sci U S A. 2012;109(49):20130–20135.

[98] Nixon PJ, Barker M, Boehm M, de Vries R, Komenda J. FtsH-mediated repair of the photosystem II complex in response to light stress. J Exp Bot. 2005;56(411):357–363.

[99] Barber.J Influence of surface charges on thylakoid structure and function. Annu Rev Plant Physiol. 1982;33:261–295.

[100] Merchant S, Bogorad L. Metal ion regulated gene expression: use of a plastocyanin-less mutant of Chlamydomonas reinhardtii to study the Cu(II)-dependent expression of cytochrome c-552. EMBO J. 1987;6(9):2531–2535.

[101] Moseley JL, Allinger T, Herzog S, Hoerth P, Wehinger E, Merchant S, et al. Adaptation to Fe-deficiency requires remodeling of the photosynthetic apparatus. Embo J. 2002;21(24):6709–6720.

[102] Tottey S, Block MA, Allen M, Westergren T, Albrieux C, Scheller HV, et al. Arabidopsis CHL27, located in both envelope and thylakoid membranes, is required for the synthesis of protochlorophyllide. Proc Natl Acad Sci U S A. 2003;100(26):16119–16124.

[103] Moseley J, Quinn J, Eriksson M, Merchant S. The Crd1 gene encodes a putative di-iron enzyme required for photosystem I accumulation in copper deficiency and hypoxia in Chlamydomonas reinhardtii. EMBO J. 2000;19(10):2139–2151.

[104] Farah J, Rappaport F, Choquet Y, Joliot P, Rochaix JD. Isolation of a psaF-deficient mutant of Chlamydomonas reinhardtii: efficient interaction of plastocyanin with the photosystem I reaction center is mediated by the PsaF subunit. Embo J. 1995;14(20): 4976–4984.

[105] Cardol P, Bailleul B, Rappaport F, Derelle E, Beal D, Breyton C, et al. An original adaptation of photosynthesis in the marine green alga Ostreococcus. Proc Natl Acad Sci U S A. 2008;105(22):7881–7886.

[106] Eberhard S, Finazzi G, Wollman FA. The dynamics of photosynthesis. Annu Rev Genet. 2008;42:463–515.

[107] Lefebvre-Legendre L, Choquet Y, Kuras R, Loubery S, Douchi D, Goldschmidt-Clermont M. A nucleus-encoded chloroplast protein regulated by iron availability governs expression of the photosystem I subunit PsaA in Chlamydomonas reinhardtii. Plant Physiol. 2015;167(4):1527–1540.

[108] Douchi D, Qu Y, Longoni P, Legendre-Lefebvre L, Johnson X, Schmitz-Linneweber C, et al. A nucleus-encoded chloroplast phsphoprotein governs expression of the photosystem I subunit PsaC in C. reinhardtii. Plant Cell. 2016;under revision.

[109] Boulouis A, Raynaud C, Bujaldon S, Aznar A, Wollman FA, Choquet Y. The nucleus-encoded trans-acting factor MCA1 plays a critical role in the regulation of cytochrome f synthesis in Chlamydomonas chloroplasts. Plant Cell. 2011;23(1):333–349.

[110] Raynaud C, Loiselay C, Wostrikoff K, Kuras R, Girard-Bascou J, Wollman FA, et al. Evidence for regulatory function of nucleus-encoded factors on mRNA stabilization and translation in the chloroplast. Proc Natl Acad Sci U S A. 2007;104(21):9093–9098.

[111] Wei L, Derrien B, Gautier A, Houille-Vernes L, Boulouis A, Saint-Marcoux D, et al. Nitric oxide-triggered remodeling of chloroplast bioenergetics and thylakoid proteins upon nitrogen starvation in Chlamydomonas reinhardtii. Plant Cell. 2014;26(1):353–372.

[112] Gfeller RP, Gibbs M. Fermentative metabolism of Chlamydomonas reinhardtii: I. Analysis of fermentative products from starch in dark and light. Plant Physiol. 1984;75(1):212–218.

[113] Gfeller RP, Gibbs M. Fermentative metabolism of Chlamydomonas reinhardtii: II. Role of Plastoquinone. Plant Physiol. 1985;77(2):509–511.

[114] Grossman AR, Catalanotti C, Yang W, Dubini A, Magneschi L, Subramanian V, et al. Multilple facets of anoxic metabolism and hyrogen production in the unicellular green alga Chlamydomonas reinhardtii. New Phytologist. 2010;doi: 10.1111/j. 1469-8137.2010.03534.x.

[115] Yildiz FH, Davies JP, Grossman AR. Characterization of sulfate transport in Chlamydomonas reinhardtii during sulfur-limited and sulfur-sufficient growth. Plant Physiol. 1994;104(3):981–987.

[116] Davies JP, Yildiz F, Grossman AR. Mutants of Chlamydomonas with aberrant responses to sulfur deprivation. Plant Cell. 1994;6(1):53–63.

[117] Wykoff DD, Davies JP, Melis A, Grossman AR. The regulation of photosynthetic electron transport during nutrient deprivation in Chlamydomonas reinhardtii. Plant Physiol. 1998;117(1):129–139.

[118] Melis A, Zhang L, Forestier M, Ghirardi ML, Seibert M. Sustained photobiological hydrogen gas production upon reversible inactivation of oxygen evolution in the green alga Chlamydomonas reinhardtii. Plant Physiol. 2000;122(1):127–136.

[119] Woodson JD, Chory J. Organelle signaling: how stressed chloroplasts communicate with the nucleus. Curr Biol. 2012;22(17):R690–R692.

[120] Johanningmeier U, Howell SH. Regulation of light-harvesting chlorophyll-binding protein mRNA accumulation in Chlamydomonas reinhardi. Possible involvement of chlorophyll synthesis precursors. J Biol Chem. 1984;259(21):13541–13549.

[121] Strand A, Asami T, Alonso J, Ecker JR, Chory J. Chloroplast to nucleus communication triggered by accumulation of Mg-protoporphyrin IX. Nature. 2003;421(6918):79–83.

[122] Mochizuki N, Tanaka R, Tanaka A, Masuda T, Nagatani A. The steady-state level of Mg-protoporphyrin IX is not a determinant of plastid-to-nucleus signaling in Arabidopsis. Proc Natl Acad Sci U S A. 2008;105(39):15184–15189. Epub 2008 Sep 25.

[123] Moulin M, McCormac AC, Terry MJ, Smith AG. Tetrapyrrole profiling in Arabidopsis seedlings reveals that retrograde plastid nuclear signaling is not due to Mg-protoporphyrin IX accumulation. Proc Natl Acad Sci U S A. 2008;105(39):15178–15183. Epub 2008 Sep 25.

[124] Kropat J, Oster U, Rudiger W, Beck CF. Chlorophyll precursors are signals of chloroplast origin involved in light induction of nuclear heat-shock genes. Proc Natl Acad Sci U S A. 1997;94(25):14168–14172.

[125] Kropat J, Oster U, Rudiger W, Beck CF. Chloroplast signalling in the light induction of nuclear HSP70 genes requires the accumulation of chlorophyll precursors and their accessibility to cytoplasm/nucleus. Plant J. 2000;24(4):523–531.

[126] von Gromoff ED, Alawady A, Meinecke L,Grimm B, Beck CF. Heme, a plastid-derived regulator of nuclear gene expression in Chlamydomonas. Plant Cell. 2008;20(3):552–567.

[127] Voss B, Meinecke L,Kurz T, Al-Babili S, Beck CF, Hess WR. Hemin and magnesium-protoporphyrin IX induce global changes in gene expression in Chlamydomonas reinhardtii. Plant Physiol. 2011;155(2):892–905.

[128] Meskauskiene R, Nater M, Goslings D, Kessler F, op den Camp R, Apel K. FLU: a negative regulator of chlorophyll biosynthesis in Arabidopsis thaliana. Proc Natl Acad Sci U S A. 2001;98(22):12826–12831.

[129] Falciatore A, Merendino L,Barneche F, Ceol M, Meskauskiene R, Apel K, et al. The FLP proteins act as regulators of chlorophyll synthesis in response to light and plastid signals in Chlamydomonas. Genes & Development. 2005;19(1):176–187.

[130] Rochaix JD. Surprising roles for bilins in a green alga. Proc Natl Acad Sci U S A. 2013;110(9):3218–3219.

[131] Duanmu D, Casero D, Dent RM, Gallaher S, Yang W, Rockwell NC, et al. Retrograde bilin signaling enables Chlamydomonas greening and phototrophic survival. Proc Natl Acad Sci U S A. 2013;110(9):3621–3626.

[132] Kobayashi Y, Imamura S, Hanaoka M, Tanaka K. A tetrapyrrole-regulated ubiquitin ligase controls algal nuclear DNA replication. Nat Cell Biol. 2011;13(4):483–487.

[133] Kobayashi Y, Kanesaki Y, Tanaka A, Kuroiwa H, Kuroiwa T, Tanaka K. Tetrapyrrole signal as a cell-cycle coordinator from organelle to nuclear DNA replication in plant cells. Proc Natl Acad Sci U S A. 2009;106(3):803–807.

[134] Tanaka K, Hanaoka M. The early days of plastid retrograde signaling with respect to replication and transcription. Frontiers in Plant Science. 2012;3:301.

[135] Pfannschmidt T, Nilsson A, Tullberg A, Link G, Allen JF. Direct transcriptional control of the chloroplast genes psbA and psaAB adjusts photosynthesis to light energy distribution in plants. IUBMB Life. 1999;48(3):271–276.

[136] Escoubas JM, Lomas M, LaRoche J, Falkowski PG. Light intensity regulation of cab gene transcription is signaled by the redox state of the plastoquinone pool. Proc Natl Acad Sci U S A. 1995;92(22):10237–10241.

[137] Brautigam K, Dietzel L,Kleine T, Stroher E, Wormuth D, Dietz KJ, et al. Dynamic plastid redox signals integrate gene expression and metabolism to induce distinct metabolic states in photosynthetic acclimation in Arabidopsis. Plant Cell. 2009;21(9):2715–2732.

[138] Mitra M, Kirst H, Dewez D, Melis A. Modulation of the light-harvesting chlorophyll antenna size in Chlamydomonas reinhardtii by TLA1 gene over-expression and RNA interference. Philos Trans R Soc Lond B Biol Sci. 2012;367(1608):3430–3443.

[139] Kirst H, Garcia-Cerdan JG, Zurbriggen A, Melis A. Assembly of the light-harvesting chlorophyll antenna in the green alga Chlamydomonas reinhardtii requires expression of the TLA2-CpFTSY gene. Plant Physiol. 2012;158(2):930–945.

[140] Kirst H, Garcia-Cerdan JG, Zurbriggen A, Ruehle T, Melis A. Truncated photosystem chlorophyll antenna size in the green microalga Chlamydomonas reinhardtii upon deletion of the TLA3-CpSRP43 gene. Plant Physiol. 2012;160(4):2251–2260.

[141] Wobbe L, Blifernez O, Schwarz C, Mussgnug JH, Nickelsen J, Kruse O. Cysteine modification of a specific repressor protein controls the translational status of nucleus-

encoded LHCII mRNAs in Chlamydomonas. Proc Natl Acad Sci U S A. 2009;106(32): 13290–13295.

[142] Blifernez O, Wobbe L, Niehaus K, Kruse O. Protein arginine methylation modulates light-harvesting antenna translation in Chlamydomonas reinhardtii. Plant J. 2011;65(1): 119–130.

[143] Frommolt R, Werner S, Paulsen H, Goss R, Wilhelm C, Zauner S, et al. Ancient recruitment by chromists of green algal genes encoding enzymes for carotenoid biosynthesis. Mol Biol Evol. 2008;25:2653–2667.

[144] Moustafa A, Beszteri B, Maier UG, Bowler C, Valentin K, Bhattacharya D. Genomic footprints of a cryptic plastid endosymbiosis in diatoms. Science. 2009;324(5935):1724–1726.

Chapter 3

Photosynthesis in Global Cycle of Biospheric Carbon

A.A. Ivlev

Additional information is available at the end of the chapter

http://dx.doi.org/10.5772/62222

Abstract

A key role of photosynthesis as a regulator of global carbon cycle dynamics is considered. According to the suggested model, global natural carbon cycle is regarded as a transition of carbon from the oxidative state, presented by carbon dioxide, bicarbonate, and carbonate species, into the reduced state, presented by different biogenic forms, produced in photosynthesis and in the following transformations. Photosynthesis provides a conversion of oxidative forms into reductive ones. The reverse transition is realized via respiration of living organisms, via microbial and chemical oxidations, accompanying transformations of "living" matter after burial. Among them the oxidation of the buried organic carbon by means of thermochemical sulfate reduction in the subduction zone, where lithospheric plates collide, is most important. Photosynthesis is under the impact of the Earth crust processes. In particular, the lithospheric plates' movement exerts the impact on photosynthesis development via periodic injections of CO_2 into "atmosphere–hydrosphere" system during the plates' collisions. The irregular lithospheric plates' movement generates orogenic cycles which consist of short-term orogenic period of active volcanism, magmatism, and mountain building and a long-term geosynclynal period of low volcanic activity and quiet development of Earth crust processes. The pulsating movement of plates affects the dynamics and development of photosynthesis, which in turn determines the periodicity of numerous processes in the nature, including climatic cycles, changes in the rate of biodiversity, irregular accumulation of organic matter in sediments, uneven stratigraphic oil distribution, sea level changes, etc. The redox carbon cycle is a self-organizing system due to negative feedback between CO_2 assimilation and photorespiration of global photosynthesis in response to oxygen growth. It made carbon cycle to shift to ecological compensation point. In this point, the system becomes sensitive to separate plates' collisions that results in short-term climatic oscillations.

Keywords: photosynthesis, CO_2 assimilation, photorespiration, "greenhouse" and "icehouse" periods, biodiversity, global carbon cycle, plate tectonics, orogenic and geosynclynal periods of orogenic cycle, sedimentary carbonates, burial organic carbon

1. Introduction

Here we concentrate one's attention on the unusual role of photosynthesis as a regulator of global carbon cycle dynamics. It stems from a new model of global natural carbon cycle which, despite the popular point of view, regards carbon turnover not only as a simple transfer of the element between different geospheres and biospheres but also as a transition of carbon from the oxidative state, presented by carbon dioxide, bicarbonate, and carbonate species, into the reduced state, presented by different biogenic forms, produced in photosynthesis and in subsequent transformations. That is why we named natural carbon turnover like a redox cycle of biospheric carbon. It has two branches – oxidative and reductive (Figure 1). The transition from oxidative species into reductive ones occurs by means of photosynthesis. The reverse transition is realized via respiration of living organisms, via microbial and chemical oxidations, accompanying transformations of "living" matter after burial. Among them, there is an oxidation of the buried organic carbon by means of thermochemical sulfate reduction occurring in the subduction zone, where lithospheric plates collide. This process is a dominant contributor to the oxidative branch of cycle.

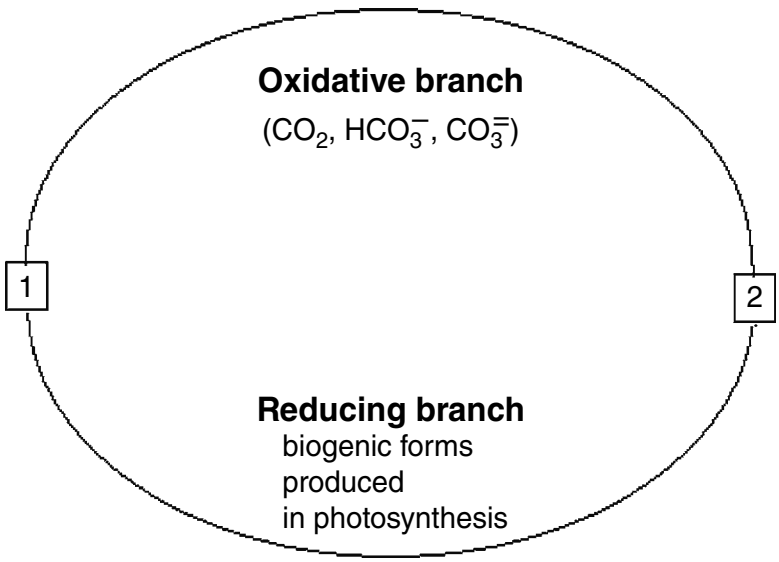

Figure 1. Putative global carbon cycle in nature. Oxidative and reductive branches. The points of carbon transition from the oxidative states to the reduced ones (in photosynthesis) and back (in sulfate reduction in subduction zone).

http://dx.doi.org/10.5772/62222

As early as 1926, a famous Russian geochemist V.I. Vernadsky put forward an idea on the interaction of biospheric and Earth crust processes [1]. This interpretation is as follows: photosynthesis developed under the impact of lithospheric plates' movement. The impact of lithospheric plates' movement on photosynthesis is transmitted via injections of CO_2 arising in plate collisions with the participation of continental plates. In the course of these collisions under high temperatures arising in subduction zones, thermochemical sulfate reduction occurs resulting in the oxidation of sedimentary organic carbon. In the suggested scheme, the lithospheric plates' movement is an experimentally established fact, but the reason causing the movement is still arbitrary. A widespread hypothesis is that the movement results from magma convective motion which makes plates, covering magma surface, to move.

The carbon cycle spans different geospheres: atmosphere, hydrosphere, upper part of lithosphere, and biosphere. Prior to the origin of photosynthesis, the atmosphere was anoxic [2, 3], and the reduced carbon was mainly methane formed by archaebacteria [4]. The redox carbon cycle changed in parallel with the expansion of photosynthesis destroying most of the methane in the atmosphere. As photosynthesis expanded, oxygen concentration in the atmosphere reached such a high level, at which its concentration stabilized. At this point, the oscillatory regime was established, and the perturbations of carbon cycle in the form of short-term (tens of thousands years) "cooling–warming" transitions have appeared, expressed as the glacial–interglacial oscillations. Carbon cycle characteristics became sensitive to separate plates' collisions and to other factors.

In this study, the author uses the previously proven claim that photosynthesis is accompanied by two photosynthetic carbon isotope effects in CO_2 assimilation and in photorespiration having opposite signs [5]. It gave him the opportunity, basing on the actualism principle, to use the differences in carbon isotope composition of sedimentary organic matter and that of coeval carbonates, as a delicate tool to investigate ^{13}C isotope discrimination in the past. It was used, in turn, to trace the climatic changes, the changes in the rate of biodiversity, to explain irregular accumulation of organic matter in sediments, uneven stratigraphic oil distribution, and many other phenomena.

2. Two geological concepts supporting natural redox carbon cycle hypothesis. The suggested mechanism of the cycle functioning

Two known geological concepts form the basis for the natural redox carbon cycle hypothesis. They are plate tectonics and orogenic cycles. The plate tectonics concept [6–8], or mobilism theory, asserts that the lithospheric plates, covering the entire Earth's surface, are in permanent motion. The motion is believed to occur due to convection of magma in the asthenosphere. Some researchers think that magma convection is a result of the impact of celestial bodies with the Earth's motion around the Sun [9]. Though the plate motion is an experimental fact, the real reason for the motion is still arbitrary. The motion is similar to the movement of an escalator. In some places of the Earth, in the zone of the mid-Atlantic ridge, where the crust is most subtle, magma erupts onto the surface and, coming into the contact with ocean water,

hardens to form a new plate. It pushes other plates, causing their movement. In other places of the Earth (Wadati-Benioff–Zavaritsky zone) the plates, moving toward each other, collide. One of them, bending and moving down under the other, is absorbed by magma. The area where the collisions occur is called the subduction zone.

The orogenic cycle's concept was developed, in particular, by Rutten [2]. He studied the spatiotemporal distribution of sedimentary strata and concluded that the intensity of geological processes on the Earth over its geological history was unequal. There were relatively short periods, named orogenic periods, and the subsequent relatively extended periods of quiet development of the crust, named geosynclynal periods. The geosynclynal and the orogenic periods both constitute the orogenic cycle. According to Rutten's estimate, the duration of orogenic periods is about 50 million years, while that of geosynclynal periods amounts to several hundreds of millions years (up to 500 million years).

Orogenic periods are characterized by intensive mountain buildup and active volcanism, accompanied by volcanic eruptions and the entry of large masses of igneous rocks onto the Earth's surface. Geosynclynal periods correspond to the time of quiet Earth crust development and slow volcanic activity. It is the time for the accumulation of sediments and photosynthesis.

I took from Rutten his idea on orogenic cycle, and from the plate tectonic concept, I adopted the idea about plates' movement and plates' collisions. Combining both ideas and assuming that plates' movement was uneven, I have developed the following model.

In orogenic periods of the cycle, plates move rapidly and their collisions are frequent. Great quantities of volatile products, including CO_2 and H_2S, go onto the Earth surface from the subduction zone. In geosynclynal periods, the plates move slowly and the collisions are rare. Photosynthesis and weathering become the dominant processes. The collisions with the participation of the continental plates, bearing the sedimentary rocks with carbon in the form of carbonates and organic matter, are most interesting from the point of view of the natural redox carbon cycle.

During its life span, a continental plate accumulates sedimentary rocks with the buried organic matter and carbonates. When a plate descends and reaches the subduction zone, the rocks under high temperatures and great pressures are destroyed, but before they are absorbed by magma, the following reactions occur:

$$\begin{aligned} &MeCO_3 + SiO_2 \rightarrow MeSiO_3 + CO_2 \\ &MeCO_3 \rightarrow MeO + CO_2 \end{aligned} \quad (1)$$

"Me" designates Ca^{2+} or Mg^{2+} cations.

These transformations do not change the redox state of carbon, and carbon transfer can be considered as a constant increment of the oxidative pool which does not affect carbon turnover.

The burial of organic matter and its transformation represent a different case. In thermochemical sulfate reduction, the organic matter reacts with evaporated sulfates according to the equation:

http://dx.doi.org/10.5772/62222

$$SO_4^{2-} + 2(CH_2O) \Leftrightarrow 2CO_2 + 2H_2O + S^{2-} \quad (2)$$

The resultant CO_2, together with sulfides, is transferred from the subduction zones onto the Earth surface. This final step of oxidation completes the transfer of the reduced carbon into the oxidative forms. The above processes occur in the orogenic period.

On the Earth surface, due to chemical exchange reactions and in accordance with thermodynamics laws, CO_2 is redistributed in the atmosphere and hydrosphere, composing the common "carbon dioxide–bicarbonate–carbonate" system:

$$CO_2(\text{gas}) \Leftrightarrow CO_2(\text{dissolved}) \Leftrightarrow H_2CO_3 \Leftrightarrow HCO_3^- \Leftrightarrow CO_3^{2-} \quad (3)$$

This system is close to equilibrium since the rate of chemical exchange is much greater than the rate of geological processes. The observed differences in carbon isotope composition of the atmospheric CO_2 ($\delta^{13}C \approx -7‰$) and of the carbonate species dissolved in seawater ($\delta^{13}C \approx 0‰$) evidence for the state close to equilibrium. In fact, the difference is about 5–7 ‰ [10, 11], corresponding to the thermodynamic (equilibrium) values of isotope separation coefficients $\alpha(CO_2/CO_3^{2-})$ and $\alpha(CO_2/HCO_3^-)$, which are equal to 1.005–1.008 [10, 12, 13] and typical to Earth surface temperatures (0–30°C).

Under the action of sunlight, photosynthesizing organisms absorb CO_2 and water and convert the oxidized forms of carbon into the reduced ones, producing "living matter." After the conversion of the buried "living matter" into the sedimentary organic matter, the latter undergoes oxidation. Then all the processes repeat. This sequence of transformations forms a close loop.

All the above are depicted in Figure 2. In orogenic periods, shown as filled triangles, CO_2 concentration in the system should increase abruptly because of frequent collisions of lithospheric plates when sedimentary rock masses fall in subduction zone and are destroyed with CO_2 evolution. The entry of CO_2 into the "atmosphere–hydrosphere" system leads to considerable growth of all oxidized carbon species in the system. Photosynthesis is stimulated by high CO_2 concentrations achievable in the orogenic period.

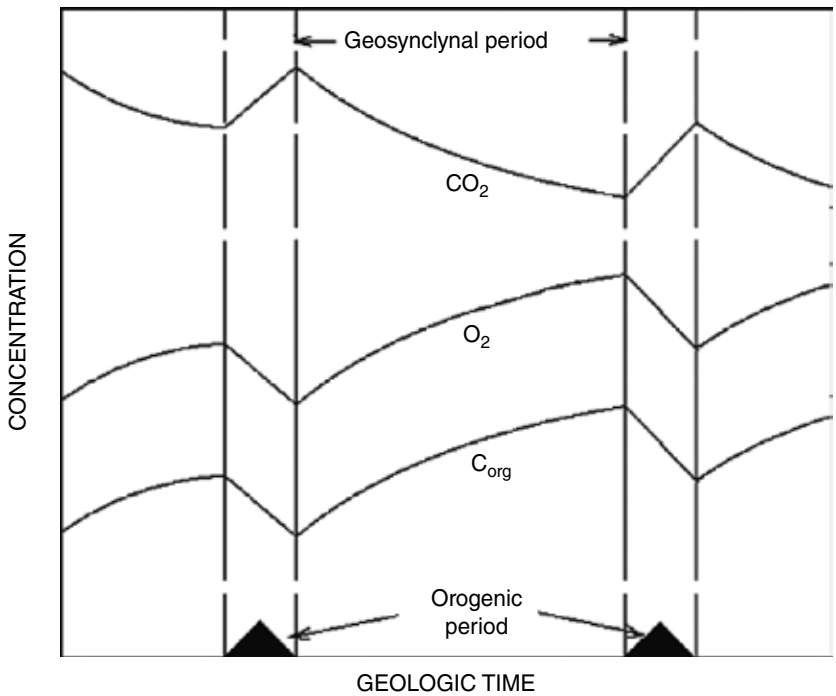

Figure 2. The scheme of the putative changes of CO_2 and O_2 in atmosphere and organic matter in sedimentary rocks in the course of orogenic cycles. Note that the variations of CO_2 and O_2 are in anti-phase, while the variations of O_2 and organic matter are in phase.

At the same time, the atmospheric O_2 concentration decreases since it is utilized in the oxidation of the reduced igneous rocks and reduced sulfur species, lifting from the subduction zones onto the Earth surface.

In the following relatively extended geosynclynal period, the rate of photosynthetic consumption of CO_2 becomes greater than its emission from the subduction zones. It results in the depletion of the oxidative pool of carbon in the "atmosphere–hydrosphere" system. Onthe contrary the O_2 concentration, due to photosynthesis, increases, achieving maximum concentration by the end of the geosynclynal period. The curve describing organic matter accumulation in sedimentary rocks in accordance with the global photosynthesis reaction $CO_2 + H_2O \xrightarrow{hv} CH_2O + O_2$ coincides with the curve of O_2 concentration, since the burial rate of organic matter changes in parallel with the growth of atmospheric oxygen concentration. Note that the atmospheric CO_2 appears as a substrate, while the oxygen and the assimilated organic matter (CH_2O in this approximation) are the products of the global photosynthesis reaction.

Thus the model claims the periodic filling/depletion of "atmosphere–hydrosphere" system with CO_2 and counter-phase parallel changes of O_2. Accordingly, the periodic strengthening of CO_2 assimilation and weakening of photorespiration should take place. In parallel with atmospheric O_2 concentration changes, the accumulation of organic matter occurs in sedi-

http://dx.doi.org/10.5772/62222

ments, since they are both the products of global photosynthesis. It means the periodic intensification of organic matter accumulation in sediments should take place.

Some important notes concerning carbon isotope fractionation in photosynthesis based on recent findings [5, 14] should be taken into account. The periodic depletion of carbon oxidative pool result in the appearance of carbon isotope Raleigh effect which affect the carbon isotope composition of sedimentary carbonates and organic matter displaying gradual ^{13}C enrichment with the extent of depletion. It allows examining orogenic cycles by means of the analysis of isotope composition of carbonate and organic carbon.

Following the actualism principle, one can take organic carbon as analog of "living" matter in the past, and coeval carbonates as analog of CO_2 , corresponding to that time. Then the isotopic difference between organic matter and carbonates should be regarded as analog of ^{13}C carbon isotope discrimination in modern plants. We denoted the above isotopic differences, after Popp et al. [15] and Hayes et al. [16] as ε parameter. If so, in the orogenic period and at the beginning of the geosynclynal period when the CO_2 concentration as well as the CO_2/O_2 concentration ratio in the environment are maximal, the ^{12}C enrichment of the organic carbon and ε parameter should be maximal too.

By the end of geosynclynal period, when the CO_2 and CO_2/O_2 concentration ratios are the lowest (photorespiration is maximal), the buried organic carbon should be the most enriched in ^{13}C (additional to Raleigh effect). Accordingly, the isotopic difference between organic matter and coeval carbonates should be minimal (Figure 3).

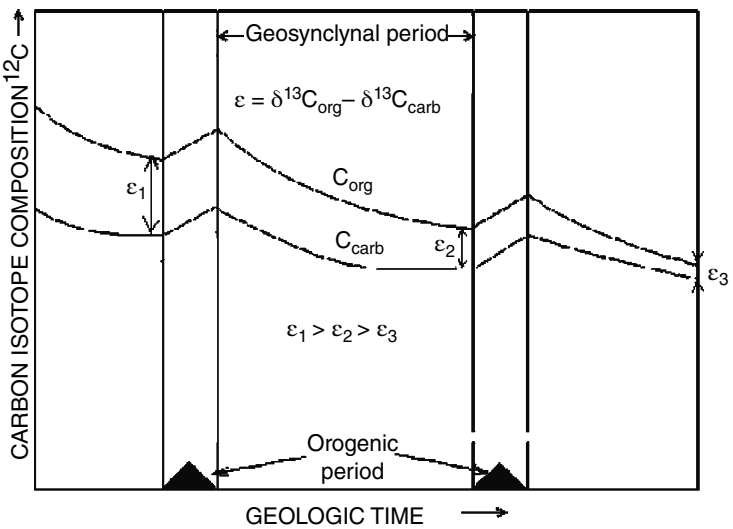

Figure 3. The scheme of putative changes of carbon isotope discrimination in photosynthesis ε in the course of geological time; ε is equal to carbon isotope difference between carbon isotope composition of sedimentary carbonates and coeval organic matter. The isotope discrimination decreases steadily with each subsequent cycle.

The validity of the assertion can be seen from the measurements of the buried organic and coeval carbonates of different age [16]. They revealed noticeable differences in ε parameter. In the Neoproterozoic era, from 1000 Ma to 541 Ma, the isotope discrimination was found to be greater than 32 ‰. In the period from Cambrian to Jurassic, ε changed to 28‰, and then in the period from Cretaceous to Late Cenozoic it was less than 28‰. They also noticed the successive growth of atmospheric O_2 concentration from the Neoproterozoic to Late Cenozoic.

Thus the isotope technique provides an immensely effective and delicate tool for the orogenic cycle studies. This claim is supported by the fact that isotope ratios of organic carbon and coeval carbonates are the main and widely used factual materials in common geological studies.

3. Isotope data support the idea on organic carbon oxidation in subduction zone during orogenic period

The oxidation of organic carbon in subduction zone coupled with sulfate reduction during orogenic period is one of the critical points of the model that requires proof. According to [17], the natural sulfur cycle, like the carbon cycle, consists of the oxidative (sulfate) and reductive (sulfide) branches. To substantiate the above assertion, let us address the data from the work of Mackenzie and Piggot [17]. Temporal curves in Figure 4 demonstrate synchronous isotopic variations of carbon and sulfur of marine carbonates and gypsum (sulfates) in time.

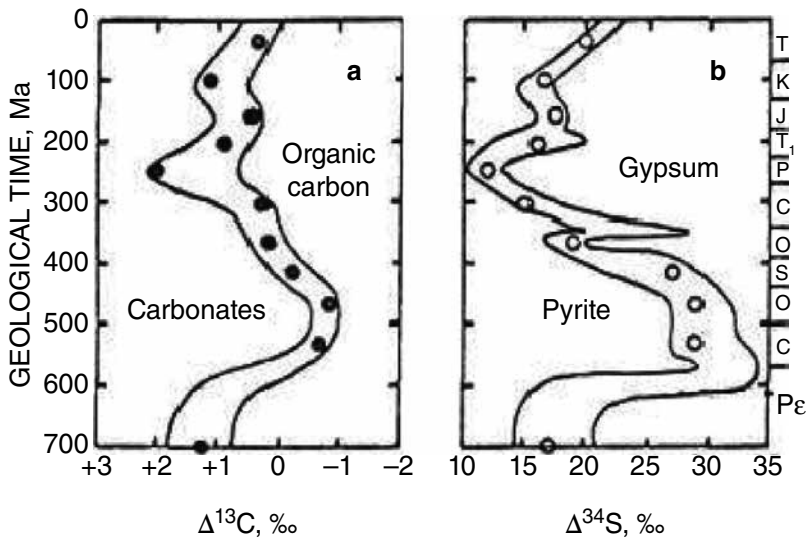

Figure 4. Coupling of global carbon and sulfur cycles. Synchronous variations of the curves of carbon isotope composition of carbonates (a) and sulfur isotope composition of sulfate sulfur in evaporates (b) for the last 700 million years in the geologic history of the Earth [17].

http://dx.doi.org/10.5772/62222

Such synchronism prompts itself that both cycles are somehow bound. Each curve has two differently directed humps. Next to them there are inscriptions, made by authors, to indicate minerals of sedimentary rocks that were mostly spread at the corresponding periods. Carbonates and pyrites correspond to the humps in lower parts of the curves. Organic matter and gypsum correspond to the humps in the upper part of the curves.

If we compare the above substances with the substrates and the products of sulfate reduction, it is easy to see that the substances corresponding to the lower humps on the curves coincide with the reaction products, and the substances corresponding to the upper humps on the curves coincide with the reaction substrates. The analysis of the isotopic changes of carbon and sulfur proves that the coincidence is not accidental.

By analyzing the dynamics of carbon and sulfur isotopic variations resulting from the curves on Figure 4, we should first note that the thermochemical sulfate reduction is followed by sulfur isotope fractionation [18, 19]. Then, due to the periodic character of the reaction, the substrate is depleted. The depletion is followed by Raleigh effect. The more the reaction proceeds and the more the substrate pool is depleted, the greater the residual substrate (gypsum) is enriched with a "heavy" sulfur isotope ^{34}S. As it follows from the analysis of the lower part of the curves, the enrichment of gypsum with ^{34}S is accompanied with the enrichment of carbonates with a "light" carbon isotope ^{12}C. Both traits evidence in favor of high extent of sulfate conversion. Indeed, in the case of high extent of sulfate conversion, another reaction product CO_2 should also be produced in a considerable amount. Thus the CO_2 inherits "light" carbon isotope composition from organic matter. Hence, when "light" CO_2 enters marine "carbon dioxide–carbonate" system with carbon enriched in ^{13}C, it makes carbon in the system "lighter" due to chemical isotope exchange.

A quite opposite scenario can be deduced from the analysis of the upper parts of the curves. The ^{32}S enrichment of gypsum evidences that the extent of sulfate conversion is low. Hence small amounts of "light" CO_2 are produced, and marine carbonates become "heavier" as compared with the previous case. Thus, the coupled isotopic changes of carbon and sulfur of marine carbonates and gypsum, in addition to chemical arguments, give firm proofs that they represent the results of sulfate reduction process occurring in the subduction zones.

An indirect argument in favor of sulfate reduction in subduction zone was the great abundance of sulfide-oxidizing bacteria in the Precambrian. It evidences for significant inflow of the reduced sulfur forms (sulfides and hydrogen sulfide) onto the Earth surface. This was favored by low oxygen concentration in the Earth's atmosphere at that time. The sulfide-oxidizing bacteria were so widely disseminated that gave grounds for Hayes et al. [16] to conclude that these bacteria were the main source of organic matter in rocks in the Proterozoic.

Thus, the coupled isotopic changes of carbon and sulfur of marine carbonates and gypsum, in addition to chemical and paleontological arguments, give firm proofs that they represent the results of sulfate reduction process occurring in the subduction zones.

4. The effect of redox carbon cycle on the climate in the past

The role of CO_2 in climate formation is a well-known fact. It is the main component of "greenhouse" gases [20]. The periodic filling of the "atmosphere–hydrosphere" system with CO_2 in orogenic time and the following depletion of CO_2 due to photosynthetic assimilation in geosynclynal period provide alternating warming–cooling change. It is even possible to use the relation between CO_2 concentrations and Earth temperature for the determination of paleotemperatures [21], although the validity of this correlation is limited due to the contribution of other greenhouse gases.

Following the logic of this model, the existence of climatic cycles is a result of the orogenic cycles. The beginning of the orogenic cycle may be considered as the warmest time of the cycle and the end as the coldest one. The latter is often accompanied with glaciations.

The mentioned ε parameter may be used as the indicator of orogenic and climatic cycles. At the beginning of the orogenic cycle, when CO_2/O_2 ratio is maximal and the contribution of photorespiration is low, ε parameter is also at its maximum and corresponds to the warming period. Conversely, at the end of the cycle, when CO_2/O_2 ratio is minimal and photorespiration increases, ε parameter reaches its minimum and corresponds to the cooling period.

Popp et al. [15] found a coherence of ε values and climatic cycles in the Cenozoic. Hayes and others [16], having examined carbon isotope composition for more than 5000 samples of coeval carbonates and sedimentary organic matter spanning the Precambrian and Phanerozoic, found statistically significant differences in ε values in interglacial periods and those in periods of glaciations. The results were supported by other researchers [22, 23].

5. The impact of redox carbon cycle on the rate of biodiversity

It is a known fact in geological history that in the past there were "explosions" of life and mass extinctions of living organisms. In some works, a periodicity in a rate of change of biodiversity (a rate of appearance of the new fauna and flora species per geological unit) in time was revealed [24]. Following the redox carbon cycle model, these facts can be reasonably explained. It was supposed that periodicity is caused by the increase of oxygen concentration in the Phanerozoic atmosphere [25]. The assumption was supported by a close coherence of the curves illustrating the time dependence of a rate of change of biodiversity and other parameters, strongly related with oxygen concentrations. The peaks of all curves fully coincided and corresponded to oxygen maximum (see Figure 7 from [25])

The physical sense of this link is quite clear. The elevated O_2 concentrations in the atmosphere stimulate (photo)respiration in photosynthesizing organisms, which is followed by superoxide radical formation. They attack gene molecules causing mutations. Though in a cell there are some enzymes, which destroy radicals reducing them to H_2O and O_2, at the time of oxygen growth, the enzymes fail to cope with the abundance of radicals and to diminish their amount to the safe level. As a result, mutations appear and the rate of change of biodiversity increases.

http://dx.doi.org/10.5772/62222

Rothman [26] found a good correlation of ε parameter and the rate of change of biodiversity for land plant families as well as for marine animals. His results prove the relation of orogenic cycles and biodiversity rate.

The observed periodicity of mass extinctions of plant and animal species on the Earth has a close agreement with the previous correlation. These events are also linked with a change of CO_2/O_2 ratio in the atmosphere over time [27]. According to the model, the abrupt change of CO_2/O_2 ratio in the atmosphere occurring in orogenic cycles' transitions should lead to the extinction events, because they are followed by the change of aerobic conditions to anoxic ones causing a mass extinction of aerobic organisms.

6. Irregular periodicity in organic carbon accumulation in sediments is the reason for uneven stratigraphic distribution of sediments rich in organic matter and oils

It stems from the model's logic that there should be uneven rate of organic matter accumulation in sediments as a result of CO_2 variations in the course of orogenic cycles. In the orogenic periods of the repeated cycles, the "atmosphere–hydrosphere" system of the Earth is filled with CO_2, coming from the subduction zone. In the subsequent geosynclynal periods, due to a dominant role of photosynthesis, the system is gradually depleted in the oxidized carbon species. It means that the photosynthesis rate is maximal at the beginning of the cycle and reaches its minimum by the end. The opposite scenario could be expected for organic matter accumulation in sediments. The maximum of organic matter accumulation should take place by the end of the cycle, when most of the CO_2, that entered the "atmosphere–hydrosphere" system in the orogenic period, after some transformation is converted into organic matter. As a result, the uneven stratigraphic distribution of sediments rich in organic matter appears. The other consequence of the uneven stratigraphic distribution is the irregular distribution of the oils generated by these sediments.

Though the kinetics of global photosynthesis and organic matter accumulation is unknown, we assumed that the mentioned kinetics is described by the simplest first-order equation. It corresponds to proportional, in-phase of O_2 and buried organic carbon variations (Figure 5), and anti-phase atmospheric CO_2 and O_2 variations (see Figure 1 from [25]). The corresponding curves, depicting the behavior of CO_2 and O_2 in the atmosphere and organic matter in sedimentary rocks obtained in climatic and depositional models, are in full agreement with the changes expected from the proposed carbon cycle model.

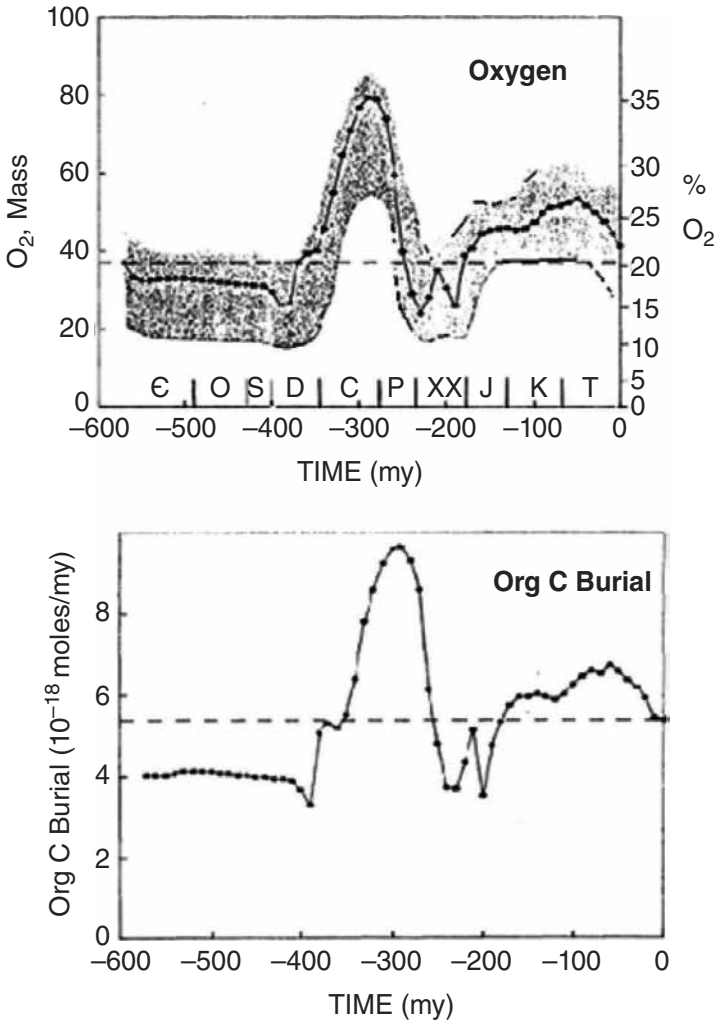

Figure 5. The in-phase changes of oxygen content in the atmosphere and burial organic matter rates in the sedimentary rocks in the Phanerozoic. The shaded zone for oxygen designates the zone of possible errors based on sensitivity analysis [29].

In fact, Bazhenova and Sokolov [28], examining the stratigraphic distribution of Domanic oil source rocks, revealed that these sediments rich in organic matter were present in different continents at the same stratigraphic levels. They are found practically in all systems of the Phanerozoic and of the Precambrian. The stratigraphic levels, where domanicoids were fixed, are Ediacaran–Cambrian, Devonian–Carboniferous, and Late Jurassic–Early Cretaceous. Such nonuniform stratigraphic distribution can be explained in the frames of the natural redox carbon cycle dynamics.

The formation of sediments rich in organic matter is likely bound to the transitions from one cycle to another when there was a change of aerobic conditions to anoxic causing mass

http://dx.doi.org/10.5772/62222

extinction of living organisms. Their biomass is a probable source of organic material. The repeatability of orogenic cycles determines the appearance of domanicoids at different stratigraphic levels in the Precambrian and the Phanerozoic.

Though the periods, indicated by Bazhenova and Sokolov [28], are rather conditional, they are known to include glacial periods. During the Ediacaran period, there were Varanger (660 to 635 Ma) and Gaskiers (590 to 575 Ma) glaciations; in Devonian, there was the Andean-Saharan (ca. 440 Ma) and then Permo-Carboniferous (320 Ma) glaciations; in Late Jurassic–Early Cretaceous period, traces of glaciations were not found with certainty, but there was a great extinction (66 Ma), which was caused by a bolide impact. Besides this, the indicated time was characterized by high oxygen concentration likely associated with glaciations and land life development. It should be stressed that Bazhenova and Sokolov [28] marked that periods of organic matter accumulation were followed by rifting process which in accordance with our model corresponds to the orogenic period, occurring behind the cooling time.

It is natural to consider that Domanic oil source rocks as well as other rocks rich in organic matter ("black" shales) are oil kitchen. Therefore, the periods of oil source rock – formation should be related to oil generation, and one could expect that the oil field discoveries are mostly related with this time with high probability. This assertion is supported by the available data. Figure 6 illustrates the stratigraphic distribution of the discovered oil fields in the world [30] and the distribution of oil fields in the former USSR [31]. The latter is presented as a ratio of number of oil fields for a given period to the total number of oil fields [Figure 6b]. As it can be seen, in both cases the distributions are very similar and irregular. Though the comparison is not very strict, Figure 6b, unlike Figure 6a, does not take into account the sizes of oil fields, nevertheless the comparison is still reasonable. The peaks in both distributions correspond to each other; the number of the peaks is the same. According to both distributions, the beginning of oil generation falls in time limits from 600 to 500 million years ago. This is in agreement with the considerable growth of oxygen concentration in the atmosphere. As it was noted, oxygen concentration is an indicator of organic matter accumulation in sediments. According to some data [32, 33], one can accept that in most of the Precambrian, oxygen concentration was less than 1%, and only by the end of the Precambrian it started to increase significantly [34]. It is logical to assume that photosynthesis needs a prolonged time to accumulate the amount of organic matter in sediments sufficient to produce hydrocarbons capable to form oil fields. One can follow it by tracing the O_2 concentration in the atmosphere.

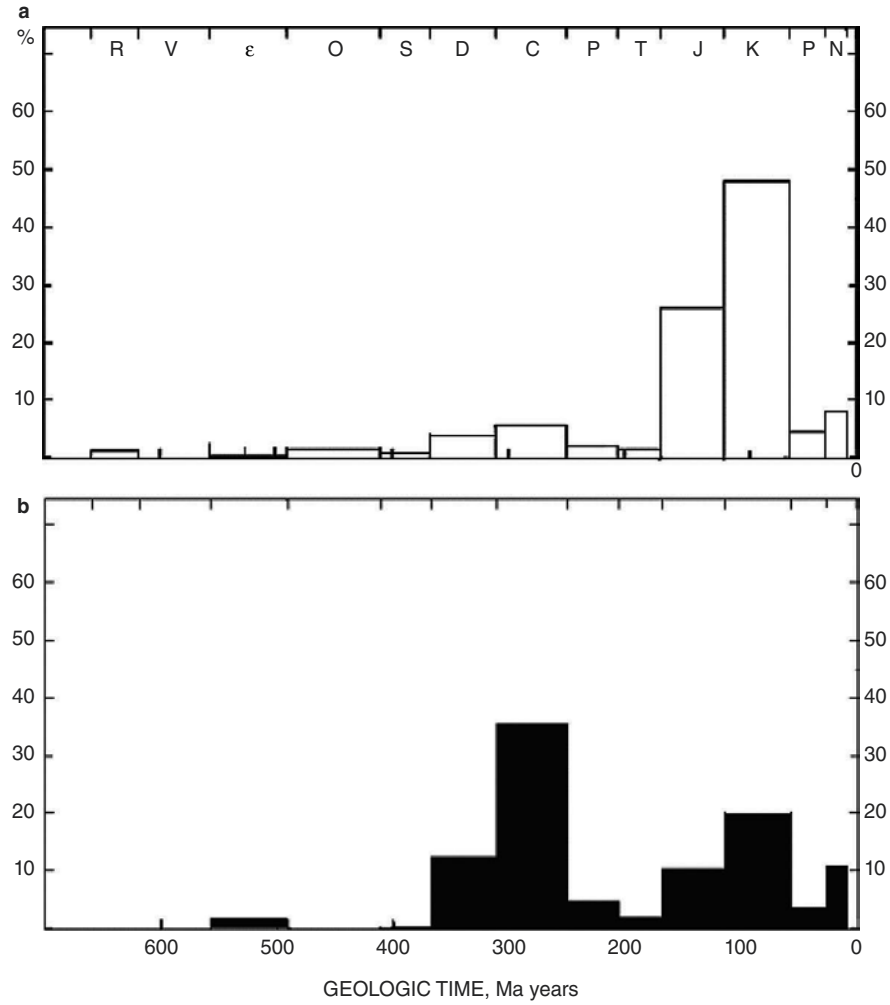

Figure 6. Comparison of distribution of explored extractable oil fields in the largest world reservoirs (Vishemirsky, Kontorovich, 1997) [30] (a) and revealed oil fields (% of the total number of oil fields) of the former USSR (Korchagin, 2001) [31] (b) with stratigraphic subdivisions.

7. ^{13}C enrichment of oils reflects O_2 growth in the atmosphere and display four orogenic cycles from the Cryogenian period of Neoproterozoic era to the Miocene epoch of Cenozoic era

Having examined the extensive collection of oils (504 oil samples) differing in age and origin, Andrusevich et al. [35, 36] established that in the course of geological time, the oils and their components have been consistently enriched in ^{13}C (Figure 7). Model's logic allows concluding that the most likely reason for this enrichment is the intensified photorespiration of photo-

http://dx.doi.org/10.5772/62222

synthesizing organisms as a result of the increase of average oxygen concentration in the atmosphere. One should take into account that, despite of variations, in the course of geological time; an average atmospheric oxygen concentration steadily grew up. The ^{13}C enrichment of oils reflects that at least four orogenic cycles took place, accompanied by an increase in average oxygen concentration in the atmosphere. Oils inherit the enrichment from organic matter. The existence of four orogenic cycles in Phanerozoic agrees with the other proofs (see the previous section), evidencing for four waves of oil generation in the Phanerozoic.

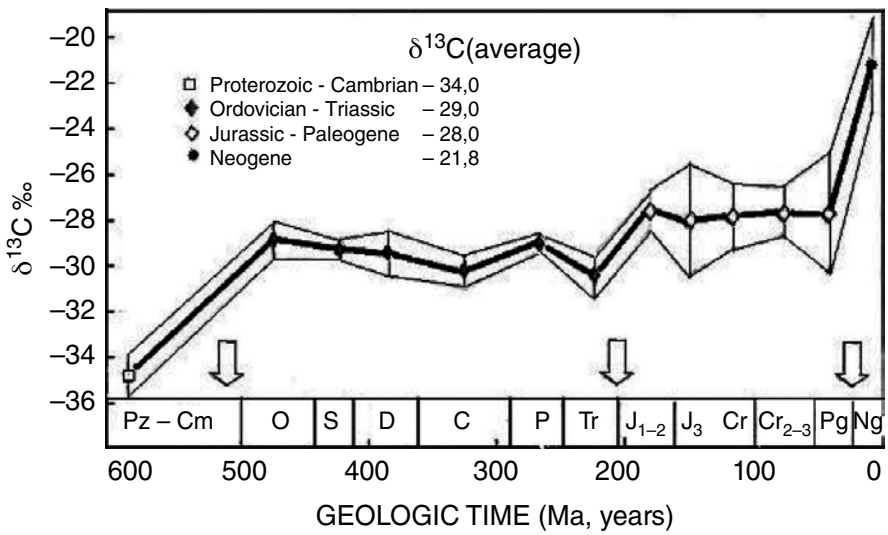

Figure 7. Change of the average carbon isotope composition ($\delta^{13}C$, ‰) for saturate fraction C_{15+} of crude oils. Vertical bars are standard deviations, which increase with decreasing age. Arrows indicate Cambrian–Ordovician, Triassic–Jurassic, and Paleogene– Neogene boundaries where ^{13}C enrichment occurs [36].

One more interesting observation indicating the validity of the model stems from the analysis of the above data. Since Jurassic, a scatter in carbon isotopic composition of oils has increased essentially. The variety of land photosynthesis conditions resulted in a wide spectra of $\delta^{13}C$ values.

8. Ecological compensation point

Global natural redox carbon cycle is a developing and self-organizing system. This feature is provided due to photosynthesis which is an essential part of the cycle. Its origin occurred in anoxic atmosphere. The photosynthesis evolution was followed by atmospheric oxygen growth. The literature data, given below, illustrate oxygen growth in the atmosphere over geological time. Atmospheric O_2 concentration prior to photosynthesis was determined by water dissociation under ultraviolet action and was equal to one thousandth part of the present oxygen level (Urey level). With the emergence of photosynthesis, the average oxygen concentration in the atmosphere began to increase from cycle to cycle.

The Early Archean oxygen concentration was up to 0.02–0.08% (Urey's level) (Rutten, 1971) [2]. From the Late Archean (3.0–2.7 Ga) to Middle Proterozoic (2.2–2.0 Ga) oxygen concentration reached 0.21% (Pasteur's level) [2, 32, 33]. In the Neoproterozoic (Tonian– Cryogenian–Ediacaran, 1000–550 Ma), oxygen concentration was estimated to be up to 5 %, reaching 8% in the end of Ediacaran [34]. In the Early Paleozoic (Cambrian, 541–485 Ma), according to different estimates, oxygen concentration was 12–13% [29, 37, 38]. In the Middle Paleozoic (Ordovician–Silurian, 485–420 Ma), oxygen concentration has been 13–15% [39]. In the Late Paleozoic (Carboniferous–Early Permian, 350–280 Ma), oxygen concentration reached about 30–35% [37, 38]. In the Early Mesozoic (Triassic) (250–200 Ma), oxygen concentration has reduced down to 15–17% [39, 40]. In the Miocene epoch of Neogene (23–5 Ma), oxygen content again increased to 25% level [41].

The oxygen growth is explained by photosynthesis expansion. In parallel, another product of global photosynthesis, "the living matter," transforming into "buried organic matter," was accumulated in sedimentary rocks. How long could it last? As free oxygen accumulated in the atmosphere, photosynthesizing organisms have acquired photorespiration which was in reciprocal relations with CO_2 uptake [42]. As known, carbon dioxide uptake increases biomass production, whereas photorespiration reduces it. As a result, photorespiration decreased the expansion of photosynthesis and brought down the accumulation of buried organic matter. Despite the absolute growth of buried organic matter in sediments, its relative input became lesser with each new orogenic cycle. The contribution of the above processes to metabolism depends on the CO_2/O_2 ratio in the environment. The latter ratio steadily grew down in the course of orogenic cycles. Thus photosynthesis performed a regulatory role in carbon cycle.

For individual photosynthesizing organisms of C_3-type, which were the first representatives of photosynthesizing life on the Earth, a term "compensation point" is applicable. It is a metabolic state of the organism at a particular concentration ratio of CO_2 and O_2 when CO_2 uptake becomes equal to CO_2 release. Below this point, the rate of photorespiration (together with respiration) exceeds the rate of photoassimilation, and the physiological existence of organisms becomes impossible. As CO_2 and O_2 are mutually related, the compensation point may be determined via consideration of either CO_2 or O_2 concentrations [43].

It was shown that the plants placed in a closed chamber due to reverse links (reciprocal relations) between main photosynthetic processes, CO_2 assimilation and photorespiration, make the CO_2/O_2 ratio in chamber atmosphere stable [43, 44]. Considering these results, Tolbert et al. [43] assumed that the same feedback mechanism acts in nature and is responsible for the achievement of stationary CO_2 and O_2 concentrations in the atmosphere. They introduced the term "ecological compensation point." The above processes are the driving forces in achieving the ecological compensation point. The numerous oxidation processes of the reductive branch, due to O_2 consumption and CO_2 evolution, play a regulatory role via common reaction intermediates, defining the real position (concentrations) of the ecological compensation point. In this position, the full conversion of the reduced carbon into the oxidized forms and back occurs. The total interaction of CO_2 assimilation and photorespiration provides the excess of reductive carbon over oxidative in period from photosynthesis origin up to the moment of achieving the ecological compensation point. The excess of the reduced carbon was accumu-

http://dx.doi.org/10.5772/62222

lated in deposits in the form of buried organic matter. The corresponding amount of oxygen was accumulated in the atmosphere.

The glacial–interglacial oscillations of CO_2 have emerged as a consequence of proximity of the system to the ecological compensation point [22,45–48]. This possibly happened in the end of Carboniferous when the great expansion of photosynthesis took place and covered the land [49]. The ecological compensation point was most likely achieved in the Neogene (Miocene). At this time, after some decline, there was a burst of atmospheric oxygen to the maximum level associated with global cooling. Right after cooling in the Miocene, there was considerable warming in the Pliocene period [50–52]. The warming was followed by mass extinction of organisms, and by the formation of sediments rich in organic matter. These sequences of climatic changes are characteristic of transitions from one orogenic cycle to another.

After achieving the ecological compensation point, global carbon cycle became very sensitive to separate plates' collisions, what is in agreement with short-term glacial–interglacial oscillations of CO_2. It allows assuming that long-term orogenic cycles and short-term oscillations have the same physical nature.

The most important conclusion from the existence of the ecological compensation point is the following. After the achievement of ecological compensation point, the system of global carbon cycle gets its stationary level. No additional accumulation of buried organic carbon occurs. It means no additional oil generation takes place, and hence the amount of oil in the Earth crust becomes stable and limited. Hence it should be concluded if the rate of oil production is greater than the rate of generation, oil resources should be exhausted with time.

9. Conclusions

New redox carbon cycle model is suggested. It claims a dominant role of photosynthesis in the mechanism of cycle functioning. According to the model, carbon transfer between geospheres and biosphere is accompanied by the changes in the redox state of carbon. Photosynthesis provides the transfer of carbon from the oxidative to the reduced state. The reverse transfer takes place in numerous processes of oxidation, including the respiration of living organisms and the processes of direct and indirect oxidation of buried organic matter. The final powerful oxidation of organic matter occurs in sulfate reduction proceeding in the subduction zones (plates' collisions zone).

Photosynthesis connects the Earth crust and biosphere processes. This link is realized by means of CO_2 pulses appearing in lithospheric plates' collisions when they move. The source of CO_2 is the oxidation of the buried organic matter in sulfate reduction in subduction zone. The last reaction is the coupling point of natural carbon and sulfur cycles.

Lithospheric plates' movement has two phases. In the short-term orogenic phase, the CO_2 coming from subduction zone fills the "atmosphere–hydrosphere" system, causing climate warming. In the long-term geosynclynal phase, weathering and photosynthesis become dominant processes, depleting the oxidative forms of carbon followed by glaciations. By this

way, photosynthesis transmits the impact of Earth crust processes on biosphere. The irregular periodicity exerts an impact on climate, biodiversity, distribution of organic matter in sedimentary deposits, etc.

Thus due to the unique combination of CO_2 assimilation and photorespiration, which are in reciprocal relations, photosynthesis plays a key regulatory role in the carbon cycle. During photosynthesis, the expansion of O_2 concentration in the environment permanently grew while that of CO_2 dropped. When they reached values limiting physiological boundaries of life, the changes ceased and the CO_2/O_2 ratio became stable. This state does correspond to ecological compensation point. In terms of global photosynthesis, it means that all biomass, produced by photosynthesis, is oxidized in numerous processes of respiration, microbial and chemical oxidation in sediments. It happened when photosynthesis had spread over the whole land. The last splash of oxygen in the atmosphere occurred in the Miocene.

Prior to this moment, the excess of photosynthesis production was accumulated in sediments as a buried organic carbon. Thus, the process of organic carbon accumulation in sediments went on from the origin of photosynthesis up to the ecological compensation point.

On achieving the ecological compensation point, further accumulation of buried organic carbon has ceased. The amount of organic matter and its derivatives in sediments became stationary. It means that the amount of oils generated by source rocks also stabilized.

It should be underlined that the isotope techniques now are a powerful instrument of examination of the processes in the past. It became possible since in many cases carbon isotopic discrepancies remain unchangeable and preserve its memory about the processes. Among them, carbon isotope technique is of special interest. In accordance with actualism principle, carbon isotopic difference between carbonate and coeval organic matter (ε parameter) is the analog of ^{13}C isotope discrimination in modern plants, while ε parameter is a function of CO_2/O_2 ratio in the environment. Moreover, the above isotopic differences are the most widely used data in geology studies. The established changes of the CO_2/O_2 ratio, found by means of carbon isotope data, reflect many events of evolution of the atmosphere, climate, and other coupled phenomena in the biosphere. Combining this technique with adequate carbon cycle model, researchers obtain a very delicate tool to study various phenomena in the past, including evolution itself. Very interesting and important results can be obtained in combination of isotopic techniques of different elements.

Author details

A.A. Ivlev

Russian State Agrarian University – Moscow Agricultural Academy of K.A. Timiryazev, Russian Federation

http://dx.doi.org/10.5772/62222

References

[1] Vernadsky V.I. The Biosphere. 1926 ed. Complete Annotated Edition: Copernicus Books; New York. 1986.

[2] Rutten M.G. The Origin of Life by Natural Causes: Elsevier; Amsterdam. 1971.

[3] Farquhar G.D., Zerkle A.L., Bekker A. Geological constraints on the origin of oxygenic photosynthesis. Photosynth. Res. 2011. 107: 11–36.

[4] Schrag D.P., Higgins J.A., Macdonald F.A., Johnston D.T. Authigenic carbonate and the history of the global carbon cycle. Science 2013. 339: 540–543.

[5] Ivlev A.A. Oscillatory nature of metabolism and carbon isotope distribution in photosynthesizing cells. In: Najafpour M.M, editor. Photosynthesis – fundamental aspects: Intech Publishers; Croatia. 2012. pp. 341–366.

[6] Wegener A. Die Entstehung der Kontinente und Ozeane (4 ed.): Friedrich Vieweg & Sohn; Akt. Ges., Braunschweig. 1929.

[7] Flint R.F. The Earth and Its History: J. Wiley & Sons; New York. 1973. 354 p.

[8] Monin A.S. Istoriya Zemli [History of the Earth]: Nauka; Leningrad. 1977. 228 p. [in Russian].

[9] Harland W.B., Armstrong R.L., Cox A.V., Craig L.E., Smith A.G., Smith D.G. A Geologic Time Scale, 1989 edition: Cambridge University Press; Cambridge. 1990.

[10] Deuser M.J.S., Degens E.T. Carbon isotope fractionation in the system $CO_{2(gas)}$ - $CO_{2(aqueos)}$ – $HCO_3^-{}_{(gas)}$. Nature 1967. 215: 1033–1037.

[11] Wendt Y., Fractionation of C isotopes and its temperature dependence in the system CO_2 (gas) - CO_2 (solution) and HCO_3^- in solution. Earth Planet Sci. Lett. 1968. 4: 132–147.

[12] Abelson P.H., Hoering T.C. Carbon isotope fractionation in the system CO_2(gas) - CO_2(aqua) – HCO_3^-(aqua). Ann. Rep. Dir. Geophys. Lab 1960. 59: 158–161.

[13] Thode H., Shima M., Rees C., Krishnamurty K. Carbon-13 isotope effects in systems containing carbon dioxide, bicarbonate, carbonate and metal ions. Can. J. Chem. 1965. 43: 582–593.

[14] Ivlev A.A. Chemical Evolution vs Biological Evolution: Coupling Effect and Consequences: Signpost Research Publisher; Kerala. 2013. 79 p.

[15] Popp B.N., Takigiku R, Hayes J.M., Louda J.W., Baker E.W. The post-Paleozoic chronology and mechanism of ^{13}C depletion in primary marine organic matter. Am. J. Sci. 1989. 289: 436–454.

[16] Hayes J.M., Strauss H., Kaufman A.J. The abundance of ^{13}C in marine organic matter and isotopic fractionation in the global biogeochemical cycle of carbon during the past 800 Ma. Chem. Geol. 1999. 161: 103–125.

[17] Mackenzie F.T., Pigott J.D. Tectonic controls of Phanerozoic sedimentary rock cycling. J. Geol. Soc. London 1981. 138: 183–196.

[18] Nakai N., Jensen M. Biogeochemistry of sulfur isotopes. J. Earth Sci. 1960. 8: 30–35.

[19] Thode H., Monster J., Dunford H. Sulfur isotope geochemistry. Geochim. Cosmochim. Acta 1961. 25: 159–174.

[20] Ivlev A.A., Voronin V.I. The mechanism of carbon isotope fractionation in photosynthesis and carbon dioxide component of the greenhouse effect. Biology Bull. 2007. 34: 603–609.

[21] Kothavala Z., Oglesby R.J., Saltzman B. Sensitivity of equilibrium surface temperature of CCM3 to systematic changes in atmospheric CO_2. Geophys. Rev. Lett. 1999. 26: 209–212.

[22] Huang Y., Street-Perrott F.A., Perrott R.A., Meitzger P., Eglinton G. Glacial-interglacial environmental changes inferred from molecular and compound-specific δ ^{13}C analyses of sediments from Sacred Lake, Mt. Kenya. Geochim. Cosmochim. Acta 1999. 63: 1383–1404.

[23] Bornemann A., Norris R.D., Friedrich O., Britta Beckmann B., Schouten S., Damsté J.S.S., Vogel J., Hofmann P., Wagner T. Isotopic evidence for glaciation during the Cretaceous super greenhouse. Science 2008. 319: 189–192.

[24] Liebermann B.S., Melott A.L. Considering the case for biodiversity cycles: re-examining the evidence for periodicity on the fossil record. PLoS One 2007. 2: e759.

[25] Igamberdiev A.U., Lea P.J. Land plants equilibrate O_2 and CO_2 concentrations in the atmosphere. Photosynth. Res. 2006. 87: 177–194.

[26] Rothman D.H. Global biodiversity and the ancient carbon cycle. Proc. Natl. Acad. Sci. USA 2001. 98: 4305–4310.

[27] Cornette J.L., Lieberman B.S., Goldstein R.H. Documenting a significant relationship between macroevolutionary origination rate and Phanerozoic pCO_2 levels. Proc. Natl. Acad. Sci. USA 2002. 99: 7832–7835.

[28] Bazhenova O.K., Sokolov B.A. Origin of oil is the fundamental problem of natural science. Geologiya Nefti i Gaza. 2002. n 1: 2–8.

[29] Berner R.A., Canfield D.E. A new model for atmospheric oxygen over Phanerozoic time. Am. J. Sci. 1989. 289: 333–361.

[30] Vyshemirskii V.S., Kontorovich A.E. Cyclic character of oil accumulation in Earth history. Geologiya & Geofizika. 1997. 38: 907–918.

[31] Korchagin V.I. General stratigraphic scale and distribution of oil and gas deposits by stratifications of subdivisions of Phanerozoic and Precambrian. Table composed based on acting stratigraphic lowbook: VNIGNI Publisher; Moscow. 2001.

[32] Rye R., Holland H.D. Paleosols and the evolution of atmospheric oxygen: a critical review. Am. J. Sci. 1998. 298: 621–672.

[33] Bjerrum C.J., Canfield D.E. New insight into the burial history of organic carbon on the early Earth. Geochim. Geophys. Geosyst. 2004. 5: 1–9.

[34] Canfield D.E., Teske A. Late Proterozoic rise in atmospheric oxygen concentration inferred from phylogenetic and sulphur-isotope studies. Nature 1996. 382: 127–132.

[35] Andrusevich V.E., Engel M.H., Zumberge J.E. Effects of paleolatitude on the stable carbon isotope composition of crude oil. Geology 2000. 28: 847–850.

[36] Andrusevich V.E., Engel M.H., Zumberge J.E., Brothers L.A. Secular, episodic changes in stable carbon isotope composition of crude oils. Chemical Geology 1998. 152: 59–72.

[37] Berner R.A., Petsch S.T., Lake J.A., Beerling D.J., Popp B.N., Lane R.S., Laws E.A., Westley M.B., Cassar N., Woodward F.I., Quick W.P. Isotope fractionation and atmospheric oxygen: implications for Phanerozoic O_2 evolution. Science 2000. 287: 1630–1633.

[38] Berner R.A. The long-term carbon cycle, fossil fuels and atmospheric composition. Nature 2003. 426: 323–326.

[39] Lenton T.M. The role of land plants, phosphorous weathering and fire in the rise and regulation of atmospheric oxygen. Global Change Biol. 2001. 7: 613–629.

[40] Bergman M.J., Lenton T.M., Watson A.G. COPSE: a new model of biogeochemical cycling over Phanerozoic time. Am. J. Sci. 2004. 304: 397–437.

[41] Berner R.A., Kothavala Z. GEOCARB III: a revised model of atmospheric CO_2 over Phanerozoic time. Am. J. Sci. 2001. 301: 184–204.

[42] Andre M.J. Modelling $^{18}O_2$ and $^{16}O_2$ unidirectional fluxes in plant: II. Analysis of Rubisco evolution. BioSystems 2011. 103: 251–264.

[43] Tolbert N.E., Benker C., Beck E. The oxygen and carbon dioxide compensation points of C_3 plants: possible role in regulating atmospheric oxygen. Proc. Natl. Acad. Sci. 1995. 92: 11230–11233.

[44] Jahren A.H., Arens N.C., Harbeson S.A. Prediction of atmospheric $\delta^{13}CO_2$ using fossil plant tissues. Rev. Geophys. 2008. 46: 1–12.

[45] Huang Y., Street-Perrott F.A., Metcalfe S.E., Brenner M., Moreland M., Freeman M. Climate change as the dominant control on glacial – interglacial variations in C_3 and C_4 plant abundance. Science 2001. 293: 1647–1651.

[46] Ratnayake N.P., Suzuki N., Okada M., Takagi M. The variations of stable carbon isotope ratio of land plant-derived n-alkanes in deep-sea sediments from the Bering Sea and the North Pacific Ocean during the last 250 000 years. Chem. Geology 2006. 228: 197–208.

[47] Korte C., Hesselbo S.P. Shallow marine carbon and oxygen isotope and elemental records indicate icehouse/greenhouse cycles during Early Jurassic. Paleoceanography 2011. 26: 4219.

[48] Riding J.R., Leng M.J., Kender S., Hesselbo S.P., Feist-Burkhardt S. Isotopic and palynological evidence for a new Early Jurassic environmental perturbation. Paleogeography, Paleoclimatology, Paleoecology 2013. 374: 16–27.

[49] Cors J., Heimhofer U., Adatte T, Hochuli P.A., Huck S., Bover-Arnal T. Climatic evolution across oceanic anoxic event 1a derived from terrestrial palynology and clay minerals (Maestrat Basin, Spain). Geol. Mag. 2015. 152: 632–647.

[50] Robinson M., Dowsett H.J., Chandler M.A. Pliocene role in assessing future climate impacts. Eos. 2008. 89: 501–502.

[51] Dwyer G.S., Chandler M.A. Mid-Pliocene sea level and continental ice volume based on coupled benthic Mg/Ca palaeotemperatures and oxygen isotopes. Phil. Trans. R. Soc. 2009. A 367: 157–168.

[52] Kotthoff U., Greenwood D. R., McCarthy F. M. G., Müller-Navarra K., Prader S., Hesselbo S.P. Late Eocene to middle Miocene (33 to 13 million years ago) vegetation and climate development on the North American Atlantic Coastal Plain (IODP Expedition 313, Site M0027). Clim. Past 2014. 10: 1523–1539.

Chapter 4

The physiology and genetics of stomatal adjustment under fluctuating and stressed environments

Mingnan Qu, Saber Hamdani and James A. Bunce

Additional information is available at the end of the chapter

http://dx.doi.org/10.5772/62223

Abstract

Stomata are pores in the leaf that allow gas exchange where water vapor leaves the plant and carbon dioxide enters. Under natural condition, plants always experience at a fluctuating light regime (shade-/sun-fleck) and due to global climate change, occasionally extreme high temperature and CO_2 enrichment will be inevitable occurred, which dramatically affects stomatal response, and trade-off between water-use efficiency and photosynthesis. Response of stomata to fluctuating and stressed environments determines optimized strategy of plants directing to water save or photosynthesis. Dynamic adjustments of stomata play an equivalent role as steady-state stomatal characteristics. Evolutionary approach indicated that stomatal-dynamic adjustments interacting with historical environments or life histories could be genetically controlled and environmentally selected. In this article, we reviewed physiological response of stomatal dynamic to changing enironments including our previous works, and discussed the possibility of genetic improvements on stomatal adjustments by estimating broad-sense heritability and SNP heritability of stomatal pattern. To gain insight into the framework of stomatal genetics, we highlighted the importance of combining multidisciplinary techniques, such as mathematic modeling, quantitative genetics, molecular biology and equipments developments.

Keywords: Stomatal dynamics, Changing environments, Photosynthesis, Evolution

1. Introduction

Stomata, from the Greek word "stoma" meaning mouth, are small pores that distributed on the epidermis of plant leaves. Their structures consist of two guard cells around a pore. For optimum efficiency, stomata must balance the gas exchange between inside and outside the leaf, in order

to maximize CO_2 uptake for photosynthetic carbon assimilation (P_N) and to minimize water loss through transpiration (E). Although the cumulative area of stomatal pores only represents a small fraction of the leaf surface, typically less than 3%, the CO_2 uptake and water loss pass through these pores. When fully open, they can promote water evaporation equivalent to one-half of a wet surface of the same area [1]. To cope with environmental stress during growth condition, plants must adjust and regulate the stomatal opening/closing process to obtain optimized transpiration and leaf water status.

On the other hand, studying the evolutionary adaptation and natural variation of stomata-related genes may represent an essential step for better understanding the mechanisms involved in the stomatal adjustment and regulation. In fact, stomata have probably undergone a crucial adaptation occurring 400 million years ago, it enabled plants to thrive on land. To survive in the dry atmosphere, plants must maintain a reasonable level of gas exchange necessary for P_N and E, in order to protect against desiccation [2]. In addition, the natural variation in stomata-related genes across different cultivars (from different origins) of particular species may indicate differing selection pressures allowing better adaptation against environmental stress [3].

To get a deeper understanding, the study of the relationship between genotype and phenotype at the organism–environment interface by identifying traits that respond to differing environmental pressures and uncovering the genetic basis for variability in these traits is highly requested. Recent researches have shown that the mode of action of stomatal movement depends on the combination of environmental and intracellular signals. These external factors (e.g., CO_2, biotic and abiotic stresses, and additionally different plant hormones) and internal signals (e.g., ion exchange, metabolites, catalyze of enzyme, and gene structure or expression) simultaneously affect stomatal dynamics, forming a complex framework behind acclimation responses of plants under fluctuating and stressed environments. The empirical evidences related to stomatal dynamics provide strong promotion for the development of model stimulating stomatal dynamics, which remains difficult to achieve so far. In this chapter, we aim to give a multidimensional review about recent works describing multiple environmental and internal factors, such as elevated CO_2, heat stress, light fluctuations, ion channel, and stomata-related genes [4–8]. Furthermore, we discussed expended research perspective regarding stomatal evolution, natural variations of stomatal traits, interactions with life history, and theoretical modeling.

2. External environments

2.1. Interactive effects of elevated CO_2 and heat wave

The global change, leading to frequent occurrence of atmospheric CO_2 enrichment and heat wave, inevitably affects the development and final productivity of plants. Most climate impact studies rely on changes in means of meteorological variables, such as temperature and rainfall, to estimate the potential climate impacts on agricultural production. However, extreme meteorological events, e.g., a short period of abnormally high temperatures, can have a

http://dx.doi.org/10.5772/62223

significant profound and lasting effect on canopy transpiration, crop growth, and final yield [9].

During heat stress, elevated CO_2 has probably less effect on C_3 plants as compared to C_4 plants [10]. In fact, elevated CO_2 can increase water-use efficiency (WUE) by decreasing stomatal conductance (g_s) and E [11], which may increase tolerance to acute heat. It was shown that the reduction in g_s (stomatal opening) is about 20% for C_3 and 50% for C_4 species [10, 12, 13]. The lower g_s in C_4 plants may induce lower transpiration (water loss) and thus higher leaf temperatures, which may increase heat-related damage in C_4 plants as compared to C_3 plants in the same habitat.

Since evaporative cooling is essential to avoid heat damage in leaves exposed to full sunlight, and time scales of stomatal adjustments are longer than fluctuations in solar irradiance within a canopy, the question arises whether elevated CO_2 can mitigate damage over transpiring leaves from extreme high temperature by decreasing g_s. If this is the case, then adaptation for cooling would appear as a more imperative driver for stomatal adjustments than the potential increase in carbon gain. To test this hypothesis, intact leaves of maize were subjected to a substantial reduction P_N due to 45°C heat stress cycle for 1hour[14]. Our previous finding showed that elevated CO_2, either during plant growth or co-heat period, does not improve the foliar thermotolerance against heat stress (Figure 1). With the lower P_N and higher g_s and subcellular CO_2 pressure (C_i) following the acute heat stress treatment, a non-stomatal inhibition of g_s occurs, contrary to other studies showing a stomatal adjustments in response to high temperature stress in grape leaves [15, 16]. In the meantime, the sudden reversal of stomatal responses to leaf temperature and CO_2 between 40°C and 45°C (Figure 1) suggests that to avoid damage, plants enhance the stomatal opening, leading to an increase in evaporative cooling.

Some studies compared elevated CO_2 effects with tolerance to heat stress in relatively heat-sensitive vs. heat-tolerant species or in species with different photosynthetic pathways [4, 17–20]. As an example, two corn cultivars (B73 and B106) were previously reported as contrasting heat stress tolerance from field investigation and evaluations [21]. When comparing the effects of elevated CO_2 and heat stress from field-based investigation using these corn cultivars, our previous results showed a reversible response of two cultivars regarding to photosynthetic activity (Figure 2), which might be due to intricate reasons: 1) change in physical function of stomatal regulation by decreasing transpiration and optimized water conservation at intact leaves scales; 2) change in kinetic activities of photosynthetic regulatory enzymes, i.e., rubisco (ribulose 1,5-bisphosphate carboxylase/oxygenase), PEPase, and MDHase (Table 1), which agrees with some reports [22, 23]; and 3) disorder of metabolite flux in Calvin cycle due to heat stress.

2.2 Fluctuating light effects

Leaves are always subjected to rapidly fluctuating irradiance due to motion of sunflecks and clouds that may span two orders of magnitude from light compensation points of shade-adapted leaves to almost full irradiance intensities [25]. Such environmental fluctuations occur at second scales, which is much shorter than the time needed for stomatal adjustments (2–60

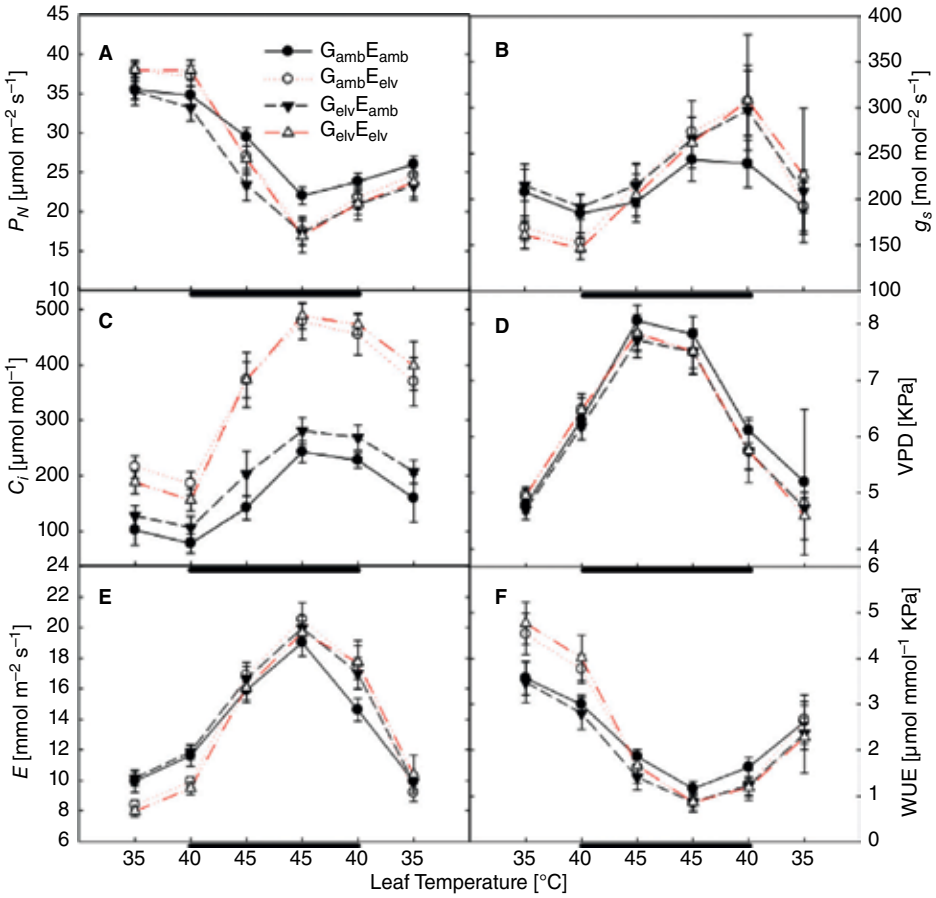

Figure 1. Dynamic changes of photosynthetic parameters during acute heat stress cycles. Lines with same color stand for treatment at same exposure CO_2 concentrations. Symbols $G_{amb}E_{amb}$, $G_{amb}E_{elv}$, $G_{elv}E_{amb}$, and $G_{elv}E_{elv}$ represent grown and exposed at ambient [CO_2], grown at ambient [CO_2] but exposed at elevated [CO_2], grown at elevated [CO_2] but exposed at ambient [CO_2], and both of grown and exposed at elevated [CO_2]. *Vertical bars* represent S.E. for n = 9 (see [14]).

min.) [26]. For leaves with slowly adjusting stomata, rapid fluctuations at shorter time scales could push leaf hydraulic and thermal status beyond operational limits resulting in xylem cavitation, overheating, or wilting.

Although the phenomena underlying dynamic responses of photosynthesis to sunflecks (such as induction requirements) were studied by physiologists and biochemists earlier [26], their role in sunfleck utilization was not recognized until the early 1980s. Evidence for the light activation requirement of the primary carboxylating enzyme, Rubisco, was first uncovered in the 1960s [27]. The components underlying induction, especially stomatal behavior, are complex and are dependent on environmental and developmental factors as well transient light changes. It was reported that water stress could reduce g_s in shade-grown, but not in sun-

http://dx.doi.org/10.5772/62223

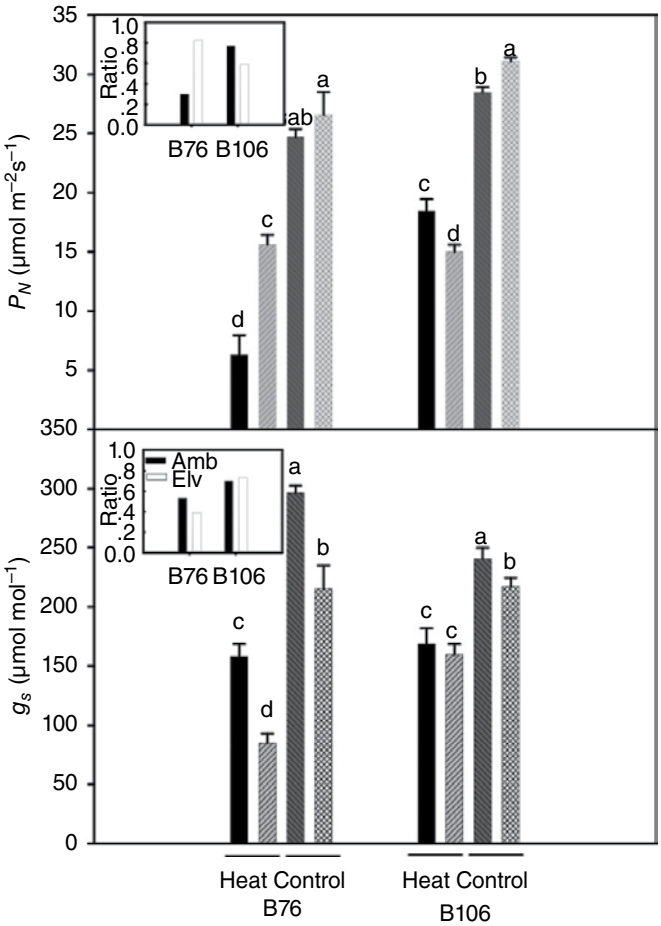

Figure 2. Heat induced decrease of photosynthesis and stomatal conductances in B76 and B106. Black and grid bars represent ambient and elevated [CO_2], respectively. Ratio of photosynthesis and stomatal conductances under heat stress over control in B76 and B106 was shown in inserted panel. (Qu et al. 2016, unpublished data).

grown for the leaves of a *Populus* species; drought also could lead to faster induction gain in shade-grown, but not in sun-grown for the leaves during simulated sunflecks [28] .

In the naturally fluctuating environment, the temporal disconnect between g_s and P_N means the coordination between carbon gain and water loss (and, therefore, WUE) is far from optimal ([29]; Figure 3). Photosynthetic induction state is a complex function of light-dependent stomatal opening and closing responses and the time courses of light-regulated enzyme activation and deactivation. All these combined factors determine the potential light-saturated P_N at any given time and therefore the potential P_N that can be achieved during a fluctuating light (shade-fleck). Under this condition, responses of g_s and P_N are not always synchronized, as stomatal movements can be an order of magnitude slower than the more rapid photosynthetic response to the same environmental stimuli ([30, 31]; Figure 3).

OTCs	Heat	PEPC activity (μmol m^{-2} s^{-1})	ME activity (μmol m^{-2} s^{-1})	MDH activity (μmol m^{-2} s^{-1})
Ambient[CO2]				
B76	aft0	15.5 ± 0.5 (33.1 ± 1.6)	3.7 ± 0.4 (31.6 ± 0.5)	7.9 ± 3.4 (24.8 ± 3.3)
	aft4	19.7 ± 0.5 (36.5 ± 1.5)	20.6 ± 0.3 (29.0 ± 0.1)	14.9 ± 1.2 (26.5 ± 0.4)
	% Change	27.1	456.8	88.6
B106	aft0	13.3 ± 0.7 (32.8 ± 0.5)	12.4 ± 1.1 (24.6 ± 0.3)	17.2 ± 0.3 (26.1 ± 0.2)
	aft4	15.8 ± 0.7 (36.6 ± 1.4)	13.9 ± 0.7 (27.7 ± 0.3)	19.0 ± 2.7 (28.9 ± 0.4)
	% Change	18.8	12.1	10.5
Elevated[CO2]				
B76	aft0	13.6 ± 1.5 (32.0 ± 0.7)	10.9 ± 0.2 (25.3 ± 0.4)	12.1 ± 1.7 (29.0 ± 1.2)
	aft4	17.9 ± 1.3 (34.4 ± 0.9)	18.1 ± 1.0 (26.3 ± 0.6)	20.9 ± 0.4 (28.8 ± 1.5)
	% Change	31.6	66.5	72.7
B106	aft0	10.5 ± 1.7 (32.2 ± 0.1)	9.0 ± 0.6 (26.7 ± 0.8)	14.6 ± 1.7 (28.6 ± 0.6)
	aft4	12.8 ± 1.0 (31.9 ± 1.0)	11.6 ± 1.6 (29.2 ± 0.5)	13.7 ± 0.9 (31.6 ± 1.1)
	% Change	21.9	29.1	-6.2

Table 1. Enzyme activities of PEPC, NADP-ME, and NADP-MDH for B76 vs. B106 grown ambient and elevated [CO_2]. Values of control experiments were shown in brackets (Qu et al. 2016, unpublished data).

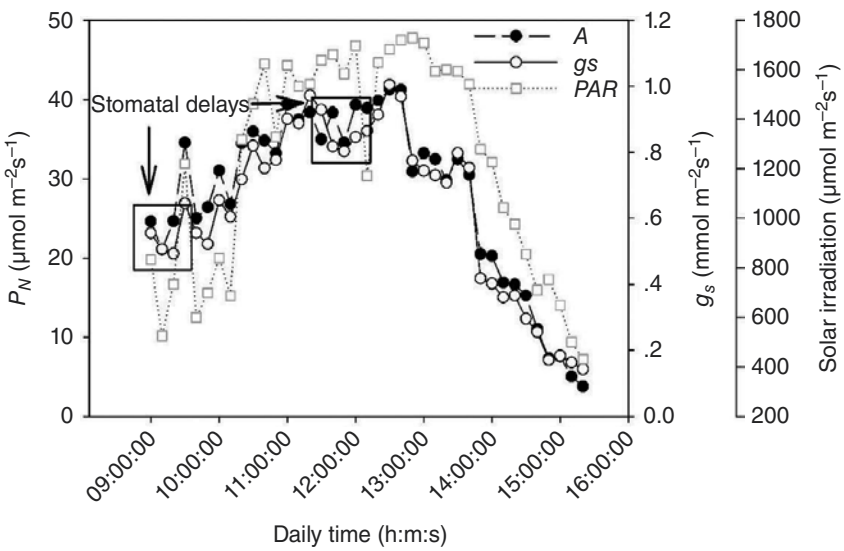

Figure 3. Photosynthesis and stomatal conductance in response to naturally light regime (Qu et al. 2016, unpublished data).

http://dx.doi.org/10.5772/62223

3. Internal signals

3.1 Ion channels and transmembrane antiporters

There is no question that stomatal movements (stomatal opening and closing) of seed plants, including crop plants, arise from the transport, accumulation, and release of osmotically active solutes (reviewed by [32]). It has been shown that the guard cell movement is controlled by movement of Cl^+, Na^+, K^+, and also changes in the sucrose and malate levels [32, 33]. It is reasonable to give expectation that ion exchange, inducing change in pH, might indirectly determine response time of stomatal adjustments during light fluctuations based on previous literatures. For example, membrane depolarization in ABA stimulates K^+ efflux within seconds through outward-rectifying K^+ channels, in Arabidopsis the GORK K^+ channel [34, 35], and these K^+ currents are enhanced during the subsequent 3–5 min as a consequence of rise in cytosolic pH [36, 37]. Stomatal aperture responds more slowly, typically with half-times of 10–20 min, reaching a new stable, (near) closed state after 45–60 min [38–40]. Thus, making a connection of ion channel antiporters to the speed and efficacy of stomatal movements is necessarily important.

3.2 Anatomical features of stomata

Responsiveness of stomatal adjustments under changing environments is also dependent on anatomical characteristics. In fact, stomatal anatomical features define the maximum theoretical conductance and also influence the speed of response [41]. Many experimental evidences have demonstrated that stomatal density is negatively correlated with stomatal size [42, 43]. The interaction/correlation between stomatal size and density and the impact on stomatal function have received much attention [44]. The latest studies have also implied that physical attributes affect stomatal response times following environmental perturbations [45]. Therefore, it is possible to manipulate the stomatal structure, for example, we can take into consideration the interaction between stomatal size and number and its impact on rapidity of stomatal movement.

3.3 Casual genes of stomatal features

Engineering and breeding crops for enhanced drought resistance become a pressing task for plant biologists and breeders. Manipulation on functional genes underlying dynamics of stomatal responses and steady-state values of g_s would be helpful for optimizing WUE and drought resistance of plants [46–51]. For example, mutation in the *SLAC1* gene, which codes for an anion channel, causes slow stomatal opening by light, low CO_2, and elevated air humidity in intact plants, due to severely reduced activity of inward K^+ channels in *slac1* guard cells [52]. Arabidopsis (*Arabidopsis thaliana*) stomatal density and distribution (*sdd1-1*) mutants, having a point mutation in a single gene that encodes a subtilisin-like Ser protease, exhibit a 2.5-fold higher stomatal density compared with their wild type [53]. Stomatal movements can also be stimulated by membrane fusion protein, soluble N-ethylmaleimide-sensitive fusion protein attachment protein receptor (SYP121), Eisenach et al. [54] demonstrated that stomatal

opening and the rise in stomatal transpiration of the *syp121* mutant were delayed in the dark–light transition and following the Ca^{2+}-evoked closure. The increase in stomatal density translates leads to an increase in g_s and 30% greater P_N under high light conditions [55]. Tanaka et al. [56] have used plants overexpressing STOMAGEN, a positive regulator of stomatal density, to produce transgenic plants with a two- to three fold greater stomatal density than the wild type. P_N in these plants is increased by 30% due to greater CO_2 diffusion into the leaf rather than changes in photosynthetic carboxylation capacity [56]. By contrast, some genes can induce low stomatal density and g_s at high light intensities, for example, upregulation of *sdd1* can restrict CO_2 diffusion limited P_N to 80% of the wild type [57].

These findings exemplify the role of both the physical and functional stomatal features in determining g_s. In particular, these works illustrate the importance of surrounding environmental conditions and ion exchange on stomatal behavior and the significance of examining g_s limitation on P_N at fluctuating light and elevated CO_2 and heat stress.

4. Natural variation and heritability of stomatal conductance

The analysis of evolution of stomata over species should depend on two strategies, i.e., fossil studies on ancestor plants and genetic studies on current plants. Fossil evidence shows that stomata have occurred in sporophytes and (briefly) gametophytes of embryophytes during the last 400 million years. Cladistic analyses with hornworts basal are consistent with a unique origin of stomata, although cladograms with hornworts as the deepest branching embryophytes require loss of stomata early in the evolution of liverworts (reviewed by [58]).

Genetic variation is a vital characteristic of every population that is required to adapt. Phenotypic trait variance within a population can be related to genetic variance as an estimation of broad-sense heritability (H^2). In theory, when a greater proportion of phenotypic variation is attributable to genetic variance, the corresponded trait is highly heritable. Exploring stomatal traits with high H^2 under multiple environments could provide strategy for artificial selection and improvements on stomatal traits. Although natural variation in photosynthetic capacity especially stomatal features is known to exist among different species [59–63], relatively few studies have examined natural variation among accessions of the same species [64–67]. Besides, studying the genetic variation of photosynthetic capacity of different rice accessions with diverse genetic background could be an effective way to improve the photosynthetic capacity of existing rice elite germplasm [67, 68].

In fact, mining natural variations of photosynthetic and stomatal parameters is regarded as a promising approach to identify new genes or alleles for crop improvement. Conventionally, the identification of genomic loci that govern complex traits has been extensively facilitated by the development of quantitative trait locus (QTL) mapping approaches. Recent advances in high-throughput and high-dimensional genotyping and phenotyping technologies enable us to reduce the gaps between genomics and phenomics using the principles of genome-wide association studies (GWAS). This biostatistic method has been widely used in food crops for identifying genes that underlie natural variation of various ecological and agricultural traits

[69–71]. Consequently, a combination of GWAS and QTL mapping as well as co-expression network would be a better option to obtain additive, dominance, and epistasis effects of genes, for example, in Arabidopsis [72] and soybean [73].

Therefore, understanding the mechanisms that underlie efficient carbon gain driven by stomatal adjustments in fluctuating light can open doors for increasing plant yields and, more broadly, can reveal fundamental principles to optimize the water cycle system in the biosphere.

5. Relation of stomatal profiling with life histories

Evolutionary responses of stomata to fluctuating light conditions are important because stomata in theory must have been subject to evolutionary pressures associated with highly variable conditions. This is always related to the life history of accession origins. Studying the evolution of photosynthesis is critical to understand how stomata or plants structure variation influence ecological interactions and adaptation to various environments [74]. Where an overlying geographical origin or environmental gradient exerts strong adaptive selection, the natural variation in both genotype and phenotype is predicted. However, this variation will depend on the relative strength of selection, demographic history, and levels of dispersal and/or gene flow among populations [75]. Differing selection pressures may include temperature, precipitation, and soil nutrient availability, growing season length, photoperiod, and biotic agents. Many of these factors are directly affected by geographic conditions and are therefore interrelated. This is already extensively reported in trees species. Genetic covariance among ecophysiological traits can be shaped by the past ecological and evolutionary processes [3]. However, for traits of ecological or evolutionary interest, studies must also address the extent to which population structure, trait variation, and genetic architecture covary along ecological gradients [3].

6. Theoretical modeling for describing stomatal delays

To describe the dynamics of g_s and P_N in response to an abrupt change in light, piecewise linear, logistic, and exponential models have been frequently employed [25, 76–78]. For instance, in terms of stomatal dynamics in time scales during closing (τ_{cl}) and opening phases (τ_{op}), significant variation insensitivity and responsiveness is known to exist among different species [25, 32, 33]. As described above, when switching from high to low light, stomata always performed a lag relative to photosynthetic reduction, and to simplify, linearizing imputation between specific time period (stepwise) on photosynthetic dynamics could be a better option to define the amplitude and speed of stomata. In Arabidopsis, Wang et al. [79] have developed a dynamic model of stomatal responses, taking into consideration ion channel and kinetic effects as components controlling g_s under steady-state and dynamic conditions. This model integrated the biophysical, molecular, and biochemical characteristics of guard cell transport, malate metabolism, and H^+ and Ca^{2+}, to predict stomatal aperture, which can be used to explore

inherent interaction between different factors controlling g_s [79, 80]. This model provided a good framework to incorporate new knowledge about controls over guard cell movements and hence help design engineering options to gain optimal steady state g_s and also optimal dynamic responses of g_s to light levels.

Author details

Mingnan Qu[1,2], Saber Hamdani[1] and James A. Bunce[2]

1 CAS-Key Laboratory for Computational Biology, CAS-MPG Partner Institute for Computational Biology, Shanghai Institutes for Biological Sciences, Chinese Academy of Sciences, Shanghai, China

2 USDA ARS, Crop Systems and Global Change Laboratory, Beltsville, MD, USA

References

[1] Willmer C, Fricker M. 1996. Stomata, 2nd edn. London: Chapman & Hall.

[2] Petersona KM, Rychela AL, Toriia KU. Out of the mouths of plants: The molecular basis of the evolution and diversity of stomatal development. *The Plant Cell* 22: 296–306.

[3] McKown AD, Guy RD, Klateps J, Geraldes A, Friedmann M, Cronk QCB, El-Kassa YA, Mansfield SD, Douglas CJ. 2014a. Geographical and environmental gradients shape phenotypic trait variation and genetic structure in *Populus trichocarpa*. The New Phytologist 201: 1263–1276.

[4] Taub , DR, Seemann JR, Coleman JS. 2000. Growth in elevated CO_2 protects photosynthesis against high-temperature damage. *Plant, Cell & Environment* 23: 649–656.

[5] Wang D, Heckathorn SA, Barua D, Joshi P, Hamilton EW, LaCroix JJ. 2008. Effects of elevated CO_2 on the tolerance of photosynthesis to acute heat stress in C_3, C_4, and CAM species. *American Journal of Botany* 95: 165–176.

[6] Wang D, Heckathorn SA, Hamiton EW, Frantz J. 2014. Effects of CO_2 on the tolerance of photosynthesis to heat stress can be affected by photosynthetic pathway and nitrogen. *American Journal of Botany* 101: 34–44.

[7] Yang Y, Han C, Liu Q, Lin B, Wang J. 2008. Effect of drought and low light on growth and enzymatic antioxidant system of *Picea asperata* seedlings. *Acta Physiologiae Plantarum* 30: 433–440.

[8] Demmig B, Winter K, Kruger A, Czygan FC. 1988. Zeaxanthin and the heat dissipation of excess light energy in *Nerium oleander* exposed to a combination of high light and water stress. *Plant Physiol*ogy 87: 17–24.

[9] Mearns LO, Katz RW, Schneider SH. 1984. Extreme high temperature events: changes in their probabilities with changes in mean temperature. *Journal of Climate and Applied Meteorology* 23: 1601–1613.

[10] Sage RF. 1994. Acclimation of photosynthesis to increasing atmospheric CO_2: The gas-exchange perspective. *Photosynthesis Research* 39: 351–368.

[11] Ainsworth EA, Davey PA, Bernacchi CJ, Dermody OC, Heaton EA, Moore DJ, Morgan PB, Naidu SL, Ra HSY, Zhu XG, Gurtis PS, Long SP. 2002. A meta-analysis of elevated CO_2 effects on soybean (*Glycine max*) physiology, growth and yield. *Global Change Biology* 8: 695–709.

[12] Reich PB, Tilman D, Craine J, Ellsworth D, Tjoelker MG, Knops J, Wedin D, Naeem S, Bahauddin D, Goth J, Bengtson W, Lee TD. 2001. Do species and functional groups differ in acquisition and use of C, N and water under varying atmospheric CO_2 and N availability regimes? A field test with 16 grassland species. *The New Phytologist* 150: 435–448.

[13] Maherali H, Reid CD, Polley HW, Johnson HB, Jackson RB. 2002. Stomatal acclimation over a subambient to elevated CO_2 gradient in a C_3/C_4 grassland. *Plant, Cell & Environment* 25: 557–566.

[14] Qu M, Bunce JA, Shi ZS. 2014. Does elevated CO_2 protect photosynthesis from damage by high temperature via modifying leaf water status in maize seedlings? *Photosynthetica* 52: 211–216.

[15] Luo HB, Ma L, Xi HF, Duan W, Li SH, Loescher W, Wang JF, Wang LJ. 2011. Photosynthetic responses to heat treatments at different temperatures and following recovery in grapevine (*Vitis amurensis* L.) leaves. *PLoS ONE* 6: e23033. doi:10.1371/journal.pone.0023033.

[16] Hamilton EW, Heckathorn SA, Joshi P, Wang D, Barua D. 2008. Interactive effects of elevated CO_2 and growth temperature on the tolerance of photosynthesis to acute heat stress in C_3 and C_4 species. *Journal of Integrative Plant Biology* 50: 1375–1387.

[17] Coleman JS, Rochefort L, Bazzaz , Woodward . 1991. Atmospheric CO_2, plant nitrogen status and the susceptibility of plants to acute heat stress. *Plant, Cell & Environment* 14: 667–674.

[18] Bassow SL, McConnaughay KDM, Bazzaz FA. 1994. The response of temperate tree seedlings grown in elevated CO_2 to extreme temperature events. *Ecological Applications* 4: 593–603.

[19] Roden JS, Ball MC. 1996. Growth and photosynthesis of two eucalypt species during high temperature stress under ambient and elevated [CO_2]. *Global Change Biology* 2: 115–128.

[20] Huxman TE, Hamerlynck EP, Loik ME, Smith SD. 1998. Gas exchange and chlorophyll fluorescence responses of three south-western Yucca species to elevated CO_2 and high temperature. *Plant, Cell & Environment* 21: 1275–1283.

[21] Chen JP, Burke JJ, Xin ZG. 2010. Role of phosphatidic acid in high temperature tolerance in maize. *Crop Science* 50: 2506–2515.

[22] Eckardt NA, Snyder GW, Portis AR Jr, Ogren WL. 1997. Growth and photosynthesis under high and low irradiance of Arabidopsis thaliana antisense mutants with reduced ribulose-1,5-bisphosphate carboxylase/oxygenase activase content. *Plant Physiology* 113: 575–586.

[23] Crafts-Brandner SJ, Salvucci ME. 2002. Sensitivity of photosynthesis in a C_4 plant, maize, to heat stress. *Plant Physiology* 129: 1773–1780.

[24] Chazdon RL. 1988. Sunflecks and their importance to forest understorey plants. *Advances in Ecological Research* 18: 1–63.

[25] Vico G, Manzoni S, Palmroth S, Katul G. 2011. Effects of stomatal delays on the economics of leaf gas exchange under intermittent light regimes. The *New Phytologist* 192: 640–652.

[26] Osterhout WJV, Haas ARC. 1918. On the dynamics of photosynthesis. *The Journal of General Physiology* 1: 1–16.

[27] Walker DA. 1973. Photosynthetic induction phenomena and the light activation of ribulose diphosphate carboxylase. *The New Phytologist* 72: 209–235.

[28] Tang Y, Liang NS. 2000. Characterization of the photosynthetic induction response in a Populus species with stomata barely responding to light changes. *Tree Physiol* 20: 969–976.

[29] Lawson T, Weyers JDB. 1999. Spatial and temporal variation in gas exchange over the lower surface of *Phaseolus vulgaris* primary leaves. *Journal of Experimental Botany* 50: 1381–1391.

[30] Pearcy RW. 1990. Sunflecks and photosynthesis in plant canopies. *Annual Review of Plant Physiology and Plant Molecular Biology* 41: 421–453.

[31] Lawson T, von Caemmerer S, Baroli I. 2010. Photosynthesis and stomatal behaviour. In: Luttge U, Beyschlag W, Budel B, Francis D, eds. Progress in Botany, Vol. 72. Heidelberg: Springer, 265–304.

[32] Lawson T, Blatt MR. 2014. Stomatal size, speed, and responsiveness impact on photosynthesis and water use efficiency. *Plant Physiology* 164: 1556–1570.

[33] Lawson T. 2009. Guard cell photosynthesis and stomatal function. The *New Phytologist* 181: 13–34.

[34] Hosy E, Vavasseur A, Mouline K, Dreyer I, Gaymard F, Porée F, Boucherez J, Lebaudy A, Bouchez D, Very AA, . 2003. The Arabidopsis outward K^+ channel GORK is involved in regulation of stomatal movements and plant transpiration. *Proceedings of the National Academy of Sciences of the United States of America* 100: 5549–5554.

[35] Suhita D, Raghavendra AS, Kwak JM, Vavasseur A. 2004. Cytoplasmic alkalization precedes reactive oxygen species production during methyl jasmonate- and abscisic acid-induced stomatal closure. *Plant Physiology* 134: 1536–1545.

[36] Blatt MR, Armstrong F. 1993. K^+ channels of stomatal guard cells: abscisic acid-evoked control of the outward rectifier mediated by cytoplasmic pH. *Planta* 191: 330–341.

[37] Grabov A, Blatt MR. 1997. Parallel control of the inward-rectifier K^+ channel by cytosolic-free Ca2+ and pH in Vicia guard cells. *Planta* 201: 84–95.

[38] Raschke K, Firn RD, Pierce M. 1975. Stomatal closure in response to xanthoxin and abscisic acid. *Planta* 125: 149–160.

[39] Roelfsema MG, Prins HA. 1995. Effect of abscisic acid on stomatal opening in isolated epidermal strips of abi mutants of *Arabidopsis thaliana*. *Physiologia Plantarum* 95: 373–378.

[40] Zhang X, Miao YC, An GY, Zhou Y, Shangguan ZP, Gao JF, Song CP. 2001. K^+ channels inhibited by hydrogen peroxide mediate abscisic acid signaling in *Vicia* guard cells. *Cell Research* 11: 195–202.

[41] Dow GJ, Bergmann DC, Berry JA. 2014. An integrated model of stomatal development and leaf physiology. *The New Phytologist* 201: 1218–1226.

[42] Hetherington AM, Woodward FI. 2003. The role of stomata in sensing and driving environmental change. *Nature* 424: 901–908.

[43] Franks PJ, Beerling DJ. 2009. CO_2-forced evolution of plant gas exchange capacity and water-use efficiency over the Phanerozoic. *Geobiology* 7: 227–236.

[44] Franks PJ, Farquhar GD. 2007. The mechanical diversity of stomata and its significance in gas-exchange control. *Plant Physiology* 143: 78–87.

[45] Drake PL, Froend RH, Franks PJ. 2013. Smaller, faster stomata: scaling of stomatal size, rate of response, and stomatal conductance. *Journal of Experimental Botany* 64: 495–505.

[46] Negi J, Matsuda O, Nagasawa T, Oba Y, Takahashi H, Kawai-Yamada M, Uchimiya H, Hashimoto M, Iba K. 2008. CO_2 regulator *SLAC*1 and its homologues are essential for anion homeostasis in plant cells. *Nature* 452: 483–486.

[47] Wang D, Maughan MW, Sun J, Feng X, Miguez F, Lee D, Dietze MC. 2012. Impact of nitrogen allocation on growth and photosynthesis of Miscanthus (*Miscanthus* × *giganteus*). *GCB Bioenergy* 4: 688–697.

[48] Merlot S, Leonhardt N, Fenzi F, Valon C, Costa M, Piette L, Vavasseur A, Genty B, Boivin K, Müller A. 2007. Constitutive activation of a plasma membrane H^+-ATPase prevents abscisic acid-mediated stomatal closure. *The EMBO Journal* 26: 3216–3226.

[49] De Angeli A, Monachello D, Ephritikhine G, Frachisse JM, Thomine S, Gambale F, Barbier-Brygoo H. 2009. Review: CLC-mediated anion transport in plant cells. *Philosophical Transactions of the Royal Society B: Biological Sciences* 364: 195–201.

[50] Gobert A, Isayenkov S, Voelker C, Czempinski K, Maathuis FJM. 2007. The two-pore channel TPK1 gene encodes the vacuolar K^+ conductance and plays a role in K^+ homeostasis. *Proceedings of the National Academy of Sciences of the United States of America* 104: 10726–10731.

[51] Valliyodan B, Nguyen HT. 2006. Understanding regulatory networks and engineering for enhanced drought tolerance in plants. *Current Opinion in Biotechnology* 9: 189–195.

[52] Laanemets K, Wang YF, Lindgren O, Wu J, Nishimura N, Lee S, Caddell D, Merilo E, Brosche M, Kilk K. 2013. Mutations in the *SLAC1* anion channel slow stomatal opening and severely reduce Kþ uptake channel activity via enhanced cytosolic [Ca2þ] and increased Ca2þ sensitivity of Kþ uptake channels. *The New Phytologist* 197: 88–98.

[53] Berger D, Altmann T. 2000. A subtilisin-like serine protease involved in the regulation of stomatal density and distribution in Arabidopsis thaliana. *Genes & Development* 14: 1119–1131.

[54] Eisenach C, Chen ZH, Grefen C, Blatt MR. 2012. The trafficking protein SYP121 of Arabidopsis connects programmed stomatal closure and K^+ channel activity with vegetative growth. *The Plant Journal* 69, 241–251.

[55] Schlüter U, Muschak M, Berger D, Altmann T .2003. Photosynthetic performance of an Arabidopsis mutant with elevated stomatal density (*sdd1-1*) under different light regimes. *Journal of Experimental Botany* 54: 867–874.

[56] Tanaka Y, Sugano SS, Shimada T, Hara-Nishimura I. 2013. Enhancement of leaf photosynthetic capacity through increased stomatal density in Arabidopsis. *The New Phytologist* 198: 757–764.

[57] Büssis D, von Groll U, Fisahn J, Altmann TA. 2006. Stomatal aperture can compensate altered stomatal density in Arabidopsis thaliana at growth light conditions. *Funct Plant Biol* 33: 1037–1043.

[58] Raven JA. 2002. Selection pressures on stomatal evolution. *The New Phytologist* 153: 371–386.

[59] Wullschleger SD.1993. Biochemical limitations to carbon assimilation in C_3 plants – a retrospective analysis of the A/C_i curves from 109 species. *Journal of Experimental Botany* 44: 907–920.

[60] Wright IJ, Reich PB, Cornelissen JHC, Falster DS, Garnier E, Hikosaka K, Lamont BB, Lee W, Oleksyn J, Osada N, Poorter H, Villar R, Warton DI, Westoby M. 2005. Assessing the generality of the global leaf trait relationships. *The New Phytologist* 166: 485–496.

[61] Hikosaka K, Shigeno A. 2009. The role of Rubisco and cell walls in the interspecific variation in photosynthetic capacity. *Oecologia* 160, 443–451.

[62] Hikosaka K. 2010. Mechanisms underlying interspecific variation in photosynthetic capacity across wild plant species. *Plant Biotechnology* 27: 223–229.

[63] Lawson T, Kramer DM, Raines CA. 2012. Improving yield by exploiting mechanisms underlying natural variation of photosynthesis. *Current Opinion in Biotechnology* 23: 215–220.

[64] Pettigrew WT. 2004. Cotton genotypic variation in the photosynthetic response to irradiance. *Photosynthetica* 42: 567–571.

[65] Gilbert ME, Zwieniecki MA, Holbrook NM. 2011. Independent variation in photosynthetic capacity and stomatal conductance leads to differences in intrinsic water use efficiency in 11 soybean genotypes before and during mild drought. *Journal of Experimental Botany* 62: 2875–2887.

[66] Flood PJ, Harbinson J, Aarts MGM. 2011. Natural genetic variation in plant photosynthesis. *Trends in Plant Science* 16: 327–335.

[67] Gu J, Yin X, Stomph T-J, Struik PC. 2014. Can exploiting natural genetic variation in leaf photosynthesis contribute to increasing rice productivity? A simulation analysis. *Plant, Cell & Environment* 37: 22–34.

[68] Hamdani S, Qu M, Xin CP, Li M, Chu C, Govindjee , Zhu XG. 2015. Variations between the photosynthetic properties of elite and landrace Chinese rice cultivars revealed by simultaneous measurements of 820 nm transmission signal and chlorophyll a fluorescence induction. *Journal of Plant Physiology* 177: 128–138.

[69] Huang X, Wei X, Sang T, Zhao Q, Feng Q, Zhao Y, Li C, Zhu C, Lu T, Zhang Z, Li M, Fan D, Guo Y, Wang A, Wang L, Deng L, Li W, Lu Y, Weng Q, Liu K, Huang T, Zhou T, Jing Y, Li W, Lin Z, Buckler ES, Qian Q, Zhang QF, Li J, Han B. 2010. Genome-wide association studies of 14 agronomic traits in rice landraces. *Nature Genetics* 42: 961–967.

[70] Huang X, Zhao Y, Wei X, Li C, Wang A, Zhao Q, Li W, Guo Y, Deng L, Zhu C, Fan D, Lu Y, Weng Q, Liu K, Zhou T, Jing Y, Si L, Dong G, Huang T, Lu T. 2012. Genome-wide association study of flowering time and grain yield traits in a worldwide collection of rice germplasm. *Nature Genetics* 44: 32–40.

[71] Mckown AD, Guy RD, Quamme L, Klapste J, Mantia JL, Constabel CP, El-Kassaby YA, Hamelin RC, Zifkin M, Azam MS. 2014b. Association genetics, geography and eco-

physiology link stomatal patterning in *Populus trichocarpa* with carbon gain and disease resistance trade-offs. *Molecular Ecology* 23: 5771–5790.

[72] Brachi B, Faure N, Horton M, Flahauw E, Vazquez A, Nordborg M, Bergelson J, Cuguen J, Roux F. 2010. Linkage and association mapping of Arabidopsis thaliana flowering time in nature. *PLoS Genetics* 6: e1000940.

[73] Sonah H, O'Donoughue L, Cober E, Rajcan I, Belzile F. 2014. Identification of loci governing eight agronomic traits using a GBS-GWAS approach and validation by QTL mapping in soybean. *Plant Biotechnology Journal*. doi: 10.1111/pbi.12249.

[74] Eckert AJ, Dyer RJ. 2012. Defining the landscape of adaptive genetic diversity. *Molecular Ecology* 21: 2836–2838.

[75] Savolainen O, Pyhajarvi T, Knurr T. 2007. Gene flow and local adaptation in trees. *Annual Review of Ecology Evolution and Systematics* 38: 595–619.

[76] Kirschbaum MUF, Gross LJ, Pearcy RW. 1988. Observed and modeled stomatal responses to dynamic light environments in the shade plant *Alocasia macrorrhiza*. *Plant, Cell & Environment* 11: 111–121.

[77] Zipperlen SW, Press MC. 1997. Photosynthetic induction and stomatal oscillations in relation to the light environment of two *dipterocarp* rain forest tree species. *Journal of Ecology* 85: 491–503.

[78] Naumburg E, Ellsworth DS, Katul GG. 2001. Modeling dynamic understory photosynthesis of contrasting species in ambient and elevated carbon dioxide. *Oecologia* 126: 487–499.

[79] Wang Y, Papanatsiou M, Eisenach C, Karnik R, Williams M, Hills A, Lew VL, Blatt MR. 2012. Systems dynamic modeling of a guard cell Cl^- channel mutant uncovers an emergent homeostatic network regulating stomatal transpiration. *Plant Physiology* 160: 1956–1967.

[80] Blatt MR, Wang YZ, Leonhardt N, Hillsa A. 2014. Exploring emergent properties in cellular homeostasis using OnGuard to model K^+ and other ion transport in guard cells. *Journal of Plant Physiology* 17: 1770–778.

Chapter 5

Monitoring of the Drought Tolerance of Various Cotton Genotypes Using Chlorophyll Fluorescence

Erkin Zakhidov, Sherzod Nematov and
Vakhobjon Kuvondikov

Additional information is available at the end of the chapter

http://dx.doi.org/10.5772/62232

Abstract

In this chapter, chlorophyll fluorescence in plant leaves of three genotypes of cotton cultivated in Uzbekistan and characterized at different degrees of drought tolerance is studied. The light and CO_2 responses of the chlorophyll fluorescence and the photosynthesis and possible mechanisms of adaptation of plants to moderate long-term drought are described. The chlorophyll fluorescence and various morpho-physiological indicators of well-watered and moderately drought-stressed cotton plants have been measured simultaneously over a long period of plant ontogenesis to establish direct correlations between them to estimate the magnitude of drought effect using fluorescence parameters. It is shown that determination of such correlations and their calibration by photoacoustic signals generated in plant leaves at application of low-frequency-modulated light may be used for monitoring of the drought tolerance of crops in the field.

Keywords: photosynthesis, chlorophyll fluorescence, cotton genotypes, drought effect

1. Introduction

Drought is an important environmental stress exerting a critical effect on plants that can reduce their productivity, on average, up to 50% [1]. Approximately one third of Earth's arable land all over the world suffers from chronic water deficiency for agriculture and by various estimations; in 2050s, this area can be doubled [2]. Particularly, in Central Asia, located mostly in desert zones, the first-limiting factor of crop yield is water deficit and the agriculture can be practiced only with additional irrigation. However, the irrational use of water resources of the region

for cotton production in the past has lead to an excessive soil salinization and to the exhaustion of its largest water resource—the Aral Sea. Therefore, revealing the adaptation potential of local agricultural crops to water deficit and creating their drought-tolerant genotypes are an important task: this would allow, in particular, to obtain higher cotton yield and quality in conditions of limited water resources and to improve local environment by stopping desertification of the region.

Creating drought-tolerant genotypes of agricultural crops is complicated because the lack of systematic knowledge on physiological parameters reflecting the genetic potential for improved productivity under conditions of water deficiency. The effect of drought stress on the photosynthetic performance and drought-induced morpho-physiological, biochemical and biophysical changes in various plant species have been extensively studied; stomatal and non-stomatal limitations to photosynthesis, their role and possible mechanisms have been suggested [3]. These studies have shown that photosynthetic performance is very informative and sensitive indicator of stress effects of drought in plants.

Nowadays, the methods of chlorophyll fluorescence control along with the classical measurements of photosynthesis based on gas-exchange analysis are widely used by agronomists in monitoring of crops and their response to environmental stresses [4]. Revealing physical characteristics of chlorophyll fluorescence in plant leaves and employing achievements in laser physics, optoelectronics and computer technologies allowed developing a variety of efficient experimental methods and easy to use devices for measuring such key fluorescence parameters, as a maximal (saturated) and a minimal (dark) fluorescence, a prompt and a delayed fluorescence, a kinetics of induction of chlorophyll fluorescence and their relationship with quantitative indicators of photosynthesis in plants [5, 6]. These methods are fast, noninvasive and estimate the photosynthetic performance of plants even under mid-day solar radiation, and portable devices commercially manufactured on their basis determine the parameters of plant photosynthetic performance with multiple replication of measurements and recording the results in a memory for subsequent statistical processing using relevant computer programs [7, 8].

Here, the results of long-term effect's study of drought on the chlorophyll fluorescence and morpho-physiological indicators of cotton plants grown under field conditions are described. Literature on researches concerning to mechanisms of stress effect of drought on photosynthesis in plants are analyzed. The long-term effect of drought on cotton plants has been studied during the key period of their ontogenesis — in flowering and maturing stages from last July to last September by simultaneously measuring indicated parameters in well-watered and moderately drought-stressed plants. Correlations between the chlorophyll fluorescence and morpho-physiological indicators (leaf blade area and thickness, relative water content and transpiration) have been defined in three genotypes of cotton with different degrees of drought tolerance.

Comparative measurements of the operating quantum efficiency of photochemistry in Photosystem II, Φ_{PSII}, and its changes during the day time in well-watered and moderately drought-stressed plants have shown that in contrary to the widely accepted idea on tight links between Φ_{PSII} and the quantum efficiency of CO_2 uptake [9], and decline of photosynthesis in

http://dx.doi.org/10.5772/62232

plants under drought stress [10, 11], the sustainable higher values of Φ_{PSII} in drought-stressed plants have been registered [12, 13]. It was also defined considerable changes in morpho-physiological parameters under drought stress.

For better understanding of mechanisms of such an unexpected increase in the quantum efficiency of primary photochemistry, the chlorophyll fluorescence was measured simultaneously with the gas-exchange analysis at different light intensities and CO_2 concentrations [14]. Drought-stressed plants displayed elevated rates of photorespiration playing a protective role in conditions of water deficit, when plants can gradually adapt to such a stress, regulating various phases of photosynthetic reactions.

The measurement of photoacoustic waves generated in plant leaves on application of a modulated light simultaneously with the chlorophyll fluorescence allowed us to determine quantitatively the magnitude of photosynthetic oxygen evolution. This has an especial importance in the case of elevated photorespiration, when tight links between Φ_{PSII} and the quantum efficiency of the CO_2 uptake is broken. Photobaric component of the photoacoustic waves at low-modulation frequencies (~10 Hz) originated in the photosynthetic oxygen evolution process [15, 16], as quantitative indicator of the photosynthetic performance of plants, may be used for the calibration of the values Φ_{PSII} determined in chlorophyll fluorescence measurements.

In this way, the chlorophyll fluorescence parameters measured simultaneously with morpho-physiological indicators of plants proposed for monitoring of the drought tolerance of various cotton genotypes in the field that can be applied in the practice of a plant breeding.

2. Materials and methods

Three local genotypes of cotton (*Gossypium hirsutum L.*), Navbakhor, Liniya-49, and Gulsara were grown on the two levels of irrigation: under well-watered and moderately drought-stressed conditions [17] at the experimental cotton station of the Institute of Genetics and Plant Experimental Biology, Uzbekistan Academy of Sciences, Tashkent (41°10′N, 69°07′E, 400 m above sea level), in 2013–2014. All plants were sown on 10th April with the scheme of 90 cm (distance between rows) × 20 cm (distance between plants) × 1 (amount of plants per hole). Thousand plants of each genotype and water treatment were grown in 4 rows, 250 plants each. During the entire period of ontogenesis, well-watered plants were irrigated 5 times: 1–before flowering, 3–during flowering-maturing, and 1–in maturing stages, and the drought-stressed plants–3 times: in the scheme 1—2—0. Thus, moderate drought stress was induced in the most sensitive stage of cotton plants—in mass flowering-maturing period. During this period, rainfall did not occur. All other growth conditions, including content of nutrients in soil, were the same.

The chlorophyll fluorescence was measured in attached leaves by using portable chlorophyll fluorometer Mini-PAM (Walz, Effeltrich, Germany) allowing up to 3000 measurements in the field without battery recharging [7]. The Mini-PAM fluorometer measures the chlorophyll

fluorescence parameters even under mid-day solar radiation by means of simultaneous application of a CW measuring light and saturating light flashes. Measurements were carried out in the early morning, from 7.00 to 8.00, on the third, matured leaves with 10-fold replication. In most of the experiments, the operating quantum efficiency of primary photochemistry, $\Phi_{PSII} = F_V' / F_M' = (F_M' - F_S') / F_M'$ (F_M'—is a maximum and F_S'—a steady state levels of fluorescence at any arbitrary moment of a leaf illumination [18]), was determined as an indicator of the photosynthetic performance. For calculation of this parameter, measurements of a dark fluorescence and, consequently, dark adaptation of leaves were not a need [19, 20], which essentially simplified field experiments. The maximum fluorescence was measured at application of saturating light flashes with duration 0.8 s and photosynthetic photon flux density (PPFD) 8000 μmol m^{-2} s^{-1}. However, in some experiments, the photochemical quenching factor $q_P = (F_M' - F') / (F_M' - F_0')$ and the non-photochemical quenching $NPQ = F_M / F_M' - 1$, characterizing efficiencies of photochemical utilization and non-photochemical losses of the absorbed light energy accordingly, were also determined. The electron transport rate $ETR = \Phi_{PSII} \times PAR \times 0.5 \times \alpha$ was controlled as an indicator of activity of the photosynthetic electron transport chain; here photosynthetic active radiation (PAR) is the solar radiation intensity in spectral range 400–750 nm expressed as PPFD in μmol m^{-2} s^{-1}, and α is leaf absorption. In general, it is assumed that α = 0.85 and a ratio $PSII : PSI = 1:1$. PAR intensities were controlled by portable luxometer Yu-116 with a dielectric multilayer filter filtering out PAR from the whole solar radiation.

The gas-exchange measurements were carried out using photosynthesis analyzer LI-6400 (Licor, USA) at temperature 24°C [21]. The curves of CO_2 response were measured in leaves of both water treatments by means of gradual lowering of the external CO_2 concentration, from 400 μmol mol^{-1} to 0 μmol mol^{-1} at PPFD 1000 μmol m^{-2} s^{-1}, and the light response curves—at ambient CO_2 concentration with step-by-step increasing of PPFD from 0 μmol m^{-2} s^{-1} to 2000 μmol m^{-2} s^{-1}. The light and CO_2 responses of the chlorophyll fluorescence and the photosynthesis were measured after adaptation of leaves to each value of PPFD and CO_2 concentration during 15 min. The operating values of the minimum fluorescence under continuous illumination during the measurements, F'_0, were calculated according to [22] using the equation $F_0' = F_0 / (F_V / F_M + F_0 / F_M')$.

Relative water content and transpiration of plant leaves were determined by their weighting [23]. In addition, a leaf thickness and a leaf blade area were also measured in each cotton genotype. For estimation of the magnitude and diurnal variations of photoinhibition, the values of Φ_{PSII} have been consistently measured simultaneously in both well-watered and drought-stressed plants every hour during 24 h.

Photoacoustic spectrometer of special design with ~1 cm^3 sample chamber having higher sensitivity at low (10–250 Hz) frequencies of light modulation [24] has been used for measuring photoacoustic characteristics of plant leaves. The sources of a CW measuring light and saturating light flashes of the spectrometer were a semiconductor LED (650 nm, 20 mW) and a halogen lamp (400–700 nm, 20 W) with a mechanical chopper, respectively. Intensity of the measuring light was supported as 50–100 μmol m^{-2} s^{-1} and intensity of the saturating flashes

http://dx.doi.org/10.5772/62232

did not exceed 2500 μmol m^{-2} s^{-1}. The photobaric component was selected from the total photoacoustic waves generated in a plant leaf at application of low-frequency (10 Hz)-modulated light by recording quadrature signal from a lock-in amplifier [25].

3. Effect of drought to photosynthesis

Drought stress is primarily affected to photosynthetic performance of plants. The long-term drought effect is expressed as reducing/delaying of a plant growth and development, premature leaf senescence, and related reduction in a crop productivity [26, 27]. The dispute, what, mainly, limits photosynthesis under conditions of water deficiency: stomata closure or impairment of the metabolism is long enough [28, 29], but in the past decade, closure of stomata was perceived by experts as the predominant factor in mild and moderate drought stress [30].

The first response of a plant to onset of drought stress is the stomata closure and associated reduction of the relative water content of leaves and intracellular CO_2 concentration, C_i [3, 31]. This, in turn, causes decrease in a leaf turgor and a water potential [32]. In such a condition, gas-exchange analysis in plant leaves would be an informative technique for assessment of stomatal limitation to CO_2 assimilation.

Non-stomatal mechanisms of the photosynthesis limitation under long-term or severe drought in the soil include changes in chlorophyll synthesis [33], structural changes in photosynthetic apparatus and depressing the Calvin cycle enzymes activities, which reduces crop yield [34] and decline in Rubisco activity [35, 36].

Short-term or mild drought-induced non-stomatal limitations to photosynthesis have smaller magnitude than stomatal ones. Closure of stomata and limited access of CO_2 bring about reduced utilization of the energy of electron transport, and, accordingly, over-excitation of the plant photosynthetic apparatus. This, accordingly, increases the susceptibility of the system to photo-damage. Accumulation of singlet oxygen or superoxide radicals, when a dynamic balance between producing of such reactive substances and functioning of the plant antioxidant defense system is broken, may cause destruction of photosynthetic proteins and membrane lipids [37, 38].

Reduced rate of transpiration, especially at higher ambient temperatures, increases the heat accumulation and relevant increase in leaf temperature. The latter can also cause decline of the plant photosynthetic performance under drought [30].

A number of experiments have shown that the closure of stomata is controlled, mostly, by reducing soil water content, but not leaf water status. This suggests response of stomata to a chemical signal from roots, i.e. presence of abscisic acid produced by dehydrating roots, while a leaf water status is constant [39, 40]. The same time it means that the efficient way to control the stomatal conductance is to change the soil water content even preserving constant level of leaf water status.

Activity of the photosynthetic electron transport chain is rigidly regulated by the availability of CO_2 in the chloroplast, limited by closure of stomata under drought stress [41]. Leaf

dehydration leads to shrinking of cells and accordingly reducing of their volume. This causes an increase in the internal viscosity of the cell contents, and interaction between proteins and, consequently, their aggregation and denaturation [42].

Comparison of the results from different studies is quite difficult due to the essential variations in responses of the stomatal conductance and photosynthesis to changes of leaf water potential and relative water content in different genotypes [3]. It is considered as well established that drought-induced stomata closure declines the net photosynthesis in all plant species, though, with different magnitudes. That is why comparative studies of the photosynthetic parameters in different plant genotypes under drought stress may provide an important information concerning to the photosynthetic performance and adaptation potential of plants to moderate long-term drought.

Analysis of the chlorophyll fluorescence and photosynthesis in plant leaves has revealed that in conditions favorable for photosynthesis, i.e. lack of environment stresses, at low light intensities, etc. when alternative mechanisms of light energy utilization did not required, the quantum efficiency of photochemistry is tightly linked with quantum efficiency of CO_2 fixation [9], and the photosynthesis rate is not sensitive to mild under drought stress [10, 43]. In this condition, photorespiration increases and its magnitude depends on the light intensity [44]. In a number of researches, the reduction in Φ_{PSII} has been observed under long-term drought, which has been attributed, mostly, to reducing of photochemistry and, in less extent, to dissipative processes in the plant photosynthetic apparatus. However, in some other researches, the increasing Φ_{PSII} has been observed in plants exposed to moderate long-term drought [12, 13]. Such contradiction in behavior of Φ_{PSII} may be explained by a heterogeneity of the photosynthetic performance across the leaf blade [14, 45]. Thus, simultaneous analysis of chlorophyll fluorescence and photosynthesis in plant leaves may reveal mechanisms and magnitude of protective changes in plants under drought stress, and correlations between changes in chlorophyll fluorescence parameters and morpho-physiological indicators, traditionally used for estimation of drought tolerance of plants, may be used as an effective instrument for monitoring of plants in the field.

4. Comparative measurements of Φ_{PSII} in different cotton genotypes

The operating quantum efficiency of photochemistry, Φ_{PSII}, has been determined simultaneously in well-watered and moderately drought-stressed plants of three genotypes of cotton cultivated in Uzbekistan with the aim of estimating the magnitude of the effect of drought on the photosynthetic performance and monitoring its changes during a key period of the ontogenesis—in flowering and maturing stages from last July to last September [12, 46]. Figure 1 shows the results of this experiment. The dates of measurements are shown on the X-axis. Stressed plants of all cotton genotypes display higher values of Φ_{PSII} in comparison with well-watered plants. Moreover, in the drought-tolerant plants of Navbakhor, this increase was maximal (up to 15% over the most period of measurements), while in Gulsara characterized by lower drought tolerance, it was minimal (approximately 2%). And, in Liniya-49 having an

http://dx.doi.org/10.5772/62232

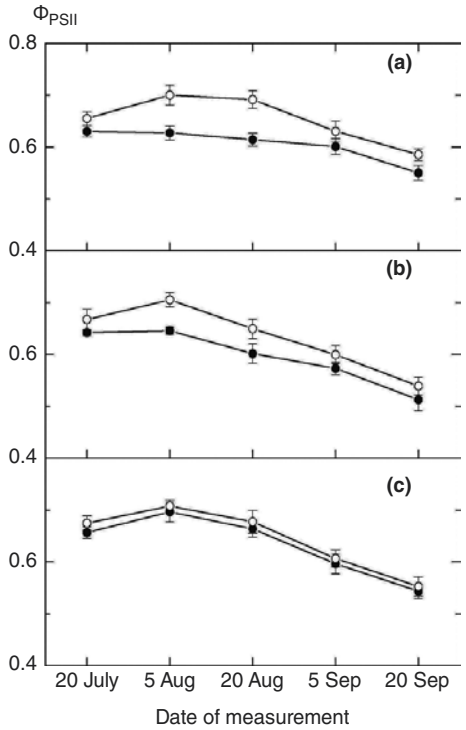

Figure 1. The changes in Φ_{PSII} in leaves of three genotypes of cotton: Navbakhor (a), Liniya-49—(b) and Gulsara—(c) growing in well-watered (•) and moderately drought-stressed (○) conditions during a long period of their ontogenesis.

intermediate degree of drought tolerance had intermediate values for differences in Φ_{PSII}. Irrigation of the drought-stressed plants on 10th September shortened this difference, though, with different extent in different genotypes.

Measurements of morpho-physiological indicators in plants of all genotypes have demonstrated considerable reduction in leaf relative water content and of leaf blade expansion and increase in leaf thickness under long-term drought stress. These changes are presented in Table 1. It is seen that in the most drought-tolerant cotton genotype Navbakhor, these changes are maximal, and in Gulsara having lower drought tolerance, these are minimal. Correlations between Φ_{PSII} and these morpho-physiological indicators have been defined in all three genotypes, but with different extent. The last may be attributed to the possibility of other protective reactions in plants affected to long-term drought stress [47].

Leaf transpiration was lower in drought-stressed plants than in well-watered plants of all genotypes for 5–15% (not shown), which may be considered as typical for the field-grown cotton plants [48]. However, diurnal changes in transpiration of plants were much more than differences between two treatments, therefore reliable correlations between changes in the

Morpho-physiological indicators	Water treatment	Cotton genotypes		
		Navbahor	Liniya-49	Gulsara
Relative water content, %	Well-watered	79.4	78.8	77.4
	Drought-stressed	72.5	74.4	74.3
	Percentage of the difference	8.7%	5.6%	5.0%
Leaf blade area, m^2	Well-watered	71.1	77.7	80.9
	Drought-stressed	63.1	73.0	77.1
	Percentage of the difference	11.3%	6.1%	4.7%
Relative leaf thickness, g m^{-2}	Well-watered	0.853	0.974	0.987
	Drought-stressed	0.981	1.09	1.052
	Percentage of the difference	15.0%	11.9%	6.6%

Table 1. Morpho-physiological indicators of the well-watered and moderately drought-stressed cotton genotypes.

transpiration and the chlorophyll fluorescence parameters under drought stress were not established.

For determination of changes in the photosynthetic performance of plants under drought stress and kinetics of photoinhibition over the day, the quantum efficiency of photochemistry has been measured hourly during 24 h. Figure 2 shows such dependencies measured in well-watered and drought-stressed plants of Navbakhor. As shown in previous figure, in the drought-stressed plants, Φ_{PSII} is higher than in well-watered plants during all the day, including a night time. In addition, decline of Φ_{PSII} in mid-day in the drought-stressed plant is smaller but occurs for longer time [12]. Such a photoinhibitory depression of the primary photochemistry under high-intensity solar radiation is characterized by various components with different relaxation periods [49, 50]. Obviously, adaptive changes in the structure and func-

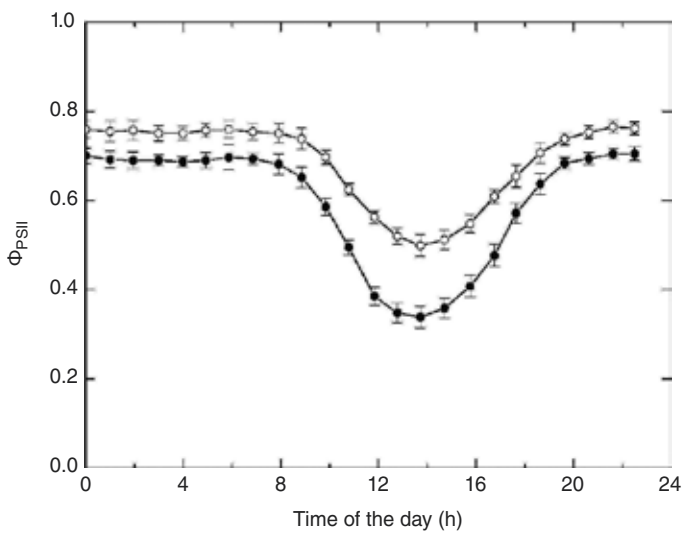

Figure 2. Diurnal changes in Φ_{PSII} measured in leaves of the cotton genotype Navbakhor grown in well-watered (•) and moderately drought-stressed (○) conditions in the field.

http://dx.doi.org/10.5772/62232

tioning of the plant photosynthetic apparatus under moderate long-term drought may bring about depressing, mainly short-period, components of photoinhibition and its long-period components will dominate in drought-stressed plants [51]. Such changes in the proportion of different components of photoinhibition results in decreasing of the amplitude and reshaping of the form of diurnal changes Φ_{PSII} as it is shown in Figure 2. It should be noted that difference in values of Φ_{PSII} measured in well-watered (0.34) and drought-stressed (0.48) plants at mid-day, 0.14, is considerably higher than those in other periods of the day. This fact may be considered as enhancing of photorespiration that may contribute in Φ_{PSII} only as a prompt component.

Therefore, protective response of cotton plants to drought stress expressed in photosynthetic indicators is the increase in quantum efficiency of primary photochemistry, in morphology is the increase of leaf thickness with decreasing leaf blade expansion and in physiology is the reduce in transpiration. If reduce in the leaf blade expansion and transpiration may be explained logically by considerations of minimizing the moisture loss [47], increase of Φ_{PSII} looks as somehow contradictory with the literature data: at the onset of drought stress, the plant should response by reducing photosynthesis to protect the photosynthetic apparatus [52]. At constant values of efficiency of alternative ways of energy utilization, this has to bring about lower quantum efficiency of photochemistry. Then, the excessive energy of absorbed light may be utilized by enhancing the activity of an alternative channel—photorespiration. Lastly, in C3 plants could be significant, particularly in cotton, which typical growth conditions are associated with higher temperatures and water deficiency. At present, protective role of photorespiration under environmental stresses are poorly studied and published researches on this matter is very minor [53].

Thus, cotton genotypes with different degrees of drought-tolerance studied displayed specific changes in the chlorophyll fluorescence parameters, as well as in morpho-physiological indicators under long-term drought stress. Diurnal curves of Φ_{PSII} variations in well-watered and moderately drought-stressed plants provide information on the magnitude and different time components of photoinhibition developed under high-intensity solar radiation.

Photoacoustic waves generated in plant leaves at application of modulated light have been studied for precise control of the photosynthetic performance and quantitative estimation of the photosynthetic oxygen evolution. Photobaric component of the photoacoustic waves related to photosynthetic evolution of oxygen has been measured in the photoacoustic cell of special design with a small measuring chamber (~1 cm^3) in lock-in amplifier by selecting quadrature signal at low frequencies [15, 54]. Figure 3 shows kinetics of changes of the photoacoustic signal from the well-watered (relative water content 100%) and short-term dehydrated (relative water content 65%) leaves of the cotton genotype Navbakhor, generated at application of low frequency (10 Hz) measuring light. It is shown from the figure that the steady-state photoacoustic signal considerably declines at application of additional CW light of high intensity (~2500 μmol m^{-2} s^{-1}) to plant leaf, which saturates photosynthetic oxygen evolution process and, accordingly, excludes periodic changes of pressure in the measuring chamber, which is the photobaric wave. Therefore, relative change in the photoacoustic signal (ratio of amplitude of change to the total photoacoustic signal) may be used as a measure of

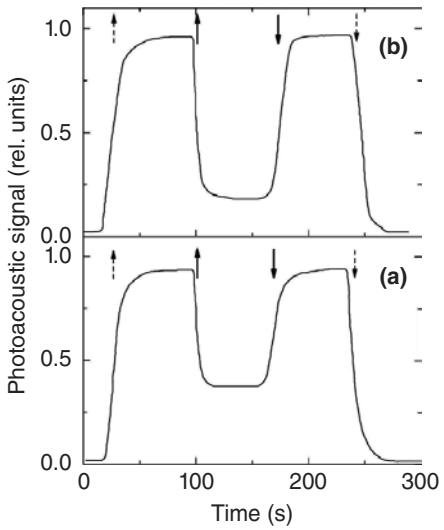

Figure 3. Induction curves of the photoacoustic signal generated in leaves of the cotton genotype Navbakhor with relative water content 100% (a) and 65% (b). Arrows up and down show switching on and off, respectively, the measuring (dashed arrows) and saturating (bolt arrows) lights.

the photosynthetic oxygen evolution. In experiments, before measuring photoacoustic signals, the plant leaves were adapted to dark for 10 min. After reaching the steady-state photoacoustic signal, the saturating CW light was applied, which causes decrease in the photoacoustic signal for 0.82 (Figure 3a) in the well-watered leaf and for 0.50 (Figure 3b) in the dehydrated leaf. Thus, the photoacoustic measurements have shown that photosynthetic oxygen evolution in plant leaves depresses in short time water deficiency: decrease in the relative water content for 45% causes decrease of photosynthetic activity 1.5 times. Simultaneous measurements of Φ_{PSII} in these two samples displayed decline of the operative quantum efficiencies of photochemistry in the same ratio (0.75:0.51). However, the advantage of photoacoustic measurements is evident in the case of significant level of photorespiration in plant leaves, when direct correlation between Φ_{PSII} and the net photosynthesis is disturbed (see the next section).

5. Simultaneous measurements of ETR and photosynthesis in well-watered and moderately drought-stressed cotton plants

Electron transport rate (ETR) and photosynthesis in cotton plants of both water treatments have been measured simultaneously for revealing the role and magnitude of alternative channels for utilization of the energy of electron transport and obtaining new insights into mechanisms of adaptation of the plant photosynthetic apparatus to long-term drought stress. Indicated photosynthesis parameters have been determined at CO_2 concentrations 0–400 μmol mol^{-1} under constant PPFD of 1000 μmol m^{-2} s^{-1} and under PPFD of 0–2000 μmol m^{-2} s^{-1} at ambient CO_2 concentration in plants of genotype Navbakhor (Figure 4). It is seen that the rate

http://dx.doi.org/10.5772/62232

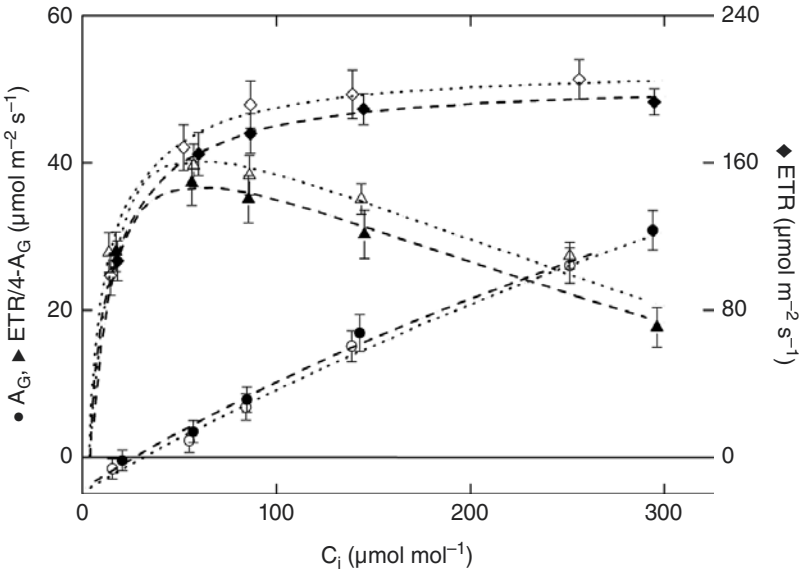

Figure 4. Response of the photosynthesis, A_G, electron transport rate, ETR, and photorespiration, estimated as ETR/4-A_G, to CO_2 concentration in leaves of the cotton genotype Navbakhor grown in well-watered (closed symbols) and moderately drought-stressed (open symbols) conditions in the field.

of CO_2 assimilation (A_G) increases linearly with increase of intracellular CO_2 concentration, C_i, while the dependence ETR *versus* C_i is non-monotonic: sharp increase of ETR with increase of CO_2 concentration at $C_i < 100$ µmol mol^{-1}, further saturates on the level of ETR ~200 µmol m^{-2} s^{-1}. The measurements were carried out in the field, early morning, from 7.00 to 8.00 at temperature 22–24°C.

At higher light intensities and/or low CO_2 concentrations, the plant photosynthetic apparatus cannot cope with the coming light energy and a portion of this energy has to be utilized through alternative channels; photorespiration or some other processes, including Mehler reaction, may play a role of a sink for electrons transported through the photosynthetic electron transport chain [55]. In most of the cases, excluding severe drought stress, the photorespiration considered as prevailing mechanism of utilization of such an excessive light energy [56]. The magnitude of this energy utilization may be estimated by comparing ETR and photosynthesis. Assuming that assimilation of one molecule CO_2 requires four electrons transported through the chain, the amount of photorespiration may be defined by dividing ETR by four and subtracting the photosynthesis [55]. By calculating this way, values of the photorespiration rate are also presented in Figure 4: photorespiration increases sharply at low concentrations up to 100 µmol mol^{-1}, and further slowly drops with increase of CO_2 concentration. The fact seems reasonable, because CO_2 is a product of photorespiration. Figure 4 shows that drought stress noticeably increases ETR and slightly decreases the photosynthesis in cotton plant leaves. As a result, the photorespiration in drought-stressed leaves calculated as above is considerably higher than in well-watered plants, especially at higher CO_2 concentrations. In

Water treatment	R_D	Φ_{PSII}
Drought-stressed	3.8 ± 0.5	0.67 ± 0.023
Well-watered	5.2 ± 0.6	0.62 ± 0.021

Table 2. "Dark"" respiration, R_D, and operating quantum efficiency of primary photochemistry in Photosystem II, Φ_{PSII}, measured in leaves of well-watered and moderately drought-stressed cotton genotype Navbakhor.

addition, the effect of drought stress to "dark" respiration has been measured in plants of both water treatments simultaneously with the quantum efficiency of primary photochemistry (Table 2). The "dark" respiration, as an additional source of bioenergy necessary for supporting vital biochemical reactions in plants, was considerably higher in drought-stressed plants. The same occurred with the quantum efficiency of photochemistry, but with less magnitude.

The light response of ETR and photosynthesis measured in plants of Navbakhor of the two treatments was similar to the CO_2 response (Figure 5). At low light intensities, most of the energy from the electron transport is utilized in photochemical reactions, and with increasing of light intensity, more and more portion of this energy is spent for photorespiration. However, the increase in ETR induced by drought stress in light response was less expressed than that in CO_2 response, particularly at higher intensities. Considerable variations of photosynthesis in different replications comparable with its difference between the treatments may be attributed to diurnal changes of stomatal conductance, g_s, which can induce relevant changes in photosynthesis [57]. In view of tightly links between stomatal conductance and photosynthesis, and efficiency of primary reactions of photosynthesis remains constant, the changes in stomatal conductivity during the day may bring about considerable changes in photosynthesis

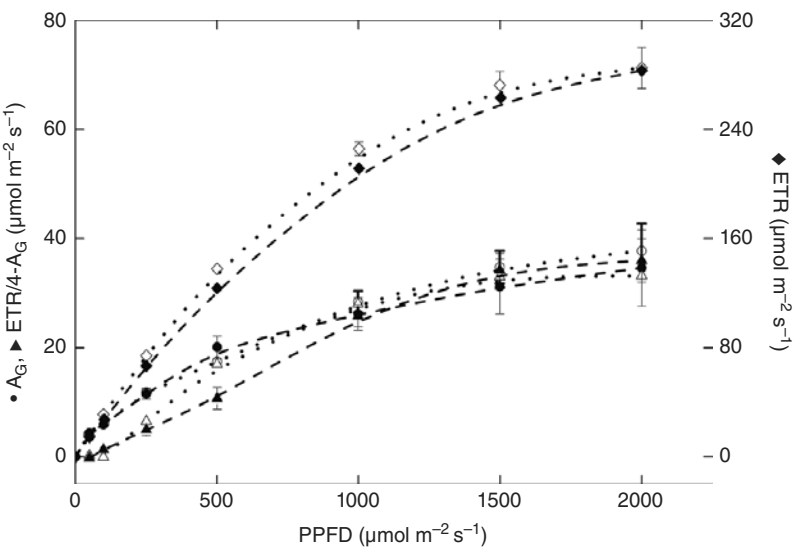

Figure 5. Response of the photosynthesis, A_G, electron transport rate, ETR, and photorespiration, estimated as ETR/4-A_G, to light intensity (PPFD) in leaves of the cotton genotype Navbakhor grown in well-watered (closed symbols) and moderately drought-stressed (open symbols) conditions in the field.

http://dx.doi.org/10.5772/62232

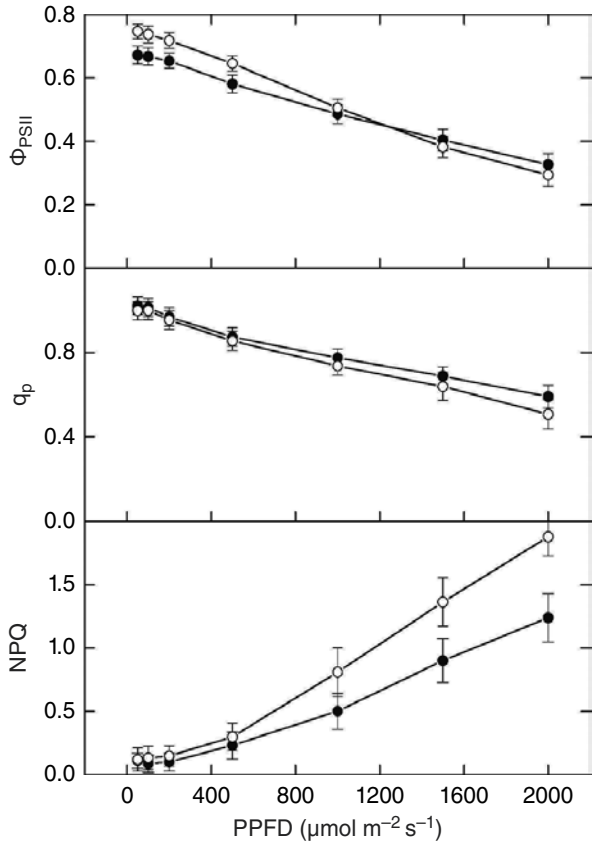

Figure 6. Light response of the chlorophyll fluorescence parameters: quantum efficiency of photochemistry in Photosystem II, Φ_{PSII}, photochemical quenching factor, q_p, and non-photochemical quenching, NPQ, in leaves of the cotton genotype Navbakhor grown in well-watered (closed symbols) and moderately drought-stressed (open symbols) conditions in the field.

[58]. In this case, the sum of photosynthesis and photorespiration, as measured using the ETR/4, is not constant, but varies during the day.

In the Figure 6 are shown the light response of the three key fluorescence parameters, operating quantum efficiency of photochemistry, Φ_{PSII}, photochemical quenching factor, q_P, and non-photochemical quenching, NPQ, determined in leaves of well-watered and moderately drought-stressed cotton genotype Navbakhor. As shown from the figure, at low and moderate light intensities, PPFD < 800 μmol m^{-2} s^{-1}, Φ_{PSII} in drought-stressed plants was higher than in well-watered plants, whereas q_P was the same and near to its maximum. However, with increase of light intensity, Φ_{PSII} and q_P decrease with increments, which are higher in drought-stressed plants. And finally, at PPFD > 800 μmol m^{-2} s^{-1}, both Φ_{PSII} and q_p become lower in drought-stressed plants in comparison with well-watered plants. What concerns to NPQ, it is negligibly low at low intensities in both treatments but increases rapidly at moderate and high

intensities and under drought stress. So, increasing light intensity activates photosynthetic performance of plants. At low and moderate intensities, when the plant photosynthetic apparatus copes with coming light energy, the efficiency of photosynthetic conversion of light energy is very high, when photochemical quenching factor is near to its maximum and non-photochemical quenching is negligibly low. Long-term drought stress due to stomatal and non-stomatal limitations to photosynthesis induces enhancement of photorespiration as an alternative sink for transported electrons in reaction centers of photosynthesis. However, further increase of light intensity increases non-photochemical quenching, and in drought-stressed plants, it is higher than in well-watered ones. This causes faster decrease of Φ_{PSII} and q_p in drought-stressed plants.

Experiments with the measurement of chlorophyll fluorescence and the gas-exchange in different cotton genotypes showed that under drought stress, CO_2 uptake slightly decreases, while ETR increases considerably. Simultaneously measuring these two parameters of photosynthesis allowed us to estimate the magnitude of photorespiration in the plant leaves, assuming that changes in the ETR/4-A_G reflect the changes in photorespiration. Photorespiration increases with increasing light intensity and decreasing CO_2 concentration. Moderate drought stress noticeably increases the rate of photorespiration, which can be considered as a characteristic response of C3 plants to a drought [44].

Leaves of drought-stressed cotton plants displayed higher Φ_{PSII} and photorespiration at low and moderate light intensities, and non-photochemical quenching, NPQ, was stronger in drought-stressed plant than that in well-watered one. Obviously, higher levels of photorespiration in plant leaves during the drought stress exerts the "pressure" to the rate of electron flow and makes Photosystem II to operate with higher efficiency.

6. Conclusion

The photosynthetic apparatus of plants supports higher performance of electron transport chain through enhancement of quantum efficiency of photochemistry in Photosystem II under drought stress. The accumulated energy in this state of over-excitation may be utilized in enhanced photorespiration. This protective reaction of the plant photosynthetic apparatus to drought stress has different magnitude depending on its drought tolerance. Field measurements of the chlorophyll fluorescence parameters simultaneously with morpho-physiological indicators of the cotton genotypes studied have displayed direct correlations between these parameters under drought stress. These correlations together with possible calibration of chlorophyll fluorescence parameters by photoacoustic characteristics determined at application of low-frequency-modulated light to plant leaves give new opportunities in monitoring of drought tolerance of various cotton genotypes in the field.

Acknowledgements

The authors thank Dr. A. Massacci from the Institute of Agro-environmental and Forest Biology, CNR, Roma, Italy, and Dr. Y. Fracheboud and Dr. J. Leipner from the Institute of Plant Sciences, ETH, Zurich, Switzerland, for fruitful discussions on the photorespiration mechanisms in plants.

Author details

Erkin Zakhidov, Sherzod Nematov and Vakhobjon Kuvondikov

*Address all correspondence to: ezakhidov@hotmail.com

Institute of Ion-Plasma and Laser Technologies, Uzbekistan Academy of sciences, Tashkent, Uzbekistan.

References

[1] Wang W, Vinocur B, Altman A . Plant responses to drought, salinity and extreme temperatures: towards genetic engineering for stress tolerance. Planta. 2003;218:1-14. DOI: 10.1007/s00425-003-1105-5

[2] Vicente-Serrano SM, Gouveiab C, Camarero JJ, Begueríae S, Trigob R, López-Morenoa JI, Azorín-Molinaa C, Pashoa E, Lorenzo-Lacruza J, Revueltoa J, Morán-Tejedaa E, Sanchez-Lorenzog A . Response of vegetation to drought time-scales across global land biomes. Proceedings of the National Academy of Sciences. 2013;110:52–57. DOI: 10.1073/pnas.1207068110

[3] Cornic G, Masacci A. Leaf photosynthesis under drought stress. In: Baker NR, editor. Photosynthesis and Environment. The Netherlands: Kluwer Academic Publishers; 1996. p. 347–366. DOI: 10.1007/0-306-48135-9_14

[4] Murchie EH, Lawson T. Chlorophyll fluorescence analysis: a guide to good practice and understanding some new applications. Journal of Experimental Botany. 2013;64:3983–3996. DOI: 10.1093/jxb/ert208

[5] Schreiber U, Bilger W, Hormann H, Neubauer C. Chlorophyll fluorescence as a diagnostic tool: basics and some aspects of practical relevance. In: Raghavendra AS, editor. Photosynthesis: a comprehensive treatise. Cambridge, UK: Cambridge University Press; 2000. p. 320–335. ISBN: 9780521784443.

[6] Strasser RJ, Tsimilli-Michael M, Srivastava A. Analysis of chlorophyll fluorescence transient. In: Papageorgiou CG, Govingee, editors. Chlorophyll fluorescence: A

signature of photosynthesis. The Netherlands: Kluwer Academic Publishers; 2004. p. 321–362. DOI: 10.1007/978-1-4020-3218-9_12

[7] Heinz Walz GmbH (Germany). PAM Chlorophyll Fluorometers [Internet]. 2015. Available from: http://www.walz.com/products/chl_p700/mini-pam-II/introduction.html [Accessed: 2015-12-17].

[8] Hansatech Instruments Ltd. (Norfolk, England). Handy-PEA and Pocket-PEA Chlorophyll Fluorometers [Internet]. 2006. Available from: http://hansatech-instruments.com/products/introduction-to-chlorophyll-fluorescence [Accessed: 2015-12-17]

[9] Genty B, Briantais JM, Baker NR. The relationship between the quantum yield of photosynthetic electron transport and quenching of chlorophyll fluorescence. Biochimica et Biophysica Acta. 1989;990:87–92. DOI: 10.1016/S0304-4165(89)80016-9

[10] Ennahli S, Earl HJ. Physiological limitations to photosynthetic carbon assimilation in cotton under water stress. Crop Science. 2005;45:2374–2382. DOI: 10.2135/cropsci2005.0147

[11] Inamullah, Isoda A. Adaptive responses of soybean and cotton to water stress II. Changes in CO2 assimilation rate, chlorophyll fluorescence and photochemical reflectance index in relation to leaf temperature. Plant Production Science. 2005;8:131–138. DOI: 10.10.1626/pps.8.13112

[12] Khabibullaev PK, Zakhidov EA, Zakhidova MA, Kasymdzhanov MA, Nematov SQ, Abdukarimov AA, Nabiev SM, Saakova NA, Stamp P, Fracheboud I. Evaluation of the effects of drought on cotton plants using characteristics of chlorophyll fluorescence. Doklady Biological Sciences. 2003;392:442–444. DOI: 10.1023/A:1026144325526

[13] Pettigrew WT. Physiological consequences of moisture deficit stress in cotton. Crop Science. 2004;44:1265–1272. DOI: 10.2135/cropsci2004.1265

[14] Massacci A, Nabiev SM, Pietrosanti L, Nematov SK, Chernikova TN, Thor K, Leipner J. Response of the photosynthetic apparatus of cotton (*Gossypium hirsutum*) to the onset of drought stress under field conditions studied by gas-exchange analysis and chlorophyll fluorescence imaging. Plant physiology and biochemistry. 2008;46:189–195. DOI: 10.1016/j.plaphy.2007.10.006

[15] Herbert S, Han T, Vogeman T. New applications of photoacoustics to the study of photosynthesis. Photosynthesis Research. 2000;66:13–31. DOI: 10.1023/A:1010788504886

[16] Hou HJM, Mauzerall D. Listening to PS II: Enthalpy, entropy, and volume changes. Journal of Photochemistry and Photobiology. B: Biology. 2011;104:357–365. DOI: 10.1016/j.jphotobiol.2011.03.007

[17] Loka DA, Oosterhuis DM, Ritchie GL. Water-deficit stress in cotton. In: Kole C, Michler C, Abbott AG, Hall TC, editors. Transgenic Crop Plants. Berlin—Heidelberg: Springer-Verlag; 2004. p. 37–72. DOI: 10.1007/978-3-642-04812-8_2

[18] Maxwell K, Johnson GN. Chlorophyll fluorescence—a practical guide. Journal of Experimental Botany. 2000;51:659–668. DOI: 10.1093/jexbot/51.345.659

[19] Fracheboud Y, Leipner J. The application of chlorophyll fluorescence to study light, temperature and drought stress. In: De Ell JR, Toivonen PMA, editors. Practical Applications of Chlorophyll Fluorescence in Plant Biology. Dordrecht: Kluwer Academic Publishers; 2003. p. 125–150. DOI: 10.1007/978-1-4615-0415-3_4

[20] Oxborough K, Baker NR. Resolving chlorophyll a fluorescence images of photosynthetic efficiency into photochemical and non-photochemical components: calculation of q_p and F_M'/F_0' without measuring F_0. Photosynthesis Research. 1997;54:135–142. DOI: 10.1023/A:1005936823310

[21] LI-COR Biosciences Inc. (Lincoln, NE, USA). Using the LI-6400 Portable Photosynthesis System. Version 5 [Internet]. 2004 . Available from: https://www.licor.com/env/products/photosynthesis [Accessed: 2015-12-17].

[22] Rosenqvist E, van Kooten O. Chlorophyll fluorescence: A general description and nomenclature. In: De Ell JR, Toivonen PMA, editors. Practical Applications of Chlorophyll Fluorescence in Plant Biology. Dordrecht: Kluwer Academic Publishers; 2003. p. 31–77. DOI: 10.1007/978-1-4615-0415-3_2

[23] Boyer JS, James RA, Munns R, Condon AG, Passioura JB. Osmotic adjustment may lead to anomalously low estimates of relative water content in wheat and barley. Functional Plant Biology. 2008;35:1172–1182. DOI: 10.1071/FP08157

[24] Zakhidov EA, Kokhkharov AM, Quvondikov VO, Nematov SQ, Saparbaev AA. Photoacoustic spectroscopy of thermal relaxation processes of solar energy in the photosynthetic apparatus of plants. Applied Solar Energy. 2012;42:62–68. DOI: 10.3103/S0003701X12010161

[25] Malkin S. Photoacoustic method in photosynthesis—monitoring and analysis of phenomena leading to pressure changes at light excitation. In: Amesz J, Hoff AJ, editors. Biophysical Technique in Photosynthesis. The Netherlands: Kluwer Academic Publishers; 1996. p. 191–206. DOI: 10.1007/0-306-47960-5_12

[26] Yordanov I, Velikova V, Tsonev T. Plant responses to drought, acclimation, and stress tolerance. Photosynthetica. 2000;38:171–186. DOI: 10.1023/A:1007201411474

[27] Wahid A, Rasul E. Photosynthesis in leaf, stem, flower and fruit. In: Pessarakli M, editor. Handbook of Photosynthesis. 2nd ed. Florida USA: CRC Press; 2005. p. 479–497. DOI: 10.1201/9781420027877.sec8

[28] Sharkey TD. Water stress effects on photosynthesis. Photosynthetica. 1990;24:651–661.

[29] Tezara W, Mitchell VJ, Driscoll SD, Lawlor DW. Water stress inhibits plant photosynthesis by decreasing coupling factor and ATP. Nature. 1999;401:914–917. DOI: 10.1038/44842

[30] Yokota A, Kawasaki S, Iwano M, Nakamura C, Miyake C, Akashi K. Citrulline and DRIP-1 Protein (ArgE Homologue) in Drought Tolerance of Wild Watermelon. Annals of Botany. 2002;89:825–832. DOI: 10.1093/aob/mcf074

[31] Mansfield TJ, Atkinson CJ. . Stomatal behaviour in water stressed plants. In: Alscher RG, Cumming JR, editors. Stress Responses in Plants: Adaptation and Acclimation Mechanisms. New York, USA: Wiley; 1990. p. 241–264. ISBN: 0-471-56810-4

[32] Ludlow MM, Muchow RC. A critical evaluation of traits for improving crop yields in water-limited environments. Advances in Agronomy. 1990;43:107–153. DOI: 10.1016/S0065-2113(08)60477-0

[33] Anjum F, Yaseen M, Rasul E, Wahid A, Anjum S. Water stress in barley (*Hordeum vulgare L.*). I. Effect on chemical composition and chlorophyll contents. Pakistan Journal of Agronomy Sciences. 2003;40:45–49. ISSN: 2076-0906

[34] Monakhova OF, Chernyadev II. Protective role of kartolin-4 in wheat plants exposed to soil drought. Applied Biochemistry. Micro+. 2002;38:373–380. DOI: 10.1023/A:1016243424428

[35] Bota J, Flexas J, Medrano H. Is photosynthesis limited by decreased Rubisco activity and RuBP content under progressive water stress? . New Phytology. 2004;162:671–681. DOI: 10.1111/j.1469-8137.2004.01056.x

[36] Parry MAJ, Andralojc PJ, Khan S, Lea PJ, Keys AJ. Rubisco activity: effects of drought stress. Annals of Botany. 2002;89:833–839. DOI: 10.1093/aob/mcf103

[37] Fu J, Huang B. Involvement of antioxidants and lipid peroxidation in the adaptation of two cool-season grasses to localized drought stress. Environment and Experimental Botany. 2001;45:105–114. DOI: 10.1016/s0098-8472(00)00084-8

[38] Reddy AR, Chaitanya KV, Vivekanandan M. Drought-induced responses of photosynthesis and antioxidant metabolism in higher plants. Journal of Plant Physiology. 2004;161:1189–1202. DOI: 10.1016/j.jplph.2004.01.013

[39] Morgan PW. Effects of abiotic stresses on plant hormone systems. In: Alscher RG, Cumming JR, editors. Stress Responses in plants: adaptation and acclimation mechanisms. New York, USA: Wiley; 1990. p. 13–146. ISBN: 0-471-56810-4

[40] Turner NC, Wright GC, Siddique KHM. Adaptation of grain legumes (pulses) to water-limited environments. Advanced in Agronomy. 2001;71:123–231. DOI: 10.1016/S0065-2113(01)71015-2

[41] Loreto F, Tricoli D, Di Marco G. On the relationship between electron transport rate and photosynthesis in leaves of the C4 plant Sorghum bicolor exposed to water stress, temperature changes and carbon metabolism inhibition. Australian Journal of Plant Physiology. 1995;22:885–892. DOI: 10.1071/PP9950885

[42] Hoekstra FA, Golovina EA, Buitink J. Mechanisms of plant desiccation tolerance. Trends in Plant Sciences. 2001;6:431–438. DOI: 10.1016/s1360-1385(01)02052-0

[43] Kitao M, Lei TT. Circumvention of over-excitation of PSII by maintaining electron transport rate in leaves of four cotton genotypes developed under long-term drought. Plant Biology. 2007;9:69–76. DOI: 10.1055/s-2006-924280

[44] Medrano H, Escalona JM, Bota J, Gulı´as J, Flexas J. Regulation of photosynthesis of C3 plants in response to progressive drought: stomatal conductance as a reference parameter. Annals of Botany. 2002;89:895–905. DOI: 10.1093/aob/mcf079

[45] Wise RR, Ortiz-Lopez A., Ort DR. Spatial distribution of photosynthesis during drought in field-grown and acclimated and nonacclimated growth chamber-grown cotton. Plant Physiology. 1992;100:26–32. DOI: 10.1104/pp.100.1.26

[46] Dubey RS. Photosynthesis in plants under stressful conditions. In: Mohammad P, editor. Handbook of Photosynthesis. New York, USA: CRC Press; 1997. p. 717–738. DOI: 10.1201/9781420027877.sec13

[47] Farooq M, Wahid A, Kobayashi N, Fujita D, Basra SMA. Plant drought stress: effects, mechanisms and management. In: Lichtfouse E, Navarrete M, Debaeke P, Veronique S, Alberola C, editors. Sustainable Agriculture. The Netherlands: Springer; 2009. p. 153–188. DOI: 10.1007/978-90-481-2666-8_12

[48] Isoda A, Wang P. Leaf temperature and transpiration of field grown cotton and soybean under arid and humid conditions. Plant Production Science. 2002;5:224–228. DOI: 10.1626/pps.5.224

[49] Zakhidov EA, Zakhidova MA, Kasymdzhanov MA, Kurbanov SS, Mirtadzhiev FM, Khabibullaev PK. Nonphotochemical Quenching of fluorescence in photosynthetic systems exposed to environmental stresses. Doklady Biochemistry and Biophysics. 2001;378:206–209. DOI: 10.1023/A:1011521514872

[50] Hodges M, Comic G, Briantais JM. Chlorophyll fluorescence from spinach leaves: resolution of non-photochemical quenching. Biochimica et Biophysica Acta (BBA)-Bioenergetics. 1989;974:289–293. DOI: 10.1016/S0005-2728(89)80246-4

[51] Long SP, Humphries S, Falkowski PG. Photoinhibition of photosynthesis in nature. Annual review of plant biology. 1994;45:633–662. DOI: 10.1146/annurev.pp.45.060194.003221

[52] Chaves MM, Flexas J, Pinheiro C. Photosynthesis under drought and salt stress: regulation mechanisms from whole plant to cell. Annals of botany. 209;103:551–560. DOI: 10.1093/aob/mcn125

[53] Chaves MM, Pereira JS, Maroco J, Rodrigues ML, Ricardo CPP, Osorio ML, Pinheiro C. How plants cope with water stress in the field? Photosynthesis and growth. Annals of botany. 2002;89:907–916. DOI: 10.1093/aob/mcf105

[54] Zakhidov EA, Kokhkharov AM, Kuvondikov VO, Nematov SK, Saparbaev AA. Photoacoustic spectroscopy of thermal relaxation processes of solar energy in the photosynthetic apparatus of plants. Applied Solar Energy. 2012;48:62–66. DOI: 10.3103/S0003701X12010161

[55] Long SP, Bernacchi CJ. Gas exchange measurements, what can they tell us about the underlying limitations to photosynthesis? Procedures and sources of error. Journal of Experimental Botany. 2003;54:2393–2401. DOI: 10.1093/jxb/erg262

[56] Cornic G, Fresneau C. Photosynthetic carbon reduction and carbon oxidation cycles are the main electron sinks for photosystem II activity during a mild drought stress. Annals of Botany. 2002;89:887–894. DOI: 10.1093/aob/mcf064

[57] Cornish K, Radin JW, Turcotte EL, Lu Z, Zeiger E. Enhanced photosynthesis and stomatal conductance of Pima cotton (Gossypium barbadense L.) bred for increased yield. Plant Physiology. 1991;97:484–489. DOI: 10.1104/pp.97.2.484

[58] Bielorai H, Mantell A, Moreshet S. Water relations of cotton. In: Koslowski TT editor. Additional Woody Crop Plants V7. NY, USA: Academic Press; 2012.p. 49–87.

Chapter 6

Absorption and Transport of Inorganic Carbon in Kelps with Emphasis on *Saccharina japonica*

Yanhui Bi and Zhigang Zhou

Additional information is available at the end of the chapter

http://dx.doi.org/10.5772/62297

Abstract

Due to the low CO_2 concentration in seawater, macroalgae including *Saccharina japonica* have developed mechanisms for using the abundant external pool of HCO_3^- as an exogenous inorganic carbon (C_i) source. Otherwise, the high photosynthetic efficiency of some macroalgae indicates that they might possess CO_2 concentrating mechanisms (CCMs) to elevate CO_2 concentration intracellularly around the active site of ribulose-1, 5-bisphosphate carboxylase/oxygenase (RuBisCo). As the photosynthetic modes of macroalgae are diverse (C3, C4 or a combination of C3 and C4 pathway), CCMs in different carbon fixation pathways should vary correspondingly. However, both in C3 and C4 pathways, carbonic anhydrase (CA) plays a key role by supplying either CO_2 to RuBisCO or HCO_3^- to PEPC. Over the past decade, although CA activities have been detected in a number of macroalgae, genes of CA family, expression levels of CA genes under different CO_2 concentrations, as well as subcellular location of each CA have been rarely reported. Based on analysis the reported high-throughput sequencing data of *S. japonica*, 12 CAs of *S. japonica* (*SjCA*) genes were obtained. Neighbor-Joining (NJ) phylogenetic tree of SjCAs constructed using Mega6.0 and the subcellular location prediction of each CA by WoLFPSORT are also conducted in this article.

Keywords: Macroalgae, Inorganic carbon uptake, C3 and C4 metabolism, Carbonic anhydrase, *Saccharina japonica*

1. Introduction

Kelps demonstrate high photosynthetic rates. According to the reports, productivity of large brown algae (e.g., *Macrocystis*, *Laminaria*, *Ecklonia*, *Sargassum*) ranges from 1000 to 3400 g $m^{-2}yr^{-1}C$ or about 3300 to 11,300 g $m^{-2}yr^{-1}$ dry weight, and red algae show a similar range of produc-

tion. Cultivated macroalgae can yield even higher values. The projected yield of cultivated *Laminaria japonica* on an annualized basis is equivalent to 1300 t ha^{-1} fresh weight or 6.5 times the maximum projected yield for sugarcane, the most productive of land plants under cultivation. In general, 45% yield of the dry weight of plants is accounted by carbon, which is assimilated in plant through Calvin cycle. The high productivities of kelps indicate their higher photosynthetic efficiency than C4 terrestrial plants [1].

The enzyme ribulose-1, 5-bisphosphate carboxylase/oxygenase (RuBisCo) is crucial in CO_2 assimilation. This bifunctional enzyme could catalyse the initial steps of photosynthetic carbon reduction and photorespiratory carbon oxidation cycles by combining CO_2 and O_2 with ribulose-1, 5-bisphosphate (RuBP) [2, 3]. RuBP carboxylation determines the net photosynthetic efficiency of photoautotrophs [4]. However, RuBisCo has a surprisingly low affinity for CO_2 and the oxygenase activity is intrinsic to RuBisCo. For kelps, the enzymatic efficiency of RuBisCo is also limited by the low concentration and diffusion coefficient of CO_2 in seawater [5]. At a natural pH of about 8, the major part of the dissolved inorganic carbon (DIC) is in the form of bicarbonate (HCO_3^-), and only about 12 μM is present as dissolved CO_2 [6], which is much lower than the half-saturation constant (Ks) of RuBisCo for CO_2 ranges from 30 μM to 60 μM in marine macroalgae [7, 8]. To support photosynthesis and growth, seaweeds require an exogenous inorganic carbon (C_i), while only CO_2 and HCO_3^- can be used as a CO_2 source for photosynthesis. Due to the low CO_2 concentration in seawater, it is not surprising that most seaweed have developed mechanisms for using the abundant external pool of HCO_3^- as an exogenous C_i source [9–11]. And it seems likely that those macrophytes that are able to use HCO_3^- would possess advantages compared with that rely solely on diffusive CO_2 entry. Here the question is how C_i is absorbed, transported to supply high CO_2 concentration around RuBisCo in kelps since unlike CO_2, HCO_3^- cannot diffuse through the lipid bilayer of the plasma membrane [12] and the produced or absorbed CO_2 are readily leaked out due to the high CO_2 permeability of cytomembrane. Otherwise, different models of photosynthesis such as C3, C4 and CAM might employ different CCMs in kelps. Thus, this review mainly focuses on the mechanisms of C_i absorption, transportation and concentration mechanisms of multicellular marine algae, including representatives of Chlorophyceae, Rhodophyceae and Phaeophyceae with different photosynthetic types.

2. Photosynthetic modes of macroalgae

As with terrestrial angiosperms where a single family may possess species with divergent photosynthetic modes [13], the marine macroalgal divisions also exhibit diversity. The photosynthetic carbon fixation pathways of marine macrophytic algae generally follow that of C3 plants [14]. However, for certain genera, a number of studies have shown photosynthesis to possess C4-like photosynthetic characteristics, including the high phosphoenolpyruvate carboxykinase (PEPCK) activity with low phosphoenolpyruvate carboxylase (PEPC) activity, little photorespiration and the labelling of malate and aspartate as an early product of carbon

http://dx.doi.org/10.5772/62297

fixation. Based on this, it has been suggested that these macroalgae are of the C4 type, or a combination of C3 and C4, type [15–17], although Kremer and Küppers [18] had contradicted the decision whether a species is a C4 plant or not based only on chromatographic and enzymatic analysis. In recent decades, our understanding of the possible metabolic pathways of macroalgae has been extended with using the available sequencing resources and molecular technologies and applying molecular approaches. Reiskind et al. [19] reported that a limited C4-like system in the green alga *Udotea* with the high PEPCK activity and low PEPC activity was a novel characteristic. Whereafter, Reiskind and Bowes [20] found that when PEPCK activity was inhibited *in vivo* with 3-mercaptopicolinic acid, thallus photosynthesis was decreased by 70% and the labelling of early photosynthetic products such as malate and aspartate was reduced by 66% and thus provided new evidences for the existence of C4 acid metabolism in this green alga. In contrast to *Udotea*, *Codium*, a macroalga closely related to *Udotea*, exhibits gas exchange characteristics that resemble terrestrial C3 plants, and neither C4 acids nor PEPCK plays a part in photosynthesis [19]. This demonstrates the diversity of photosynthetic mechanisms in the Chlorophyta. *Ulva*, a common green seaweed, was previously reported as a typical C3 plant based on some biochemical evidences that 3-phosphoglyceric acid (3-PGA) was the main primary product formed photosynthetically and a high RuBPcase/PEPcase ratio was found in it [21], while, recently, it was reported that *Ulva* possessed rather comprehensive carbon fixation pathways including C3, C4 and CAM mechanisms because key genes of enzymes involved in these photosynthetic modes were got from the expressed sequence tag (EST) using Kyoto encyclopedia of genes and genomes (KEGG) [22]. Recently, C4-like carbon fixation pathway was also found in representatives of Rhodophyceae and Phaeophyceae based on the analysis of ESTs or transcriptomes. In red algae, Fan et al. [23] speculated that the sporophyte of *Pyropia haitanensis* most likely possesses a C4-like carbon fixation pathway since genes of the key enzymes in the PCK-type C4 carbon-fixation pathway were abundantly transcribed. Wang et al. [24] assumed that a C4-like carbon-fixation pathway might play a special role in fixing inorganic CO_2 in *Porphyra yezoensis* with the evidence that except pyruvate-phosphate dikinase all genes involved in C4-pathway were discovered from the transcriptome. Xu et al. [25] had reported that PEPCK, an important enzyme in carbon fixation in C4 plants, had very high activity in the sporophyte of *L. japonica*. Besides, haploid gametophytes and diploid sporophytes of some marine macroalgae with dimorphic life cycles might even employ different photosynthetic mode. Wang et al. [24] found that both the RuBisCo content and the initial carboxylase activity were notably higher in gametophytes than in the sporophytes of four seaweed species — *P. yezoensis*, *P. haitanensis*, *Bangia fuscopurpurea* (Rhodophyte) and *L. japonica* (Phaeophyceae). They assumed that in the sporophyte of these algae, the major carbon fixation pathway may be a C4-like carbon fixation pathway, and thus a high abundance of RuBisCo would not be necessary for the sporophytes. And for *L. japonica*, the higher RuBisCo content and activity in gametophyte was corresponding to the lower photosynthetic rate, which implied there might be a greater difference between sporophytes and gametophytes of this alga in their photosynthetic mode. Conclusively, the existence of C4-like pathway in macroalgae has been verified using more evidence, while the distribution between C3 and C4 pathways was unknown during growth of macroalgae with comprehensive carbon fixation pathways including C3 and C4.

In C3 and C4 metabolisms, CO_2 is the substrate of RuBisCo and assimilated through the Calvin cycle. In this cycle, CO_2, catalysed with RuBisCo, combines with RuBP to form two molecules of 3-PGA. PGA is reduced to triose. RuBisCo, a bifunctional enzyme, may catalyse the combination of RuBP and CO_2 for photosynthetic carbon reduction or may combine with O_2 for C_2 photorespiration [3]. The ratio of CO_2 to O_2 around RuBisCo is a major factor for the enzyme to choose the photosynthetic carbon reduction or C_2 photorespiration carbon oxidation [26]. The low CO_2 concentration around RuBisCo may not only impose restrictions on photosynthesis but also cause permanent light injuries to photosynthetic organelle [27–29]. The speciation of DIC (C_i) is pH dependent. Above pH 4.5, the proportion occurring as CO_2 (aq) decreases and HCO_3^- increases, while above pH 8.3, the bicarbonate equivalence point, the equilibrium begins to shift towards carbonate (CO_3^{2-}). In the upper layer of the oceans, HCO_3^- ions predominate, and the dissolved CO_2 represents only about 1% of the total dissolved carbon with a concentration of about 21 μM [30]. The *K*m (CO_2) value of RuBisCO is significantly higher than this, having been reported as being as high as 200 μM in some cyanobacteria [31]. To survive under the selective pressure of low CO_2 concentration, high permeability of CO_2 for plasma membrane and low affinity of CO_2 for RuBisCo, many algae, including macroalgae living in the subtidal zone, have evolved with inorganic CCM that allows them to overcome this potentially limiting shortage of CO_2 [9, 32–36]. So, the productivity of most macroalgae is not currently considered limited by DIC. Unlike terrestrial C4 plants possessing Kranz anatomy to prevent futile recycling of CO_2 by segregating the initial carboxylation and decarboxylation reactions in different cells, macroalgae concentrate CO_2 internally, which is mediated by C_i transporters at the plasma membrane or chloroplast envelope and CA. As for carboxylases are different between C3 and C4 metabolism, C_i acquisition, transportation and concentration mechanisms might be diverse.

Based on a series of reports on the presence of CCM in blue-green algae and *Chlamydomonas* (*Chlamydomonas reinhardtii*) and some other microalgae [37–40], Badger [41] reported that the CCM of algae possess at least three functional elements: (1) the transportation of the C_i dissolved in seawater into cells in the form of CO_2 and/or HCO_3^-; (2) the accumulation of the C_i in cells in the form of HCO_3^-, forming pools of the dissolved C_i and (3) the delivery of CO_2 to the periphery of RuBisCo from such pools.

3. Inorganic carbon absorption mechanisms of macroalgae

The methods of CO_2 and/or HCO_3^- absorption of macroalgae cells (Figure 1) include the following: (1) non-CCM macroalgae (that do not possess or use CCM) rely exclusively on diffusive uptake of CO_2, (2) CCM macroalgae uptake of C_i, as CO_2 and/or HCO_3^- via mechanisms of the external carbonic anhydrase (CA_{ext}) mechanism, the anion exchange (AE) transport mechanism, the plasma membrane associated with H^+-ATPase mechanism and passive transport of CO_2 by diffusion. In the first mechanism, HCO_3^- in the periplasmic space is converted to CO_2 at the presence of CA_{ext}, an enzyme that is located in the cell wall in the

http://dx.doi.org/10.5772/62297

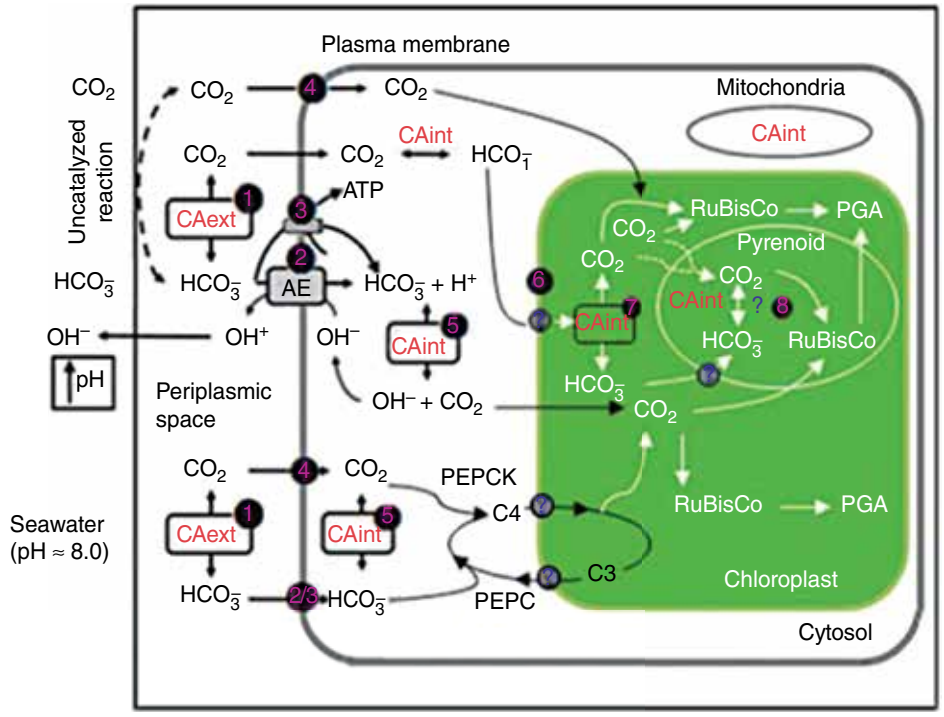

Figure 1. A schematic diagram on the photosynthetic carbon physiology of some macroalgae revised from [45].

majority of seaweeds and could be inhibited by the membrane impermeable acetazolamide (AZ), and then the resulting CO_2 is readily taken into the cell by passive diffusion. This seems to be the most prevalent for HCO_3^- utilization among seaweeds [42, 43], but it may be non-functional under high pH (>9.00) [44, 45]. The AE transport mechanism is HCO_3^- direct uptake through the AE protein in plasma membrane [11, 43, 46–48], which is 4,4'-diisothiocyanostilbene-2,2'-disulfonate (DIDS) sensitive. This operates equally well at pH 8.4 and 9.4 [44, 45]. H^+-ATPase mechanism refers to a plasma membrane associated H^+-ATPase pump that extrudes the excess cellular H^+ to the outside of the plasma membrane facilitating a H^+/HCO_3^- co-transportation or enhancement of the external uncatalysed dehydration of HCO_3^- to CO_2 in the periplasmic space [49]. However, this has only been reported in some Laminariales such as *S. latissima* and *L. digitata*. Along with the uptake of CO_2 and/or HCO_3^-, the internal charge balance (OH^-/H^+) will be absolutely changed. To maintain intracellular ion balance, macroalgae employ diverse strategies. In AE mechanism, the active transport of HCO_3^- into the cell might result in an outward flux of OH^- [50–53, 45] as this mechanism is involved in a one-for-one exchange of anions across the plasma membrane. The OH^- efflux can increase H^+ in the cell [52]. To maintain the intracellular OH^-/H^+ balance, H^+ extrusion might be required. In macroalgae possessing H^+-ATPase mechanism, their plasma membrane associated with H^+-

ATPase pump might extrude excess cellular H^+ to the outside of the plasma membrane, while in macroalgae that do not have H^+-ATPase pump in their plasma membrane, the regulation of intracellular ion balance might be related to a high activity of internal carbonic anhydrase (CA_{int}), including the CA in cytoplasm, chloroplast stroma, thylakoid lumen and mitochondria [45].

The extent to which marine macroalgae are able to acquire HCO_3^- for photosynthesis varies among taxa and/or species, and the special strategies by which the alga acquire C_i is closely related to habitat including pH and depth, conferring as adaptation advantage to the alga [9, 33, 36, 54–56]. Cornwall et al. [57] reported when light is low, CCM activity of macroalgae is reduced in favour of diffusive CO_2 uptake and the proportion of non-CCM (diffusive uptake of CO_2) species increased with depth. Otherwise, pH might also control C_i use by macroalgae. In *U. lactuca*, the CA_{ext}-mediated mechanism is the main method of HCO_3^- utilization under normal pH conditions, whereas when they were grown at high pH, direct uptake of HCO_3^- via a DIDS-sensitive mechanism can be induced [44]. Similar HCO_3^- utilizing mechanisms were found in another green macroalgae *Enteromorpha intestinalis* [54]. For the red alga *Gracilaria gaditana*, the HCO_3^- use is also carried out by the two DIC uptake mechanisms, in which the indirect use of HCO_3^- by an external CA activity being the main pathway and the potential contribution to HCO_3^- acquisition by the DIDS-sensitive AE mechanism was higher after culturing at a high pH [58]. However, these two mechanisms do not occur simultaneously, and the DIDS-sensitive mechanism is induced only under high pH. *Solieria filiformis*, another red marine macroalgae, in which the general form of C_i transported across the plasma membrane is CO_2, but HCO_3^- acquisition takes place simultaneously between CA_{ext} mechanism and direct uptake [59]. CA_{ext} mechanism is also the main pathway for DIC acquisition for the species of Phaeophyta. *S. latissima* mainly uses CA_{ext} mechanism for HCO_3^- absorption, since when AZ is used to treat *S. latissima*, its photosynthetic efficiency drops by 80% [11]. Otherwise, *S. latissima* also has a H^+-ATPase mechanism, of which the proton pump may support the antiport of H^+/HCO_3^- or the discharge of H^+, creating an acid environment in the periplasmic space and causing the dehydration of HCO_3^- into CO_2 with CA to quickly diffuse into cells [49]. *S*imilar to *S. latissima*, *L. digitata* also has a CA_{ext} mechanism of absorbing HCO_3^- and a P-H^+-ATPase mechanism [49]. Gametophytes of *Ectocarpus siliculosus* utilize the CA_{ext} mechanism and the HCO_3^- transport protein [60] on the cell membrane to absorb HCO_3^-. *Macrocystis pyrifera* utilizes the CA_{ext} mechanism and the AE protein mechanism to absorb HCO_3^-, in which the main mechanism of HCO_3^- uptake is via AE protein and CA_{ext} contributes little [45]. For *Sargassum henslowianum*, like most seaweed, the main Ci acquisition strategy is also CA_{ext} metabolism, since its photosynthetic O_2 evolution could be drastically depressed by AZ at pH 8.1 (i.e., the normal seawater pH value) and at pH 9.0. And direct uptake for HCO_3^- via DIDS-sensitive AE protein mechanism was unlikely to be present in C_i acquisition of this kelp, because the photosynthesis in either blade or receptacle tissue of this alga was not affected by DIDS [61]. For *Hizikia fusiformis*, CA_{ext}+ diffusive uptake of CO_2 could support its metabolic

http://dx.doi.org/10.5772/62297

requirements sufficiently since there is no known other active C_i transport mechanisms [62]. For *S. japonica*, Yue et al. [63] found that the C_i absorption of the CA_{ext} mechanism in its juvenile sporophytes accounts for 75% of the total C_i absorption in algae cells, whereas free CO_2 absorption accounts for 25% only.

Thus, the CA_{ext} mechanism plays an important role in the CCM macroalgae absorption and the utilization of the relatively abundant HCO_3^- in seawater.

4. C_i transition process in CCMs of macroalgae

C_i acquisition mechanisms are extensively studied and well-known in microalgae [44, 38]. For instance, regardless of the C_i form (CO_2 or HCO_3^-) taken up by the microalga *C. reinhardtii*, HCO_3^- is the primary form accumulated into the cell to prevent CO_2 leakage [38]. In macroalgae, most C_i use processes are speculated based on some biochemical evidence. For C3 photosynthesis, the CO_2 that entered the cytoplasm is transformed into HCO_3^- under the catalytic action of CA in the cytoplasm and stored in the cytoplasm [38] to maintain the equilibrium of different forms of C_i and to regulate the pH value of the cytoplasm [26, 38]. The HCO_3^- in the cytoplasm enters the chloroplast stroma via the C_i transport protein on the chloroplast membrane, and the CO_2 in the cytoplasm directly enters the stroma via the chloroplast membrane. In diatom *Phaeodactylum tricornutum*, genes with homology to bicarbonate transporters from SLC4 and SLC6 families, two HCO_3^- transporters studied thoroughly in human, were got from its genome and one of these SLC4-type HCO_3^- transporters has recently been confirmed to function as a Na^+-dependent HCO_3^- transporter on the outer membrane [64, 65]. However, the molecular nature of HCO_3^- transporters of macroalgae is unknown now, and their similarity to those found in diatoms is uncertain. The transportation of C_i from the cytoplasm to the chloroplast is the major C_i flux in the cell and the primary driving force for the CCM. This flux drives the accumulation of C_i in the chloroplast stroma and generates a CO_2 deficit in the cytoplasm, inducing CO_2 influx into the cell. Given that the pH value of the chloroplast stroma is closer to 8, the stroma C_i is mostly enriched in the form of HCO_3^-, forming C_i pools [66]. In macroalgae, which have pyrenoids, HCO_3^- is putatively carried into the thylakoid by the C_i transport protein on the thylakoid membrane, forming CO_2 in the thylakoid space under the catalytic action of thylakoid CA [67, 68]. The thylakoid membrane partially sinks into the pyrenoids [69], where the diffused CO_2 is quickly fixed by the RuBisCo in the pyrenoids. The diffused CO_2 from the thylakoid space outside the pyrenoids or the unfixed CO_2 leaked from the pyrenoids is transformed into HCO_3^- under the action of CA in the starch sheath on the periphery of the pyrenoid, thus increasing the number of HCO_3^- pools in the matrix [70]. For macroalgae without pyrenoids, such as *L. japonica*, HCO_3^- entered the chloroplast stroma after being dehydrated under the action of chloroplast stroma CA and provided CO_2 for the RuBisCo in the matrix (Figure 1).

For C4 photosynthesis, CA is required to convert CO_2 to HCO_3^- in the cytosol, and thus supply PEPC with substrate. HCO_3^- will be fixed into malate. For non-PEPC algae with PEPCK, the CO_2 entering the cytoplasm will be directly fixed in the form of four-carbon acid [71]. The produced four-carbon acid may be transported into the mitochondria, forming pyruvate after decarboxylation and CO_2 release, which is fixed in the form of carbohydrate in the Calvin cycle. In fact, the presence of CA in C4 plants has been suggested to accelerate the rate of photosynthesis in C4 plants 10^4-fold over what it would be if this enzyme were absent [72].

In conclusion, CA (CA_{ext}+CA_{int}) is essential for the reversible HCO_3^-–CO_2 conversion both in the cell and in the periplasm. They participate in photosynthesis by supplying either CO_2 to RuBisCO or HCO_3^- to PEPC for C4 type.

5. Carbonic anhydrase

CAs are metalloenzymes that catalyse the reversible interconversion of CO_2 and HCO_3^- [73]. They are encoded by six evolutionary divergent gene families and the corresponding enzymes are designated as α, β, γ, δ, ε and ζ-CA [39]. These six types of CAs share no sequence similarity in their primary amino acid sequences and seem to have evolved independently [26, 74]. In macroalgae, almost all known CAs belong to α, β and γ classes, with the β class predominating [26, 39]. The δ, ε and ζ classes of CA are found only in some diatoms [75], bacteria [76] and marine protists [77, 78]. The active site of CA contains a zinc ion (Zn^{2+}), which plays a critical role in the catalytic activity of the enzyme. The ζ and γ classes of CAs represent exceptions to this rule since they can use cadmium (ζ), iron (γ) or cobalt (γ) as cofactors [79–81]. CA plays an important role in photosynthesis by supplying either CO_2 to RuBPCO or HCO_3^- to PEPC. They also participate in some other physiological reactions such as respiration, pH homeostasis, ion transport and catalysis of key steps in the pathways for the biosynthesis of physiologically important metabolites [41]. The CA synthesis in the cytoplasm [82] is located in the periplasmic space, mitochondria, chloroplast stroma and chloroplast thylakoid lumen, carboxysome and pyrenoid [66, 70, 83, 84]. Different subcellular localizations make different CA functions in CCM. Periplasmic CA (CA_{ext}) can catalyse the conversion of HCO_3^- into CO_2 to promote the diffusion of CO_2 at the cell surface across the plasma membrane [85, 86]. Therefore, CA_{ext} has been postulated to be part of the CCM in most macroalgae. The cytoplasm CA stores Ci in the form of HCO_3^- to avoid leakage of CO_2 and to regulate the pH value of cytoplasm by maintaining the equilibrium of different forms of Ci, which is important for algal CCM [39]. CAs on the chloroplast membrane and in the stroma mainly provide CO_2 for RuBisCo [26, 38, 87]. In cyanobacteria, CAs in the carboxysomal shell function to convert accumulated HCO_3^- into CO_2 and pass it to RuBisCo inside the cytoxysome [88]. CA in the thylakoid lumen was proposed to function to create an efficient CO_2 supply to RuBisCo by taking advantage of the acidity of the lumenal compartment [69]. Stromal CA is also thought to operate by converting leaking CO_2 into HCO_3^- [70]. Recently, data provided by various genome sequencing studies have revealed the multiplicity of CA isoforms in algae. For

http://dx.doi.org/10.5772/62297

example, in the model microalga *C. reinhardtii*, there are at least 12 genes that encode CA isoforms, including three α, six β and three γ or γ-like CAs [39]. For marine diatom, nine and thirteen CA sequences were found in the genomes of *P. tricornutum* and *Thalassiosira pseudonana*, respectively [89]. *P. tricornutum* contains two β-CA genes, five α and two γ CA genes, whereas *T. pseudonana* has three α-, five γ-, four δ- and one ζ-CA genes [89]. As for macroalgae, CA genes have only been reported in few species. Six full-length CA of *P. haitanensis* (PhCA) genes were reported, which include two α-CAs, three β-CAs and one γ-CA [90]. Besides, one β-CA and one α-CA were reported in *P. yezoensis* [91] and *S. japonica* [92, 93]. Otherwise, although the activity of CA_{ext} and CA_{int} has been detected in many macroalgae, the subcellular localization and functions of CA_{ext} and CA_{int} remain unclear [71, 93].

Conclusively, CAs, including CA_{ext} and CA_{int} (Figure 1), play an important role in the transportation or concentration process of the C_i. And as for C3 and C4 metablisms have different carboxylase, CAs might play different roles in CCMs of macroalgae with different photosynthetic mode. Thus, isolating of the *CA* genes, studies on their expression levels in different CO_2 concentrations, in different life phase, and under different environmental stress, as well as studies on subcellular locations of CAs should be conducted in macroalgae to help reveal their Ci assimilation processes.

6. Studies of *S. japonica* CCM

S. japonica is an economically important brown seaweed. It has been cultivated extensively for food and industrial alginate in East Asia, such as in China, Japan and South Korea. China is by far the largest producer, and in 2009, its production in China rose sharply to 4.14×10^9 kg wet weight [94], accounting for approximately 80% of the global production, over several decades. This has been attributed to both its large-scale farming and high kelp yield per unit area. Production of this kelp in China under natural conditions is within the range of 3,300 to 11,300 g dry matter $m^{-2}\cdot year^{-1}$, whereas that under artificial conditions is higher [1]. For example, its production during the 7-month cultivation is 15,000 g dry matter m^{-2} area (equivalent to 150 t per ha), which is 2.8 times higher than the maximum productivity of sugarcane in the United States (fresh weight about 95 t per ha·year) [1], which indicates that *S. japonica* has higher photosynthetic efficiency than sugarcane and other C4 plants. In fact, the photosynthetic efficiency of macroalgae (e.g., kelp) is 6%–8%, which is 1.8%–2.2% higher than that of land plants [95]. In seawater, the dominant species of Ci is HCO_3^- [11]. Since there is a fairly high photosynthetic rate in these kelps [34], a CCM involving an efficient HCO_3^- utilization mechanism is expected to exist. Indeed, 75% of the total C_i absorption in the juvenile sporophytes of this kelp is via the CA_{ext} mechanism [63], whereas CO_2 diffusion accounts for 25% only. By analysis of genome annotation data of *S. japonica* [96], all the essential genes related to C3-pathway (23 unigenes) were discovered (Table 1), which provided the unequivocal molecular evidence that there existed C3-pathway in *S. japonica*. Otherwise, 16 enzyme-encoding unigenes involved in C4-pathway were found, covering almost all enzymes needed

for C4-carbon fixation except the malic enzyme (Table 1). The results helped us to understand the carbon fixation process of this species.

Photosynthesis modes	Enzyme names	Unigenes
C3-pathway		23
	Glyceraldehyde-3-phosphate dehydrogenase (phosphorylating) (GAPDH)	4
	Transketolase	1
	Phosphoribulokinase	2
	Phosphoglycerate kinase (PGK)	5
	Fructose-1,6-bisphosphatase (FBPase)	1
	Sedoheptulose-bisphosphatase (SBPase)	3
	Fructose-bisphosphate aldolase	1
	Ribulose-phosphate 3-epimerase	2
	Triose-phosphate isomerase (TIM)	1
	Ribose-5-phosphate isomerase	1
	Ribulose-1,5-bisphosphate carboxylase/oxygenase (RuBisCo), small	1
	Ribulose-1,5-bisphosphate carboxylase/oxygenase(RuBisCo), large	1
C4-pathway		16
	Malate dehydrogenase	4
	Aspartate aminotransferase (AST)	4
	Pyruvate kinase	4
	Phosphoenolpyruvate carboxylase (PEPC)	1
	Phosphoenolpyruvate carboxykinase (PEPCK)	1
	Pyruvate phosphate dikinase	1
	Arginine/alanine aminopeptidase	1
Total		39

Table 1. Statistics of C3/C4-pathway related enzymes of *S. japonica*.

Considering CAs play key roles in CCMs of macroalgae, it is important to determine the numbers and characterizations of CA genes of *S. japonica*. Herein, based on unigene sequences [96], the high-throughput sequencing data of *S. japonica* [97, 98] and *S. latissima* [99], as well as combined with the preparatory work of our group [92, 93], 12 CAs of *S. japonica* (*SjCA*) genes were obtained. Among them, we have cloned the full-length complementary DNA (cDNA) sequences of SjαCA1, SjβCA1 and SjβCA2 using rapid amplification of cDNA ends, which are 2804 [94], 1291 and 1261 nucleotides, respectively. The encoded proteins were 290, 314 and 307 amino acids. For further analysis the gene subtypes of CAs, a phylogenetic tree was constructed

http://dx.doi.org/10.5772/62297

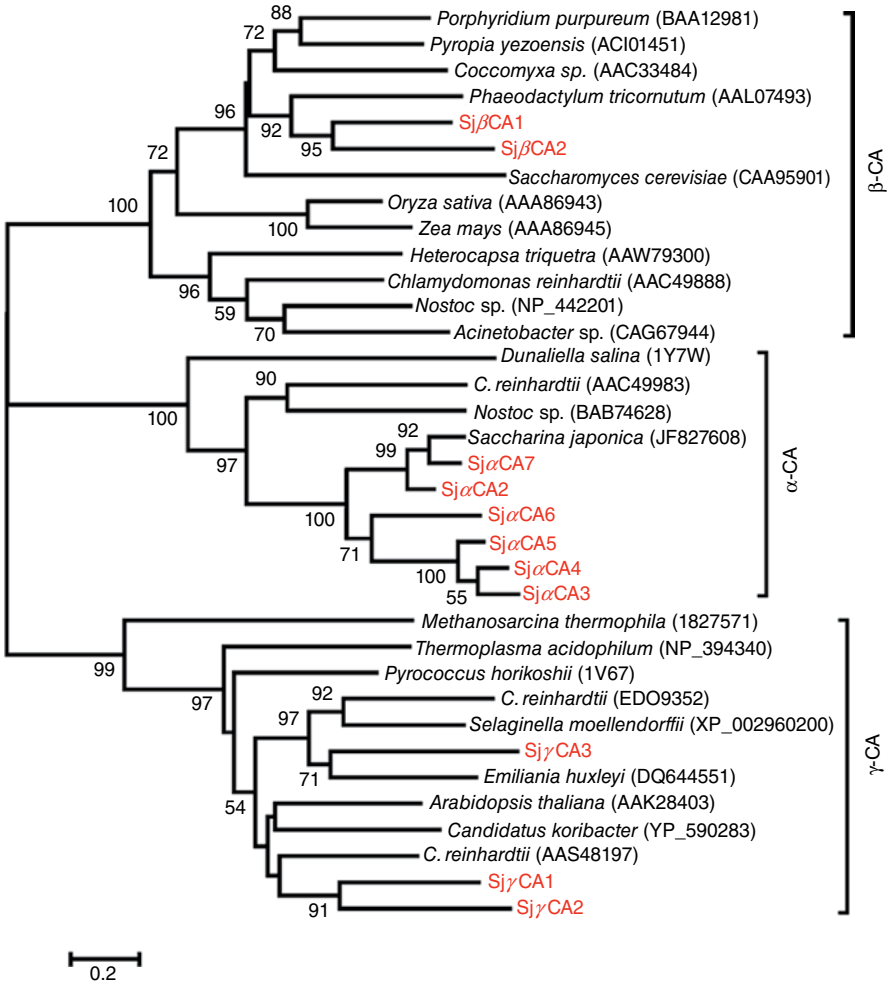

Figure 2. Phylogenetic tree constructed using SjCA amino acid sequences.

by using the neighbour-joining algorithm of the MEGA6.0 software [100] with Poisson correction and pairwise deletion parameters. A total of 1000 bootstrap replicates were performed. On the basis of conserved motifs and phylogenetic tree analysis (Figure 2), the *SjCA*s were divided into three CA classes: from SjαCA1 to SjαCA7 are α-CA; SjβCA1 and SjβCA2 are β-CA; SjγCA1, SjγCA2 and SjγCA3 are γ-CA. Among them, only one α-CA (SjαCA1) has been localized in the chloroplast and thylakoid membrane of the gametocytes of *S. japonica* under immunogold electron microscopy [93]. To get a general idea of functions of each SjCA, herein, the subcellular localizations of SjCAs were predicted using WoLFPSORT (http://www.genscript.com/wolf-psort.html). Based on the predicted results (Table 2), SjαCA2 might be an external CA and exist in periplasmic space, SjαCA3; SjαCA4, SjαCA6, SjαCA7 and SjγCA1 might be cytoplasmic CA; SjαCA5, SjβCA2 and SjγCA2 might present in mito-

chondria; SjβCA1 and SjγCA3 might exist in chloroplasts. However, most of the SjCAs' subcellular localizations are predicted, which need to be verified by further studies. Otherwise, sporophyte and gametophyte of this kelp might employ different carbon fixation process since the content and activity of RuBisCo enzyme in gametophyte are significantly higher than those in sporophyte implying they may have different types of photosynthetic metabolism [24]. As for CA might play different role in CCMs of C3 and C4 pathway, full-length cDNA as well as DNA sequences of each SjCA should be cloned from sporophytes and gametophytes of this kelp in the future studies. CA gene expression levels under different CO_2 concentrations and the subcellular location of each CA should also be conducted to help reveal C_i assimilation process of *S japonica*.

Enzyme	Gene ID[a]	AA no.	Full length (Y/N)	Subcellular location prediction
SjαCA1	JF827608	290	Y	Chloroplast and thylakoid membrane [93]
SjαCA2	SJ07762	205	N	Secreted
SjαCA3	SJ07765	160	N	Cytoplasmic
SjαCA4	SJ13238	151	N	Cytoplasmic
SjαCA5	SJ13240	294	N	Mitochondrial inner membrane
SjαCA6	SJ18135	257	N	Cytoplasmic
SjαCA7	SJ18141	189	N	Cytoplasmic
SjβCA1	SJ12311	314	Y	Chloroplast thylakoid membrane
SjβCA2	SJ17783	307	Y	Mitochondrial
SjγCA1	SJ07587	305	N	Cytoplasmic
SjγCA2	SJ22175	161	N	Mitochondrial
SjγCA3	SJ21158	246	N	Chloroplast

Abbreviation: *AA,* amino acid.
[a] JF827608 is the NCBI gene accession number; 'SJ' in the table stands for the gene IDs for *S. japonica.*

Table 2. Prediction of subcellular locations of SjCAs.

The completion of the CCM modelling of sporophyte and gametophyte in *S. japonica* will give a solid foundation for further exploring its highly efficient photosynthetic mechanism. In addition, conducting studies on the inorganic carbon metabolism of macroalgae is of positive significance on developing the biomass energy from kelp and other algae and slowing down seawater acidification and global warming.

Author details

Yanhui Bi and Zhigang Zhou*

*Address all correspondence to: zgzhou@shou.edu.cn

College of Fisheries and Life Science, Shanghai Ocean University, Shanghai, People's, Republic of China

References

[1] Gao K, McKinley KR. Use of macroalgae for marine biomass production and CO_2 remediation: a review. *Journal of Applied Phycology*. 1994; 6(1): 45–60. DOI: 10.1007/BF02185904

[2] Berry JA, Osmond CB, Lorimer G. Fixation of CO_2 during photorespiration. *Plant Physiology*. 1978; 62: 954–967.

[3] Mizohata E, Matsumura H, Okano Y. Crystal structure of activated ribulose-1,5-bisphosphate carboxylase/oxygenase from green alga *Chlamydomonas reinhardtii* complexed with 2-carboxyarabinitol-1,5-bisphosphate. *Journal of Molecular Biology*. 2002; 316: 679–691. DOI: 10.1006/jmbi.2001.5381

[4] Jensen GR, Bahr TJ. Ribulose 1,5-bisphosphate carboxylase-oxygenase. *Annual Review of Plant Physiology*. 1977; 28: 379–400. DOI: 10.1146/annurev.bi.52.070183.002451

[5] Reinfelder JR. Carbon concentrating mechanisms in eukaryotic marine phytoplankton. *Annual Review of Marine Science*. 2011; 3: 291–315. DOI: 10.1146/annurev-marine-120709-142720

[6] Stumm W, Morgan JJ. Aquatic Chemistry: Chemical Equilibria and Rates in Natural Waters. 3rd ed. New York: Wiley; 1996. 1022 p.

[7] Kerby NW, Raven JA. Transport and fixation of inorganic carbon by marine algae. *Advances in Botanical Research*. 1985; 2: 71–123.

[8] Cook CM, Colman B. Some characteristics of photosynthetic inorganic carbon uptake of a marine macrophytic red alga. *Plant, Cell and Environment*. 1987; 10: 275–278. DOI: 10.1111/1365-3040.ep11602301

[9] Maberly SC. Exogenous sources of inorganic carbon for photosynthesis by marine macroalgae. *Journal of Phycology*. 1990; 26(3): 439–449. DOI: 10.1111/j.0022-3646.1990.00439.x

[10] Larsson C, Axelsson L. Bicarbonate uptake and utilization in marine macroalgae. *European Journal of Phycology*. 1999; 34: 79–86. DOI: 10.1080/09670269910001736112

[11] Axelsson L, Mercado JM, Figueroa FL. Utilization of HCO_3^- at high pH by the brown macroalga *Laminaria saccharina*. *European Journal of Phycology*. 2000; 35(1): 53–59.

[12] Gutknecht JM, Bisson A, Tosteson FC. Diffusion of carbon dioxide through lipid bilayer membranes. Effects of carbonic anhydrase, bicarbonate, and unstirred layers. *Journal of General Physiology*. 1977; 69: 779–794. DOI: 10.1085/jgp.69.6.779

[13] Edwards GE, Huber SC. The C4 pathway. In: Hatch MD, Boardman NK, editors. The Biochemistry of Plants. A Comprehensive Treatise. Vol. 8, Photosynthesis. New York: Academic Press; 1981. p. 237–281.

[14] Kremer BP. Aspects of carbon metabolism in marine macroalgae. *Oceanography and Marine Biology: An Annual Review*. 1981; 19: 41–94.

[15] Johsi GV, Karekar MD, Gowda CA. Photosynthetic carbon metabolism and carboxylating enzymes in algae and mangrove under saline conditions. *Photosynthetica*. 1974; 8: 51–52.

[16] Karekar MD, Joshi GV. Photosynthetic carbon metabolism in marine algae. *Botanica Marina*. 1973; 16(4): 216–220. DOI: 10.1515/botm.1973.16.4.216

[17] Patil BA, Joshi GV. Photosynthetic studies in *Ulva lactuca*. *Botanica Marina*. 1970; 13(2): 111–115. DOI: 10.1515/botm.1970.13.2.111

[18] Kremer BP, Küppers U. Carboxylating enzymes and pathway of photosynthetic carbon assimilation in different marine algae—Evidence for the C4-pathway? *Planta*. 1977; 133(2): 191–196. DOI: 10.1007/BF00391918

[19] Reiskind JB, Seamon PT, Bowes G. Alternative methods of photosynthetic carbon assimilation in marine macroalgae. *Plant Physiology*. 1988; 87(3): 686–692. DOI: 10.1104/pp.87.3.686

[20] Reiskind JB, Bowes G. The role of phosphoenolpyruvate carboxykinase in a marine macroalga with C4-like photosynthetic characteristics. *Proceedings of the National Academy of Sciences of the United States of America*. 1991; 88(7): 2883–2887. DOI: 10.1073/pnas.88.7.2883

[21] Beer S, Israel A. Photosynthesis of *Ulva* sp III. O_2 effects, carboxylase activities, and the CO_2 incorporation pattern. *Plant Physiology*. 1986; 81(3): 937–938. DOI: 10.1104/pp.81.3.937

[22] Niu J, Hu H, Hu S. Analysis of expressed sequence tags from the *Ulva prolifera* (Chlorophyta). *Chinese Journal of Oceanology and Limnology*. 2010; 28: 26–36. DOI: 10.1007/s00343-010-9120-4

[23] Fan XL, Fang YJ, Hu SN. Generation and analysis of 5318 expressed sequence tags from the filamentous sporophyte of *Porphyra haitanensis* (Rhodophyta). *Journal of Phycology*. 2007; 43(6): 1287–1294. DOI: 10.1111/j.1529-8817.2007.00415.x

[24] Wang C, Fan X, Wang G. Differential expression of RuBisCo in sporophytes and gametophytes of some marine macroalgae. *PloS One*. 2011; 6(1): e16351. DOI: 10.1371/journal.pone.0016351

[25] Xu ZM, Yao NY, Li JZ. Studies on the activity of PEPck in *L. japonica*. *Marine Science*. 1991; 2: 41–45.

[26] Moroney JV, Bartlett SG, Samuelsson G. Carbonic anhydrases in plants and algae. *Plant, Cell & Environment*. 2001; 24(2): 141–153. DOI: 10.1111/j.1365-3040.2001.00669.x

[27] Krause GH. Photoinhibition of photosynthesis. An evaluation of damaging and protective mechanisms. *Physiologia Plantarum*. 1988; 74(3): 566–574. DOI: 10.1111/j.1399-3054.1988.tb02020.x

[28] Hanelt D, Huppertz K, Nultsch W. Photoinhibition of photosynthesis and its recovery in red algae. *Botanica Acta*. 1992; 105(4): 278–284. DOI: 10.1111/j.1438-8677.1992.tb00299.x

[29] Hanelt D, Huppertz K, Nultsch W. Daily course of photosynthesis and photoinhibition in marine macroalgae investigated in the laboratory and field. *Marine Ecology Progress Series*. 1993; 97(1): 31–37. DOI: 10.3354/meps097031

[30] Roleda MY, Hurd CL. Seaweed responses to ocean acidification//Seaweed Biology. *Springer Berlin Heidelberg*. 2012; 219: 407–431. DOI: 10.1007/978-3-642-28451-9_19

[31] Moroney J V, Somanchi A. How do algae concentrate CO_2 to increase the efficiency of photosynthetic carbon fixation? *Plant Physiology*. 1999, 119(1): 9–16. DOI: 10.1104/pp.119.1.9

[32] Cook CM, Lanaras T, Colman B. Evidence for bicarbonate transport in species of red and brown macrophytic marine algae. *Journal of Experimental Botany*. 1986; 37(7): 977–984. DOI: 10.1093/jxb/37.7.977

[33] Surif MB, Raven JA. Exogenous inorganic carbon sources for photosynthesis in seawater by members of the Fucales and the Laminariales (Phaeophyta): ecological and taxonomic implications. *Oecologia*. 1989; 78(1): 97–105. DOI: 10.1007/BF00377203

[34] Axelsson L, Uusitalo J, Ryberg H. Mechanisms for concentrating and storage of inorganic carbon in marine macroalgae. Seaweed Cellular Biotechnology, Physiology and Intensive Cultivation. COST-48. Universidad de las Palmas de Gran Canaria, España. 1991; 185–198.

[35] Johnston AM, Maberly SC, Raven JA. The acquisition of inorganic carbon by four red macroalgae. *Oecologia*. 92(3): 317–326. DOI: 10.1007/BF00317457

[36] Mercado JM, Gordillo FJL, Figueroa FL. External carbonic anhydrase and affinity for inorganic carbon in intertidal macroalgae. *Journal of Experimental Marine Biology and Ecology*. 1998; 221(2): 209–220. DOI: 10.1016/S0022-0981(97)00127-5

[37] Badger MR, Hanson D, Price GD. Evolution and diversity of CO_2 concentrating mechanisms in cyanobacteria. *Functional Plant Biology*. 2002; 29(3): 161–173. DOI: 10.1071/PP01213

[38] Spalding MH. Microalgal carbon-dioxide-concentrating mechanisms: *Chlamydomonas* inorganic carbon transporters. *Journal of Experimental Botany*. 2008; 59(7): 1463–1473. DOI: 10.1093/jxb/erm128

[39] Moroney JV, Ma YB, Frey WD. The carbonic anhydrase isoforms of *Chlamydomonas reinhardtii*: intracellular location, expression, and physiological roles. *Photosynthesis Research*. 2011; 109(1–3): 133–149. DOI: 10.1007/s11120-011-9635-3

[40] Price GD. Inorganic carbon transporters of the cyanobacterial CO_2 concentrating mechanism. *Photosynthesis Research*. 2011; 109(1–3): 47–57. DOI: 10.1007/s11120-010-9608-y

[41] Badger M. The roles of carbonic anhydrases in photosynthetic CO_2 concentrating mechanisms. *Photosynthesis Research*. 2003; 77(2–3): 83–94. DOI: 10.1023/A:1025821717773

[42] Israel A, Hophy M. Growth, photosynthetic properties and RuBisCo activities and amounts of marine macroalgae grown under current and elevated seawater CO_2 concentrations. *Global Change Biology*. 2002; 8(9): 831–840. DOI: 10.1046/j.1365-2486.2002.00518.x

[43] Fernández PA, Roleda MY, Hurd CL. Effects of ocean acidification on the photosynthetic performance, carbonic anhydrase activity and growth of the giant kelp *Macrocystis pyrifera*. *Photosynthesis Research*. 2015; 124: 293–304. DOI: 10.1007/s11120-015-0138-5

[44] Axelsson L, Ryberg H, Beer S. Two modes of bicarbonate utilization in the marine green macroalga *Ulva lactuca*. *Plant, Cell & Environment*. 1995; 18(4): 439–445. DOI: 10.1111/j.1365-3040.1995.tb00378.x

[45] Fernández PA, Hurd CL, Roleda MY. Bicarbonate uptake via an anion exchange protein is the main mechanism of inorganic carbon acquisition by the giant kelp *Macrocystis pyrifera* (Laminariales, Phaeophyceae) under variable pH. *Journal of Phycology*. 2014; 50(6): 998–1008. DOI: 10.1111/jpy.12247

[46] Drechsler Z, Sharkia R, Cabantchik ZI. Bicarbonate uptake in the marine macroalga *Ulva* sp. is inhibited by classica probes of anion exchange by red blood cells. *Planta*. 1993; 191: 34–40. DOI: 10.1007/BF00240893

[47] Axelsson L, Larsson C, Ryberg H. Affinity, capacity and oxygen sensitivity of two different mechanisms for bicarbonate utilization in *Ulva lactuca* L.(Chlorophyta). *Plant, Cell & Environment*. 1999; 22(8): 969–978. DOI: 10.1046/j.1365-3040.1999.00470.x

[48] Giordano M, Beardall J, Raven JA. CO_2 concentrating mechanisms in algae: mechanisms, environmental modulation, and evolution. *Annual Review of Plant Biology*. 2005; 56: 99–131. DOI: 10.1146/annurev.arplant.56.032604.144052

[49] Klenell M, Snoeijs P, Pedersén M. Active carbon uptake in *Laminaria digitata* and *L. saccharina* (Phaeophyta) is driven by a proton pump in the plasma membrane. *Hydrobiologia*. 2004; 514(1–3): 41–53. DOI: 10.1023/B:hydr.0000018205.80186.3e

[50] Smith RG, Bidwell RGS. Mechanism of photosynthetic carbon dioxide uptake by the red macroalga, *Chondrus crispus*. *Plant Physiology*. 1989; 89(1): 93–99. DOI: 10.1104/pp.89.1.93

[51] Choo K, Snoeijs P, Pedersén M. Uptake of inorganic carbon by *Cladophora glomerata* (Chlorophyta) from the Baltic Sea. *Journal of Phycology*. 2002; 38(3): 493–502. DOI: 10.1046/j.1529-8817.2002.01083.x

[52] Beer S. Mechanisms of inorganic carbon acquisition in marine microalgae (with special reference to the Chlorophyta). *Progress in Phycological Research*. 1994; 10: 179–207.

[53] Beer S. Photosynthetic utilization of inorganic carbon in *Ulva*. *Scientia Marina*. 1996; 60(Supl. 1): 125–128.

[54] Larsson C, Axelsson L, Ryberg H. Photosynthetic carbon utilization by *Enteromorpha intestinalis* (Chlorophyta) from a Swedish rockpool. *European Journal of Phycology*. 1997; 32(1): 49–54. DOI: 10.1080/09541449710001719365

[55] Snoeijs P, Klenell M, Choo K. Strategies for carbon acquisition in the red marine macroalga *Coccotylus truncatus* from the Baltic Sea. *Marine Biology*. 2002; 140(3): 435–444. DOI: 10.1007/s00227-001-0729-x

[56] Murru M, Sandgren CD. Habitat matters for inorganic carbon acquisition in 38 species of red macroalgae (Rhodophyta) from Puget Sound, Washington, USA. *Journal of Phycology*. 2004; 40(5): 837–845. DOI: 10.1111/j.1529-8817.2004.03182.x

[57] Cornwall CE, Revill AT, Hurd CL. High prevalence of diffusive uptake of CO_2 by macroalgae in a temperate subtidal ecosystem. *Photosynthesis Research*. 2015; 124(2): 181–190. DOI: 10.1007/s11120-015-0114-0

[58] Andría JR, Pérez-Lloréns JL, Vergara JJ. Mechanisms of inorganic carbon acquisition in *Gracilaria gaditana* nom. prov.(Rhodophyta). *Planta*. 1999; 208(4): 564–573. DOI: 10.1007/s004250050594

[59] Gómez-Pinchetti JL, Ramazanov Z, García-Reina G. Effect of inhibitors of carbonic anhydrase activity on photosynthesis in the red alga *Soliera filiformis* (Gigartinales: Rhodophyta). *Marine Biology*. 1992; 114(2): 335–339. DOI: 10.1007/BF00349536

[60] Gravot A, Dittami SM, Rousvoal S. Diurnal oscillations of metabolite abundances and gene analysis provide new insights into central metabolic processes of the brown alga *Ectocarpus siliculosus*. *New Phytologist*. 2010; 188(1): 98–110. DOI: 10.1111/j.1469-8137.2010.03400.x

[61] Zou D, Gao K, Chen W. Photosynthetic carbon acquisition in *Sargassum henslowianum* (Fucales, Phaeophyta), with special reference to the comparison between the vegetative

and reproductive tissues. *Photosynthesis Research*. 2011; 107(2): 159–168. DOI: 10.1007/s11120-010-9612-2

[62] Zou DH, Gao KS, Xia JR. Photosynthetic utilization of inorganic carbon in the economic brown alga, *Hizikia fusiforme* (Sargassaceae) from the South China Sea. *Journal of Phycology*. 2003; 36: 1095–1100. DOI: 10.1111/j.0022-3646.2003.03-038.x

[63] Yue GF, Wang JX, Wang JF. Inorganic carbon acquisition by juvenile sporophyte of Laminarials (*L. japonica* ×*L. longissima*). *Oceanologia et Limnologia Sinica*. 2001; 32(6): 647–652.

[64] Nakajima K, Tanaka A, Matsuda Y. SLC4 family transporters in a marine diatom directly pump bicarbonate from seawater. *Proceedings of the National Academy of Sciences of the United States of America*. 2013; 110(5): 1767–1772. DOI: 10.1073/pnas.1216234110

[65] Hopkinson BM. A chloroplast pump model for the CO_2 concentrating mechanism in the diatom *Phaeodactylum tricornutum*. *Photosynthesis Research*. 2014; 121(2–3): 223–233. DOI: 10.1007/s11120-013-9954-7

[66] Karlsson J, Clarke AK, Chen ZY. A novel α-type carbonic anhydrase associated with the thylakoid membrane in *Chlamydomonas reinhardtii* is required for growth at ambient CO_2. *EMBO Journal*. 1998; 17(5): 1208–1216. DOI: 10.1093/emboj/17.5.1208

[67] Karlsson J, Hiltonen T, Husic HD. Intracellular carbonic anhydrase of *Chlamydomonas reinhardtii*. *Plant Physiology*. 1995; 109(2): 533–539. DOI: 10.1104/pp.109.2.533

[68] Hanson DT, Franklin LA, Samuelsson G. The *Chlamydomonas reinhardtii* cia3 mutant lacking a thylakoid lumen-localized carbonic anhydrase is limited by CO_2 supply to RuBisCo and not photosystem II function in vivo. *Plant Physiology*. 2003; 132(4): 2267–2275. DOI: 10.1104/pp.103.023481

[69] Raven JA. CO_2-concentrating mechanisms: a direct role for thylakoid lumen acidification? *Plant, Cell & Environment*. 1997; 20(2): 147–154. DOI: 10.1046/j.1365-3040.1997.d01-67.x

[70] Mitra M, Lato SM, Ynalvez RA. Identification of a new chloroplast carbonic anhydrase in *Chlamydomonas reinhardtii*. *Plant Physiology*. 2004; 135(1): 173–182. DOI: 10.1104/pp.103.037283

[71] Sültemeyer D. Carbonic anhydrase in eukaryotic algae: characterization, regulation, and possible function during photosynthesis. *Canadian Journal of Botany*. 1998; 76(6): 962–972. DOI: 10.1139/b98-082

[72] Badger MR, Price GD. The role of carbonic anhydrase in photosynthesis. *Annual Review of Plant Biology*. 1994; 45(1): 369–392. DOI: 10.1146/annurev.pp.45.060194.002101

[73] Badger MR, Price GD. The CO_2 concentrating mechanism in cyanobacteria and microalgae. *Physiologia Plantarum*. 1992; 84(4): 606–615. DOI: 10.1034/j.1399-3054.1992.840416.x

[74] Hewett-Emmett D, Tashian RE. Functional diversity, conservation, and convergence in the evolution of the α-, β-, and γ-carbonic anhydrase gene families. *Molecular Phylogenetics and Evolution*. 1996; 5(1): 50–77. DOI: 10.1006/mpev.1996.0006

[75] Roberts SB, Lane TW, Morel FMM. Carbonic anhydrase in the marine diatom *Thalassiosira weissflogii* (Bacillariophyceae). *Journal of Phycology*. 1997; 33: 845–850. DOI: 10.1111/j.0022-3646.1997.00845.x

[76] So AK, Espie GS, Williams EB.A novel evolutionary lineage of carbonic anhydrase (epsilon class) is a component of the carboxysome shell. Journal of Bacteriology. 2004; 186: 623–630. DOI: 10.1128/JB.186.3.623-630.2004

[77] Lane TW, Morel FMM. Regulation of carbonic anhydrase expression by zinc, cobalt, and carbon dioxide in the marine diatom *Thalassiosira weissflogii*. *Plant Physiology*. 2000; 123: 345–352. DOI: 10.1104/pp.123.1.345

[78] Park H, Song B, Morel FMM. Diversity of the cadmium-containing carbonic anhydrase in marine diatoms and natural waters. *Environmental Microbiology*. 2007; 9(2): 403–413. DOI: 10.1111/j.1462-2920.2006.01151.x

[79] Lane TW, Saito MA, George GN. Biochemistry: a cadmium enzyme from a marine diatom. *Nature*. 2005; 435(7038): 42. DOI: 10.1038/435042a

[80] Xu Y, Feng L, Jeffrey PD. Structure and metal exchange in the cadmium carbonic anhydrase of marine diatoms. *Nature*. 2008; 452(7183): 56–61. DOI: 10.1038/nature06636

[81] Ferry JG. The γ class of carbonic anhydrases. *Biochimica et Biophysica Acta*. 2010; 1804(2): 374–381. DOI: 10.1016/j.bbapap.2009.08.026

[82] Coleman JR, Grossman AR. Biosynthesis of carbonic anhydrase in *Chlamydomonas reinhardtii* during adaptation to low CO_2. *Proceedings of the National Academy of Sciences of the United States of America*. 1984; 81(19): 6049–6053. DOI: 10.1073/pnas.81.19.6049

[83] Fujiwara S, Fukuzawa H, Tachiki A. Structure and differential expression of two genes encoding carbonic anhydrase in *Chlamydomonas reinhardtii*. *Proceedings of the National Academy of Sciences of the United States of America*. 1990; 87(24): 9779–9783. DOI: 10.1073/pnas.87.24.9779

[84] Eriksson M, Karlsson J, Ramazanov Z. Discovery of an algal mitochondrial carbonic anhydrase: molecular cloning and characterization of a low-CO_2-induced polypeptide in *Chlamydomonas reinhardtii*. *Proceedings of the National Academy of Sciences of the United States of America*. 1996; 93(21): 12031–12034. DOI: 10.1073/pnas.93.21.12031

[85] Moroney JV, Husic HD, Tolbert NE. Effect of carbonic anhydrase inhibitors on inorganic carbon accumulation by *Chlamydomonas reinhardtii*. *Plant Physiology*. 1985; 79(1): 177–183. DOI: 10.1104/pp.79.1.177

[86] Van K, Spalding MH. Periplasmic carbonic anhydrase structural gene (Cah1) mutant in *Chlamydomonas reinhardtii*. *Plant Physiology*. 1999; 120(3): 757–764. DOI: 10.1104/pp.120.3.757

[87] Lucas WJ. Photosynthetic assimilation of exogenous HCO_3^- by aquatic plants. *Annual Review of Plant Physiology*. 1983; 34(1): 71–104. DOI: 10.1146/annurev.pp.34.060183.000443

[88] Peña KL, Castel SE, de Araujo C. Structural basis of the oxidative activation of the carboxysomal γ-carbonic anhydrase, CcmM. *Proceedings of the National Academy of Sciences of the United States of America*. 2010; 107(6): 2455–2460. DOI: 10.1073/pnas.0910866107

[89] Tachibana M, Allen AE, Kikutani S. Localization of putative carbonic anhydrases in two marine diatoms, *Phaeodactylum tricornutum* and *Thalassiosira pseudonana*. *Photosynthesis Research*. 2011; 109(1–3): 205–221. DOI: 10.1007/s11120-011-9634-4

[90] Chen C, Dai Z, Xu Y. Cloning, expression, and characterization of carbonic anhydrase genes from *Pyropia haitanensis* (Bangiales, Rhodophyta). *Journal of Applied Phycology*. DOI: 10.1007/s10811-015-0646-x

[91] Zhang BY, Yang F, Wang GC. Cloning and quantitative analysis of the carbonic anhydrase gene from *Porphyra yezoensis*. *Journal of Phycology*. 2010; 46: 290–296. DOI: 10.1111/j.1529-8817.2009.00801.x

[92] Yu Z, Bi YH, Zhou ZG. Cloning and characterization of carbonic anhydrase (CA) gene from *Laminaria japonica* gametophytes. *Journal of Fisheries of China*. 2011; 35: 1343–1353.

[93] Ye RX, Yu Z, Shi WW. Characterization of α-type carbonic anhydrase (CA) gene and subcellular localization of α-CA in the gametophytes of *Saccharina japonica*. *Journal of Applied Phycology*. 2014; 26: 881–890. DOI: 10.1007/s10811-013-0221-2

[94] The FAO yearbook of Fishery and Aquaculture Statistics: Aquaculture Production. Rome: Food and Agriculture Organization of the United Nations; 2009. 221 p.

[95] Ross AB, Jones JM, Kubacki ML. Classification of macroalgae as fuel and its thermochemical behaviour. *Bioresource Technology*. 2008; 99(14): 6494–6504. DOI: 10.1016/j.biortech.2007.11.036

[96] Ye N, Zhang X, Miao M. *Saccharina* genomes provide novel insight into kelp biology. *Nature Communications*. 2015; 6: 6986. DOI: 10.1038/ncomms7986

[97] Deng YY, Yao JT, Wang XL. Transcriptome sequencing and comparative analysis of *Saccharina japonica* (Laminariales, Phaeophyceae) under blue light induction. *PLoS One*. 2012; 7(6): e39704. DOI: 10.1371/journal.pone.0039704

[98] Wang WJ, Wang FJ, Sun XT. Comparison of transcriptome under red and blue light culture of *Saccharina japonica* (Phaeophyceae). *Planta*. 2013; 237(4): 1123–1133. DOI: 10.1007/s00425-012-1831-7

[99] Heinrich S, Valentin K, Frickenhaus S. Transcriptomic analysis of acclimation to temperature and light stress in *Saccharina latissima* (Phaeophyceae). *PloS One*. 2012; 7(8): e44342. DOI: 10.1371/journal.pone.0044342

[100] Tamura K, Stecher G, Peterson D. MEGA6: molecular evolutionary genetics analysis Version 6.0. *Molecular Biology and Evolution*. 2013; 30: 2725–2729. DOI: 10.1093/molbev/mst197

Chapter 7

The Photosynthetic Pancreas: From Fantasy to Reality

Yoav Evron, Tali Goldman, Shiri Maimon,
Nurit Shalev, Karina Yavriants, Dimitry Azarov,
Dr. Baruch Zimerman and Dr. Avi Rotem

Additional information is available at the end of the chapter

http://dx.doi.org/10.5772/62237

Abstract

Islets of Langerhans implantation is a viable method to treat type I diabetes. Unfortunately, during islets isolation their vascular system is disrupted, and they need external supply of oxygen and other nutrients. A photosynthetic bioartificial device was constructed to support the oxygen consumption of the islets and to treat type I diabetes. The bioartificial device is built in layers where the core is an illumination module composed of a LED array and a light guide. The next layer is immobilized photosynthetic organism (*Synechococcus lividus*). An oxygen-permeable silicon/Teflon membrane separates the photosynthetic layer from the islets of Langerhans layer. This layer is protected from the immune system of the body by a porous Teflon membrane. The device is powered by batteries that supply electricity to a LED array. The oxygen produced by *S. lividus* is consumed by implanted islets of Langerhans that produce insulin and allow the reversal of diabetes in the patient. In this chapter, we demonstrate the ability of *S. lividus* to produce oxygen after being implanted for prolonged periods and eventually the ability of the device containing *S. lividus* and the islets of Langerhans to reverse diabetes for 10 days. To achieve this task, we developed improved media to grow cyanobacteria and, inter alia, developed a method to disperse light uniformly and in very short distances.

Keywords: Bioartificial device, Cyanobacteria, Diabetes, Implanted islets of Langerhans, Synechococcus *lividus*

1. Introduction

Type I diabetes (T1D) is a severe disease resulting from the destruction of the beta cells in the islets of Langerhans (islets) residing in the pancreas. The loss of beta cells leads to lack of insulin and increased glucose levels in the blood (hyperglycemia). If untreated, T1D 1 leads to permanent damage to small blood vessels which in turn causes blindness, kidney failure, heart failure and eventually premature death [1,2]. Even when treated with external insulin, blood glucose levels are not stable and fluctuate according to eating habits and insulin administration. On the other hand, too much insulin can cause a dangerous drop in the blood glucose level (hypoglycaemia), which leads to confusion, loss of conscience and, if not immediately treated, sudden death.

Great efforts are made to develop a "closed loop" insulin pump that will secrete insulin when needed (after a meal) and sense the glucose level in order to stop secretion when glucose levels drop to normal levels. Islet implantation is another successful approach that utilizes donor's islets isolated from the pancreas to replace the missing islets of the patient. This approach, although promising, faces several obstacles that decrease its feasibility.

1. Harvesting of the islets from the donor pancreas is performed by enzymatic process, completely disrupting the blood vessels to the islets. As a result, all nutrients supply and insulin secretion from the islet rely on slow diffusion mechanism. The solubility of oxygen in blood fluid is low and its consumption is high. Therefore, it is the first nutrient becoming the limiting factor and it must be supplied [3].

2. Donor islets will be rejected by the immune system of the host, and therefore, constant harmful immune suppression drugs are needed [4,5].

To approach these two fundamental problems, Beta-O2 Technologies had designed implantable flat geometry device containing islets that were supplied with oxygen by immobilized and illuminated cyanobacteria. The implanted islets are partly protected from the attack of the immune system by a porous Teflon membrane. **Photosynthesis** was the source of the supply of oxygen, which is the focus of this chapter . Indeed, the designed device termed bioartificial pancreas contains battery-powered illumination module, photosynthetic organisms that produce oxygen and islets that produce insulin upon demand.

To create this "science fiction" bio-artificial pancreas device, a multidisciplinary approach was needed involving optics, material science, diffusion models, plant and islet biochemistry and other fields.

2. The construction of the photosynthetic bioartificial pancreas

A. To construct such a complex device, several requirements had to be set:

1. The device must be as compact as possible to reduce the trauma after implantation.

http://dx.doi.org/10.5772/62237

2. The batteries driving the operation of the device should last at least one month for the proof of concept.
3. The power unit (batteries) must be separated from the bioreactor to decrease the immune response against foreign body, which depends upon size.
4. The light distribution must be even in all the active areas to ensure uniform oxygen production.
5. All materials exposed to body fluids must be biocompatible to provoke minimum response of the immune system.
6. The photosynthetic organism must be functional in body temperatures and withstand immobilization in the device and implantation conditions. It must also be spread even so that oxygen production will be uniform, constant and in direct contact with the islets.
7. There should be no hindrance in the diffusion of the oxygen from the oxygen producers to the oxygen consumers — the islets.
8. The islets must be active insulin producers and must be spread and immobilized evenly in the device to maximize diffusion quality.
9. The device must be protected from the body's immune system.
10. The electrical parts of the device must be completely insulated from fluid penetration.

B. The selection of the photosynthetic organism

The constraints: The aim of the photosynthetic organism in this system is producing oxygen for the islets**.** Body temperature is too high for most photosynthetic organisms. The organism has to withstand temperatures between 37 and 42°C. Since the organism has to be embedded in aqueous matrix or hydrogel, microalgae were the organism of choice. Indeed, the first work showing the beneficial effect of photosynthetic oxygen production on insulin secretion was conducted with the green algae *Chlorella* [6], but it was an in vitro study. Very few green algae can survive and be active at 37°C, and fewer still can withstand the much higher temperatures needed for immobilization in agarose. Therefore, we chose to introduce thermophilic cyanobacteria. Cyanobacteria are the first photosynthetic oxygen-evolving organisms on earth, and during the 3.5 billion years of their existence they adapted to any environment containing light, humidity and few minerals. Many cyanobacteria species grow at relatively low illumination, can survive hard conditions and still grow and produce oxygen. Several members of this large group of organisms live in proximity to geysers at temperatures reaching 70°C [7]. We chose to use *Synechococcus lividus* (*S. lividus*), a unicellular cyanobacteria found in hot springs in Yellowstone National Park, USA [8]. This strain was obtained from the Pasteur culture collection (PCC6717). PCC 6717 has an optimum growth at 52–57°C but grows well also Between 37°C and 42°C. To acclimate the *S. lividus* to body temperatures, it was grown for 10 generations in liquid culture at 40°C before being taken for immobilization in the device. Its oxygen production characteristics were checked prior to immobilization and

were shown to be stable. In nature (**Figure 1**), *S. lividus* creates bacterial mats with other organisms. Therefore, it is used to survive and function in the immobilized state. Occasionally, *S. lividus* will be termed algae for convenience, especially with relation to the device.

Figure 1. Bacterial mat containing thermophile cyanobacteria. A slice of bacterial mat (right) from Octopus spring (left) in Yellowstone National Park, USA. On top there is a layer of (mostly) cyanobacteria. Right panel is a picture by Prof. David M. Ward (October 13, 2008, by Charles Fergus, Penn State News).

C. The choice of growth medium for *S. lividus*: How much is good enough?

The cyanobacteria are enclosed within a silicon box to be protected from the host's immune system. All gas exchange (uptake of CO_2 and secretion of O_2) are performed via the silicon membrane. Therefore, all nutrients must be supplied within the silicon box for the period of implantation. This poses two problems:1. The osmolality of the BG-11 medium which is the standard medium for the growth of cyanobacteria is about 40 mOsmol/l of water, compared with 275–295 mOsmol/l of body liquid. To equilibrate the osmolalities, water molecules as vapor will escape the algae medium, leading to drying of the algae compartment. 2. BG 11 medium can support cyanobacterial growth when the medium is changed frequently, but cannot support long-term growth or photosynthesis without frequent changes of the medium. In the design of the bioartificial pancreas, the first milestone was to show treatment of diabetes for a month supported by oxygen produced by the cyanobacteria. It was difficult to obtain such a performance of the cyanobacteria based on BG-11, so efforts were made to improve the medium in order to extend its ability to support the photosynthetic activity of *S. lividus*. After several futile efforts of elevating individual components of the medium, the overall BG-11 concentration was increased. Surprisingly, increasing the BG-11 medium concentration 5 to 7-fold resulted in a 3-fold increase of the *S. lividus* cell density (**Fig. 2**B). This result indicates that BG-11x5-7 is a superior medium for the growth of *S. lividus* in solution, compared to BG-11. Also, since the osmolarity was increased it resembles that of body fluids, so no water loss from the algae compartment is anticipated. These findings enabled the use of medium that can support a long-term oxygen production by the *S. lividus* under the conditions set in the bio-artificial pancreas. It was later shown that indeed, *S. lividus* immobilized and im-

http://dx.doi.org/10.5772/62237

planted with BG-11x5 developed much better than *S. lividus* implanted in the original BG-11, produced higher oxygen amounts and maintained its volume under immobilized conditions.

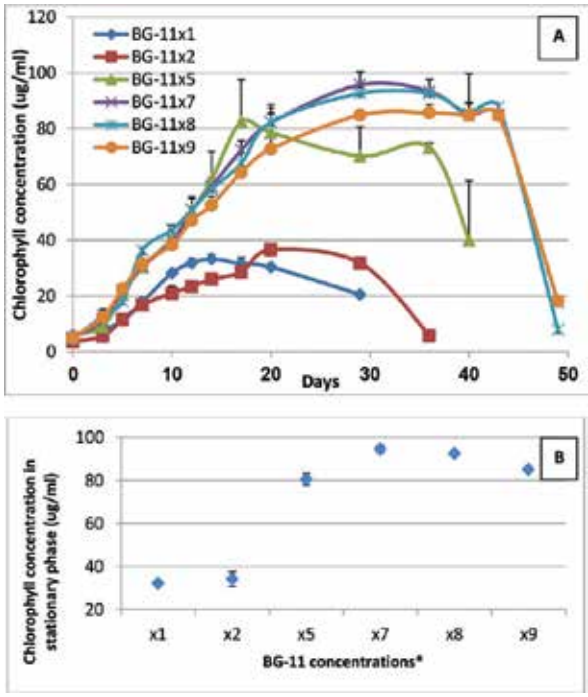

Figure 2. Dependence of bacterial growth on BG-11 concentration. Panel A: Dependence of *S. lividus* culture growth on the BG-11 concentration over time. Panel B illustrates the maximum concentration each culture has reached. Each result is the average of at least three experiments, apart of BG-11×2 that was tried only once.

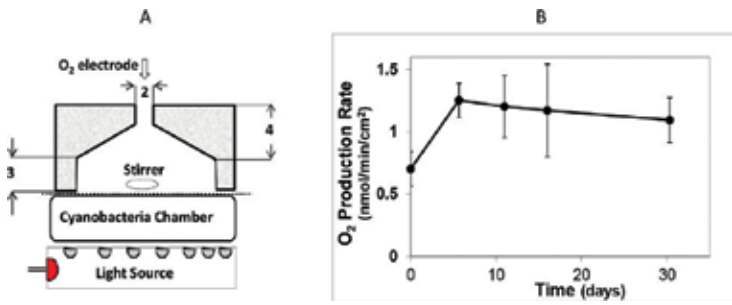

Figure 3. The oxygen measurement setup of the bioartificial pancreas. A device containing algae only (*S. lividus*) immobilized in agarose plus BG-11x5 was placed in a home-made oxygen measurement cell where a Clark-type oxygen microelectrode is inserted (Panel **A**). *S. lividus* is illuminated by a LED array as described later. The device was kept in vitro under identical conditions to the implanted device and tested periodically (Panel **B**) for oxygen production.

As shown in **Figure 3B**, the oxygen production did not diminish, but actually improved during the one month the device was tested. The BG-11 concentration in this device was BG-11×5.

The ability of the media with elevated BG-11 concentrations to support oxygen production in the device was shown both before and after implantation. It was shown that *S. lividus* alone was able to produce oxygen that will diffuse into the islets of Langerhans compartment and will allow the islets to function properly. As can be seen in **Figure 4**, an oxygen electrode is inserted into the islet part of the bioartificial pancreas. The deeper the electrode penetrates into the islet slab and gets closer to the *S. lividus* chamber, the higher is the oxygen concentration. The oxygen levels detected can support islet activity at any location and depth of the electrode.

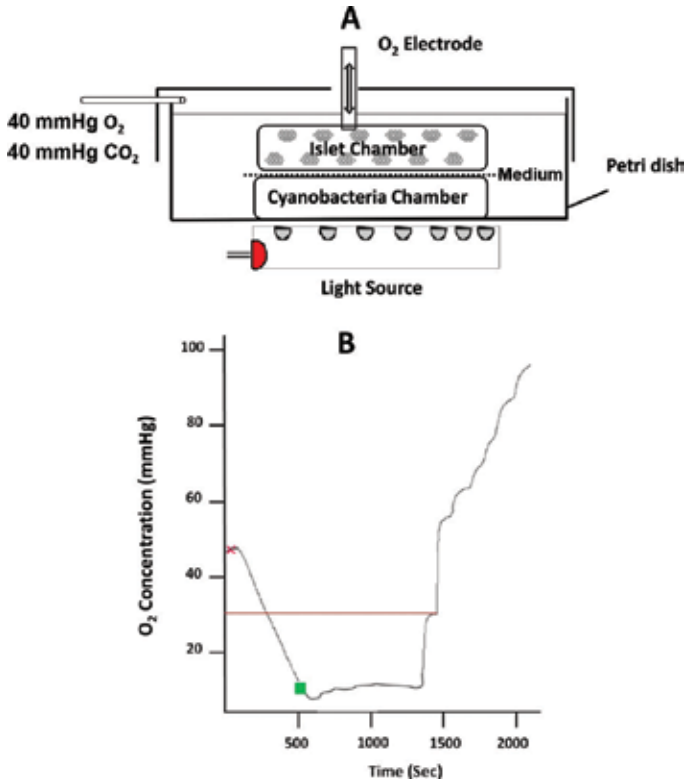

Figure 4. Measurement of the O_2 gradient in the islet slab in the device. Panel A: Device with oxygen electrode. Oxygen microelectrode was inserted by a micromanipulator at increments of 0.1mm into the islet slab with a thickness of 0.6 mm. Panel B: The O_2 concentration as a function of illumination and location of the oxygen electrode. At the start of the test, the electrode tip is located at the surface of the islet slab, the furthest point from the O_2 source. The light is turned off and the oxygen is consumed (concentration drops). The light is turned on leading to balanced O_2 concentration. Under illumination the electrode is inserted into the islet slab at 0.1mm increments, leading to a gradual increase in O_2 concentration The horizontal line indicates the O_2 concetration sufficient to support the islet's O_2 consumption.

http://dx.doi.org/10.5772/62237

D. The illumination requirements for growth and oxygen production: the struggle for homogeneous light

The cyanobacteria were chosen for their ability to produce oxygen even at very low light intensities, below 1 μE/m²/s. Since the device operates on batteries, the longer the batteries Last, the longer the device would work. The milestone was achieving normoglycemia for one month in diabetic rats, and for that time span the batteries should hold. The light

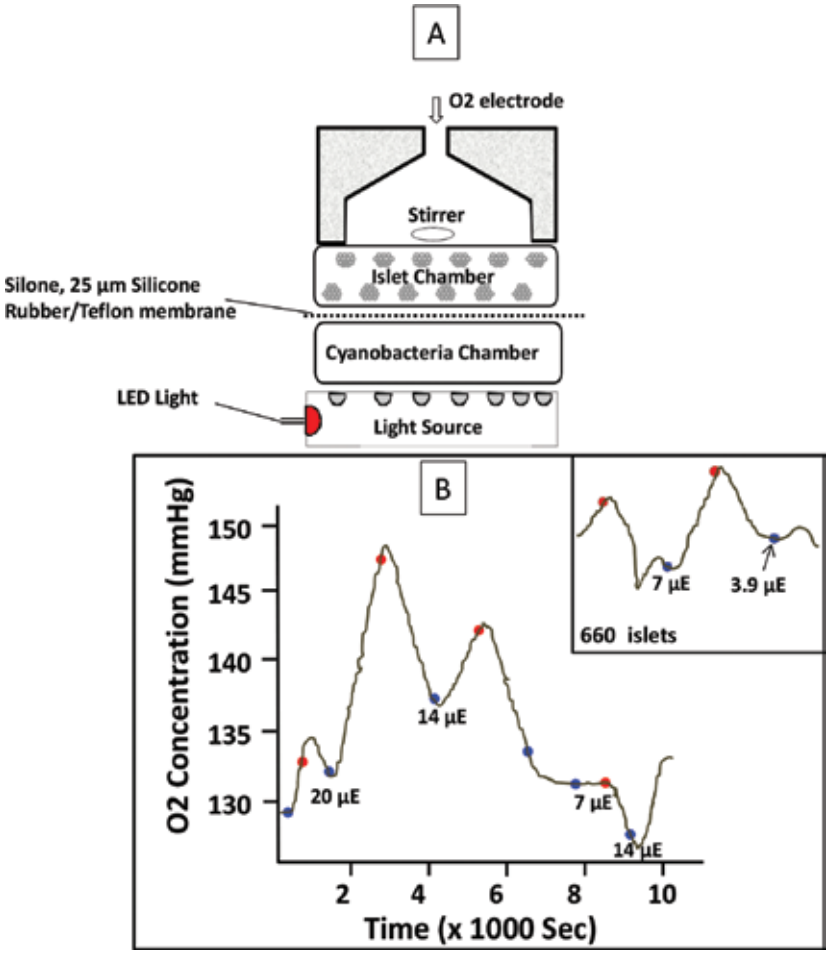

Figure 5. Compensation between oxygen production by *S. lividus* and oxygen consumption by the islets. Panel A. Schematic view of the oxygen measurement setup of the full device. Panel B. Measuring the oxygen production rate of *S. lividus* (cyanobacteria) plus the islets in order to determine the light intensity required for achieving the compensation point of the device. 1,200 islets of Langerhans, each consuming 2.5–3 pmole/min O_2, were embedded in alginate and placed on top of the *S. lividus* slab. Light intensity of 7μE/m²/s was needed to reach the compensation point. The insert (600 islets) demonstrates that compensation point is reached with light intensity (3.9μE/m²/s) which is half the light intensity needed for reaching the compensation point with 1,200 islets.

intensity needs to be such that it allows *S. lividus* to produce enough oxygen for the consumption of the islets. Therefore, the oxygen production should be equal to the oxygen consumption by the islets, what we termed **the compensation point** of the device (**Figure 5B**).

Higher intensities cause excess oxygen production that can lead to oxidative stress for both *S. lividus* and the implanted islets. Also, over-illumination causes loss of battery power and early termination of the trial.

Light quality: After checking several LED types with different wavelengths, 660nm wavelength was chosen since it is absorbed well by chlorophyll. It proved best both for oxygen evolution and also was electrically most efficient. ($E = hC/\lambda$, where E is the energy, h is Planck's constant, C is the speed of light and λ is the wavelength. The longer the wavelength, the lower is the energy of the photon, and the electric energy needed for its production.). The second, more formidable task was to disperse the light as much as possible when it enters the *S. lividus* chamber. The reasons for that are: the direct result of the illumination is oxygen production from *S. lividus*. We need the oxygen production to be uniform at all parts of the algae compartment because the oxygen diffuses directly to the islets compartment. The islets, too, need the oxygen in the most even manner, so as not to have parts with too little oxygen that will lead to islet necrosis. On the other hand, too high intensity will lead to oxidative stress, followed by bleaching of the cyanobacteria. At such short distance of less than a millimetre, it is extremely hard to disperse the LED light uniformly. Early attempts (**Figure 6**) show non-uniform growth of *S. lividus* as a result of exposure to non-uniform light.

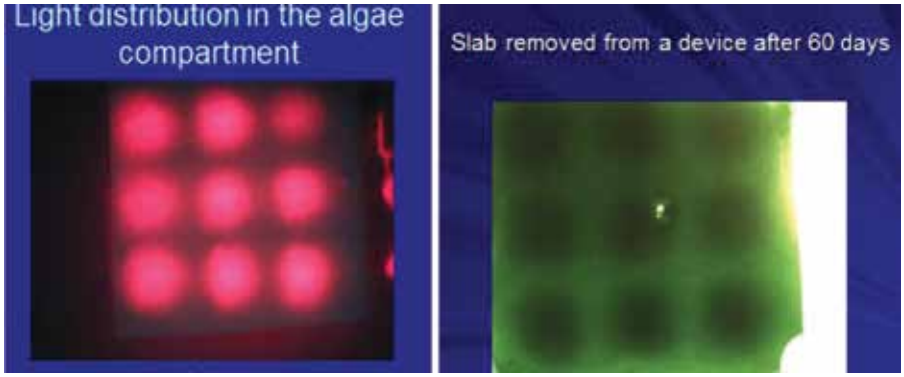

Figure 6. Correlation between light distribution in the device and *S. lividus* growth Left: The LED array on which the immobilized *S. lividus* was implanted Right: an agarose slab of *S. lividus* implanted in a rat for 60 days on a LED array.

To achieve uniform light source we constructed a LED light guide that allows light dispersion (patent no.) and uniform light to the *S. lividus* compartment (**Figure 7**).

http://dx.doi.org/10.5772/62237

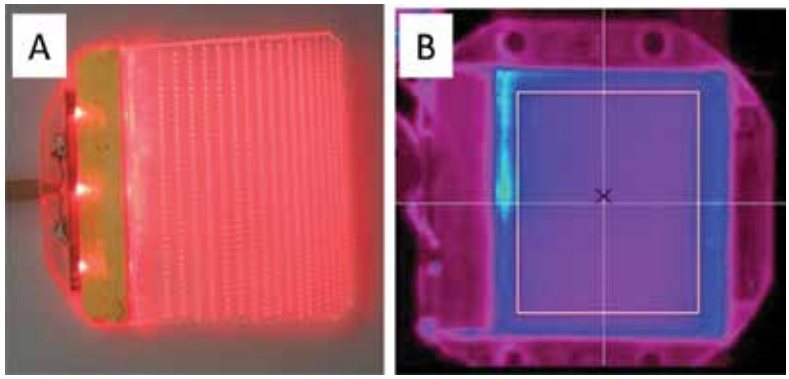

Figure 7. The bioreactor light guide Panel A. the LED operated light guide Panel B: *S. lividus* immobilized in agarose slab, illuminated by the light guide. The blue colour is an artefact of the camera.

E. The immobilization of the organism: several approaches

To avoid coalescence of both organisms, the islets and the cyanobacteria have to be separated from each other. We used hydrogels for immobilization. Two general methods were used to immobilize the unicellular *S. lividus* in the device. The first one was immobilization in alginate. Alginate is a polysaccharide extracted from brown algae (kelp). It provides flexibility and strength for the kelp to withstand the ocean currents and waves without breaking or tearing. It is provided as a viscous liquid similar to glycerol, which solidifies rapidly upon exposure to divalent ions, like calcium ions. We used it in the first devices, but stopped when we started to inject the algae with its immobilizer into a closed compartment. It was impossible to inject the alginate because of its high viscosity. Therefore, we decided to use agarose as the immobilizer. The fact that we use thermophile cyanobacteria helped to mix *S. lividus* with the liquid agarose brought to 50°C and inject it into the device under sterile conditions. For immobilization of the islets we used alginate, and cross-linked it with strontium.

F. The construction of the bioartificial pancreas

Physically, the best approach to supply oxygen to the islet by photosynthetic microorganisms is to mix them in the same compartment [6]. Attempts to combine the photosynthetic organisms with the islets in the same chamber and the same medium (DMED or RPMI) resulted in the rapid death of *S. lividus*. Attempts to construct mini balls of *S. lividus* isolated by a sol–gel coat or other protection failed as well. It was clear early on that the *S. lividus* chamber and the islet chamber must be separated by a membrane that allows the diffusion of only gases. This approach holds the risk of gas diffusion constraints from the algae chamber to the islets chamber and vice versa. To minimize this problem, a thin silicone/Teflon membrane is used between the algae and the islet chambers. A second membrane that allows insulin to diffuse out and nutrients in, but blocks the immune cells, was needed between the islets and the body.

Several approaches were tested, but eventually we embarked with a flat device illuminating both directions having the illumination panel at the core, coated with immobilized *S. lividus* and above it two islets chambers, again on both sides (**Figure 8**).

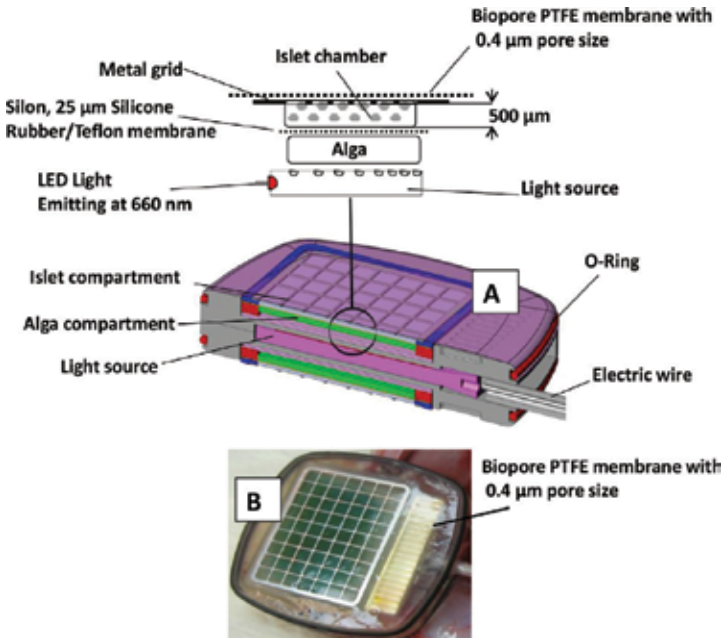

Figure 8. The photosynthetic bioartificial pancreas. The device has a core illumination panel directing the 660 nm light to both sides. The algae chamber is laid directly on the illumination panel and is separated from the islet chamber with gas-permeable thin silicone/Teflon membrane. The islet chamber is protected from the immune cells by porous biopore membrane. Panel A: Detailed cross-section of the device. **Panel B**: Actual view of the device.

G. The implantation of the device: reversing diabetes in rats

As stated before, the designed device was aimed to treat type 1 diabetic (T1D) rats as model animals. Initially, to learn the dose needed to cure STZ (Streptozotocine) diabetic rat, we implanted various islet doses under the kidney capsule, and found that about 2400 islets are sufficient to reverse diabetes. Therefore, we constructed our device with 2400 islets. To allow implantation into non-suffering animal, it was treated with slow-release insulin capsule (**Figure 9**, LPin). T1D animals were implanted with the device containing 2400 islets and the slow-release insulin capsule was removed (**Figure 9**, LPout). At this stage, the only entity that can produce insulin and reverse the diabetes is the implanted device (**Figure 9**).

This experiment, which is the culmination of efforts ranging from physics, optics, material engineering, islet biology and microbial photosynthesis, is a remarkable multidisciplinary project ending in success, although only partial.

http://dx.doi.org/10.5772/62237

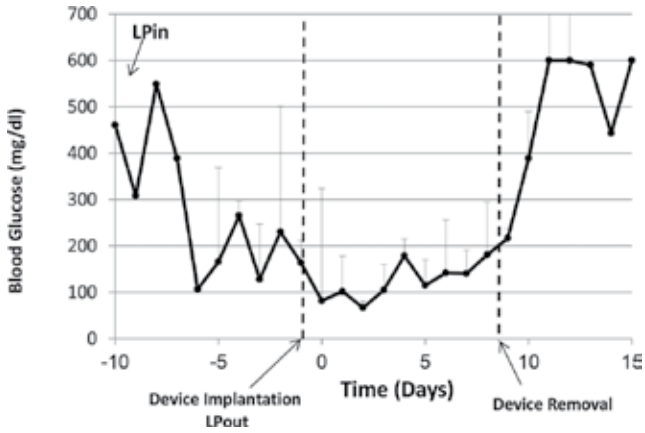

Figure 9. The effect of bioartificial pancreas implantation on the glycemic state of the implanted diabetic rat. The implanted device, driven by light and supplies oxygen by photosynthesis, allowed the implanted islets to function well and produce enough insulin to reverse diabetes in rats for 10 days (day 0 to day 9).

H. Conclusions and further possibilities

Several issues should be addressed when planning to continue toward a working device to treat lab animals and later, humans, with the bioartificial photosynthetic device.

1. The device can probably be active in the body for few months. However, the implanted batteries which power the light need to be recharged. Therefore, a recharging mechanism is needed.

2. Most of the oxygen is produced from photosynthesis during the logarithmic phase. The growth leads to self-shading that increasingly leads to light limitation. Overall produced oxygen will then eventually decrease. Example of that can be seen in **Figure 6**, where above the LEDs, *S. lividus* is much darker than the surroundings. A possible solution is developing a method of removing the excess cyanobacteria (see next paragraph).

3. Although great advances were made in improving *S. lividus* growth medium, eventually it will be exhausted, leading to a culture in the stationary phase and lack of oxygen production. A method must be found to exchange the medium periodically.

4. Scaling up the device to human size will require more islets packed at a higher density. To compensate for the increased islet density, more O_2 has to be produced. However, using this type of solid-state bioreactor, we reached the maximum O_2 production rate. Therefore, in order to supply O_2 to bioartificial pancreas with dimensions that are practical for implantation in human, the photosynthesis approach should be greatly improved.

To summarize, we showed the ability to combine cells of two organisms, one that produce O_2 and the other that consume it, into one implantable device, achieving normoglycemia in

T1D rat. In addition, we developed the effective means to disperse light in water and at very short distances.

Author details

Yoav Evron[1], Tali Goldman[2], Shiri Maimon[2], Nurit Shalev[2], Karina Yavriants[2], Dimitry Azarov[2], Dr. Baruch Zimerman[2] and Dr. Avi Rotem[2]

1 Greenonyx Technologies, Israel

2 Beta-O2 Technologies Ltd., Israel

References

[1] Bloch K, Papismedov E, Yavriyants K, Vorobeychik M, Beer S, Vardi P. Immobilized microalgal cells as an oxygen supply system for encapsulated pancreatic islets: a feasibility study. Artif Organs 2006; 30: 715–718

[2] Cryer PE. Severe hypoglycemia predicts mortality in diabetes. Diab Care 2012; 35: 1814–1816

[3] Carlsson PO, Palm F, Andersson A, Liss P. Markedly decreased oxygen tension in transplanted rat pancreatic islets irrespective of the implantation site. Diabetes 2001; 50: 489–495

[4] Hyder A, Laue C, Schrezenmeir J. Effect of the immunosuppressive regime of Edmonton protocol on the long-term in vitro insulin secretion from islets of two different species and age categories. Toxicol In Vitro 2005; 19: 541–546

[5] Lohmann T, List C, Lamesch P, Kohlhaw K, Wenzke M, Schwarz C, Richter O, Hauss J, Seissler J. Diabetes mellitus and islet cell specific autoimmunity as adverse effects of immunsuppressive therapy by FK506/tacrolimus. Exp Clin Endocrinol Diabetes 2000; 108: 347–352

[6] Bloch K, Papismedov E, Yavriyants K, Vorobeychik M, Beer S, Vardi P. Immobilized microalgal cells as an oxygen supply system for encapsulated pancreatic islets: a feasibility study. Artif Organs 2006; 30: 715–718

[7] Castenholz RW. 1969a. Thermophilic blue-green algae and the thermal environment. Bacteriol. Rev. 33,476-504.

[8] Meeks JC, Castenholz RW. Growth and photosynthesis in an extreme thermophile, Synechococcus lividus (Cyanophyta). Archiv fur Mikrobiologie 1971; 78: 25–41

Chapter 8

Recent Progress in Semiconductor Photocatalysis for Organic Fine Chemical Synthesis

Suzan A. Khayyat, Rosilda Selvin and L. Selva Roselin

Additional information is available at the end of the chapter

http://dx.doi.org/10.5772/62220

Abstract

Photocatalytic process is a well-known reaction in photosynthesis by plants and algae. Artificial photosynthesis is a chemical process that mimics the natural plant photosynthesis to make important chemicals by using man-made materials. One of the most promising methods of artificial photosynthesis is synthesis of organic chemicals, including biodegradable plastics, pharmaceutical drugs, liquid fuels and intermediates for valuable chemicals, etc. In 1972, Fujishima and Honda discovered photocatalytic process using TiO_2 semiconductor oxide electrodes to generate hydrogen from water. Researchers have achieved a single-step system that uses semiconductor particles for organic fine chemical synthesis under UV or visible radiation. This chapter summarizes the recent research trends on artificial photosynthesis by photocatalytic process for organic fine chemical synthesis on selected photocatalytic organic transformations, especially photocatalytic transformations by oxidation, carbon-carbon and carbon-heteroatom coupling, cyclization, etc.

Keywords: artificial photosynthesis, photocatalysis, organic synthesis, oxidation, cyclization, UV light, visible light, C-C bond formation

1. Introduction

The Earth receives energy of about 3×10^{24} joules in a year from sun, which is higher than the global energy consumption. Plants utilize the solar energy to fix atmospheric carbon dioxide and produce carbohydrates and oxygen by photosynthesis. Warburg and Negelein disclosed the photosynthesis, in which reaction occurs between CO_2 and H_2O in the presence of chlorophyll and form O_2 and carbohydrates [1]. It is worth to utilize the solar energy for various energy-consuming processes, since it is clean, sustainable and abundant resource. Artificial

photosynthesis is a process in which fundamental scientific principles of natural photosynthesis are applied to design a solar energy conversion to make important chemicals by using man-made materials. Many approaches are reported. One of the successful reports provides an outline for solar energy storage in fuels [2]. Another important approach is finding a new route for the chemical production and synthesis by utilizing solar energy, which is an energy-decisive industrial process. The method to synthesize organic chemical by photochemical process was first reported by Giacomo Ciamician in 1912 [3]. Presently, photochemistry is a well-developed field of chemistry and the majority of the experiments use direct excitation of molecules by UV light [4]. To activate the photoreaction under visible light, sensitizers are applied, which transfer energy or an electron from the excited state to the molecule to be converted. Various homogeneous sensitizers are successfully used for various organic transformations [5]. The homogeneous sensitizers are substituted by heterogeneous photosensitizers using photocatalytic process and which are easily separable and therefore recycled. In 1972, Fujishima and Honda reported a photocatalytic process using TiO_2 semiconductor oxide e1ectrodes to generate hydrogen from water [6]. Semiconductors can act as photocatalysts for light-induced chemical transformations because of their unique electronic structure, which is characterized by a filled valence band and an empty conduction band. When a photon with an energy of hν matches or exceeds the band gap energy (Eg) of the semiconductor (SC), an electron in the valence band (VB) is promoted to the conduction band (CB), leaving a positive hole (h^+) in VB. The photo-excitation can be written as [7]:

$$SC + h\nu \rightarrow SC\left(h^+\right)_{(vb)} + SC(e^-)_{(cb)} \quad (1)$$

Where SC is semiconductor, vb and cb represent the valance band and the conduction band, respectively. The reactive species, h^+ and e^- are powerful oxidizing and reducing agents, respectively. Subsequently, various oxidizing species such as $^{\bullet}OH$, $O_2^{\bullet-}$, various forms of active oxygen species, such as HO_2, H_2O_2 and O, are produced [8,9].

The photo-excitation process over semiconductor photocatalyst is presented in **Figure 1**.

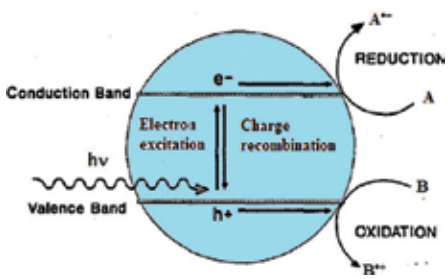

Figure 1 Semiconductor photocatalysed reaction.

Different semiconductors (e.g., TiO_2, ZnO, α-Fe_2O_3 and WO_3) are considered for their potential use as photocatalysts. In early 1980s, great effort was placed on organic synthesis by semicon-

http://dx.doi.org/10.5772/62220

ductor photocatalysis [10]. Photocatalysis in synthetic route has attracted many researchers, because this method presents a greener approach to organic synthesis [11,12]. Recent studies have revealed that highly selective redox reactions could be achieved by visible light irradiation. The studies employed in photocatalytic organic transformation includes, oxidation, reduction, carbon-carbon and carbon-hetero atom coupling, cyclization, isomerization, etc. This chapter deals with various studies performed in oxidation, carbon-carbon and carbon-heteroatom coupling, cyclization by UV and visible light-induced photocatalysis.

In photocatalytic process, photo-oxidation is the most studied because the VB edge in most of the semiconductor catalysts have more positive than the oxidation potential of the functional group in the organic compounds. The oxidation reactions are mainly focused on the oxidation of alcohols, amines, cyclohexane and aromatic alkanes. The conversion and product selectivity could be controlled by tuning the reaction conditions, such as nature of solvent, excitation wavelength of the light, interface engineering such as surface modification to change the adsorption mode or electron transfer pathway.

2. Oxidation of hydrocarbon

Selective partial oxidation of hydrocarbon into its oxidation products, such as aldehyde, ketone, and carboxylic acid, by photocatalytic process is of great importance for chemical industries. Selective oxidation of methane into its useful oxygenates such as methanol and formaldehyde by photocatalytic method is of great challenge. Gondala et al. [13], for the first time, reported the photocatalytic transformation of methane into methanol over WO_3, TiO_2 (rutile) and NiO semiconductor photocatalysts, at room temperature, under the irradiation of a strong UV laser beam at 355 nm. The methanol yield in all three catalysts observed was low due to the degradation of methanol immediately after its formation in the aqueous suspension. Methane activation at low temperature and at atmospheric pressure using supported molybdena TiO_2 catalyst [14] excited by band gap illumination motivated the researchers to test this reaction with various catalysts [15,16]. However, the conversion of methane was low and an advancement in the source of methane such as methane hydrates was used. Methane hydrates available in the ocean at depths between ~280 and 4000 m have higher concentration of methane in water, which is higher than that of water–methane pressurized systems. Comparison of photocatalytic conversion of methane dissolved in water and methane hydrate showed that the conversion of methane dissolved in water was observed at temperatures below 70°C. On the other hand, the photocatalytic conversions of the methane hydrate occurred at temperatures below −5°C [17]. The comparison of the photocatalytic reaction under visible and the full spectrum of UV-visible showed that the production of methanol was 50% greater in visible compared to that with the full spectrum lamp of UV-visible. Complete oxidation of methane could be avoided by changing the atmospheric condition. V-MCM-41 (acid) catalyst prepared under acidic conditions resulted in the selective formation of methanol with NO oxidant compared to O_2 as oxidant under UV radiation accompanied by the formation of trace amounts of CO_2 and acetaldehyde. Metal doping is used to improve the photocatalytic activity by avoiding charge recombination and to achieve visible-driven photocatalysis. Silver-

impregnated WO_3 was studied for the conversion of methane to methanol under laser illumination (100 mJ) in the aqueous medium [18]. The overall photonic efficiency of photocatalytic conversion process based on hydroxyl radicals is ~8%. The remaining portion of photogenerated hydroxyl radicals is consumed in oxygen formation, interaction with methanol, interaction with methanol by-products such as formaldehyde and recombination.

Photocatalytic oxidation of cyclohexane to cyclohexanol and cyclohexanone is an important commercial reaction, used as precursors in the synthesis of adipic acid and caprolactam, in turn used in the manufacture of nylon 66 and nylon 6, respectively. The selective oxidation of cyclohexane to cyclohexanol and cyclohexanone both under liquid and gaseous phase at room temperature and pressure by photocatalytic process was studied [10,19–21]. The product selectivity depends on the nature of the catalyst, irradiation wavelength and presence of solvent and O_2, etc. The comparison of oxidation of cyclohexane with and without TiO_2 photocatalyst showed that under photolytic oxidation at $\lambda < 275$ nm (i.e., in the absence of catalyst) yielded a high selectivity to cyclohexanol (>85%). However, under photocatalytic condition with TiO_2 catalyst at $\lambda < 275$ nm, the selectivity shifted to the ketone (>95%) [21]. In cyclohexane oxidation, nature and composition of the solvent plays an important role in the distribution of products and by-products [20]. The composition of the mixed solvent has a strong influence on the selectivity of the process: an increase in the content of dichloromethane up to 50% brings an enhancement in the rate of formation of mono-oxygenated products. At the same time, the alcohol to ketone ratio increases in the mixed solvent. Studies performed with various polar and nonpolar solvents showed that in nonpolar solvents, cyclohexanol preferentially adsorbed onto the titanium dioxide particles and underwent deep oxidation, ultimately to carbon dioxide and water. Therefore, in nonpolar solvents, the selectivity of the reaction to cyclohexanol was very low. However, in polar solvents, cyclohexanol adsorbed to the titanium dioxide particles to a lesser extent due to the competition for adsorption sites with the solvent, and the selectivity of the reaction to cyclohexanol significantly increased. Of the various solvents studied such as acetone, isopropanol, dichloromethane, chloroform, carbon tetrachloride, benzene and n-hexane, dichloromethane was the best solvent with regard to the formation rate of cyclohexanol and cyclohexanone. The most unfavorable solvents were isopropanol, chloroform and benzene [21]. Studies under different O_2 partial pressures showed that the process is unaffected for O_2 partial pressures >200 Torr. For lower values, the formation of dicyclohexyl becomes significant and reaches a maximum at a pO_2 of 60 Torr. In O_2-free media containing $C(NO_2)_4$ as the electron scavenger, the formation of cyclohexanone decreases markedly while that of cyclohexanol is essentially the same as that in oxygenated media. Studies on cyclohexane photocatalytic oxidation with $^{18}O_2$ over anatase TiO_2 was analyzed by in situ attenuated total reflection Fourier transform infrared (ATR-FTIR) spectroscopy suggests that oxygen incorporated in cyclohexanone, as well as in deactivating carbonates and carboxylates, originates from the catalyst surface, rather than from dissolved O_2. The proposed Mars-van Krevelen cycle is completed by regeneration of surface sites by reaction with $^{18}O_2$ [22]. In studies conducted at dry nitrogen containing 10–20% of oxygen, cyclohexanone is produced with high selectivity (>90%). In humidified nitrogen/oxygen gas, the cyclohexanol selectivity was increased [23]. This suggests the participation of surface hydroxyl group in the reaction mechanism. A recent study by She et al. [24] showed that the $Cl^{\bullet}$ radicals enhance the

http://dx.doi.org/10.5772/62220

oxygenation of cyclohexane by N_2O to cyclohexanone. Metal doping influences the catalytic activity and selectivity in the photocatalytic oxidation of cyclohexane. Silica-entrapped Cr catalyst for cyclohexane in acetonitrile prevents the decomposition of cyclohexane, there by increased selectivity was observed. The highest turnover number of 2.5 with cyclohexanone selectivity of 68% was observed. Increasing the Cr content resulted in red shift absorption between 500 and 800 nm, which is due to the d-d transition of octahedral Cr^{3+} in Cr_2O_3. Comparison of V-doped hollow TS-1, sulfated hollow TS-1 and sulfated V-doped hollow TS-1 demonstrated that sulfated V-doped TS-1 catalysts are more efficient for selective formation of valuable products (alcohols and ketones) [25].

3. Oxidation of alcohol

Selective oxidation of various primary and secondary alcohols in a gas-phase photochemical reactor using immobilized TiO_2 catalyst at 463 K showed that in the absence of UV light radiation 8% conversion was obtained [26]. Irradiation of the catalyst with the UV light increased the conversion dramatically to 48%. In the presence of UV light, benzaldehyde was formed in preference to phenyl acetaldehyde, in addition to small amounts of other secondary and tertiary reaction products. Benzylic alcohols gave higher conversions, however, with more secondary reaction products. The presence of oxygen was found to be critical for photo-oxidation. The conversion increased from 13 to 20% when a very small quantity of oxygen (O_2/alcohol = 1) was added to the nitrogen carrier gas. There was significant improvement in the conversion, from 13 to 36%, when nitrogen was replaced by air as the carrier gas. Aldehyde is formed only in the presence of O_2. Mohamed et al. [27] studied the photocatalytic oxidation of selected aryl alcohols, such as benzyl alcohol, 1-phenylethanol, benzhydrol, 4-chlorobenz-hydrol, hydrobenzoin, 4,4'-dichlorohydrobenzoi and 4,4'-dimethoxyhydrobenzoin, in a polar, nonhydroxylic solvent (CH_3CN). The main products formed are aldehydes or ketones; the carboxylic acids are formed in small amount. The selective oxidation of alcohol to aldehyde by photocatalytic process was demonstrated for the conversion of 4-methoxybenzyl alcohol (MBA) into 4-methoxybenzaldehyde (p-anisaldehyde, PAA) in organic-free water containing aqueous suspensions of commercial and home-prepared TiO_2 [28]. The home-prepared catalysts, obtained under mild conditions, showed to be much more selective than TiO_2 Merck and TiO_2 Degussa P25 with highest selectivity to PAA. The nanostructured anatase TiO_2 samples synthesized by simply boiling the aqueous solutions of titanium tetrachloride ($TiCl_4$) showed a yield much higher (42% mol for conversions of ca. 65%) than the commercial TiO_2 samples. The least crystalline sample showed higher quantum efficiency (0.116%) [29]. Wang et al. [30] showed that the photocatalytic oxidation of alcohol with O_2 is accelerated by Brønsted acids adsorbed onto TiO_2 or TiO_2/SiO_2 photocatalysts.

The photocatalytic oxidation of benzyl alcohol and its derivatives, such as 4-methoxybenzyl alcohol, 4-chlorobenzyl alcohol, 4-nitrobenzyl alcohol, 4-methylbenzyl alcohol, 4-(trifluoro-methyl)benzyl alcohol and 4-tertiary-butylbenzyl alcohol, into corresponding aldehydes was achieved at stoichiometric conversion and selectivity (>99%) on a TiO_2 photocatalyst under irradiation of light from a blue LED (λmax = 460 nm) in O_2 atmosphere [31]. A red shift of the wavelength of light could be achieved by Au/CeO_2, which exhibited stronger photo-absorption

due to SPR than Au/TiO_2 [32]. Aromatic alcohols (benzyl alcohol and substituted benzyl alcohol such as o-CH_3, m-CH_3 and p-CH_3, m-Cl and p-Cl substituted benzyl alcohol) oxidized to corresponding aldehydes almost quantitatively (>99% conversion, >99% selectivity and >99% carbon balance), in an aqueous suspension of Au/CeO_2 under irradiation of green light [33]. The electronic properties of the substituent groups play a very significant role on the reaction rate, which is enhanced by electron donating substituents and retarded by electron-withdrawing substituents [34].

4. Hydroxylation of aromatics

Conversion of benzene to phenol is an industrially important reaction. With TiO_2 based photocatalysis, the yield and selectivity of phenol production from benzene were about ca. 0.5 and 80%, respectively [35], which are lower than the conventional Fenton process (5% and 80–90%) [36]. The by-product formed in the photocatalytic oxidation of benzene is biphenol. The efficiency of the photocatalytic phenol synthesis can be enhanced by structural modification of the catalyst, and by using additives. Noble metal deposits on TiO_2 surface often enhance the photocatalytic reactivity because they trap CB electrons with reducing charge pair recombination and promoting interfacial electron transfer. Pt/TiO_2 exhibited an enhanced yield (1.7 times, i.e., 4.4%) and selectivity (96%). The addition of various electron acceptors such as O_2, Fe^{3+}, H_2O_2, Ag^+ and N_2O further enhanced the yield and selectivity. TiO_2 along with polyoxometalate $PW_{12}O_{40}^{3-}$ increased the phenol production yield (i.e., 11 and 70% selectivity) [37]. Here, polyoxometalate performs dual roles of both as a photocatalyst and as an electron shuttle. 2 atom % vanadium incorporated into the lattice of disordered mesoporous titania, 1 wt% Au incorporated into $Ti_{0.98}V_{0.02}O_2$ (TV2), showed two times higher activity than bare TV2 [38]. Zheng et al. [39] compared three photocatalysts M@TiO_2 (M = Au, Pt, Ag) for the oxidation of benzene to phenol in aqueous phenol under visible light ($\lambda \geq 400$ nm). Au@TiO_2 exhibited a high yield (63%) and selectivity (91%) compared to Pt@TiO_2-(yield = 34% and selectivity = 53%). Ag@TiO_2-microspheres resulted in negligible activity. The optimum Au loading for higher yield and selectivity was 2 wt% in Au@TiO_2 loading and this catalyst exhibited enhanced visible-light absorption as well as the strongest SPR effect. Comparison of the photocatalytic activity of Au@TiO_2-nanosheets and Au@TiO_2-microspheres showed that Au@TiO_2-nanosheets resulted in lower activity compared with that of Au@TiO_2-microspheres. The Au@TiO_2-microspheres produced a strong interaction between Au and TiO_2. Comparison of the synthesis of Au@TiO_2 by two different methods such as Ti^{3+} ion-assisted method and direct photodeposition route showed that the catalyst prepared by direct photodeposition route produced only traces of phenol. The direct photodeposition route leads to an inhomogeneous loading of noble metal on TiO_2, and the Au NPs exhibit a wide size distribution in the range of 20–80 nm. By changing the hydrophobicity of the catalyst, the adsorption of reactants (benzene, hydrophobic) and the desorption of the desired products (phenol, hydrophilic) could be improved [40]. With this idea, titania is incorporated in hydrophobically modified mesocellular siliceous foam (MCF) and is used for the photocatalytic hydroxylation of benzene to phenol in aqueous solutions. The inner environment of the MCF cage was turned hydro-

http://dx.doi.org/10.5772/62220

phobic by surface organo-grafting with silylation agent (TiO_2-MCF/CH_3). The hydrophobically modified TiO_2@MCF/CH_3/UV sample showed the highest phenol selectivity (70%) and phenol yield (12.5%) after 2 hours of irradiation. $FeCl_3$ and mesoporous carbon nitride ($FeCl_3$/mpg-C_3N_4) hybrids exhibited 38% benzene conversion with 97% selectivity for phenol under visible light [41], which is due to faster reduction of Fe^{3+} to Fe^{2+} by light-irradiated electrons from mpg-C_3N_4. Metal-exchanged BEA zeolites dispersed in benzene-acetonitrile-water mixtures at room temperature with O_2 as oxidant showed that Pd^{2+}-, Fe^{3+}- and Cu^{2+}-exchanged BEA were shown to be effective for the formation of phenols (hydroquinone, resorcinol, catechol and phenol) [42].

5. Epoxidation of alkenes

Epoxidation of alkenes to epoxide is a very useful transformation in organic synthesis. A series of highly dispersed transition metals such as Ti^{4+}, Cr^{6+}, Mg^{2+} and Zn^{2+}, in SiO_2 matrix, exhibited photocatalytic activity for propene oxide formation [43]. Various studies reported on silica supported that metal oxide catalysts are effective photocatalysts for propylene epoxidation in a closed reactor system. Studies on silica supported on V, Ti and Cr showed that the conversion rate of propylene and the formation rate of propylene oxide were increased in the order Cr < Ti < V oxides on silica [44]. Gradual deactivation was observed for CrO_3/SiO_2 with the course of the photoreaction, although the initial activity was almost same as that of TiO_2/SiO_2. Shiraishi et al. [45] prepared Cr-SiO_2 catalyst containing highly dispersed chromate species by a sol-gel method and when subjected to photocatalytic oxidation reaction under visible light irradiation (λ > 400 nm) showed very high selectivity (>90%), which is higher than Cr/SiO_2 catalysts prepared by an impregnation method or Cr/MCM-41 prepared by a templating method. The yield and selectivity to propylene oxide were improved significantly by modification of silica with 1 wt% magnesium oxide loading [46]. Photo-oxidation of propene over V_2O_5/SiO_2 with O_2 under UV irradiation in a closed circulation reactor produced ethanal (acetaldehyde, AA), acrylaldehyde (AL) and propanal (propionaldehyde, PA). However, propene oxide was not detected as a product [47]. On the other hand, the same catalyst system with flow reactor system, which provide short contact time between the substrates and the catalysts produced acetaldehyde and propene oxide as main products; the selectivities were 43 and 30%, respectively [48]. The non-loaded amorphous SiO_2 did not show any photocatalytic activity. It is clear that the surface vanadium oxide species are the photocatalytic active sites. Comparison of commercial and home-prepared TiO_2 catalysts for partial photo-oxidation of cyclopentene oxidation produced cyclopent-2-en-1-one, cyclopent-2-en-1-ol, 6-oxabicyclo[3.1.0]hexane, penta-1,5-dial (glutaraldehyde) [49]. The commercial catalysts showed lower photo-activity in terms of cyclopentene conversion (51–57%) compared to the home-prepared ones (53–69%). The commercial photocatalyst produced ketone as the major fraction in the range of 35–49% and epoxide fraction in the range of 12–17%, while the home-prepared catalysts gave mainly the epoxide fraction in the range of 26–49% and ketone fraction in the range 9–16%. The difference in catalytic behavior of TiO_2 commercial and TiO_2 homemade is due to the difference in structural properties, which resulted in different reaction mechanisms. Selective epoxidation was achieved by Shiraishi et al. [50] in Ti-containing MCM-41 mesoporous silica (T-S) with

isolated and tetrahedrally coordinated Ti-oxide species (Ti-O4), when photo-activated in acetonitrile (MeCN) with molecular oxygen. The high epoxide selectivity (>98%) of the T-S system is due to a "shield effect" driven by MeCN. TiO_2 photocatalyst incorporated in highly hydrophobic Y zeolite under UV-light irradiation using molecular oxygen as an oxygen source exhibited a markedly enhanced photocatalytic activity compared with bare TiO_2 [51].

6. Oxidation of amines to imines

In organic synthesis, selective oxidation of amines to imines are considered as important reactions, because imines and their derivatives have immense applications in the synthesis of nitrogen heterocycles, especially alkaloid synthesis, which are biologically important compounds. Lang et al. [52] have studied extensively and achieved highly selective photocatalytic conversion of various amines into its corresponding imines on TiO_2 using 1 atm of air as the oxidant in acetonitrile under UV irradiation. It is documented that it is a challenging task to achieve high selectivity in water medium as complete degradation is potential to occur by over oxidation. The reaction rate in terms of conversion of amine is much higher in water medium than in CH_3CN with high selectivity of imine formation [53]. However, the selectivity decreased to some extent because of free radical intermediates, which are comparable to photocatalytic oxidation of amine in CH_3CN. Studies on substituents' effect on the catalytic activity of amine to imine showed that substituents on the benzylic amines did not affect the selectivity significantly both in CH_3CN and in water medium [59]. The presence of electron-donating substituents (CH_3– and CH_3O–) and electron withdrawing substituents (F– and Cl–) on the phenyl ring had little effect on the reaction rate and product selectivity of the oxidation reaction. The halo-substituted benzylamines provided good selectivity, as the halo-substituted positions along with the imine functionality are useful for further transformations. Comparison of benzylic and nonbenzylic amines showed that no imines formation occurred in nonbenzylic amines such as cyclohexylamine and n-hexylamine and only fragmentation products were detected by unselective auto-oxidation at multiple reactive sites. Utilization of visible/solar energy is the prime concept to make the synthesis a economically and environmentally viable process. Nb_2O_5 converts amine to imine with high selectivity under visible light >390 nm to about 460 nm in benzene [54]. Studies on the photocatalytic activity and selectivity in the aerobic oxidation of benzylamine over various metal oxides illustrate that TiO_2 exhibited higher yield than Nb_2O_5 and ZnO. However, the selectivity to N-benzylidene benzylamine was comparatively low because benzaldehyde was formed as a by-product. In V_2O_5, benzylamine-N-carbaldehyde was formed as a main by-product. Hiroaki Tada and his research group have used the "plasmon photocatalysts", in which noble metal nanoparticles are dispersed into semiconductor photocatalysts, which possesses two prominent features: a Schottky junction and localized surface plasmonic resonance (LSPR) [55]. Au NPs supported on various metal oxides (anatase and rutile TiO_2, $SrTiO_3$, ZnO, WO_3, In_2O_3, Nb_2O_5) under visible-light irradiation ($\lambda > 430$ nm) showed that Au supported on rutile TiO_2 exhibited high level of visible-light activity for aerobic oxidation of amines to yield the corresponding imines with high selectivity (>99%) compared to other supports. The high activity of Au NP on rutile

http://dx.doi.org/10.5772/62220

TiO_2 is due to multiple factors such as significant red shift of the LSPR peak of Au/ rutile TiO_2 due to its very large permittivity (ε = 114) as compared with that of anatase TiO_2 (ε = 48), smaller Au particle size, good adsorptivity of rutile TiO_2 for amine owing to the presence of acid sites on the surface.

7. Oxidation of polycyclic aromatic hydrocarbons

Polycyclic aromatic compounds (PHA) are compounds containing multiple aromatic rings which are fused together. The highly efficient photocatalytic method was adopted to various PAHs and it was found that it can be degraded under UV or visible light irradiation [56]. The reaction mechanism illustrated that the toxic PAHs degraded through various useful intermediates. The selectivity of the product depends on the type of catalysts used. Other factors which influence the catalytic activity are solvent medium, atmospheric condition and wave length of light radiation, etc. Photocatalytic oxidation of naphthalene in water medium with Degussa P25 under UV radiation (345 nm, 500 Watt) produced 2-formyl-3-hydroxycinnamaldehyde and 5,8-dihydroxy-2,4-naphthaquinone as stable intermediates [57]. Bahnemann and coworkers found 15 different intermediates when naphthalene is in water medium with Degussa P25 under UV radiation (366 nm, 50 Watt) [56]. The main intermediates observed are coumarin, 1,4-naphthalenedione, 2,3-dihydro-2,3-epoxy-1,4-naphthalenedione, 2-formyl-Z-cinnamaldehyde, 1,2-benzenedicarboxaldehyde and phthalic acid. Karam et al. synthesized 1,4-naphthaquinone in a closed system reactor under UV radiation [58]. Solvent plays an important role in the photocatalytic degradation of naphthalene. In water containing 1% MeCN produced significant amounts of three intermediates: isomeric 2-formylcinnamaldehydes and 1,4-naphthoquinone. In organic solvent, the oxidation rate was almost an order of magnitude slower than in water and produced significant amount of naphthoquinone and phthalic anhydride [59]. In acetonitrile and water mixture, with UV light (λ < 340 nm) produced 2-formylcinnamaldehyde (85%), Z isomer is the original product that is spontaneously transformed into the thermodynamically more stable E isomer. Addition of acetone can cause an accumulation of intermediates. For example, higher concentrations and more types of intermediates were found in degradation of naphthalene with the high acetone level [60]. In mixed solvents such as acetonitrile and water bubbled with molecular oxygen, naphthalene is efficiently oxidized to 2-formylcinnamaldehyde when irradiated with 500 W super-high-pressure mercury lamp (λ < 340 nm) light [61]. Under the same condition, phenanthrene was converted into a coumarin compound with 45% yield [62]. Photocatalytic activity of different kinds of TiO_2 powders for naphthalene oxidation showed that Degussa P25 TiO_2 powders, which contain mixture of anatase and rutile, showed the highest photocatalytic activity for the production of 2-formylcinnamaldehyde from naphthalene. Similarly, powders containing both rutile and anatase phases showed high activity, even if the component of the anatase phase is a few percent. Pure anatase particles and pure rutile particles exhibited lower activity for the photocatalytic oxidation of naphthalene into 2-formylcinnamaldehyde [63]. Visible active photocatalysts are developed to convert the PAHs to useful compounds. Kohtani and coworkers showed that $BiVO_4$ (band gap 2.4 eV) [64] and Ag-loaded $BiVO_4$ photocatalysts are

visible light-driven for photo-oxidation of various PAHs in acetonitrile in O_2 atmosphere. Compared to pure $BiVO_4$, Ag-loaded $BiVO_4$ photocatalyst remarkably improves adsorptive and photo-oxidative performance on the degradation. Anthraquinone is obtained in both pure and Ag-loaded $BiVO_4$ solutions, while the amount of formation using Ag-$BiVO_4$ is much larger than that using pure $BiVO_4$. Anthrone is obtained only from the irradiated Ag-$BiVO_4$ solution but not from the pure $BiVO_4$ one. The amount of anthraquinone formation is largest in O_2-saturated solution compared to that in N_2 atmosphere. Bz[a]A was degraded by Ag-$BiVO_4$ and converted into a considerable amount of 7,12-dione. Substituent effects on the photocatalytic oxidation of naphthalene demonstrate that in dinitronaphthalene isomers, namely 1,3-dinitronaphthalene (1,3-diNN), 1,5-dinitronaphthalene (1,5-diNN) and 1,8-dinitronaphthalene (1,8-diNN), the photocatalytic oxidation rates followed in the order 1,3-diNN > 1,8-diNN > 1,5-diNN [65].

8. C-C bond formation

The C-C bond formation between an electrophilic alkene and adamantane was achieved by the irradiation of TiO_2 suspensions in the presence of isopropylydenmalonitrile (IPMN, 0.02 M, with adamantane likewise 0.02 M) and under nitrogen forms a new product as an adduct, 2-[1-(1-adamantyl)-1-methyl)]ethylpropanedicarbonitrile (35% yield), together with traces of oxygenated products, such as 1-adamantanol, 2-adamantanol and 2-adamantanone [66]. By adding silver sulfate as a sacrificial electron acceptor, the yield increased to 75%. The single-electron transfer oxidation of adamantane is followed by deprotonation leading to the 1-adamantyl radical that couples with isopropylydenmalonitrile.

9. Cyclization reaction

Intramolecular cyclization of N-(β-hydroxypropyl)-ethylenediamine in the presence of a semiconductor (TiO_2 or CdS or ZnO)-zeolite composite catalysts in O_2 atmosphere produces 2-methylpiperazine and piperazine [67]. The yield of 2-methylpiperazine and piperazine depends on the type of semiconductor and zeolite. Zeolites modified with TiO_2 (5 wt% TiO_2–Hβ) composite considerably facilitated the intramolecular cyclization with a yield of 31.9%. Zeolites modified with semiconductors ZnO and CdS showed lower activity. This is due to moderate hydrophobicity and acid site strength offered by TiO_2-zeolite composite for the cyclization reaction. Selvam and Swaminathan have shown one-pot synthesis of quinaldines from nitroarenes by combined redox-cyclization reaction assisted by photocatalytic method using pure TiO_2 and Au-loaded TiO_2 catalyst in absolute ethanolic solution under UV radiation (λ = 365 nm) [68]. The Au-loaded TiO_2 catalyst exhibited higher efficiency and selectivity for the formation of quinaldine and substituted quinaldine from nitrobenzene and substituted nitrobenzene. For instance, TiO_2 produced 60% yield and Au/TiO_2 produced 75% yield. The reaction involves two steps: in the first step nitro group is reduced to amine, which is followed by condensation with aldehyde and cyclization occurs. The substituted nitrobenzene influen-

http://dx.doi.org/10.5772/62220

ces the activity and selectivity. The authors suggested that the electron-releasing group at para-position inhibits the condensation of amino group with aldehyde. 4-Methoxynitrobenzene has a strong electron-releasing group at para-position and showed lower quinaldine yield (60%). Steric effect also plays an important role in product formation. In 3,5-dimethylnitrobenzene and 3-nitrotolune, the cyclization reaction is hindered due to steric effect in 3,5-dimethylnitrobenzene and decreased the product yield (70%) when compared to 3-nitrotolune (80%).

10. Conclusions

There is an extensive research and dramatic growth going on in the field of heterogeneous photocatalysis. This method has been commercialized in various aspects of environmental detoxification. Photocatalysis method can be successfully applied for fine organic chemical synthesis. The advantages of photocatalysis method in organic synthesis include the possibility of utilizing clean and abundant renewable energy source, harmless chemicals used as catalysts, reaction can be carried out at room temperature, product type and its selectivity can be tuned by varying the nature of solvent, atmospheric condition, and wavelength of light source used, catalyst reusability, etc. Various challenging aspects have to be considered before implementing in industrial scale. Most commonly, simulated sunlight or UV sources are used in the laboratory. Experiments need to be devised to monitor the performance of the catalyst in sunlight. In future, more catalysts need to be devised that can trap the visible radiations as well. Since organic solvents are utilized in organic transformations, the band gap of the metal oxide photocatalysts in organic medium has to be explored. Systematic study has to be conducted to optimize the reaction parameters and understand the reaction mechanism, thereby the product yield could be improved.

Author details

Suzan A. Khayyat[1,2*], Rosilda Selvin[2] and L. Selva Roselin[1]

*Address all correspondence to: saekhayyat@kau.edu.sa

1 King Abdulaziz University, Rabigh, Saudi Arabia

2 King Abdulaziz University, Jeddah, Saudi Arabia

References

[1] Warburg O., Negelein E., Z. phys. Chem., 1069 (1923) 191.

[2] Peter D.F., Mahata K., Würthner F., Chem. Soc. Rev., 2013, 42, 1847.

[3] Ciamician G., Science, 36 (1912) 385.

[4] Inoue Y., Chem. Rev., 92 (1992) 741.

[5] Narayanam J.M R., Stephenson C.R.J., Chem. Soc. Rev. 40 (2011) 102.

[6] Fujishima A., K. Honda. Nature 238 (1972) 37.

[7] Hoffmann R.M., Martin S.T., Choi W., Bahnemann D.W., Chem. Rev. 95, (1995) 69.

[8] Roselin L.S., Rajarajeswari G.R., Selvin R., Sadasivam V., Sivasankar B., K. Rengaraj. React. Kinetics Catal. Lett., 78 (2003) 259.

[9] Linsebigler A.L., Lu G., Yates T., Jr. Chem. Rev., 95 (1995) 735.

[10] Giannotti C., Legreneur S., O. Watts. Tetrahedron Lett. 24 (1983) 5071.

[11] Palmisano G., Augugliaro V., Pagliarob M., L. Palmisano. Chem. Commun., (2007) 3425.

[12] Gambarotti C., Punta C., Recupero F., Caronna T., L. Palmisano. Curr. Org. Chem., 14 (2010) 1153.

[13] Gondala M.A., Hameedb A., Yamanic Z.H., A. Arfaja. Chem. Phys. Lett., 392 (2004) 372.

[14] Thampi K.R., Kiwi J., M. Gra¨tzel, Catal. Lett. 1 (1988) 109.

[15] Suzuki T., Wada K., Shima M., Watanabe Y., J. Chem. Soc. Chem. Commun., (1990) 1059.

[16] Wada K., Yoshida K., Watanabe Y., Suzuki T., J. Chem. Soc., Chem. Commun., (1991) 726.

[17] Taylor C.E., Top. Catal. 32 (2005) 2005.

[18] Hameeda A., Ismail I.M.I., Aslam M., .Gonda M.A., Appl. Catal. A, 470 (2014) 327.

[19] Sclafani A., Herrmann J.M., J. Phys. Chem., 100 (1996) 13655.

[20] Boarini P., Carassiti V., Maldotti A., Amadelli R., Langmuir 14 (1998) 2080.

[21] Du P., Moulijn J.A., MulG., J. Catal. 238 (2006) 342.

[22] Almeida A.R., J.A. Moulijn‡, Mul G., J. Phys. Chem. C, 115 (2011) 1330.

[23] van Dijk V.H.A., Simmelink G., G. Mul. Appl. Catal. A, 470 (2014) 63.

[24] She J., Fu Z., Lia J., Zeng B., Tang S., Wu W., Zhao H., Yin D., Kirk S.R., Appl. Catal. B, 182 (2016) 392.

[25] Zhong W., Qiao T., Dai J., Mao L., Xu Q., Zou G., Liu X., Yin D., F. Zhao. J. Catal., 330 (2015) 208.

[26] Pillai U.R. and Sahle-Demessie E., J. Catal., 211 (2002) 434.

[27] Mohamed O.S., El-Aal A., Gaber M., Abdel-Wahab A.A., J. Photochem. Photobiol. A, 148 (2002) 205.

[28] Addamo M., Augugliaro V., Di Paola A., García-López E., Loddo V., Marcì G., Palmisano L., Colloids. Surf. A: Physicochem. Eng. Aspects, 265 (2005) 23.

[29] Yurdakal S., Palmisano G., Loddo V., Augugliaro V., Palmisano L., J. Am. Chem. Soc., 130 (2008) 1568.

[30] Wang Q., Zhang M., Chen C.C., Ma W.H., Zhao J.C., Angew. Chem., Int. Ed., 49 (2010) 7976.

[31] Higashimoto S., Kitao N., Yoshida N., Sakura T., Azuma M., Ohue H., Y. Sakata. J. Catal., 266 (2009) 279.

[32] Naya S., Teranishi M., Isobe T., Tada H., Chem. Commun., 46 (2010) 815.

[33] Tanaka A., Hashimoto K., Kominami H., Chem. Commun., 47 (2011) 10446.

[34] Yurdakal S., Palmisano G., Loddo V., Alagçz O., Augugliaro V., Palmisano L., Green Chem., 11 (2009) 510.

[35] Fujihira M., Satoh Y., Osa T., Nature, 293 (1981) 206; M. Fujihira, Y. Satoh, T. Osa. Chem. Lett., (1981) 1053.

[36] Seo Y.J., Tagawa T., Goto S., React. Kinet. Catal. Lett., 54 (1995) 265.

[37] Park H., W. Choi. Catal. Today, 101 (2005) 291.

[38] Devaraji P., Sathu N.K., Gopinath C.S., ACS Catal., 4 (2014) 2844.

[39] Zheng Z., Huang B., Qin X., Zhang X., Dai Y., M. Whangbo. J. Mater. Chem., 21 (2011) 9079.

[40] Zhang G., Yi J., Shim J., Lee J., Choi W., Appl. Catal. B-Environ., 102 (2011) 132.

[41] Zhang P., Gong Y., Li H., Chen Z., Wang Y., RSC Adv., 3 (2013) 5121–5126.

[42] Shimizu K.-I., Akahane H., Kodama T., Kitayama Y., Appl. Catal. A-Gen., 269 (2004) 75.

[43] Amano F., Yamaguchi T., Tanaka T., J. Phys. Chem. B, 110 (2006) 281.

[44] Amano F., Yamaguchi T., Tanaka T., J. Phys. Chem. B, 110 (2006) 281.

[45] Shiraishi Y., Teshima Y., Hirai T., J. Phys. Chem. B, 110 (2006) 6257.

[46] Yoshida H., Tanaka T., Yamamoto M., Yoshida T., Funabiki T., Yoshida S., J. Catal., 171 (1997) 351.

[47] Tanaka T., Ooe M., Funabiki T., Yoshida S.J., J. Chem. Soc., Faraday Trans. 82 (1986) 35.

[48] Amano F., Tanaka T., Funabiki T., Langmuir, 11 (2004) 4236.

[49] Kluson P., Luskova H., Cerveny L., Klisakova J., Cajthaml T., J. Mol. Catal. A-Chem., 242 (2005) 62.

[50] Shiraishi Y., Morishita M., Hirai T., Chem. Commun. (2005) 5977.

[51] Yasutaka K., Yasuhiro M., Hiromi Y., Rapid Commun. Photosci., 4 (2015) 19.

[52] Lang X.J., Ji H.W., Chen C.C., Ma W.H., Zhao J.C., Angew. Chem., Int. Ed. 50 (2011) 3934.

[53] Furukawa S., Ohno Y., Shishido T., Teramura K., Tanaka T., ACS Catal., 1 (2011) 1150.

[54] Naya S., Kimura K., H. Tada. ACS Catal., 3 (2013) 10.

[55] Theurich J., Bahmemann D.W., Vogel R., Ehamed F.E., Alhakimi G., Raja I., Res. Chem. Intermed., 23 (1997) 247.

[56] Das S., Muneer M., Gopidas K.R., J. Photochem. Photo. A: Chem., 77 (1994) 83.

[57] Karam F. F., Kadhim M.I., Alkaim A.F., Int. J. Chem. Sci., 13 (2015) 650.

[58] Soana F., Sturini M., Cermenati L., Albini A., J. Chem. Soc., Perkin Trans., 2 (2000) 699.

[59] Woo O.T., Chung W.K., Wong K.H., Alex T., Chow B.C., Wong P.K., J. Hazard Mater., 168 (2009) 1192.

[60] Ohno T., Tokieda K., Higashida S., Matsumura M., Appl. Catal. A, 244 (2003) 383.

[61] Higashida S., Harada A., Kawakatsu R., Fujiwara N., Matsumura M., Chem. Commun., (2006) 2804.

[62] Ohno T., Tokieda K., Higashida S., Matsumura M., Appl. Catal. A, 244 (2003) 383.

[63] Kohtani S., Tomohiro M., Tokumura K., Nakagaki R., Appl. Catal. B, 58 (2005) 265.

[64] Bekbolet M., Çınar Z., Kılıç M., Senem Uyguner C., Minero C., Pelizzetti E., Chemosphere, 75 (2009) 1008.

[65] Geerlings P., De Proft F., Langenaeker W., Chem. Rev., 103 (2003) 1793.

[66] Cermenati L., Dondi D., Fagnoni M., Albini A., Tetrahedron, 59 (2003) 6409.

[67] Subba Rao K.V., Subrahmanyam M. Photochem. Photobiol. Sci., 1 (2002) 597.

[68] Selvam S., Swaminathan M., Catal. Commun., 12 (2011) 389.

Chapter 9

Components of Natural Photosynthetic Apparatus in Solar Cells

Roman A. Voloshin, Margarita V. Rodionova, Sergey K. Zharmukhamedov, Harvey J.M. Hou, Jian-Ren Shen and Suleyman I. Allakhverdiev

Additional information is available at the end of the chapter

http://dx.doi.org/10.5772/62238

Abstract

Oxygenic photosynthesis is a process of light energy conversion into the chemical energy using water and carbon dioxide. The efficiency of energy conversion in the primary processes of photosynthesis is close to 100%. Therefore, for many years, photosynthesis has attracted the attention of researchers as the most efficient and eco-friendly pathway of solar energy conversion for alternative energy systems. The recent advances in the design of optimal solar cells include the creation of converters, in which thylakoid membranes, photosystems and whole cells of cyanobacteria immobilized on nanostructured electrode are used. As the mechanism of solar energy conversion in photosynthesis is sustainable and environmentally safe, it has a great potential as an example of renewable energy device. Application of pigments such as Chl *f* and Chl *d* will extend the spectral diapason of light transforming systems allow to absorb the far-red and near infra-red photons of the spectrum (in the range 700-750 nm). This article presents the recent achievements and challenges in the area of solar cells based on photosynthetic systems.

Keywords: Solar cell, Thylakoids, Photosystem I, Photosystem II, Sensibilizator

1. Introduction

The energy crisis and environmental problems are among the most important challenges for humanity to solve in the twenty-first century. Many of the actual investigations are focused on the development of renewable, sustainable and eco-friendly energy sources [1].

Nowadays, the available sources of renewable energy, including solar, wind, rain energy, energy of waves and geothermal heat, could generate only approximately 16% of the energy used [2]. Global energy consumption is about 17 TW according to the information of the year 2014 [3]. The flux density of sunlight emission near the ground surface is about 100 PW, which exceeds 5000 times our current needs [4]. Even though the solar period and the presence of clouds are taken into account, the sun is the extremely attractive source of energy, given we know how to extract it. Thus, sunlight is the most accessible and reliable source among the other renewable energy sources.

Photosynthesis is one of the main pathways of solar energy conversion, performed by higher plants, microalgae and some bacteria. Over 2.5 billion years, plant photosynthesis has evolved to convert solar energy into the chemical energy using only water as electron donor and proton source. This photosynthesis realises oxygen and is called oxygenic. Water, carbon dioxide and light are necessary for oxygenic phototrophic organisms to produce carbohydrates. The light-dependent reaction of photosynthesis takes place in the thylakoid membrane of photosynthetic organisms. The thylakoid membrane involves two photosystems (PSI and PSII), cytochrome b_6f complex and other protein complexes embedded in a lipid bilayer. PSI and PSII can capture sunlight and create an electron-hole pair [5, 6]. The latter process operates with a quantum yield closer to 100%. Water, one of the most abundant substances on Earth, is the donor of electron for PSII [2].

For several decades, photovoltaic semiconductor devices have also been developed to generate electric power by converting sunlight directly into the electricity. The coefficient of efficiency of the light energy conversion into the electric current produced by commercial silicon photovoltaic cells is typically less than 20% [7]. Unfortunately, exhaustible materials and components used in photovoltaic systems cannot be fully recycled. Considering that the efficiency of energy conversion in the primary processes of photosynthesis is close to 100%, it is reasonable to use this natural process for energy conversion applications.

Recently, after critical analysis of the photosynthetic and photovoltaic energy conversion mechanisms, experts in the area of artificial photosynthesis concluded that it is difficult to compare the conversion efficiency of the current photovoltaic cells with that of the living photosynthesizing cells, as they are completely different systems [7]. The efficiency of photovoltaic cells can be calculated by dividing the cell's output power by the total solar radiation spectrum. However, the storage and energy transfer are not considered by this approach. Photovoltaic batteries, in which energy is stored, have high production cost and the expenses required for the maintenance of such systems. Photosynthesis stores solar energy in the form of chemical energy, which can further be converted into electrical energy [2].

2. Photosynthesis

Photosynthesis is the process of conversion of the sunlight energy into chemical energy of various organic compounds, which is carried out by photosynthesizing organisms. Photosynthesis serves as the primary source of energy for all kinds of life on Earth. Photosynthetic

http://dx.doi.org/10.5772/62238

organisms are sources of energy and essential metabolites for heterotrophic organisms [8, 9]. This process proceeds in two stages: the light stage of the light absorption by photosynthetic pigments and the formation of adenosine triphosphate (ATP) and nicotinamide adenine dinucleotide phosphate (NADPH) and the dark stage when the biosynthesis of carbohydrates occurs. During the dark stage, carbon dioxide (CO_2) acts as a carbon substrate, NADPH molecule is a proton source, and ATP molecule is a source of energy. The electron transport chain (ETC) is an essential element of the light stage of photosynthesis. An electron is transferred to the $NADP^+$ molecule through ETC, which leads to the reduction of the $NADP^+$ to NADPH. An external source of electrons is required to reduce the oxidized pigment molecule. The type of photosynthesis using water as an electron source is called oxygenic one, since molecular oxygen is a by-product of the water decomposition [10].

The oxygenic photosynthesis is explicit in all plants, microalgae and cyanobacteria. It is the key source of oxygen in the atmosphere.

The oxygenic photosynthesis could be summarized through the following general equation:

$$CO_2 + H_2O \xrightarrow{h\nu} [CH_2O] + O_2$$

Light stage processes of the oxygenic photosynthesis occur in membrane structures called thylakoids. In eukaryotic cells of green plants, thylakoids are localized in specific photosynthetic organelles - chloroplasts. The space limited by chloroplast membrane is determined as stroma, and the space inside the thylakoid is determined as lumen. Thus, one side of the thylakoid membrane faces the stroma, and the other side faces the lumen. In cyanobacteria cells, thylakoids are located directly in the cytoplasm [11].

Light energy is not immediately converted into ATP energy. In fact, it is initially stored in the form of a transmembrane electrochemical potential formed due to the proton transfer by lipophilic transporters through the thylakoid membrane from the stroma to the lumen. As a result, the lumen becomes acidic and the stroma is alkalized. Due to the energy of the created potential difference ($\Delta\mu H^+$), the enzyme ATP-synthase embedded in the thylakoid membrane starts to function [12].

The light stage of photosynthesis is a sequence of enzymatic reactions. There are four transmembrane protein enzymes that catalyse these reactions in higher plants: PSI, PSII, cytochrome b_6f complex (Cyt b_6f) and ATP-synthase [11]. PSII catalyses the electron transfer reaction from the water molecule to plastoquinone (PQ). The Cyt b_6f is involved in the oxidation of plastoquinole and reduction of plastocyanin (Pc). It mediates the transfer of electrons from PSII to PSI as well as of protons from stroma to lumen [12]. PSI catalyses the oxidation of lipophilic electron carrier plastocyanine, and the ferredoxin (Fd) reduction. The enzyme ferredoxin: $NADP^+$ oxidoreductase (FNR) catalyses the $NADP^+$ reduction due to the electrons from the reduced Fd (Fig. 1).

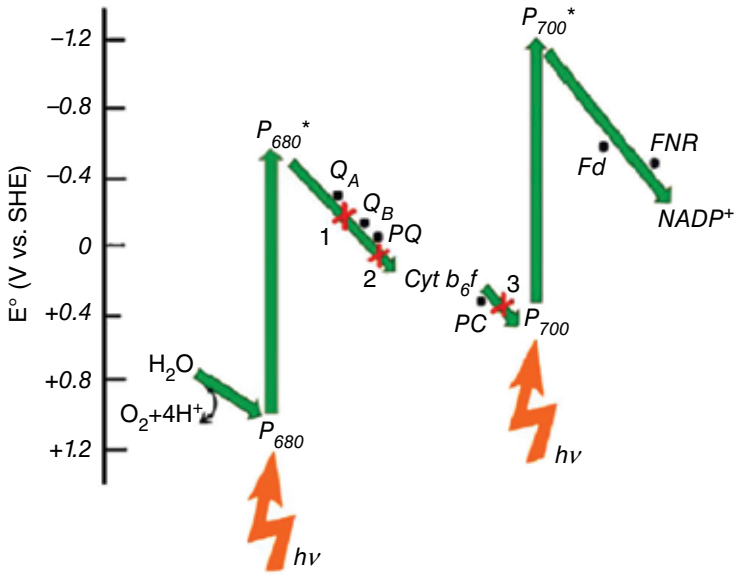

Figure 1 The scheme of the non-cyclic electron transport pathway in thylakoids of higher plants and the redox potentials of the components of electron transport chain. P_{680} – primary electron donor in photosystem II; P_{680}* – singlet exited state of P_{680}; P_{700} – primary electron donor in photosystem I; P_{700}* – singlet exited state of P_{700}; Q_A and Q_B are primary and secondary quinone electron acceptors, respectively. Red crosses represent reactions that can be inhibited by a) 3-(3,4-dichlorophenyl)-1,1-dimethylurea (DCMU); b) dibromothymoquinone (DBMIB); c) potassium cyanide (KCN) (adapted from [2]).

The primary charge separation involving photosynthetic pigments occurs in the special part of photosystem complex called photosynthetic reaction centre (RC). In the RC, the primary electron donor is at the inner lumenal side of thylakoid membrane, whereas the primary electron acceptor is closer to the outer stromal side. Thus, an electron from the molecules of the primary electron donor moves onto the opposite side of the thylakoid membrane [12].

The ETC is activated by light. First, photons are absorbed by the pigments of special antenna complex. Then, the energy of the light quanta is transferred to RC by hopping mechanism [13]. In the RC, a special pair of chlorophyll is excited by the photon energy. Chlorophyll is the pigment molecule that can be excited by light of a certain wavelength (Fig. 2). The basis of the chlorophyll structure is a heterocyclic ring consisting of four pyrrole rings connected by methine bridges [14]. Four nitrogen atoms within the chlorine ring are associated with magnesium ion (Mg^{2+}). A long hydrophobic phytol tail is attached to the fourth pyrrole ring, whereas a pigment molecule is correctly oriented in the membrane. In nature, there are two widespread forms of chlorophyll: Chl *a* and Chl *b*.

Chl *a* serves as the primary electron donor in the RC, and Chl *b* is the accessory pigment of the antenna complexes. A free Chl *a* molecule absorbs light preferably in the wavelength ranges of 400-500 nm and 600-700 nm. Due to the usage of other pigments, for example, carotenoids, the absorption spectrum of the photosystems is much broader [16]. In addition to Chl *a* and Chl *b*, other forms of chlorophyll, Chl *d* and Chl *f*, could also be found in antenna complexes

http://dx.doi.org/10.5772/62238

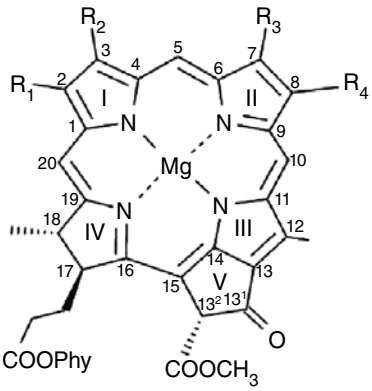

Name	R_1	R_2	R_3	R_4
Chlorophyll *a*	CH_3	$CH{=}CH_2$	CH_3	$CH_2{-}CH_3$
Chlorophyll *b*	CH_3	$CH{=}CH_2$	CHO	$CH_2{-}CH_3$
Chlorophyll *d*	CH_3	CHO	CH_3	$CH_2{-}CH_3$
Chlorophyll *f*	CHO	$CH{=}CH_2$	CH_3	$CH_2{-}CH_3$

Figure 2 The structural formula of chlorophylls: Chl *a*, Chl *b*, Chl *d*, and Chl *f* (adapted from [15]).

of phototrophic organisms, such as cyanobacteria. Also Chl *d* can be found in the photosynthetic RC [17, 18]. The chemical difference among the Chl *b*, Chl *d*, Chl *f* and the Chl *a* is that methyl or vinyl group is substituted by formyl one. The chlorophylls also differ from each other in their absorption spectra. More specifically, the long-wavelength maximum in the absorption spectrum of Chl *d* and Chl *f* markedly shifts towards longer wavelengths compared to that of the Chl *a* (shift up to 40 nm). The energy region (i.e., 380-710 nm) consists of photosynthetically active radiations that constitute about 40% of the total solar radiation reaching the Earth's surface [19]. However, further expansion in the region ranging from 700 to 750 nm leads to the increase in the overall energy conversion intensity by about 19% [20].

3. Solar cells

Solar cells are used to convert solar energy into electrical energy. The development of effective and inexpensive solar cells is of particular interest because of the importance of alternate energy sources. Currently, there are many different types of solar energy converters. The solar cells, or photoelements, are devices that can convert solar energy into usable electrical energy. They are divided into two types: regenerative cells and photosynthetic cells [21]. In the regenerative cells, the sunlight energy is converted into electricity. This process is unaccompanied by any subsequent chemical reactions. Sometimes, such cells are called photobioelectrochemical cells. In photosynthetic cells, the sunlight energy is converted to the molecular

fuel energy, for example, that of hydrogen [20-23]. Photosynthetic cells based on biological objects such as isolated photosystems [22] or the whole bacterial cells [23] are called photo-biochemical fuel cells. This article focuses generally on the regenerative solar cells.

3.1. Operating of solar cells

The main steps can be identified for all types of solar cells [24]:

1. *Absorption of light by photoactive component.*

Photoactive component is the substance that absorbs photons inside the solar cell. A semiconductor acts as a photoactive component in conventional photovoltaic solar cells; while an organic pigment (photosensitizer molecule) serves as a photoactive component in dye-sensitized solar cells. Absorption of a photon leads to certain changes in the energy of the photosensitizer molecule, which is necessary for the further generation of current or the synthesis of molecular hydrogen [20].

2. *The charge separation.*

In photoelements using plant or bacterial photosystems, charge separation occurs due to a series of redox reactions. After the absorption of incident photon energy by special pigment molecule, a primary electron donor, a charge separation between primary electron donor and primary electron acceptor occurs. Then, the molecule of the primary donor is reduced by electrons from the secondary one and electron from the primary acceptor is transferred into ETC components. This stage is termed as charge stabilization. Some voltage is generated in the photoelement as a result of these processes.

3. *The transfer of electrons to an external circuit for biofuel generation.*

For the elements acting as a photoelectric converter (regenerative cells), this step implies an electron transfer to the electrode, and further to an external circuit. For photosynthetic cells, charge separation leads to the activation of the sequence of redox reactions, resulting in the formation of molecular hydrogen [20].

3.2. The coefficient of efficiency of regenerative solar cells

One of the basic estimation parameters of regenerative solar cells is the coefficient of efficiency. The efficiency of solar cell energy conversion is determined as a ratio of power electrical output to the intensity of incident light.

$$\eta = \frac{P_{\text{ell}}}{J_{\text{light}}} \tag{1}$$

Some conditions of accepted standard tests of solar cells are: air mass of AM 1.5, light intensity of 1 kW/m^2 with a temperature of 298 K. Air mass is a ratio of the way, where sunlight passes in the atmosphere, to the thickness of the atmosphere; the value of AM 1.5 means that the sun is set at an angle of 48° to its position in zenith point [4], which is explained in Figure 3.

http://dx.doi.org/10.5772/62238

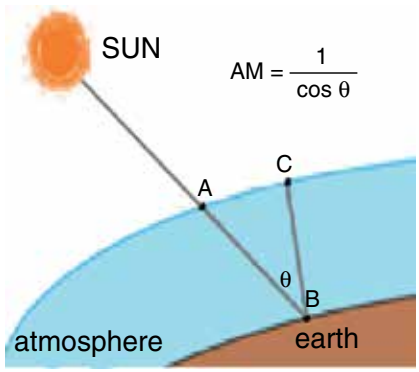

Figure 3 Explanation of air mass (AM) notion.

Traditionally, the efficiency coefficient of photoelement is defined by means of voltammetric methods [25]. The controlled voltage source is attached to the solar cell. Then, the values of the current passing through the photoelement under different values of voltage are obtained using galvanometer. Current dependence on voltage received is called current–voltage characteristic (I–V). A typical I–V curve of photoelement in the darkness and in the light is presented in Figure 4. In the darkness, the photoelement acts as a diode in reverse bias, almost no current flows through the cell in conditions of increasing voltage – there is no free charge carrier. Once the external voltage becomes higher than the potentials, which are holding the electrons in atoms, a sharp increase of the current occurs. This phenomenon is called breakdown. In the light of sufficient intensity, there will be the current in the circuit even under the voltage equal to zero: at the light, solar cell generates photovoltage. The direction of this current will be the opposite to that in case of breakdown. While the external voltage acting in the reverse direction increases, the photocurrent will decrease until it reaches value of zero. Then, there will be the situation similar to the breakdown: the reverse current significantly increases.

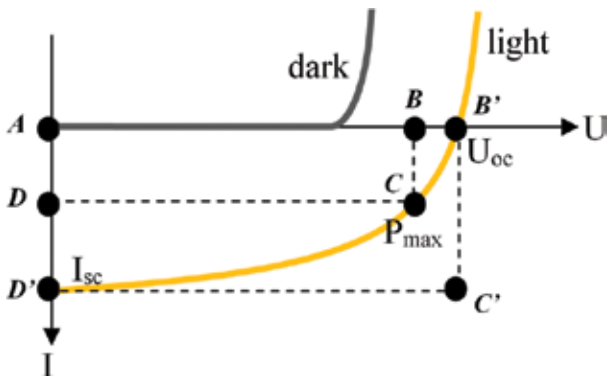

Figure 4 Typical I–V curve of photoelement.

On the I–V curve, it is possible to determine four parameters of the cell: short-circuit current, open-circuit voltage, values of current and voltage defining maximum power generated by the cell [25].

Short-circuit current I_{sc} (the current at an external voltage equal to zero) is the point of I–V intersection with the vertical axis. Open-circuit voltage V_{oc} is the voltage equal in absolute value to photovoltage and opposite to it in sign: if it is applied to the cell, no current flows. Open-circuit voltage is determined by the I–V curve intersection with the axis of abscissa. Current power generated on the cell is determined by the voltage V and current I.

$$P_{ell} = I \cdot V \tag{2}$$

There is a point on the I–V curve, where the value P reaches its maximum, P_{max}. The product of I_{sc} and V_{oc} presents the value proportionate to an area of rectangle AB'C'D' (Fig. 4). The ratio of maximum power P_{max}, corresponded to the area of rectangle ABCD, to the product of I_{sc} by V_{oc} is called fill factor.

$$FF = \frac{S_{ABCD}}{S_{AB'C'D'}} = \frac{P_{\max}}{I_{sc} \cdot V_{oc}} \tag{3}$$

Thereby, the maximum coefficient of efficiency could be expressed by the following equation:

$$\eta_{\max} = \frac{P_{\max}}{J_{\text{light}}} = \frac{I_{sc} \cdot V_{oc} \cdot FF}{J_{\text{light}}} \tag{4}$$

4. The use of components/systems of the photosynthetic apparatus to generate electricity

Nowadays, solar cells containing mono- and polycrystalline silicon as inorganic semiconductors are used for commercial applications in small devices, such as solar panels on roofs, pocket calculators, water pumps, and also in space technologies. Common traditional solar batteries can use less than 20% of the incident solar light [4]. Production of silicon solar cells requires energy-intensive processes, high temperatures (400-1400 °C) and pure vacuum conditions, which results in high cost of such cells [24]. In contrast, production of solar cells based on biological photoactive components does not require these conditions. It suggests that biological-based solar cells are less expensive. The main disadvantage is the fact that they do not reach the efficiency of the inorganic solar cells [21, 24].

In recent researches, the thylakoid membrane and isolated PSI and PSII have been used in solar cells [26-28] and in optoelectronic devices by immobilizing these photoactive components directly onto the electrode surface [29-31] or via linker molecule [32-39].

http://dx.doi.org/10.5772/62238

4.1. Thylakoids as photobiocatalysts

Thylakoid membranes can be isolated from plant leaves and immobilized on the electrode surface to generate a photocurrent. A team of researchers led by Robert Carpentier [40] has been the first to begin using thylakoid membranes isolated from spinach leaves as a photosensitizer. In their work, a platinum electrode was used as a final acceptor. Studies were carried out in the light and in the dark, in the presence and in the absence of potassium ferrocyanide as a mediator. Native thylakoids generated a photocurrent up to 6-9 μA without a mediator, and four times more current in the presence of potassium ferrocyanide. This study has shown that the photocurrent generation without any mediators is associated with direct electron transfer from the membrane proteins to the electrode surface or through the molecules in the electrolyte that can function as mediators. Oxygen capable of producing the superoxide radical may be viewed as a mediator. In 2011, Bedford et al. [41] immobilized thylakoids on conductive nanofibers, using the electrospinning technique. The maximum electric power generated by the cell surface was 24 mW/cm^2 upon illumination by red light with a wavelength of 625 nm.

It is possible to create a stable solar cell by combining the photosynthetic anode and biocatalytic cathode. There is an idea to use photosynthetic organisms/organelle/photosystems for the water oxidation at the anode and the conversion of oxygen into water at the cathode.

Calkins et al. [32] created solar cells using thylakoids isolated from spinach. Thylakoids were immobilized on the anode modified with multi-walled carbon nanotubes (MWCNT). Glass electrode modified by laccase/MWCNT system was used as the cathode (Fig. 5a). The study has demonstrated a maximum current density of 68 mA/cm^2 and a maximum power density of 5.3 mW/cm^2 (Fig. 5b). Composite electrode based on thylakoid/MWCNT produced a current density of 38 mA/cm^2 that is by two orders higher than predicted. The fact that the transmembrane chlorophyll-protein complexes remain in their native state during the isolation process is the main advantage of the usage of membrane thylakoids for photocurrent. This may lead to greater stability and greater power output as compared to the results that can be achieved by using isolated chlorophyll-protein complexes or RCs.

4.2. Photosystem I as photobiocatalyst

Besides the thylakoid membrane preparations, some researchers have conducted studies of photocurrent generating using cells based on isolated photosystems. There are two major benefits of using photosystems as a photosensitizers compared to thylakoids [20]:

a. There is less influence exerted by the other redox systems on the electron transfer in the photosystem chain.

b. RCs are closer to the electrode; it facilitates direct electron transfer to the electrode.

Fourmond et al. [42] developed a photobioelectrochemical system with PSI as the main photocatalytic subunit, cytochrome C_6 and ferredoxin as electron carriers and FNR as an electron acceptor (Fig. 1). They used a gold electrode in the experiment. In an earlier investigation, Frolov et al. [43] created a photobioelectrochemical cell that could generate a voltage of 0.498±0.02 V. They used the PSI preparations isolated from the cyanobacteria *Synechocystis*

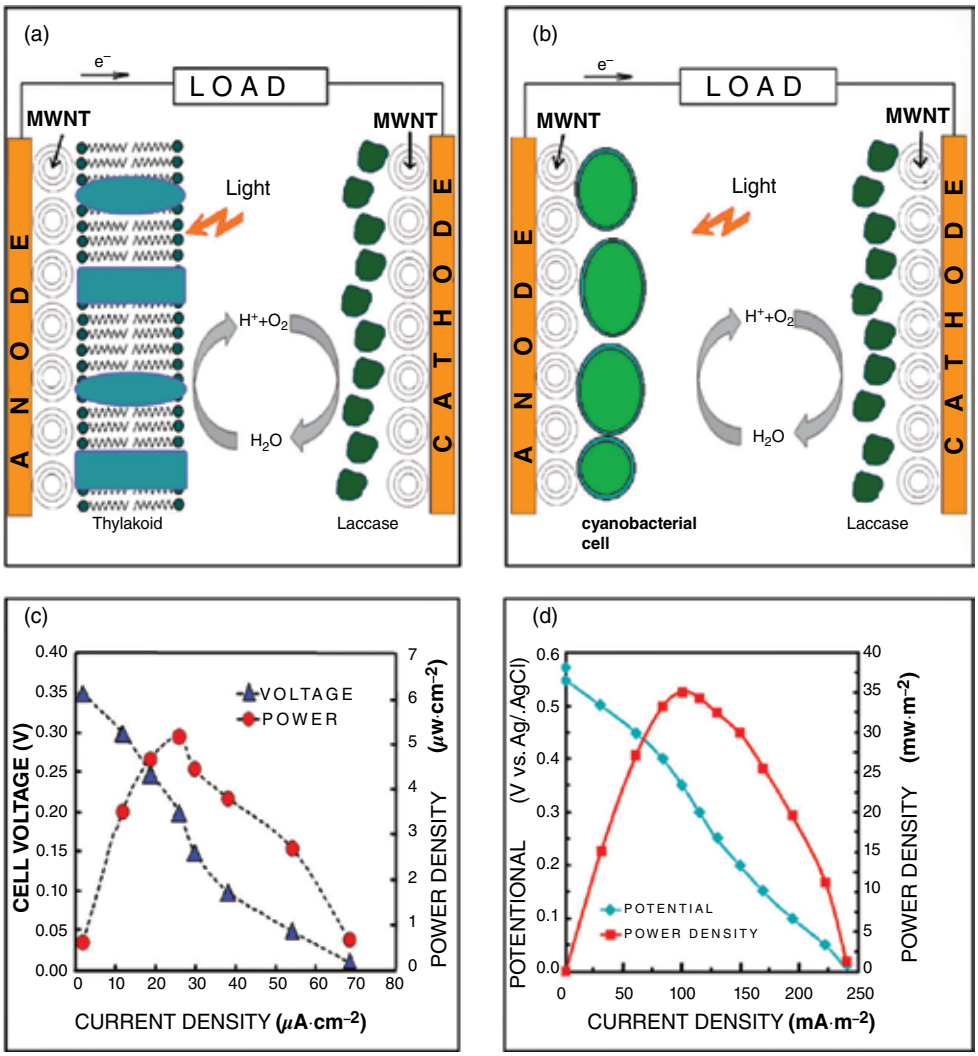

Figure 5 Schematic representation of the functioning photobioelectrochemical cells based on, a) the thylakoid/MWCNT; b) cyanobacteria *Nostoc*/MWCNT; c) and d) the dependences of the voltage and the flux density of the received energy on the current density for each of the cells shown (adapted from [20, 32]).

sp. PCC 6803. These systems are more stable than plant systems due to the antenna pigment molecule's integration into the core subunits. More specifically, unlike plant systems, the antenna pigments are associated only with chlorophyll-protein complex attached to core subunits. Surfactant peptides necessary for the stabilization of other plant and bacterial RCs were not required to stabilize such PSI. In their work, another important factor was the mutation-based replacement of specific amino acids of the PSI by cysteines. Properly oriented stable monolayer of PSI was formed through the formation of Au-S bonds between the thiol group of cysteine and purified hydrophilic gold surface. The procedure for creating the

http://dx.doi.org/10.5772/62238

corresponding gold electrode included thermal treatment at 350 °C. In studies carried out by Das et al [24], mutation-modified PSI complexes were attached to the gold electrode by Ni^{2+}-nitrilotriacetic acid (Ni^{2+}-NTA). In these complexes, native subunit PsaD was replaced by PsaD-His_6 one (Fig. 6a).

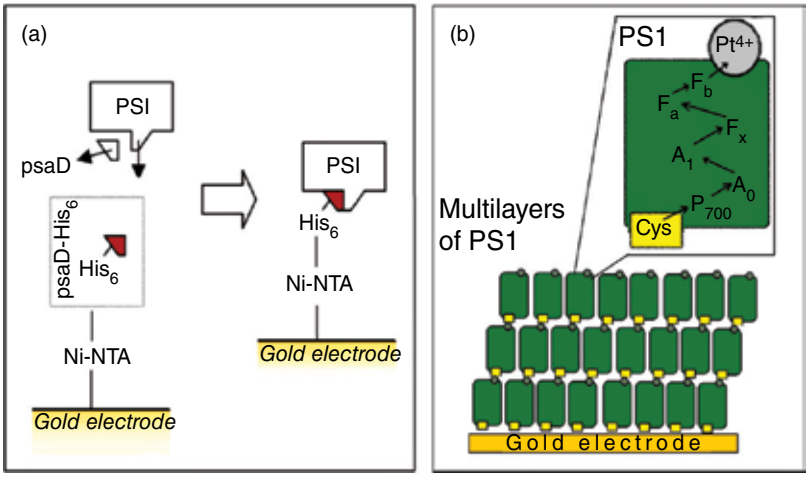

Figure 6 Models used for immobilizing photosystem I on the electrode. a) Native PsaD subunit of PSI replaced by PsaD-His, which clings to the histidine tag, and the entire structure is associated with the gold electrode through a Ni^{2+}-NTA (adapted from [20, 24]). b) The scheme of the cysteine mutants of the PSI with Pt ions and the multilayer structure of such PSI on a gold substrate (adapted from [20, 45]).

In another study, Faulkner et al. [44] reported a fast way to create a dense monolayer of PSI isolated from spinach leaves on a gold electrode. This method of the monolayer creation requiring vacuum conditions was 80 times faster than method of photosystem precipitation from a solution. More specifically, PSI was immobilized on the electrode modified with gold nanoparticles (GNP). In the presence of suitable mediators, the cell generated a photocurrent of 100 nA/cm^2 [44].

However, photobioelectrochemical elements based on the PSI monolayer were not sufficiently effective in cases when a large cross-sectional area of light absorption was required. A photobioelectrochemical cell based on multilayer structures of PSI was created in the same year [45]. The PSI complexes were platinised on the stromal side to form the multilayer structures. The platinum ions facilitated the binding of the lumenal side of PSI and the stromal side of another PSI complex that resulted in the electrically connected multilayer. The first PSI monolayer was attached to the gold surface through the bonds between the cysteine's thiol groups of the mutant PSI and the gold atoms. Then, the next layer was formed through the connection between the photosystem donor side of the next layer and the platinum atoms (Fig. 6b). The devices developed on the basis of the two and three layers generated photovoltage outputs of 0.330 and 0.386 V, respectively [45]. Hereafter, the investigations of solar cells based on multilayer structures of PSI were continued. Method suggested by Ciesielski et al. [46] did not require the use of photosystems isolated from mutated cyanobacteria, nor the use

of a high vacuum, so it was more economical and less time-consuming. In their study, a plate of gold (thickness of about 125 nm) immobilized on a silicon substrate served as cathode and a working surface of transparent plastic plate coated with lead oxide doped with indium served as anode of the photoelement, respectively. A cavity between them was half-filled with an electrolyte composed of 5 mM 2,6-dichlorphenolindophenol, 100 mM ascorbic acid (Asc), and 100 mM NaCl in 5 mM phosphate buffer at pH 7.0. In the other half, there was a buffer solution containing PSI complexes (about 9 μM), Triton-X100 (0.05% w/v), 0.14 M in 0.2 M NaH_2PO_4 at pH 7.0. The PSI complexes were precipitated on a gold electrode for seven days. As a result, a multilayer of the PSI complexes with a thickness of 1-2 μm was obtained. The obtained solar cell generated a photocurrent at a density of about 2 mA/cm^2 under illumination by a standard light intensity (clear sky at noon). The device demonstrated a considerable stability and retained activity under ambient conditions for at least 280 days [46].

According to the review of the recent advances in photosynthetic energy conversion made by Sekar and Ramasamy [2], to the present day the highest current density of 362 mA/cm^2 and the energy flux density of 81 mkW/cm^2 using PSI were obtained by Mershin et al. [47]. In their work, they compared the efficiency of solar cells with two different semiconductor substrates: nanocrystalline titanium dioxide TiO_2 and nanowires of zinc oxide (ZnO) (Fig. 7). The measurements were carried out under normal sunlight. The PSI complexes were adsorbed on each of these two substrates. Stability of the isolated PSI complexes was increased by the treatment with surfactant Ac-AAAAAAK-NH_2 – a sequence of six alanines and one lysine (A_6K). This also promoted the selective adsorption of the PSI on the substrates and increased the absorption of light. Such approach improved the photovoltaic performance. In this artificial system, cobalt electrolyte performed the role of plastocyanine, and ferredoxin was replaced by nanocrystalline TiO_2, or nanofiber ZnO [47]. Overall, PSI is a good photobiocatalyst, but it has several disadvantages as a photosensitizer. First, the process of the complex isolation is more laborious compared with the isolation of thylakoid membranes. Second, the isolated PSI complex is less stable. Third, for getting a continuous electron transfer to P_{700}, RC requires an external electron donor with a redox potential approximately equal to the redox potential of plastocyanin. Thus, the photosystem depends on other electron sources.

4.3. Photosystem II as photobiocatalyst

The main advantage of PSII against PSI is the fact that water is the electron source required to activate the electron transfer, and it is abundant in the environment [2]. Unlike the PSI, which requires an electron donor, PSII has an internal oxygen-evolving complex, also known as water-splitting complex. Thus, PSII depends on the availability of water and light. Here, electrons from P_{680} are transferred to pheophytin, then to plastoquinone and further to the other ETC components [8]. There are two major rate-limiting steps in this process: reduction of plastoquinone in QB-site by two electrons from plastoquinone in QA-site and diffusion of the double reduced quinone (PQH_2) inside membrane [8]. Therefore, it is assumed that the water oxidation in PSII should be accelerated if electrons from QA-site could be efficiently transferred to an external electron acceptor [48]. Thus, in order for the electrons from PSII to be transferred onto the electrode, the complex should come in contact with the surface of the

http://dx.doi.org/10.5772/62238

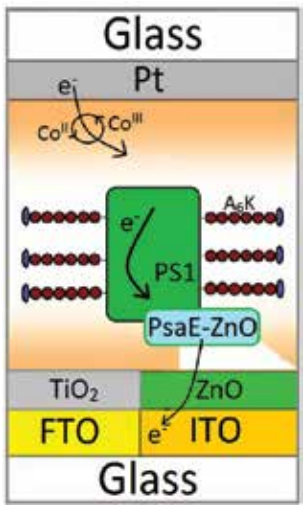

Figure 7 Schematic presentation of two Mershin's cells with zinc oxide and titanium dioxide. FTO – a layer of fluorine doped with tin oxide, ITO – a layer of indium doped with tin oxide, and PsaE-ZnO – mutant subunit (adapted from [20, 47]).

electrode, or the electron transfer should be carried out by a mediator. In fact, it is difficult to achieve direct electron transfer from the PSII to the electrode due to the deep localization of the Pheo-PQ site inside the PSII [38].

For the creation of efficient solar cell based on PSII, it is important to improve its stability and increase electron transport efficiency. To achieve that, Vittadello et al. [49] reported the application of histidine-tagged protein complex of PSII from *Synechococcus elongatus* covalently bound to a gold electrode treated with Ni^{2+}-nitrilotriacetic acid (Ni^{2+}-NTA). The current density of the resulting photobioelectrochemical cell has reached 43 mkA/cm^2 [49]. On the other hand, while the photochemical energy conversion efficiency of the freshly isolated PSII was 0.7, the same parameter for the PSII immobilized on gold was 0.53. This clearly indicated that the PSII complexes were photochemically stable even after immobilization [49].

Utilization of osmium-containing redox polymer based on poly-1-vinylimidazole is also an effective immobilization method, which could help maintain the stability as well as enhance the coating degree of the electrode by the PSII complexes (Fig. 8a) [38]. The polymer works both as an immobilization matrix and a mediator. This kind of system could facilitate the electron transfer from the PSII complex to the electrode. The correct orientation of the immobilized complex could also support the electron transfer. Recently, Noji et al. [50] developed a nanodevice for the artificial water decomposition controlled by light, using a conjugate of PSII-GNP. The core of the PSII complex comprising a histidine tag on the C-terminus of CP47 protein was immobilized on a GNP by Ni^{2+}-NTA (Fig. 8b). In this work, the diameter of GNPs was about 20 nm, and GNPs could bind four or five PSII complexes. The efficiency of oxygen evolution by the developed PSII-GNP was comparable to that of the unbound PSII [50].

Israeli scientists developed the photocell on the basis of bacterial PSII complexes isolated from the thermophilic cyanobacterium *Mastigocladus laminosus*. The photoanode consisting of a matrix of 2-mercapto-1,4-benzoquinone was electro-polymerized on the gold surface. Then, PSII complexes were immobilized on this surface. The anode was electrically connected to the cathode by bilirubin oxidase/carbon nanotubes (BOD/CNT). It is claimed that photo-induced quinone-mediated electron transfer led to the generation of photocurrent with an output power of 0.1 W [37].

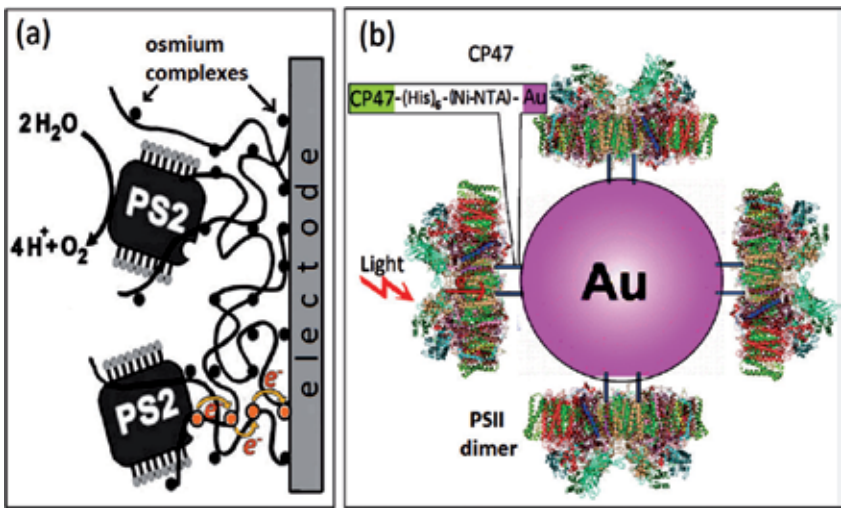

Figure 8 Models used for immobilizing photosystem II on the electrode. a) PSII associated with an osmium redox polymer containing a mediator network (adapted from [20, 38]). Yellow arrows depict the electron transfer pathway by a hopping mechanism. b) Connection of PSII with gold nanoparticle through histidine tag with Ni^{2+}-nitrilotriacetic acid (Ni^{2+}-NTA) attached to the C-terminus of the CP47 protein (adapted from [20, 50]).

Special protective compounds located inside the chloroplast protect highly sensitive photosystems (PSI and PSII) from photoinhibition [2]. It is evident that the stability of isolated photosystems will be impaired after their isolation from native environments. It should be noted that isolated PSII is less stable compared to PSI. Thus, photocurrent of higher density could be achieved in cells using PSI complexes [20].

4.4. The bacterial cell as photobiocatalyst

Photocells with isolated photosynthetic structures such as thylakoids, PSI and PSII suffer from significant disadvantages. The components of these cells are relatively unstable; they have a short running time and require labour-consuming laboratory procedures such as isolation/purification. These limitations could be overcome if whole cells of photosynthetic microorganisms were used as a biocatalyst and/or sensitizer. In the past few years, some studies have been conducted to construct a photosynthetic microbial fuel cell (PMFC) based on whole cells of photosynthetic organisms such as cyanobacteria [2]. In the anode chamber of PMFCs, there are photosynthetic organisms that are able to oxidize water using light. PMFC requires only sunlight and water for the functioning, whereas traditional MFCs based on bacteria, for

http://dx.doi.org/10.5772/62238

example, *Gejbacter* and *Shewanella*, require organic carbon sources such as glucose/lactate, and they produce CO_2 as final product. Figure 9 shows the general scheme of the combined cell.

Various cyanobacteria were used in the most effective PMFCs [51-53]. In particular, the ability of the cyanobacteria *Nostoc sp*. in generating a photocurrent was investigated using various electrochemical methods. In a recent investigation, the mechanism of direct electron transfer from ETC of *Nostoc* to electrode was studied using the site-specific photosynthetic inhibitors (Fig. 1) [54]. It was shown that the solar cell with *Nostoc* immobilized on the MWCNT-modified carbon electrode as an anode and laccase/MWCNT-modified cathode (Fig. 5c) generated a current density of 25 mA/cm^2, while the maximum energy flux density achieved without mediators was only at 3.5 mW/cm^2 (Fig. 5d). In comparison, the cell based on thylakoids generated a maximum current density of 10 mA/cm^2 (Fig. 5a), and the maximum energy flux density achieved without mediators was of 5 mW/cm^2 (Fig. 5b). Overall, the maximum current density from the solar element based on the native photosynthetic cells was higher than that from the photoelement based on thylakoids.

One of the main advantages of cyanobacteria compared with individual components of the photosynthetic apparatus is that they are considerably less susceptible to dehydration. Currently, the power that could be generated by PMFCs is less than that achieved by the biofuel cell [2]. However, many of their advantages such as simplicity of operation, the utilization of available substrates, for example, water, as well as stress-resistance of PMFCs in comparison with the other biofuel cells mark them as promising solar cell structure for the future.

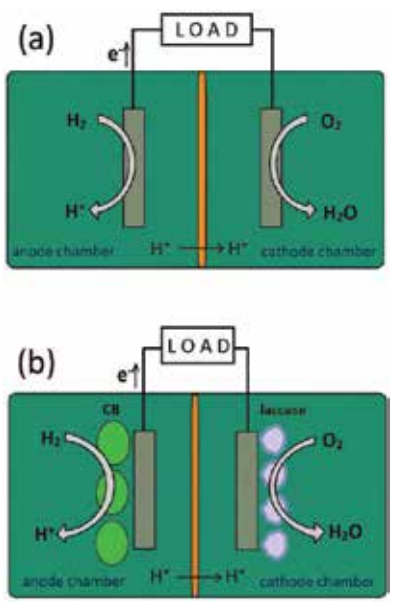

Figure 9 Schematic representation of the different forms of fuel cells: a) hydrogen fuel cell with a platinum catalyst on the anode and the cathode and b) photobioelectrochemical cell based on cyanobacterial cell (CB) on the anode and laccase enzyme on the cathode (adapted from [2, 20]).

5. Improving the efficiency of solar cells

5.1. The redox-active components: changing the direction of the electron flow

Various redox-active components accept electrons from specific sites of ETC in accordance with their redox potential. Redox active sites of metalloproteins are usually hidden inside the PSII complex [38]. Therefore, the electron transfer from immobilized photosystems onto the electrode may be limited. This limitation could be overcome by redirecting the electrons from the inner part of the protein to the surface [2]. For instance, Larom et al. [55] successfully used an artificial mediator to redirect electrons from QA-site to an artificial acceptor at a distance of about 1.3 nm from the stromal side of the membrane. This change in the direction of electron flow together with additional blocking of QB-site has reduced oxidative damages at the expense of reducing the time of the intermediate electron transfer at the QA/QB stage. In another study, Sekar et al. [54] used whole cells of cyanobacteria as photobiocatalysts in a solar cell. They achieved a power density of about 10 μW/cm^2 by adding 1,4-benzoquinone (BQ) as a mediator. It was three times higher in comparison with power density of photoelements without a mediator using the systems *Nostoc*/MWCNT and laccase/MWCNT. Since both BQ and PQ have the similar structure, this addition facilitated electron transfer from the PSII to the MWCNT [54]. Previously, mediators such as BQ, 2,6-dimethyl-1-benzoquinone (DMBIB) and 2-hydroxy-1,4-naphthoquinone (HNQ) have been also used for accepting the electrons from the cyanobacterial photosynthetic ETC [51, 52].

5.2. Bioengineering of photosynthetic RCs

Primary processes of photosynthesis have a high quantum yield reaching almost 100%, but the energy storage efficiency can reach about 27% under ideal conditions, and much less under non-ideal ones [56]. This value is comparable to the efficiency of the modern silicon-based solar panels operating with an efficiency of approximately 20%. It is notable that some laboratory models have demonstrated an efficiency of 40% [2, 7, 21]. Moreover, the photosynthetic pigments usually absorb light only from the visible region of the spectrum (from 400 to 700 nm) [7] unlike photovoltaic cells that are capable of absorbing the light from ultraviolet and near infra-red regions as well. Thus, photosynthetic organisms utilize only about a half of the incident solar energy. Nevertheless, photosynthetic efficiency can be improved by expanding the region of photosynthetic absorption using bioengineering techniques. Since two photosystems used in photosynthesis absorb light under the same conditions, the variation of absorbance could increase the efficiency [20]. This approach may be performed using photoelements based on RC containing far-red and infra-red absorbing pigments similar to bacteriochlorophyll that absorbs light in the region up to 900 nm [57] or Chl *d* or Chl *f* capable of absorbing light in the region of 400-750 nm [21]. As a result, the absorption region may be significantly increased.

http://dx.doi.org/10.5772/62238

5.3. Biomimetics

Biomimetic approach is aimed to construct an artificial systems mimicing the natural photosynthesis for the production of electricity or hydrogen. Synthetic sensitizers and catalysts are considered as a suitable alternative to unstable native systems. As a first-line strategy, porphyrins, phthalocyanines and their metal complexes that absorb light in the same optical region as the native chlorophyll molecules are regarded as such synthetic RCs. Covalently linked cyclic porphyrins are more durable, but they are difficult to synthesize [58]. Non-covalently associated porphyrins easily degrade due to their sensitivity to changing environmental conditions [59]. The advantages of utilizing the porphyrin structures include stability of the RCs and accessibility compared to synthetic products, while their disadvantage is the short lifetime in their excited state. Polypyridines containing transition metals have a longer lifetime in their high energy excited states [60]. Nevertheless, they generally require more expensive metals [53]. It should be noted that the biomimetic-based semiconductor materials mimicking the oxygen-evolved complex were designed to create energy devices during the early 1970s [61].

6. The key challenges in photosystem-based solar cell development

6.1. Methods of immobilization and orientation of biocatalysts

It is necessary to immobilize photoactive molecules on a conductive substrate for the optimum functioning of a solar cell. Most of these cells require peptides for immobilization of pigments on the electrode surface. Another important question is the correct orientation of pigment molecules. The studies conducted at Stanford [62] were focused on the orientation of photosynthetic RCs towards the electrode surface. According to this construction, a poly-histidine tag was attached to the C-terminus of the M-subunit of the *Rhodobacter sphaeroides* RC. With the help of the tag, the construction was immobilized on a gold electrode containing self-assembling layer of alkanethiols with Ni^{2+}-NTA as a head part. It has been experimentally shown that the proximity of RCs to the electrode is important for the cell effective operation [63].

Many techniques were used for immobilization of photosynthetic complexes, including bioelectrocatalystic self-assembling monolayers (bio-SAMs) [45, 47, 63, 64]; Ni^{2+}-NTA attached to poly-histidine tagged PSI complexes (Fig. 6a) [24, 54]; the redox-active hydrogels [38] (Fig. 8a) and fixation on CNTs by means of molecular binding reagents [32]. Each of these techniques provides various beneficial properties, including the increase of the electrode surface area, the rise of the electron transfer rate between the electrode and photobiocatalyst and/or orientation of specific enzymes on the electrode. Unfortunately, enzyme immobilization reduces their activity in comparison with their native state. Therefore, the enzyme activity should be retained for a long time with the help of correct immobilization methods. In a study conducted by Meunier et al. [65], thylakoids were adsorbed on a silicon matrix, thereby the stability of the native thylakoid suspension increased and it remained active for 30 days. Immobilization should provide an optimum rate of electron transfer from the protein to the

electrode, with minimal resistance. This can be achieved by correct orientation of proteins on the electrode surface or by the usage of intermediate carriers. Many investigations have shown that the correct orientation of a photosystem on the electrode results in an improved electron transport [45]. In many studies, the correct orientation of the photosystems provides specific binding of a histidine-tagged protein complex with Ni^{2+}-NTA molecule anchored to a gold electrode [24, 50]. Badura et al. [38] used the osmium-containing polymer of polyvinyl-imidazole as modified electrode acting as both an immobilizing agent and an electron acceptor for the PSII complex (Fig. 8a). Binding of sensitizer with redox polymer is rather interesting way of sensitizer immobilization. Due to that, an electron transfer between neighbouring redox centres covalently bound to the polymer backbone is possible by means of a hopping mechanism. Thus, there could be the shuttling of electrons from a reactive site within a redox protein towards an electrode surface. Several parameters determine the rate of electron transfer: the polymer backbone composition (flexibility, swelling behaviour, and amount of cross-linking), the distance between the polymer-bound redox centres and potential of the mediator. Hence, the properties of the redox polymer can be adapted to find an appropriate redox polymer for a specific application. In these modified systems, immobilized PSII were capable of generating a current density of 45 mA/cm^2 at light intensity of 2.65 mW/cm^2 (maximum wavelength at 675 nm) [38].

6.2. The stability of the isolated proteins

The main problem of the usage of isolated proteins as photosensitizers in photovoltaic cells is their extremely low stability. Photoinhibition of photosystems is the main reason for protein destruction, especially in case of the PSII. Caused by an excessive amount of radiation, photoinhibition may damage the photosynthetic apparatus and hence destroy the chloroplast proteins. Photosystems are provided with some protective mechanisms in vivo [2]. However, once the proteins are isolated, natural self-healing mechanisms do not work. Thus, isolated proteins are more susceptible to damage and have a short lifetime. There is one of the methods to stabilize the photosynthetic complexes through the simulation of the natural states of proteins. Surfactant peptides can be used to imitate the lipid membrane naturally stabilizing photosynthetic complexes. Such surfactants are designed as molecular nanomaterial to study the membrane protein's stability [47]. It consists of hydrophilic amino acids (aspartate or lysine) as the head of the chain and hydrophobic amino acids (alanine) as the tail. For the stabilization of the photosynthetic complex during the construction of a solid electrical device, Das et al. [24] used the peptides A_6K and V_6D, a sequence of six valines and one aspartic acid (VVVVVVD), as cationic and anionic surfactant peptides, respectively. They showed a short-circuit current density of 0.12 mA/cm^2 at the excitation light intensity of 10 W/cm^2 with a wavelength of 808 nm. Presumably, this direction is promising.

6.3. Increase of surface area

The increase of the electrode surface area is a method conventionally used to improve the efficiency of functioning solar cells. In many cases, the electrode itself is originally flat, and changes of its geometry can destroy its structure. However, the electrode can be modified via

http://dx.doi.org/10.5772/62238

nanomaterials, which could increase the real surface area due to the formation of nanostructures with non-planar topology on the electrode surface. In this case, the working electrode area is larger than the area of the initial flat surface, and it can absorb more pigment molecules. In their study, Mershin et al. [47] compared two different forms of electrode modification using nanocrystals of titanium dioxide and zinc oxide nanowires (Fig. 7). In contrast with the flat electrodes of the same size, the electrodes using TiO_2 and ZnO had 200 and 30 times larger active areas, respectively. The results of this study demonstrated that the samples based on ZnO were less effective due to the smaller coefficient of roughness. On the other hand, ZnO was found to be more conductive and less expensive in comparison with the TiO_2 [47].

The cells of that construction used in Mershin's experiments are worth discussing in more detail. It is a stable and acknowledged design of solar cells. These cells are called dye-sensitized solar cells (DSSC) or Grätzel cell named after the one of its inventors, Michael Grätzel [21]. The advantage of such cells over the others is exactly in the usage of mesoscopic material as a substrate for photoactivator. The mesoscopic material is the material with a complicated inner structure represented by interpenetrating network of inorganic or organic semiconductor particles of mesoscopic size (2–50 nm) forming connections of very high contact area [4]. The structure of DSSC can be described as follows (Fig. 10). The main components of DSSC are two flat glass electrodes. Each of them has one conductive side. The conductive side is provided by application of thin layer of indium tin oxide (ITO) or fluorine tin oxide (FTO). The layer of mesoscopic semiconductive material is deposited on the one of the electrodes. Also, there is a monolayer of the dye attached to the surface of the nanocrystalline film. Photoexcitation of the dye results in the injection of an electron into the conduction band of the semiconductor. For the original state of the dye to be subsequently restored, there is the electrolyte, usually an organic solution containing redox system, such as the iodide/triiodide couple. It donates an electron to the dye. Timely regeneration of the sensitizer by iodide retards the recapture of the conduction band electron by the oxidized dye. The reduction of triiodide at the counter electrode regenerates the iodide, and the circuit is completed via electron migration through the external load. The mesoscopic oxide films are made of networks of thin crystals of a few nanometers. The components mostly preferred are the oxides such as TiO_2, ZnO, SnO_2, Nb_2O_5 or chalcogenides such as CdSe. They are bound inside and this allows the electron conduction to occur. Generally, the size of TiO_2 particles is about 20 nm [4]. Before Grätzel cells, many cells were designed by the application of photosensitizer on flat electrode. In case of flat topology solar cells, a low density of pigments is one of low efficiency reasons. In DSSC, there are several advantages of nanocrystalline structure of semiconducting oxide (usually TiO_2) used for sensitizer support [4]:

1. It enables the effective capture of light by the surface with sensitizer absorbed. On the flat surface, a monolayer absorbs less than a few percent of light as it covers an area approximately two order of magnitude larger than its optical cross-section [4]. The use of multilayered sensitizer would not solve this problem as molecules only in contact with semiconductor could excite it; the others act like filter. Significant increase of interface enhances absorption and leads to thousand-fold increase of photocurrent in comparison with flat surface DSSC.

2. Nanocrystals of TiO_2 should not be somehow doped to have the conductivity. Injection of one electron from sensitizer to TiO_2 particle is enough for titanium dioxide to get its conducting state. This photo-induced conductivity allows gathering the electron without any significant ohmic losses. In contrast, it is necessary for compact semiconductive films to be n-doped so that semiconductor could conduct the current. In this case, the energy transport from excited sensitizer to conducting band of semiconductor will inevitably decrease the coefficient of efficiency.

3. Size of TiO_2 particles allows effectively screening electrons from the electrolyte or hole conductor present in pores. As a result, photocurrent is not declined by a repulse between electrons diffusing through the particle network.

Ruthenium dyes are used as sensitizers in most studies connected with Grätzel cells [4, 21]. But isolated components of photosynthetic apparatus as dyes are also quite attractive since ruthenium dyes are rather expensive. Some studies including Mershin's investigations offer significant possibilities in this area.

As it has already been shown, the mesoscopic materials cannot be the only way to increase an active surface area of solar cell. In fuel cells of another kind, nanotextured surfaces are also used to increase the amount of absorbed dye molecules. As the technique for creating nanowires, nanotubes and other structures for carbon materials is quite well developed, carbon is rather attractive as a material for the creation of such surfaces. These approaches include the usage of GNPs [50], nanoporous gold electrodes [46] and redox hydrogels [38].

6.4. Direct or mediated transfer of electrons

Another way to achieve the maximum current density in the cells based on photosynthetic sensitizers is to create a system that carries out direct electron transfer from photosystem to electrode without using a mediator. As was mentioned earlier, the mediators have lower redox potential required for the efficient electron transfer compared to the native electron source. If the electrons are transferred to the mediator, they lose some part of their energy in contrast to transfer from the real source. The distance between the redox site and the electrode should also be minimized in order to ensure efficient transfer of electrons. The difficulty in ensuring continuous contact between the electron source and the electrode is the main disadvantage of direct electron transfer.

Furukawa et al. used polyaniline as an electronic catalyst instead of mediators to develop a photosynthetic biofuel cell [66]. Polyaniline has a good electrical conductivity; it is compatible with the photosystem. Due to its nanostructure, polyaniline also increases the surface area. During their experiment, they managed to achieve a good efficiency of the developed cell: peak current density was about 150 mA/cm^2 and power density was measured at 5.3 mkW/cm^2. According to the study conducted by Sekar et al. [54], MWCNTs were successfully used for direct electron transfer, both in isolated spinach thylakoids and cyanobacteria *Nostoc sp*.

http://dx.doi.org/10.5772/62238

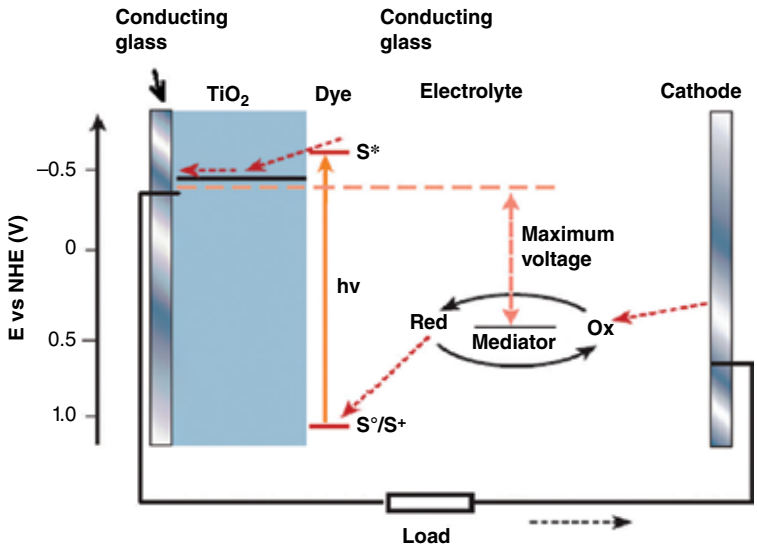

Figure 10 Scheme of operation of the dye-sensitized solar cell. The photoanode, made of a mesoporous dye-sensitized semiconductor, receives electrons from the photo-excited dye which is thereby oxidized, and which in turn oxidizes the mediator, a redox species dissolved in the electrolyte. The mediator is regenerated by reduction at the cathode by the electrons circulated through the external circuit. Energy levels are measured in relation to normal hydrogen electrode (NHE). S –ground state of dye molecule. S^+ – its oxidized state, S* – its exited state (adapted from [21]).

6.5. Extension of the spectral range of the light absorption by photosystems

Previous four problems were closely linked: stability of isolated complexes directly depends on the way of its immobilization on electrode. For creating electrodes with complex surface, it is necessary to consider the ability of the surface to adsorb sensitizer molecules. In their experiments, Badura et al. [38] have been solving all these four problems at once. Ni^{2+}-NTA and 6-His tag are both mediators of electron transport and a means of photosystem attachment on electrode surface. Immobilization, dye stability, working surface area and mediation of electron transport are connected with 'dye/electrode' contact. The increase of the spectral absorption region is the matter that is connected only with sensitizer. Extension of the spectral range of the light absorption is possible using Chl *d* or *f* [15,21,67-70]. Though the creation of artificial solar cells based on these chlorophylls is still at the early stages of its development. Overall, designing of solar cells using these chlorophylls seems to be quite promising.

7. Conclusion

Researchers in the area of artificial photosynthesis have focused on the development of total inorganic and hybrid semi-natural systems [71, 72] that could effectively produce a sustainable energy from sunlight without requiring external fuels. These systems should have a high quantum yield and generate energy fluxes of high density to satisfy the energy requirements.

The more we learn about the nature, the closer we come to the creation of the efficient energy solar cells using the components of photosynthetic apparatus. The usage of systems imitating the photosynthetic apparatus and the elements of photosynthetic systems in current energy generators and fuel cells is a quite promising direction [72, 73]. However, the biophotovoltaics requires a lot of changes and improvements to be widely used.

Acknowledgements

The work was supported by the Russian Science Foundation №14-14-00039 (to S.I.A.) and by the grant-in-aid for Specially Promoted Research No. 24000018 (J.-R.S.) from JSPS, MEXT, Japan.

Author details

Roman A. Voloshin[1*], Margarita V. Rodionova[1], Sergey K. Zharmukhamedov[2], Harvey J.M. Hou[3], Jian-Ren Shen[4] and Suleyman I. Allakhverdiev[1,2,5*]

*Address all correspondence to: voloshinra@gmail.com

*Address all correspondence to: suleyman.allakhverdiev@gmail.com

1 Controlled Photobiosynthesis Laboratory, Institute of Plant Physiology, Russian Academy of Sciences, Moscow, Russia

2 Institute of Basic Biological Problems, Russian Academy of Sciences, Pushchino, Moscow, Russia

3 Department of Physical Sciences, Alabama State University, Montgomery, USA

4 Photosynthesis Research Center, Graduate School of Natural Science and Technology/ Faculty of Science, Okayama University, Japan

5 Department of Plant Physiology, Faculty of Biology, M.V. Lomonosov Moscow State University, Moscow, Russia

References

[1] Ort D.R., Merchant S.S., Alric J., Barkan A., Blankenship R.E., Bock R., Croce R., Hanson M.R., Hibberd J.M., Long S.P., Moore T.A., Moroney J., Niyogi K.K., Parry M.A.J., Peralta-Yahya P.P., Prince R.C., Redding K.E., Spalding M.H., van Wijk K.J., Vermaas

W.F.J., von Caemmerer S., Weber A.P.M., Yeates T.O., Yuan J.S., and Zhu X.G. Redesigning photosynthesis to sustainably meet global food and bioenergy demand. *Proceedings of the National Academy of Sciences of the United States of America*. 2015;112(28): 8529-8536.

[2] Sekar N., Ramasamy R. Recent advances in photosynthetic energy. *Journal of Photochemistry and Photobiology C: Photochemistry*. 2015;22:19-33.

[3] Lewis N.S., Nocera D.G. Powering the planet: Chemical challenges in solar energy utilization. *Proceedings of the National Academy of Sciences of the United States of America*. 2006;103(43):15729–15735.

[4] Grätzel M. Photovoltaic and photoelectrochemical conversion of solar energy. *Philosophical Transactions of the Royal Society*. 2007;365:993-1005.

[5] Mazor Y., Borovikova A., Nelson N. The structure of plant photosystem I supercomplex at 2.8 Å resolution. *eLife*. 2015;4. DOI: 10.7554/eLife.07433.

[6] Suga M., Akita F., Hirata K., Ueno G., Murakami H., Nakajima Y., Shimizu T., Yamashita K., Yamamoto M., Ago H., ShShen J.-R. Native structure of photosystem II at 1.95 Å resolution viewed by femtosecond X-ray pulses. *Nature*. 2015;517: 99–103. DOI: 10.1038/nature13991.

[7] Blankenship R.E., Tiede D.M., Barber J., Brudvig G.W., Fleming G., Ghirardi M.R., Gunner M., Junge W., Kramer D.M., Melis A., Moore T.A., Moser C.C., Nocera D.G., Nozik A.J., Ort D.R., Parson W.W., Prince R.C., Sayre R.T. Comparing photosynthetic and photovoltaic efficiencies and recognizing the potential for improvement. *Science*. 2011;332:805-809.

[8] Blankenship R.E., editors. *Molecular Mechanisms of Photosynthesis*. Oxford: Blackwell Science; 2002. 321 p. DOI: 10.1002/9780470758472.

[9] Blankenship R.E. Early evolution of photosynthesis. *Plant Physiology*. 2010;154:434-438.

[10] Blankenship R.E., Hartman H. The origin and evolution of oxygenic photosynthesis. *Trends in Biochemical Sciences*. 1998;23:94-97.

[11] Nelson N., Yocum C.F. Structure and function of photosystem I and II. *Annual Review of Plant Biology*. 2006;57:521-565.

[12] Andralojc J., Harris D.A. The chloroplast ATP-synthase - A light regulated enzyme. *Biochemical Education*. 1992;20(1):44-48.

[13] Qin X., Suga M., Kuang T., Shen J.-R. Structural basis for energy transfer pathways in the plant PSI-LHCI supercomplex. *Science*. 2015;348(6238):989-995.

[14] Scheer H. An overview of chlorophylls and bacteriochlorophylls: Biochemistry, biophysics, functions and applications. In: Grimm B., Porra R.J., Rüdiger W., Scheer H, editors. *Chlorophylls and Bacteriochlorophylls: Biochemistry, Biophysics, Functions and Applications*. Dordrecht: Springer; 2006. pp. 4-11.

[15] Loughlin P., Lin Y., Chen M. Chlorophyll d and Acaryochloris marina: Current status. *Photosynthesis Research*. 2013;116(2-3):277-293.

[16] Sandman G. Evolution of carotenoid desaturation: The complication of a simple pathway. *Archives of Biochemistry and Biophysics*. 2009;483:169-174.

[17] Tomo T., Akimoto S., Tsuchiya T., Fukuya M., Tanaka K., Mimuro M. Isolation and spectral characterization of photosystem II reaction center from *Synechocystis sp*. PCC 6803. *Photosynthesis Research*. 2008;98:293–302.

[18] Tomo T., Shinoda T., Chen M., Allakhverdiev S.I., Akimoto S. Energy transfer processes in chlorophyll f-containing cyanobacteria using time-resolved fluorescence spectroscopy on intact cells. *Biochimica et Biophysica Acta* . 2014;1837:1484-1489.

[19] Blankenship R.E., Chen M. Spectral expansion and antenna reduction can enhance photosynthesis for energy production. *Current Opinion in Chemical Biology*. 2013;17:457-461.

[20] Voloshin R.A., Kreslavski V.D., Zharmukhamedov S.K., Bedbenov V.S., Ramakrishna S., Allakhverdiev S.I. Photoelectrochemical cells based on photosynthetic systems: A review. *Biofuel Research Journal*. 2015;6:227-235.

[21] Grätzel M. Photoelectrochemical cells. *Nature*. 2001;414:338-344.

[22] Lubner C.E., Applegate A.M., Knörzer P., Ganago A., Bryant D.A., Happe T., Golbeck J.H. Solar hydrogen-producing bionanodevice outperforms natural photosynthesis. *Proceedings of the National Academy of Sciences of the United States of America*. 2011;108(52): 20988-20991.

[23] Torella J.P., Gagliardi C.J., Chen J.S., Bediako D.K., Colón B., Way J.C., Silver P.A., Nocera D.G. Efficient solar-to-fuels production from a hybrid microbial–water-splitting catalyst system. *Proceedings of the National Academy of Sciences of the United States of America*. 2015;112(8):2337-2342.

[24] Das R., Kiley P.J., Segal M., Norville J., Yu A.A., Wang L.Y., Trammell S. A., Reddick L. E., Kumar R., Stellacci F., Lebedev N., Schnur J., Bruce B.D., Zhang S.G., Baldo M. Integration of photosynthetic protein molecular complexes in solid-state electronic devices. *Nano Letters*. 2004;4:1079-1083.

[25] Gamry Instruments. DSSC: Dye Sensitized Solar Cells [Internet]. 2015 [Updated: 2015]. Available from: http://www.gamry.com/application-notes/physechem/dssc-dye-sensitized-solar-cells/ [Accessed: 2015].

[26] Tel-Vered R., Willner I. Photo-bioelectrochemical cells for energy conversion, sensing, and optoelectronic applications. *ChemElectroChem*. 2014;1:1778-1797.

[27] Kato M., Zhang J.Z., Pau N., Reisner E. Protein film photoelectrochemistry of the water oxidation enzyme photosystem II. *Chemical Society Reviews*. 2014;43:6485-6497.

[28] Lam K.B., Irwin E.F., Healy K.E., Lin L. Bioelectrocatalytic self-assembled thylakoids for micro-power and sensing applications. *Sensors and Actuators* B: *Chemical*. 2006;117:480-487.

[29] Kato M., Cardona T., Rutherford A.W., Reisner E. Photoelectrochemical water oxidation with photosystem II integrated in a mesoporous indium–tin oxide electrode. *Journal of the American Chemical Society*. 2012;134:8332-8335.

[30] Shah V.B., Henson W.R., Chadha T.S., Lakin G., Liu H., Blankenship R.E., Biswas P. Linker-free deposition and adhesion of photosystem I onto nanostructured TiO_2 for biohybrid photoelectrochemical cells. *Langmuir*. 2015;31:1675-1682.

[31] LeBlanc G., Chen G., Gizzie E.A., Jennings G.K., Cliffel D.E. Enhanced photocurrents of photosystem I films on p-doped silicon. *Advanced Materials*. 2012;24:5959-5962.

[32] Calkins J.O., Umasankar Y., O'Neill H., Ramasamy R.P. High photoelectrochemical activity of thylakoid-carbon nanotube composites for photosynthetic energy conversion. *Energy & Environmental Science*. 2013;6:1891–1900.

[33] Yehezkeli O., Wilner O.I., Tel-Vered R., Roizman-Sade D., Nechushtai R., Willner I. generation of photocurrents by bis-aniline-cross-linked Pt nanoparticle/photosystem I composites on electrodes. *Journal of Physical Chemistry B*. 2010;114:14383-14388.

[34] Rao K.K., Hall D.O., Vlachopoulos N., Grätzel M., Evans M.C.W., Seibert M. Photoelectrochemical responses of photosystem II particles immobilized on dye-derivatized TiO_2 films. *Journal of Photochemistry and Photobiology B: Biology*. 1990;5:379-389.

[35] Efrati A., Tel-Vered R., Michaeli D., Nechushtai R., Willner I. Cytochrome c-coupled photosystem I and photosystem II (PSI/PSII) photo-bioelectrochemical cells. *Energy & Environmental Science*. 2013;6:2950-2956.

[36] Kothe T., Plumeré N., Badura A., Nowaczyk M.M., Guschin D.A., Rögner M., Schuhmann W. Combination of a photosystem 1-based photocathode and a photosystem 2-based photoanode to a Z-scheme mimic for biophotovoltaic applications. *Angewandte Chemie International Edition*. 2013;52:14233-14236.

[37] Yehezkeli O., Tel-Vered R., Wasserman J., Trifonov A., Michaeli D., Nechushtai R., Willner I. Integrated photosystem II-based photo-bioelectrochemical cells. *Nature Communications*. 2012;742(3):1-7. DOI: 10.1038/ncomms1741.

[38] Badura A., Guschin D., Esper B., Kothe T., Neugebauer S., Schuhmann W., Rogner M. Photo-induced electron transfer between photosystem II via crosslinked redox hydrogels. *Electroanalysis*. 2008;20:1043-1047.

[39] Badura A., Guschin D., Kothe T., Kopczak M.J., Schuhmann W., Rogner M. Photocurrent generation by photosystem 1 integrated in crosslinked redox hydrogels. *Energy & Environmental Science*. 2011;4:2435-2440.

[40] Carpentier R., Lemieux S., Mimeault M., Purcell M., Goetze D.C. A photoelectrochemical cell using immobilized photosynthetic membranes. *Bioelectrochemistry and Bioenergetics*. 1999;22:391-401.

[41] Bedford N.M., Winget G.D., Punnamaraju S., Steckl A.J. Immobilization of stable thylakoid vesicles in conductive nanofibers by electrospinning. *Biomacromolecules*. 2011;12:778-784.

[42] Fourmond V., Lagoutte B., Setif P., Leibl W., Demaille C. Electrochemical study of a reconstituted photosynthetic electron-transfer chain. *Journal of the American Chemical Society*. 2007;129:9201-9209.

[43] Frolov L., Rosenwaks Y., Carmeli C., Carmeli I. Fabrication of a photoelectronic device by direct chemical binding of the photosynthetic reaction center protein to metal surfaces. *Advanced Materials*. 2005;17:2434–2437. DOI: 10.1002/adma.200500295.

[44] Faulkner C.J., Lees S., Ciesielski P.N., Cliffel D.E., Jennings G.K. Rapid assembly of photosystem I monolayers on gold electrodes. *Langmuir*. 2008;24:8409-8412.

[45] Frolov L., Wilner O., Carmeli C., Carmeli I. Fabrication of oriented multilayers of photosystem I proteins on solid surfaces by auto-metallization. *Advanced Materials*. 2008;20:263–266.

[46] Ciesielski P.N., Hijazi F.M., Scott A.M., Faulkner C.J., Beard L., Emmett K., Rosenthal S.J., Cliffel D., Jennings G.K. Photosystem I – Based biohybrid photoelectrochemical cells. *Bioresource Technology*. 2010;101:3047-3053.

[47] Mershin A., Matsumoto K., Kaiser L., Yu D.Y., Vaughn M., Nazeeruddin M.K., Bruce B.D., Graetzel M., Zhang S.G. Self-assembled photosystem-I biophotovoltaics on nanostructured TiO_2 and ZnO. *Scientific Reports*. 2012;234(2}):1-7. DOI: 10.1038/srep00234.

[48] Ulas G., Brudvig G.W. Redirecting electron transfer in photosystem II from water to redox-active metal complexes. *Journal of the American Chemical Society*. 2011;133:13260–13263.

[49] Vittadello M., Gorbunov M.Y., Mastrogiovanni D.T., Wielunski L.S., Garfunkel E.L., Guerrero F., Kirilovsky D., Sugiura M., Rutherford A.W., Safari A., Falkowski P.G. Photoelectron generation by photosystem II core complexes tethered to gold surfaces. *ChemSusChem*. 2010;3:471-475.

[50] Noji T., Suzuki H., Gotoh T., Iwai M., Ikeuchi M., Tomo T., Noguchi T. Photosystem II - Gold nanoparticle conjugate as a nanodevice for the development of artificial light-driven water-splitting systems. *Journal of Physical Chemistry Letters*. 2011;2:2448-2452.

[51] Yagishita T., Horigome T., Tanaka K. Effects of light, CO2 and inhibitors on the current output of biofuel cells containing the photosynthetic organism *Synechococcus sp*. *Journal of Chemical Technology and Biotechnology*. 1993;56:393-399.

[52] Torimura M., Miki A., Wadano A., Kano K., Ikeda T. Electrochemical investigation of cyanobacteria *Synechococcus sp*. PCC7942-catalyzed photoreduction of exogenous quinones and photoelectrochemical oxidation of water. *Journal of Electroanalytical Chemistry*. 2001;496:21-28.

[53] Pisciotta J.M., Zou Y., Baskakov I.V. Light-dependent electrogenic activity of cyanobacteria. *PLoS ONE*. 2010;5:1-10. DOI: 10.1371/journal.pone.0010821.

[54] Sekar N., Umasankar Y., Ramasamy R.P. Photocurrent generation by immobilized cyanobacteria via direct electron transport in photo-bioelectrochemical cells. *Physical Chemistry Chemical Physics*. 2014;16(17):7862-7871.

[55] Larom S., Salama F., Schuster G., Adir N. Engineering of an alternative electron transfer path in photosystem II. *Proceedings of the National Academy of Sciences of the United States of America*. 2010;107:9650-9655.

[56] Fultz M.L., Durst R.A. Mediator compounds for the electrochemical study of biological redox systems – A compilation. *Analytica Chimica Acta*. 1982;140:1-18.

[57] Hanna M.C., Nozik A.J. Solar conversion efficiency of photovoltaic and photoelectrolysis cells with carrier multiplication absorbers. *Journal of Applied Physics*. 2006;100:1-8.

[58] Sanders J.K.M., editors. *Porphyrin Handbook*. New York: Academic Press; 2000.

[59] Iengo E., Zangrando E., Alessio E. Discrete supramolecular assemblies of porphyrins mediated by coordination compounds. *European Journal of Inorganic Chemistry*. 2003;2003:2371–2384.

[60] Krassen H., Ott S., Heberle J. In vitro hydrogen production – Using energy from the sun. *Physical Chemistry Chemical Physics*. 2011;13:47-57.

[61] Fujishima A., Honda K. Electrochemical photolysis of water at a semiconductor electrode. *Nature*. 1972;238:37-38.

[62] Goldsmith J.O., Boxer S.G. Rapid isolation of bacterial photosynthetic reaction centers with an engineered poly-histidine tag. *Biochimica et Biophysica Acta*. 1996;1276:171–175.

[63] Kincaid H.A., Niedringhaus T., Ciobanu M., Cliffel D.E., Jennings G.K. Entrapment of photosystem I within self-assembled films. *Langmuir*. 2006;22:8114-8120.

[64] Nakamura C., Hasegawa M., Yasuda Y., Miyake J. Self-assembling photosynthetic reaction centers on electrodes for current generation. *Biotechnology and Applied Biochemistry*. 2000;84(6):401-408.

[65] Meunier C.F., Van Cutsem P., Kwon Y.U., Su B.L. Thylakoids entrapped within porous silica gel: Towards living matter able to convert energy. *Journal of Materials Chemistry*. 2009;19:1535-1542.

[66] Furukawa Y., Moriuchi T., Morishima K. Design principle and prototyping of a direct photosynthetic/metabolic biofuel cell (DPMFC). *Journal of Micromechanics and Microengineering*. 2006;16:220–225.

[67] Allakhverdiev S.I., Tomo T., Shimada Y., Kindo H., Nagao R., Klimov V.V., Mimuro M. Redox potential of pheophytin a in photosystem II of two cyanobacteria having the different special pair chlorophylls. *Proceedings of the National Academy of Sciences of the United States of America*. 2010;107:3924-3929.

[68] Chen M., Schliep M., Willows R.D., Cai Z.-L., Neilan B.A., Scheer H. A red-shifted chlorophyll. *Science*. 2010;329:1318-1319.

[69] Chen M., Scheer H. Extending the limit of natural photosynthesis and implications of technical light harvesting. *Journal of Porphyrins and Phthalocyanines*. 2013;17:1-15.

[70] Tomo T., Allakhverdiev S.I., Mimuro M. Constitution and energetics of photosystem I and photosystem II in the chlorophyll d-dominated cyanobacterium Acaryochloris marina. *Journal of Photochemistry and Photobiology B: Biology*. 2011; 104:333-340.

[71] Hou H.J.M., Allakhverdiev S.I., Najafpour M.M., Govindjee. Current challenges in photosynthesis: From natural to artificial. *Frontiers Publishers*. 2014;5:1-3.

[72] Allakhverdiev S.I., Ramakrishna S. A random walk to and through the photoelectrochemical cells based on photosynthetic systems. *Biofuel Research Journal*. 2015;6:222.

[73] Marshall J. Solar energy: Springtime for the artificial leaf. *Nature*. 2014;510:22-24.

Chapter 10

Visible Light-Driven Water Oxidation Catalyzed by Ruthenium Complexes

Markus D. Kärkäs, Tanja M. Laine,
Eric V. Johnston and Björn Åkermark

Additional information is available at the end of the chapter

http://dx.doi.org/10.5772/62272

Abstract

A shift in energy dependence from fossil fuels to sustainable and carbon-neutral alternatives is a daunting challenge that faces the human society. Light harvesting for the production of solar fuels has been extensively investigated as an attractive approach to clean and abundant energy. An essential component in solar energy conversion schemes is a catalyst for water oxidation. Ruthenium-based catalysts have received significant attention due to their ability to efficiently mediate the oxidation of water. In this context, the design of robust catalysts capable of driving water oxidation at low overpotential is a key challenge for realizing efficient visible light-driven water splitting. Herein, recent progress in the development within this field is presented with a focus on homogeneous ruthenium-based systems and surface-immobilized ruthenium assemblies for photo-induced oxidation of water.

Keywords: water splitting, ruthenium, photochemistry, sustainable chemistry

1. Introduction

The search for inexpensive and renewable energy is currently one of society's greatest technological challenges. As light energy from the sun continuously strikes the earth's surface, harnessing this energy would solve the increasing future energy demand and lead to a more sustainable society. An appealing solution would therefore be to convert light energy to storable fuels, such as hydrogen gas or reduced carbon compounds. For realizing this scenario, novel technologies have to be developed that efficiently utilize solar energy. Furthermore, such systems also need to rely on abundant and inexpensive feedstocks in order to become viable on a large

scale. As water is plentiful, it would be attractive to use it as a feedstock for obtaining the necessary reducing equivalents—protons and electrons [1–6].

The natural system constitutes an excellent source of inspiration for how to design an artificial system that is capable of harnessing solar energy for fuel production. The concept of artificial photosynthesis emerged in the 1970s and is inspired by nature where light-induced charge separation events sequentially oxidize a Mn_4Ca cluster (Figure 1) known as the oxygen-evolving complex (OEC) [7, 8]. After four electrons have been abstracted from the OEC, two molecules of water are oxidized to molecular oxygen, thus releasing four electrons and four protons. The natural photosynthetic apparatus subsequently utilizes the generated reducing equivalents to reduce CO_2 to carbohydrates [9, 10]. However, instead of using the generated reducing equivalents to reduce CO_2 to carbohydrates as in the natural photosynthetic apparatus, these "artificial leafs" would produce hydrogen gas from the protons and electrons that are liberated when water is oxidized (Eq. 1) [11, 12].

$$2H_2O \rightarrow O_2 + 2H_2 \tag{1}$$

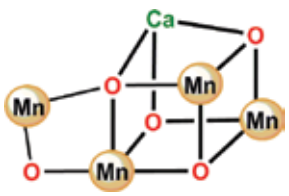

Figure 1. Depiction of the Mn_4Ca cubane core of the oxygen-evolving complex (OEC).

Water splitting can be divided into two half-reactions; proton reduction and water oxidation. The reductive side of water splitting involves the generation of hydrogen gas from the generated protons and electrons. In contrast to hydrocarbons, hydrogen gas is considered to be environmentally benign, as water is the only combustion product. Although deceptively simple, the other half-reaction, water oxidation (Eq. 2), is a mechanistically complex process and is currently considered as the bottleneck. The oxidation of water thus requires a single catalytic entity capable of accumulating four oxidizing equivalents, breaking several bonds and forming the crucial O–O bond. Splitting of water is an energy demanding process with a Gibbs free energy of 237.18 kJ mol^{-1} and a minimum electrochemical potential of 1.229 V vs. normal hydrogen electrode (NHE) is required. The basic thermodynamic requirements for splitting water suggest that any light with a wavelength shorter than 1 mm has enough energy to split a molecule of water. Consequently, this allows the use of the entire visible solar spectrum and a majority of the near-infrared spectrum, which collectively constitutes ~80% of the total solar irradiance [13].

$$2H_2O \rightarrow O_2 + 4H^+ + 4e^- \tag{2}$$

http://dx.doi.org/10.5772/62272

The first example of photoelectrochemical water splitting was reported by Fujishima and Honda in the early 1970s. Their system consisted of a titanium dioxide (TiO_2) photoanode which upon irradiation with ultraviolet (UV) light generated oxygen at the anode and hydrogen gas at an unilluminated platinum cathode [14]. Since the seminal work by Fujishima and Honda, several research groups have attempted to improve the system in order to enable the reaction to be driven by visible light instead of UV light [15, 16].

A simple depiction of an artificial photosynthetic system is shown in Figure 2 and consists of three components: a chromophore (photosensitizer) for light-absorption, a water oxidation catalyst (WOC), and a reduction catalyst for proton reduction. The light-absorbing component, the molecular chromophore, is in general coordinated to the surface of a semiconductor, such as TiO_2. The initial step in such a system involves light absorption by the photosensitizer, generating a long-lived charge-separated state by transferring an electron to the conduction band of the semiconductor. The oxidized photosensitizer subsequently recovers an electron from the covalently bound oxidation catalyst (the WOC) or from the functionalized semiconductor surface to regenerate the ground state photosensitizer. After four successive electron transfers, the highly oxidized WOC is reduced by oxidizing two molecules of water, thus releasing molecular oxygen. Although the events seem trivial, the overall process of light-driven water splitting requires interfacing of several nontrivial chemical steps such as accumulation and abstraction of several electrons at the reduction and oxidation catalyst, respectively. This requires the integration of efficient light absorption, generation of long-lived charge separation, organized proton reduction at the cathode, and fast oxidation of water at the anode [17–19].

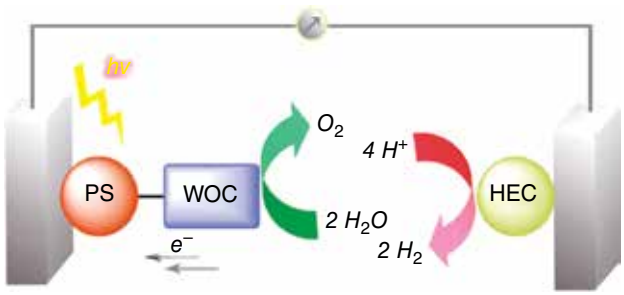

Figure 2. Three-component molecular assembly for water splitting consisting of a photosensitizer (PS), a water oxidation catalyst (WOC), and a hydrogen-evolving catalyst (HEC). Reprinted with permission from ref. 29. Copyright 2014 American Chemical Society.

2. Ruthenium-Based Photosensitizers

The first step in solar energy conversion schemes involves light absorption by a chromophore. In the natural photosynthetic system, a set of specialized chlorophyll-based pigments is responsible for the absorption of visible light, and subsequently transfers the excitation energy

to the reaction centers of photosystem II and I. Mimicking these events for constructing artificial photosynthetic devices is a crucial objective and requires tailored photosensitizers that are photostable and efficiently absorb photons across a wide range of wavelengths in the visible spectral region. Furthermore, they should also be easy to modify to allow for straightforward tuning of the photophysical features. The main requirement is that the reduction potential of the oxidized photosensitizer is more positive than that of the WOC and the onset potential for water oxidation (and any overpotential that is produced in the designed system) [20, 21].

2.1. Photophysical Description of Ruthenium-Type Photosensitizers

Perhaps the most extensively studied metal-based photosensitizers are the $[Ru(bpy)_3]^{2+}$-type complexes (Figure 3; bpy = 2,2′-bipyridine). Shortly after the seminal report on UV-light-mediated water splitting at TiO_2 photoanodes by Honda and Fujishima [14], the basis for artificial photosynthesis appeared when it was realized that metal complexes, such as $[Ru(bpy)_3]^{2+}$ (**1**), are efficiently quenched by organic compounds [22, 23]. Flash photolysis experiments have revealed that light absorption ($\lambda_{max} \approx 450$ nm) by the $[Ru(bpy)_3]^{2+}$-type photosensitizers triggers excitation of an electron in a metal-centered orbital to a π^* orbital located on the ancillary polypyridyl ligand. This metal-to-ligand charge transfer (MLCT) results in a singlet excited state, $^1[Ru(bpy)_3]^{2+*}$, that undergoes rapid intersystem crossing (ISC), affording a triplet state, $^3[Ru(bpy)_3]^{2+*}$. This excited state is relatively long lived and has a dual nature, being that it can participate in either a single-electron oxidation or a single-electron reduction in the presence of an acceptor or a donor, respectively (Figure 4). The $[Ru(bpy)_3]^{2+}$-type photosensitizers possess several desirable features: 1) photostability, 2) the produced excited state has a sufficient lifetime for it to participate in chemical reactions, 3) they exhibit compatibility with a wide pH range, 4) they display broad absorption of visible light, and 5) the relative ease by which the photophysical properties of the ruthenium photosensitizers can be tuned, allowing e.g. that the absorption of light can be extended from the near infrared to the UV region by simply modifying the ancillary ligands (see Figure 3) [24–26].

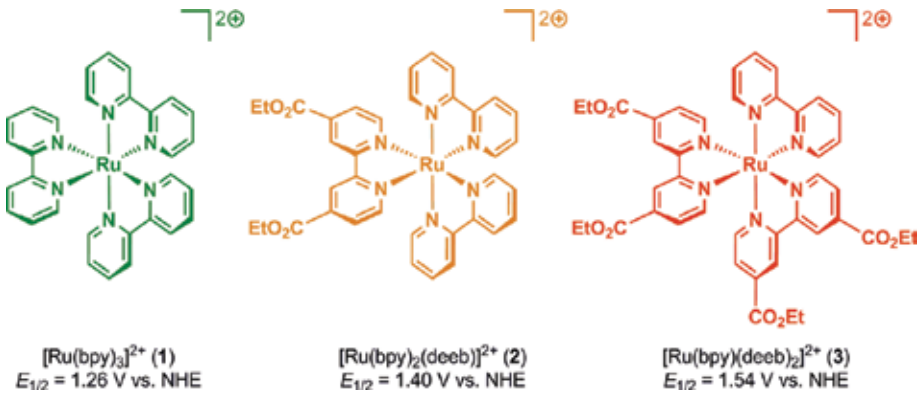

Figure 3. Examples of $[Ru(bpy_3)]^{2+}$-type photosensitizers.

http://dx.doi.org/10.5772/62272

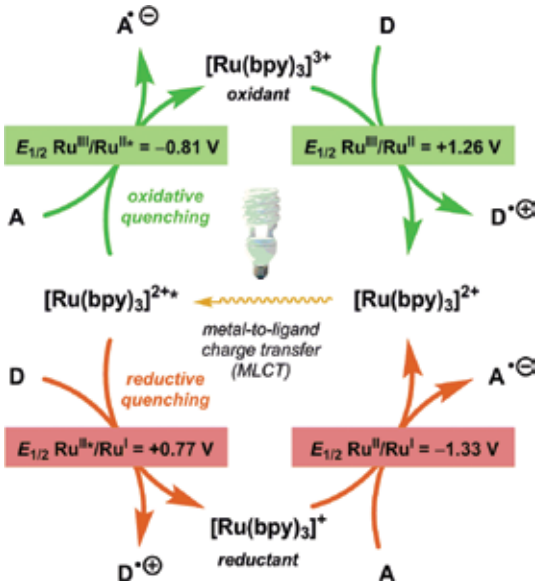

Figure 4. Photophysical properties of the $[Ru(bpy)_3]^{2+}$ complex (**1**).

2.2. Evaluating Light-Driven Water Oxidation with Ruthenium Complexes

A three-component system is typically employed for evaluating light-driven water oxidation and consists of a photosensitizer, a water oxidation catalyst, and a sacrificial electron acceptor (Figure 5). As the sacrificial electron acceptor, sodium persulfate is usually employed since the recombination or reversed electron transfer can be ruled out, thereby simplifying the kinetic analysis of subsequent steps in the catalytic process. The three-component light-driven system using the persulfate anion ($S_2O_8^{2-}$) and a metal-based photosensitizer has been well documented and is believed to commence with oxidative quenching of the excited state of the photosensitizer, such as $[Ru(bpy)_3]^{2+*}$. This results in the generation of $[Ru(bpy)_3]^{3+}$, sulfate, and a sulfate radical ($SO_4^{-\bullet}$), which is a strong oxidant ($E° > 2.40$ V vs. NHE[27]) and has the ability to directly oxidize a second equivalent of $[Ru(bpy)_3]^{2+}$ [28]. The reduction of two equivalents affords the four equivalents of $[Ru(bpy)_3]^{3+}$ that are needed to oxidize the WOC, which in turn oxidizes water to molecular oxygen. The processes involved in the light-driven persulfate system are summarized by Eqs. 3–6.

Figure 5. Three-component system for light-driven water oxidation consisting of a water oxidation catalyst, a $[Ru(bpy)_3]^{2+}$-type photosensitizer and persulfate as the sacrificial electron acceptor.

$$2\left[\mathrm{Ru(bpy)_3}\right]^{2+} + 2h\nu \rightarrow 2\left[\mathrm{Ru(bpy)_3}\right]^{2+*} \quad (3)$$

$$2\left[\mathrm{Ru(bpy)_3}\right]^{2+*} + 2\mathrm{S_2O_8^{2-}} \rightarrow 2\left[\mathrm{Ru(bpy)_3}\right]^{3+} + 2\mathrm{SO_4^{2-}} + 2\mathrm{SO_4^{-}} \quad (4)$$

$$2\left[\mathrm{Ru(bpy)_3}\right]^{2+} + 2\mathrm{SO_4^{-}} \rightarrow 2\left[\mathrm{Ru(bpy)_3}\right]^{3+} + 2\mathrm{SO_4^{2-}} \quad (5)$$

$$4\left[\mathrm{Ru(bpy)_3}\right]^{2+} + 2\mathrm{S_2O_8^{2-}} + 2h\nu \rightarrow 4\left[\mathrm{Ru(bpy)_3}\right]^{3+} + 4\,\mathrm{SO_4^{2-}} \quad (6)$$

3. Ruthenium-Based Water Oxidation Catalysts—Oxidatively Robust Catalytic Entities

One of the main challenges in realizing water splitting is the development of efficient and robust WOCs that possess low overpotentials and high turnover rates. The development of homogeneous WOCs is an intense and rapidly expanding research field. During the past decade, considerable progress in constructing molecular catalysts capable of oxidizing water has been made using transition metal-based catalysts in the presence of strong chemical oxidants, such as Ce^{IV} [29, 30]. Homogeneous catalysts are advantageous as they facilitate mechanistic studies, thus stimulating the design of new and improved WOCs [31]. Owing to their high abundance and low toxicity, several WOCs based on first-row transition metals, such as cobalt (Figure 6) [32–35], copper (Figure 7) [36–38], iron (Figure 8) [39–42], and manganese (Figure 9) [43–47], have been designed. However, their design has proven particularly challenging as these WOCs suffer from insufficient stability and are rapidly deactivated/decomposed under the harsh conditions required to oxidize water. In contrast, catalysts based on the third-row transition metal ruthenium have shown to produce robust catalysts that are able to deliver high turnover numbers (TONs) and high turnover frequencies (TOFs) [29, 30]. This chapter summarizes the recent advances that have been made in designing ruthenium-based WOCs for visible light-driven water oxidation.

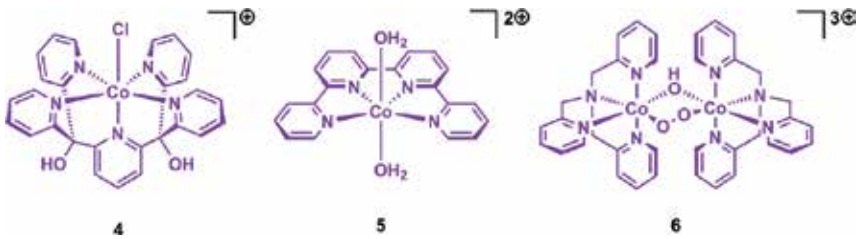

Figure 6. Examples of cobalt-based water oxidation catalysts.

http://dx.doi.org/10.5772/62272

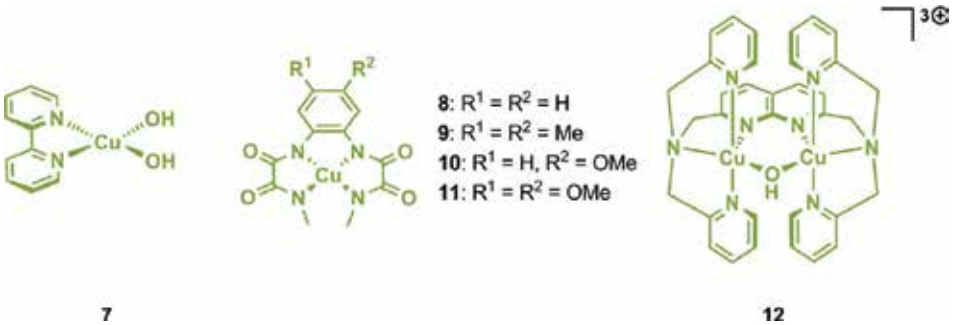

Figure 7. Examples of copper-based water oxidation catalysts.

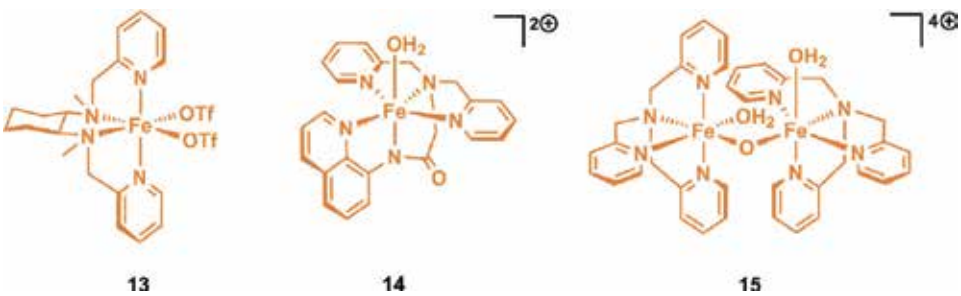

Figure 8. Examples of iron-based water oxidation catalysts.

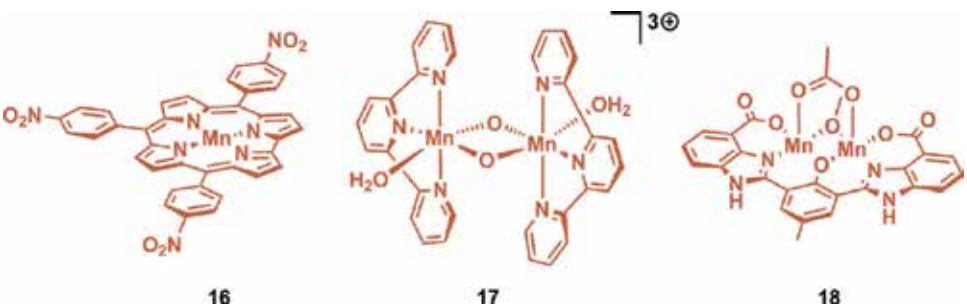

Figure 9. Examples of manganese-based water oxidation catalysts.

3.1. Dinuclear Ruthenium Complexes Capable of Mediating Light-Driven Water Oxidation

Intensive attempts to develop efficient WOCs have been made since the first homogeneous ruthenium catalyst, the "blue dimer" (**19**, Figure 10), was presented by Meyer and coworkers in the early 1980s [48, 49]. Light-driven water oxidation by a mononuclear "blue dimer", *cis*-$[(bpy)_2Ru(OH_2)_2]^{2+}$, derivative which presumably resulted in the formation of the dinuclear derivative **20** (Figure 10), was reported in 1987 [50]. In addition to the coordinated aqua ligands,

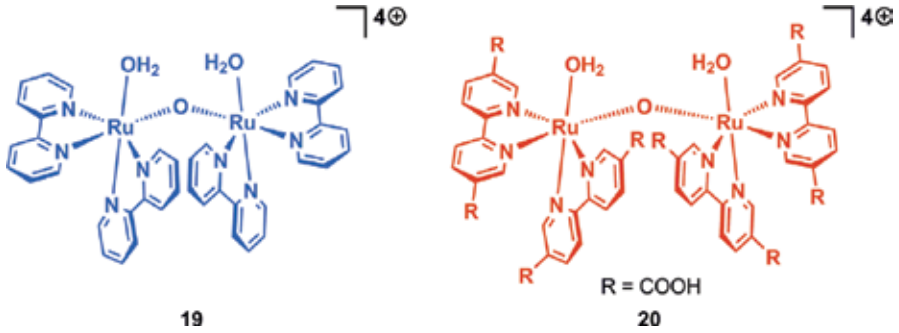

19 20

Figure 10. Depiction of the "blue dimer" (**19**) and dinuclear ruthenium complex **20**.

this ruthenium-aqua complex consisted of two ruthenium metal centers connected via a μ-oxo bridge and two carboxylate substituted bpy ligands. Cyclic voltammetry displayed a reversible wave at ~1.20 V vs. NHE, assigned to the $Ru_2^{III,IV}/Ru_2^{III,III}$ redox couple and a catalytic onset for water oxidation at approximately 1.54 V vs. NHE. When using $[Ru(deeb)_3]^{2+}$ as the photosensitizer and sodium persulfate as the sacrificial electron acceptor, molecular oxygen was evolved at a rate of 330 μL h^{-1} during the first 15 min, after which the oxygen production dropped.

The groups of Sun and Åkermark designed a dinuclear ruthenium complex (**21**, Figure 11) where the two ruthenium centers were positioned in an *anti*-fashion about a central pyridazine moiety [51]. In addition to the central pyridazine unit, the ligand scaffold contained two pyridine groups with negatively charged carboxylate groups, which have been shown to lower the redox potentials of metal complexes and stabilize high-valent redox states. The electrochemical properties of the complex were studied by cyclic voltammetry in dry acetonitrile and showed two reversible one-electron waves at ~0.54 and ~1.04 V vs. NHE, which were assigned as the $Ru_2^{II,III}/Ru_2^{II,II}$ and $Ru_2^{III,III}/Ru_2^{II,III}$ redox couples. At pH 7, a catalytic current for water oxidation was observed at ~1.45 V vs. NHE.

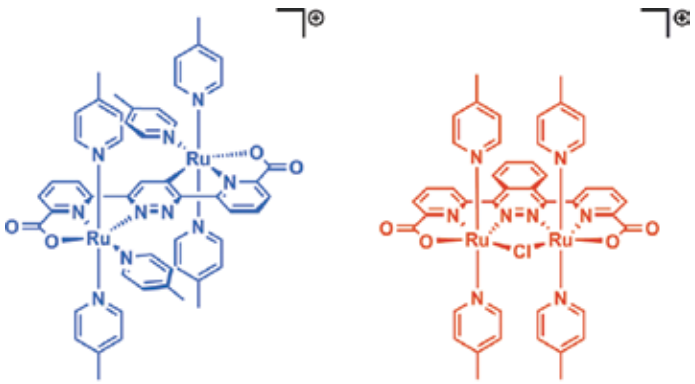

21 22

http://dx.doi.org/10.5772/62272

Figure 11. Structures of the dinuclear ruthenium complexes **21** and **22**.

Three different $[Ru(bpy)_3]^{2+}$-type photosensitizer derivatives were employed for visible light-driven water oxidation [52]. It could be shown that the TONs and TOFs increased with the increasing potential of the photosensitizer, which is ascribed to the stronger driving force. When employing the $[Ru(bpy)(deeb)_2]^{2+}$ photosensitizer, a TON of 370 and a TOF of 0.26 s^{-1} was obtained for ruthenium complex **21**. During the catalytic process, the pH was found to drop significantly and had to be adjusted. However, this allowed for a total TON of 1270 after four consecutive runs. Unfortunately, using a more concentrated buffer solution (0.2 M) resulted in deactivation of the catalytic system. In the presence of catalyst **21,** minimal decomposition of the photosensitizers was observed upon illumination, whereas in the absence of catalyst **21,** significant decomposition of the photosensitizers was observed, indicating efficient electron transfer from the catalyst unit to the oxidized photosensitizer.

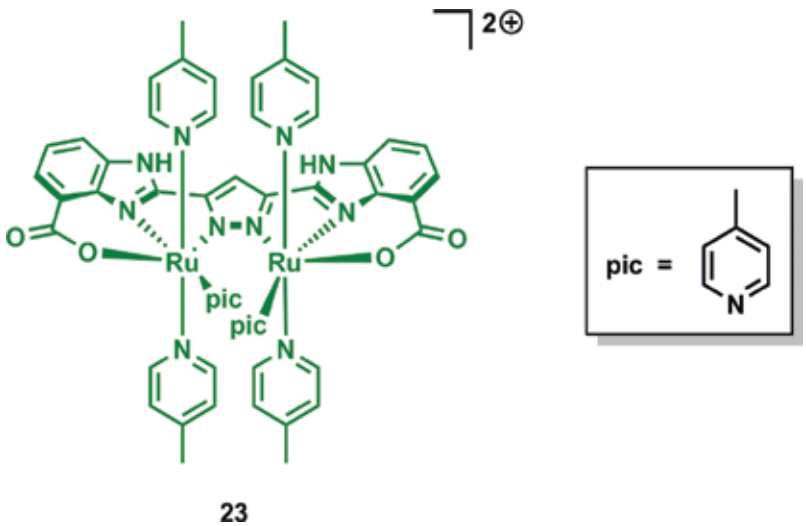

23

Figure 12. Structure of dinuclear ruthenium complex **23**.

Subsequent studies by the group of Sun and Åkermark focused on the dinuclear ruthenium complex **22**, which adopts a *cis* structure with phtalazine as the bridging unit (Figure 11) [53]. The electrochemical properties of the complex were studied by cyclic voltammetry in dry acetonitrile and exhibited two one-electron waves at 0.903 and 1.396 V vs. NHE. These were assigned to the redox processes $Ru_2^{II,III}/Ru_2^{II,II}$ and $Ru_2^{III,III}/Ru_2^{II,III}$, respectively. Despite the fact that the two ruthenium centers were oriented in a *cis* fashion, the redox potentials were higher than for ruthenium complex **21**, probably due to the strong electron donation from the aryl carbon bond to one of the ruthenium centers in complex **21**. The catalytic current for water oxidation for complex **22** takes place at onset potential of approximately 1.20 V vs. NHE in phosphate buffer at pH 7.2, which is lower than for complex **21**. TONs of 60, 420, 580, and TOFs of 0.1, 0.77, and 0.83 s^{-1} were obtained for the three photosensitizers **1–3**, respectively. Ruthenium complex **22** was shown to retain its catalytic activity upon the addition of photosensitizer

and sodium persulfate, and after the neutralization of pH, highlighting the stability of ruthenium complex **22** in the studied photochemical system.

A dinuclear ruthenium complex (**23**) for visible light-driven water oxidation was recently reported by the Åkermark group (Figure 12) [54]. Based on previous studies where a phenolate-based bridging ligand was utilized [55], it was envisioned that a ligand backbone consisting of a central pyrazole moiety would allow for the accommodation of two ruthenium centers. Employing an ancillary ligand scaffold consisting of a central pyrazole moiety and two benzimidazole units functionalized with carboxylate groups produced the dinuclear ruthenium complex **23** where the two metal centers are held in close proximity [54].

Several redox active species were observed in the electrochemical studies in phosphate buffer at pH 7.2. Oxidation peaks at potentials of approximately 0.05, 0.38, 0.70, 0.90, and 1.20 V vs. NHE were observed, with a catalytic current for water oxidation appeared at an onset potential of 1.20 V vs. NHE. The photochemical oxidation of water was initially carried out at pH 7.2, using $[Ru(bpy)_2(deeb)]^{2+}$ as photosensitizer. At a 3.0 μM catalyst concentration, the amount of evolved oxygen corresponded to a TON of 830. Lowering the pH led to a slight increase of the TON (890); however, a further decrease of the pH to 5.2 resulted in a substantial reduction in oxygen production, presumably due to the lower driving force. An increase of the pH to 8.2 also resulted in a significantly lower oxygen formation and was ascribed to the decomposition of the ruthenium-based photosensitizer [54]. A subsequent study has suggested that the designed ligand scaffold in dinuclear ruthenium complex **23** has a non-innocent behavior, in which the metal–ligand cooperation is an important feature during the four-electron oxidation of water and thus explains the observed catalytic efficiency of complex **23** [56].

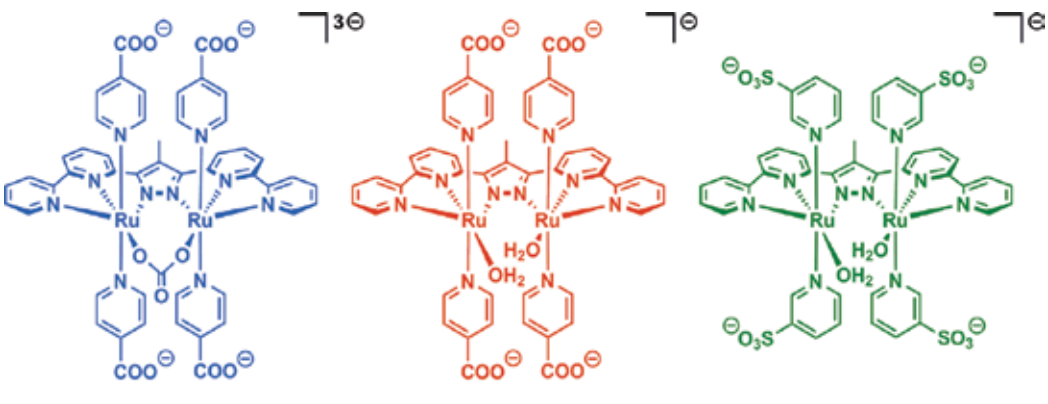

Figure 13. Dinuclear ruthenium complexes **24–26**.

Llobet and coworkers reported a pyrazolate bpy-based dinuclear ruthenium complex **24** (Figure 13) [57]. The complex accommodates two ruthenium centers in a slightly distorted octahedral conformation. The metal ions are closely located within the pyrazole plane with a twisted carbonate bridging the two metals. The twisted conformation facilitates the exchange

http://dx.doi.org/10.5772/62272

of the carbonate with two water molecules in aqueous media, resulting in the formation of catalyst **25**. Electrochemical studies of complex **25** were conducted in phosphate buffer at pH 7. Two quasi-reversible redox processes at 0.59 and 0.88 V vs. NHE and the catalytic onset potential for water oxidation at 1.48 V vs. NHE could be observed, employing cyclic voltammetry.

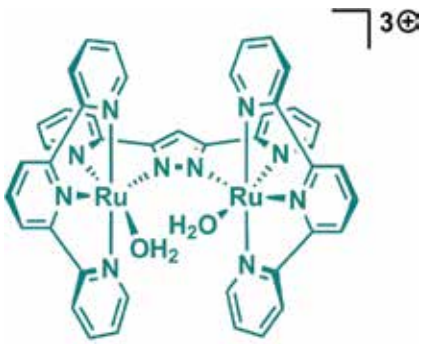

27

Figure 14. Depiction of the previously developed dinuclear ruthenium–pyrazole complex **27**.

The catalytic activity for light-driven water oxidation was measured at pH 7, using the $[Ru(bpy)(deeb)_2]^{2+}$ photosensitizer (**3**) together with sodium persulfate as the sacrificial electron acceptor. Sulfonate-based complex **26** gave rise to a TON of 2373 and a TOF of 11.1 s^{-1} in a single run. The experiments were repeated twice, resulting in a total TON of 5300. Complex **25** exhibited similar activity, producing a TON of >2300 and a TOF of 9.2 s^{-1}. The quantum yield (amount of molecular oxygen produced per absorbed photon) for complex **25**, under the above-mentioned conditions, reached 4.8% during 100 s of irradiation. The ligand design thus permits formation of a water soluble and oxidatively stable ruthenium complex, where the active catalyst reaches high TONs and TOFs for visible light-driven water oxidation [57].

The activity of **25** and **26** was compared with the previously reported complex **27** [58, 59] (Figure 14) under the exact same conditions, which further revealed the dramatic catalytic difference as catalyst **27** only yielded a TON of 67 and a TOF of 0.13 s^{-1}. An explanation for the lower activity of ruthenium complex **27** was assumed to be the high onset potential for water oxidation, occurring at 1.60 V vs. NHE, which is close to the redox potential provided by the $[Ru(bpy)(deeb)_2]^{2+}$ photosensitizer [57].

The catalytic efficiencies for the developed ruthenium-based complexes housing carboxylate-functionalized ligands and related complexes containing negatively charged ligand backbones highlight the robustness of these WOCs and suggest that such catalysts can be further heterogenized and applied onto photoanodes, which constitute an important part for the fabrication of devices for artificial photosynthesis.

3.2. Light-Driven Water Oxidation Catalyzed by Single-Site Ruthenium Complexes

Thummel and coworkers demonstrated that the ruthenium(II) polypyridyl complex **28** (Figure 15) was a viable catalyst for visible light-induced water oxidation [60]. The examination of the catalytic activity was carried out in a three-component homogeneous system containing $[Ru(bpy)_3]^{2+}$ (**1**) as photosensitizer, persulfate as a sacrificial electron acceptor, and catalyst **28**. Under these conditions, complex **28** provided a TON of 103, a TOF of 0.12 s^{-1}, and a quantum yield of 9%. Mechanistic studies suggested that a unique proton-coupled low-energy pathway via a ruthenium(IV)-oxo intermediate takes place when using the mild photogenerated oxidant $[Ru(bpy)_3]^{3+}$ (1.26 V vs. NHE) to drive water oxidation [60, 61].

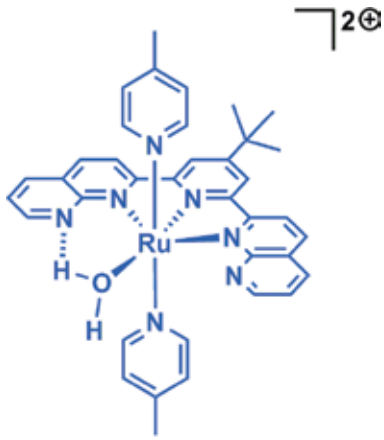

28

Figure 15. Structure of ruthenium(II) polypyridyl complex **28**.

Although a plethora of single-site ruthenium-based WOCs have been designed, only a handful has been shown to catalyze light-driven water oxidation. A majority of the ruthenium complexes that have been successful in driving water oxidation with visible light contain negatively charged ligand scaffolds, which are essential for lowering the redox potentials, allowing water oxidation to be driven by $[Ru(bpy)_3]^{2+}$-type photosensitizers.

The $[Ru(bda)(pic)_2(OH_2)]$ complex (**29**, Figure 16; bda = 2,2′-bipyridine-6,6′-dicarboxylic acid) is a rare example of a ruthenium complex containing a seven-coordinated ruthenium center [62]. The complex displays relatively low redox potentials, which makes it compatible with $[Ru(bpy)_3]^{2+}$-type photosensitizers. By using a three-component system consisting of ruthenium catalyst **29**, a $[Ru(bpy)_3]^{2+}$-type photosensitizer and sodium persulfate or $[Co(NH_3)_5Cl]Cl_2$ as sacrificial electron acceptors, molecular oxygen was generated [63, 64]. It was found that the catalytic system was rapidly deactivated due to the pH-dependent properties of ruthenium complex **29**. During the catalytic process, a rapid decrease of the pH of the reaction solution is observed, which affects the redox properties of catalyst **29** and decreases the catalytic activity. The authors found that adjusting the pH to 7.1 allowed for continued evolution of molecular

http://dx.doi.org/10.5772/62272

oxygen, highlighting that the observed fast deactivation is a result of the rapidly decreasing pH. The oxidative degradation of ruthenium complex **29** was also observed in both solution and the solid state under aerobic conditions. It could be established that complex **29** gradually decomposed via oxidative degradation of the axial picoline ligands, resulting in C(sp^3)–H bond-oxidized ruthenium species.

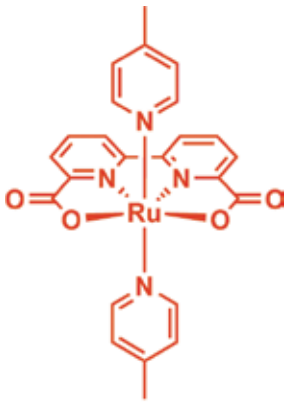

29

Figure 16. Structure of the [Ru(bda)$(pic)_2(OH_2)$] complex **29**.

The two structurally related ruthenium complexes **30** and **31** based on the tridentate 2,6-pyridinedicarboxylic acid ligand have also been studied for visible light-driven water oxidation (Figure 17) [65]. Despite their high structural resemblance, the two ruthenium complexes displayed significant difference in the activity in photochemical water oxidation. Using the $[Ru(bpy)_2(deeb)]^{2+}$ (**2**)/$S_2O_8^{2-}$ system, catalyst **30** triggered immediate oxygen evolution, producing a TON of 62 after 1 h of illumination. A linear dependence of the initial rate on complex **30** was observed using Ce^{IV} as chemical oxidant, implying that the catalyst most likely follows a mechanism involving the generation of a high-valent ruthenium-oxo species. Subsequent water nucleophilic attack on this species produces the key O–O bond, where additional oxidation events of the formed ruthenium-peroxo result in the liberation of molecular oxygen. In contrast to ruthenium complex **30**, complex **31** only generated a TON of 3.7, highlighting the dramatic difference in reactivity for the two ruthenium complexes. This difference was ascribed to the relative ease by which the complexes undergo picoline water ligand exchange, which was supported by mechanistic studies utilizing electrochemistry and ^{1}H NMR spectroscopy. In complex **30**, the equatorially bound picoline is rapidly replaced by a solvent water molecule, thus producing the catalytically important ruthenium-aqua species. By contrast, the ruthenium complex **31**, where bpy occupies the equatorial position, no such exchange was observed. These observations highlight that subtle changes in the ancillary ligand environments can dramatically affect the catalytic efficiencies of the studied ruthenium catalysts and are fundamental for designing WOCs with improved catalytic efficiencies.

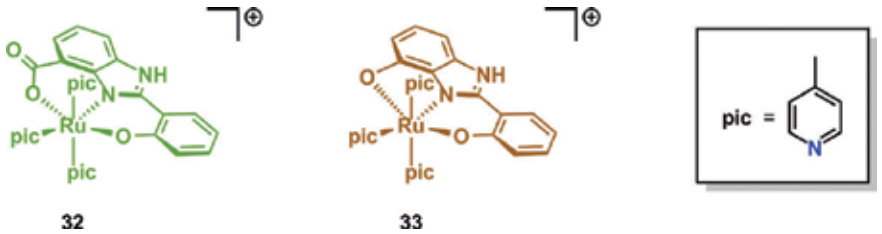

Figure 18. Molecular structures of ruthenium complexes **32** and **33**.

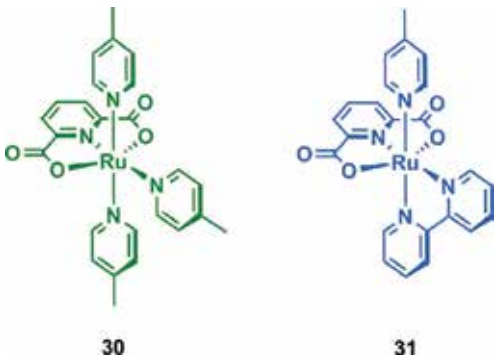

Figure 17. Depiction of the two structurally related ruthenium complexes **30** and **31**.

Åkermark and coworkers have recently reported on the two single-site ruthenium complexes $[Ru(Hhpbc)(pic)_3]^+$ (**32**; H_3hpbc = 2-(2-hydroxyphenyl)-1*H*-benzo[*d*]imidazole-7-carboxylic acid) and $[Ru(Hhpb)(pic)_3]^+$ (**33**; H_3hpb = 2-(2-hydroxyphenyl)-1*H*-benzo[*d*]imidazol-7-ol) that contain two benzimidazole-based tridentate meridionally coordinating ligand frameworks (Figure 18) [66]. Inspired by nature, it was envisioned that the incorporation of negatively charged functional groups imidazole, phenol, and carboxylate, which have important functions in the natural photosynthetic system, would lower the redox potentials of the ruthenium complexes. Furthermore, inclusion of these potential proton transfer mediator motifs into the WOCs would also be expected to facilitate the simultaneous transfer of electrons and protons via proton-coupled electron transfer (PCET), which is crucial for avoiding charge buildup and high-energy intermediates. Catalytic experiments revealed that both ruthenium complexes were capable of mediating oxidation of water to molecular oxygen, both by use of pregenerated $[Ru(bpy)_3]^{3+}$ as oxidant and driven by visible light. When using pregenerated $[Ru(bpy)_3]^{3+}$, ruthenium complex **32** was able to generate a TON of ~4000 and TOF of ~7 s^{-1}. In the photochemical setup, TONs of ~200 were obtained for the two ruthenium complexes **32** and **33** under neutral conditions using a three-component system consisting of $[Ru(bpy)_2(deeb)]^{2+}$ (**2**) as photosensitizer and persulfate as sacrificial electron acceptor. A recent study has suggested that O–O bond formation for the developed ruthenium complex **32** proceeds via a high-valent ruthenium(VI) species, where the capability of accessing this species is derived from the non-innocent ligand architecture (Figure 19) [67]. This cooperative catalytic involvement and the ability of accessing such high-valent species are intriguing and distinguish this ruthenium

http://dx.doi.org/10.5772/62272

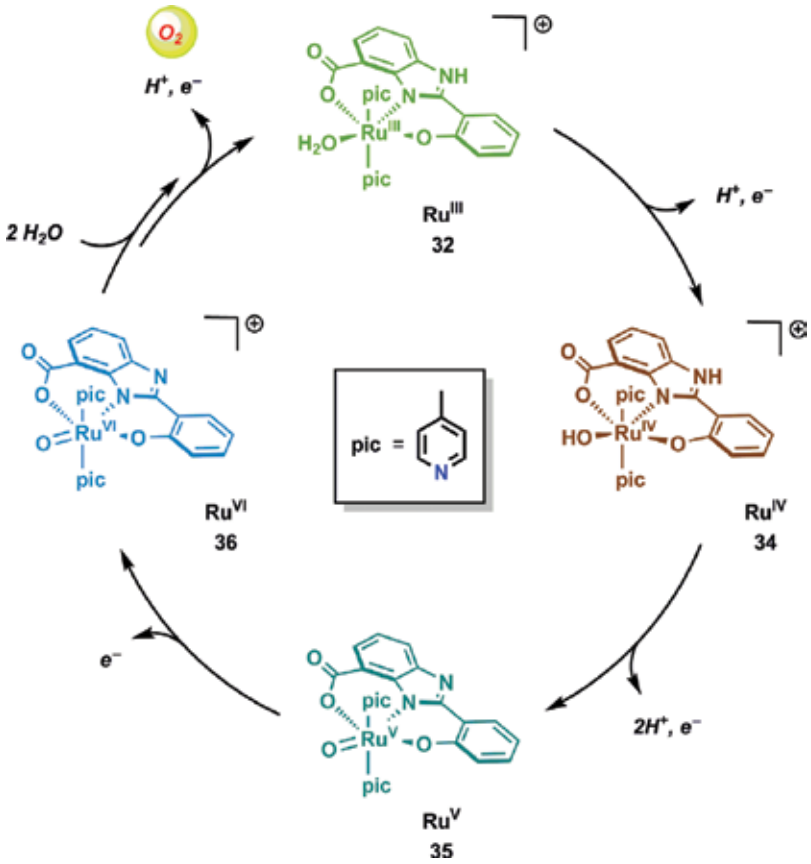

Figure 19. Proposed catalytic cycle for single-site ruthenium complex **32**.

catalyst from the majority of previously reported complexes, which typically proceed via the generation of ruthenium(IV) or ruthenium(V) species as the catalytic key intermediate for O–O bond formation. This could thus provide the foundation for new pathways for the activation of small molecules such as water.

4. Molecular Chromophore–Catalyst Assemblies for Water Oxidation

Due to the progress that has been made in developing ruthenium-based catalysts for water oxidation, increased attention has recently been given to constructing supramolecular dyads where a photosensitizer and a WOC are covalently linked. These assemblies can subsequently be grafted onto solid electrodes, which would ultimately allow for visible light-driven water splitting [68, 69]. This chapter highlights some of the representative ruthenium-based assemblies and devices that have been constructed for photochemical and photoelectrochemical water oxidation.

4.1. Chromophore–Catalyst Assemblies for Homogeneous Water Oxidation

As a result of the synthetic complexity associated with linking a chromophore to a catalyst, there are only a limited number of examples of reported chromophore–catalyst assemblies. Here, the design of an appropriate linker is essential as these supramolecular assemblies have been shown to suffer from fast back electron transfer from the excited photosensitizer to the oxidized WOC entity [70].

Based on the promising results obtained with the $[Ru(bda)(pic)_2(OH_2)]$ complex **29** in visible light-driven water oxidation in the three-component component system using sodium persulfate as sacrificial electron acceptor [63], Sun and coworkers decided to design supramolecular assemblies utilizing ruthenium complex **29** as the WOC unit [71]. For synthetic simplicity, the authors decided to introduce the photosensitizer moiety to the catalyst from its axial ligands. Two structurally different ruthenium-based photosensitizers were coupled to the WOC unit, which afforded the two ruthenium triads **37** and **38** (Figure 20). Due to the electron-rich bda ligand, the onset potential for water oxidation for triad **37** was observed at 0.96 V vs. NHE under neutral conditions, suggesting that the catalytic properties of the WOC unit are not significantly altered by linking it to the ruthenium photosensitizer. Furthermore, this also implies that water oxidation would be thermodynamically favorable. For ruthenium system **38**, the onset potential was observed at a slightly higher potential, yet still thermodynamically feasible. Photocatalytic experiments were performed in degassed phosphate buffer solutions, using sodium persulftate as the sacrificial electron acceptor. Upon irradiation with visible light ($\lambda > 400$ nm), triad **37** rapidly generated molecular oxygen with a TOF of 0.078 s^{-1}. Control experiments confirmed that light, assembly, and electron acceptor were all required to achieve the evolution of molecular oxygen. A vital question was whether assembly **37** would be more effective than the corresponding separate system consisting of $[Ru(bda)(pic)_2]$ (**29**), $[Ru(bpy)_3]^{2+}$ (**1**), and sodium persulfate. This comparison revealed an almost fivefold difference in activity, where assembly **37** provided a TON of 38 vs. a TON of 8 for the non-coupled system. The degradation pathway for the coupled system **37** was also addressed by the use of mass spectrometry, which revealed a correlation between slow ligand dissociation of one of the two axial photosensitizer units of the assembly and the decrease in water oxidation activity over time. In contrast to ruthenium triad **37**, no oxygen was generated when using **38**. This dramatic difference in reactivity was attributed to the significantly shorter excited state lifetime of the $[Ru(tpy)_2]^{2+}$-units (tpy = 2,2′;6′,2″-terpyridine) in assembly **38** relative to that of the $[Ru(bpy)_3]^{2+}$-units of **37**. Although system **38** proved to be inactive, this work highlights that supramolecular assemblies for visible light-driven water oxidation can be constructed by matching two light-harvesting sites and a catalytic WOC unit. Subsequent studies on ruthenium triad **39** (Figure 20) established that this produced a significantly higher TON of 200 when driven by visible light [72]. Here, photocatalytic experiments in combination with time-resolved spectroscopy showed that the linked catalyst in its ruthenium(II) state rapidly quenches the photosensitizer, predominantly by energy transfer. The higher photostability of assembly **39** compared to the three component system was attributed to kinetic stabilization by rapid photosensitizer regeneration. A supramolecular assembly where $[Ru(bda)(pic)_2]$ complex (**29**) was incorporated into a cyclodextrin-modified $[Ru(bpy)_3]^{2+}$-type photosensitizer

http://dx.doi.org/10.5772/62272

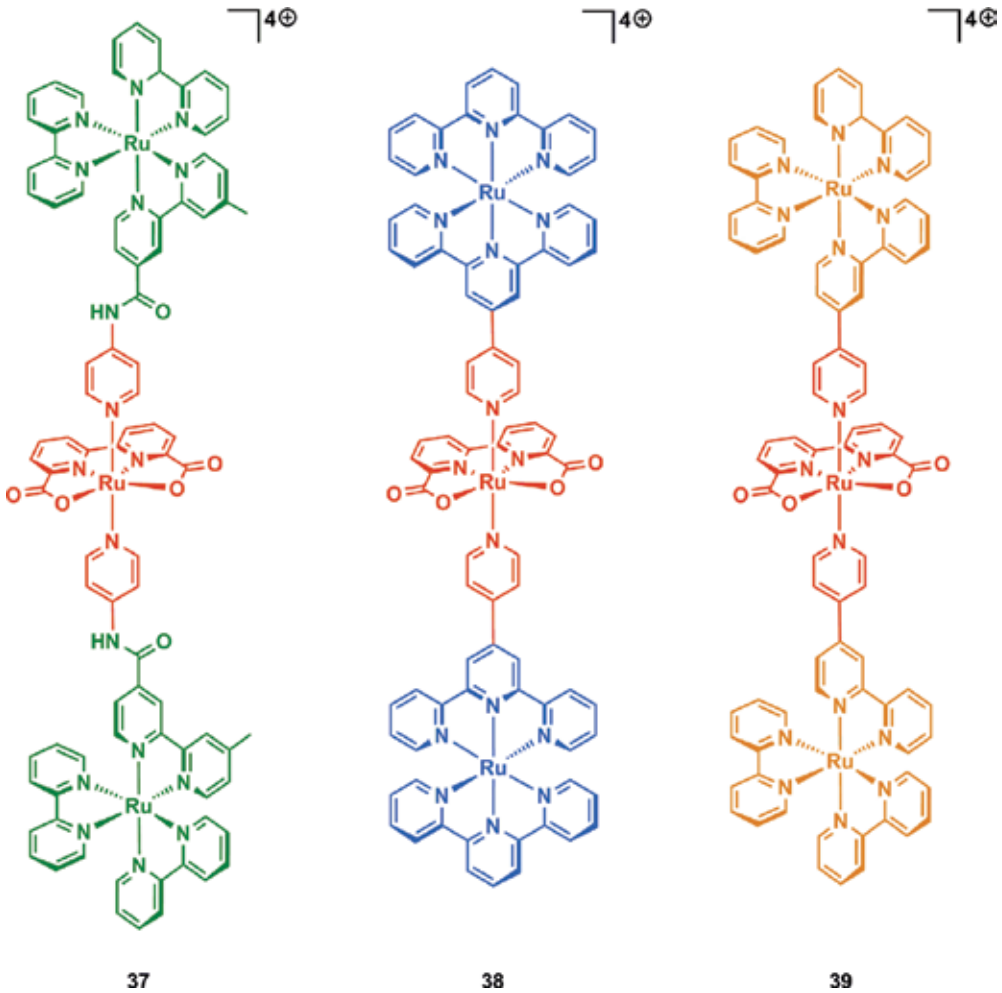

Figure 20. Depiction of the molecular assemblies **37–39** based on the $[Ru(bda)(pic)_2(OH_2)]$ complex **29**.

has recently also been developed for visible light-driven water oxidation employing persulfate as the sacrificial electron acceptor [73]. A remarkable quantum efficiency of 84% was determined for the host–guest adduct under visible light irradiation, which is nearly one order of magnitude higher than that of non-interaction system, indicating that noncovalent incorporation of photosensitizer and catalyst entities is an appealing approach for realizing efficient conversion of solar energy into fuels.

4.2. Surface-Bound Chromophore–Catalyst Assemblies

Dye-sensitized photoelectrochemical cells (DSPECs) for water splitting consist of a photoanode, which is connected via an external circuit to a cathode. A characteristic feature is also the use of a membrane, which is supposed to prevent mixing of the generated gaseous products. The membrane should also be permeable to proton diffusion, in order to allow

equilibration between the cell compartments. In a majority of water-splitting cells based on TiO_2, an external bias of ~0.2 V is needed for efficient reduction of the produced protons to hydrogen gas and maximize water splitting [74–76].

At the core of DSPECs for water splitting, is the chromophore–catalyst assembly that is supposed to mediate water oxidation. Important characteristics of this are 1) robust anchoring to the electrode surface, which also allows electron transfer events to take place through electronic orbital coupling, 2) chromophores that display broad absorption of visible light that 3) upon excitation undergo electron injection into the conduction band of the photoanode, and 4) a stable and efficient WOC entity, having catalytic rates that exceed the rate of solar insolation. It is also essential that the oxidized chromophore is rapidly reduced by the WOC. The ruthenium-based chromophores are in general highly unstable in their oxidized state, which facilitates degradation via nucleophilic attack of water or buffer anions, and back electron transfer events can occur from the semiconductor, thus regenerating the reduced state of the chromophore resulting in low quantum yields [74–77].

The covalent attachment of chromophores and/or WOC to the high surface area of the oxide-based semiconductor is a critical feature that needs to be targeted in order to prevent detachment of the molecular entity from the oxide surface. A variety of strategies for anchoring molecular chromophores, WOCs, and chromophore–catalyst assemblies to oxide surfaces have therefore been evaluated. Reported examples include the use of acetylacetonates [78], alkoxides [79], hydroxamates [80], and siloxanes [81]. However, the most widely used functional groups are carboxylic (–COOH) and phosphonic acid ($–PO_3H_2$) derivatives. Carboxylic acids are the most frequently used linking groups in dye-sensitized solar cells (DSSCs) where they provide strong electronic coupling for ultrafast electron injection from the excited state of the dye. Under nonaqueous conditions, surface detachment is not a limiting factor; however, photoanodes for water splitting operate in aqueous solutions, thus causing irreversible hydrolysis of the covalently attached molecular scaffold and limiting the lifetime of the assemblies. An attractive alternative is the use of phosphonate linkers (Figure 21), which provide more robust surface binding and are typically resistant to hydrolysis/desorption at pH > 5 with added buffer bases [82–85].

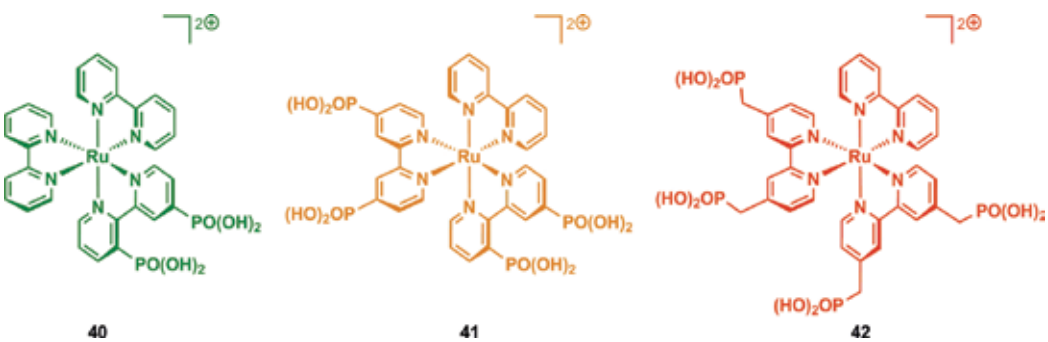

Figure 21. Structures of phosphonate-derivatized ruthenium(II) photosensitizers **40–42**.

http://dx.doi.org/10.5772/62272

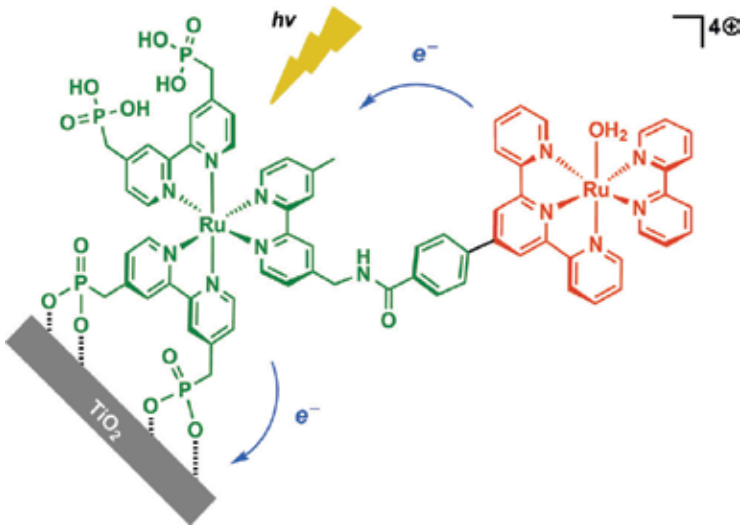

Figure 22. Structure of chromophore–catalyst assembly **43**.

It has been suggested that the presence of molecular oxygen facilitates the photodesorption of phosphonate-linked dyes in aqueous solutions, presumably due to the formation of superoxide ions through back electron transfer from TiO_2. This problem can partially be circumvented by constructing chromophores with multiple ligating phosphonate units. However, the electron injection ability of the chromophores decreases with increasing number of phosphonate groups, highlighting that additional work on designing chromophores for surface stabilization is needed [86].

From the aforementioned discussion, it is apparent that fast electron transfer between the WOC and the oxidized photosensitizer is vital for achieving efficient and robust water-splitting cells. Recent work has shown that the use of phosphonate linkages has limited impact on the reactivity or properties of surface-bound assemblies, thus maintaining the reactivity observed for the homogeneous system [87].

Meyer and coworkers have designed several chromophore–catalyst assemblies that upon attachment to oxide surfaces are able to mediate electrocatalytic water oxidation [88–90]. For the chromophore–catalyst **43** depicted in Figure 22, an amide-based linker ligand was utilized to couple the WOC unit to the chromophore. The synthetically flexible saturated amide bridge ligand was designed to enable long-lived charge-separated states. Interfacial dynamics analysis of dyad **43** by nanosecond transient absorption measurements revealed that upon excitation of the ruthenium chromophore, rapid electron injection into TiO_2 occurred, which was followed by intra-assembly electron transfer from the ruthenium–WOC unit to the oxidized chromophore. This process takes place on the subnanosecond timescale and was followed by microsecond–millisecond back electron transfer from the semiconductor to the oxidized WOC entity (Eq. 7) [91].

$$\left[\mathrm{TiO_2}\left(\mathrm{e^-}\right)-\mathrm{Ru}_{\mathrm{chrom^{II}}}-\mathrm{Ru}_{\mathrm{WOC^{III}}}-\mathrm{OH_2}\right]^{4+}\rightarrow\left[\mathrm{TiO_2}-\mathrm{Ru}_{\mathrm{chrom^{II}}}-\mathrm{Ru}_{\mathrm{WOC^{II}}}-\mathrm{OH_2}\right]^{4+} \quad (7)$$

An attractive approach for constructing catalytic assemblies for light-driven water splitting involves the layer-by-layer addition of a chromophore followed by a catalyst overlayer. Such co-loading strategies allow for straightforward, and potentially practical, approaches for surface attachment and are considered to be general and simple alternatives for producing functioning DSPEC photoanodes [92–94].

An example of such an approach can be seen in Sun and coworkers' photoanode where a derivative of a previously developed ruthenium-based WOC **29** (**44**) was immobilized together with a molecular ruthenium photosensitizer (**45**) on nanostructured TiO_2 particles on fluorine-doped tin oxide (FTO) conducting glass (Figure 23) [95]. Electrochemical measurements revealed an irreversible oxidation peak at E_{pa} = 1.40 V vs. NHE, which was assigned to the Ru^{III}/Ru^{II} redox couple of photosensitizer **45**. A redox process at $E_{1/2}$ = 0.71 V vs. NHE, assigned to the Ru^{III}/Ru^{II} redox couple of catalyst **44**, was also observed, which was followed by a catalytic wave with an onset potential of 1.14 V vs. NHE corresponding to the oxidation of water. From the electrochemical experiments, it could also be established that the ratio of photosensitizer/catalyst was 3:1. A three-electrode PEC cell was constructed using the synthesized photoanode as working electrode, Ag/AgCl as the reference electrode and platinum wire as the cathode for visible light-driven ($\lambda > 400$ nm) water splitting. An external bias of 0.2 V vs. NHE was applied in order to allow for efficient electron transfer. The incident photo-to-current conversion efficiency (IPCE) spectrum of the constructed PEC cell was also measured and showed a maximum IPCE value of 14% at ~450 nm, which corresponds well with the UV–vis absorption spectrum of the developed photoanode. After ~500 s of visible light illumination, the amount of molecular oxygen and hydrogen gas produced was calculated. A TON of almost 500 and a TOF of 1.0 s^{-1} (based on catalyst **44**) were calculated with Faradaic efficiencies of 83% and 74%, respectively, highlighting the efficiency of the fabricated PEC cell. Subsequent work has focused on employing different anchoring groups on the WOC entity (Figure 24) and includes the use of the phosphonate-functionalized catalyst **46** [96], the acrylate-functionalized catalyst **47** [97], and the vinyl-functionalized catalyst **48** [98, 99], which was used for electrochemical polymerization onto nanoporous TiO_2 and Fe_2O_3 films, and a ruthenium-based catalyst containing a long carbon chain in combination with poly(methyl methacrylate) as the auxiliary material [100].

5. Conclusions

As a consequence of the depleting energy resources and the increasing need for energy, modern society faces a daunting task of realizing sustainable, carbon-neutral alternatives. In this context, the development of solar-to-fuel conversion technologies by mimicking the natural photosynthetic apparatus is considered as an attractive solution. While significant effort has been devoted to designing artificial systems for solar energy conversion, replicating the essential functions of natural photosynthesis has proved to be intricate.

http://dx.doi.org/10.5772/62272

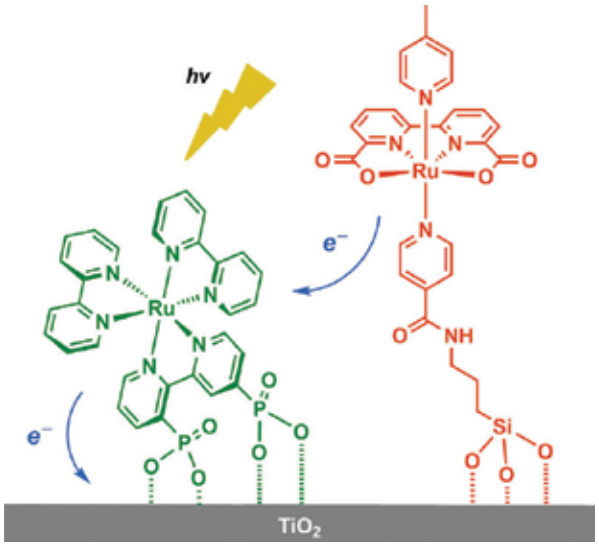

Figure 23. Co-immobilization of ruthenium WOC **44** and ruthenium photosensitizer **45** onto nanostructured TiO_2 particles for visible light-driven water splitting.

An essential component in light-harvesting devices is a catalyst that is able to oxidize water to molecular oxygen, thereby providing the necessary reducing equivalents for reduction of protons to hydrogen gas. Photo-induced charge separation and buildup of multiple redox equivalents is also an essential part of solar-to-fuel conversion schemes. The catalysts reviewed here represent the state of the art and are hence capable of mediating homogeneous light-driven water oxidation through the accumulation of multiple redox equivalents at the catalytic center. The envisioned assemblies for water splitting consist of three parts—a chromophore, a catalyst for water oxidation, and a semiconductor—and have mainly been developed

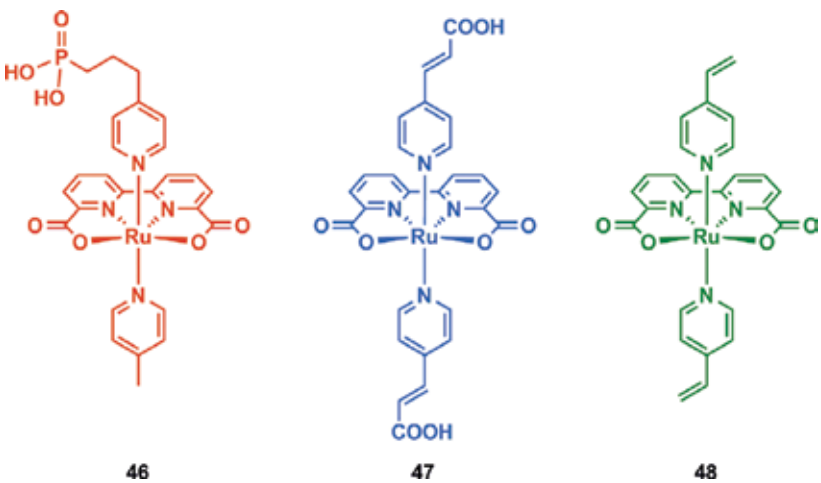

Figure 24. Ruthenium-based catalysts **46–48** employed for fabrication of photoanodes.

separately. The current limitation of these assemblies is related to the inefficient coupling of the individual catalytic events, which is necessary for the development of efficient artificial photosynthetic systems.

Considerable progress has been made during the last decade in constructing photochemical cells capable of splitting water. However, the fundamental aspects, including their synthesis, their long-term durability, and the mechanistic understanding, are far from resolved and are of significant concern. Further elaboration and assembling of all of the integral components through cooperative interplay will certainly continue, thereby realizing efficient artificial photosynthesis in a not too distant future.

Acknowledgements

Financial support from the Swedish Research Council (637-2013-7314, 2015-04995 and 621-2013-4872), Swedish Foundation for Strategic Research, Stiftelsen Olle Engkvist Byggmästare, the Knut and Alice Wallenberg Foundation, and the Carl Trygger Foundation is gratefully acknowledged.

Author details

Markus D. Kärkäs*, Tanja M. Laine, Eric V. Johnston* and Björn Åkermark*

*Address all correspondence to: markus.karkas@su.se (M. D. K.)

*Address all correspondence to: eric.johnston@su.se (E. V. J.)

*Address all correspondence to: bjorn.akermark@su.se (B. Å.)

Department of Organic Chemistry, Arrhenius Laboratory, Stockholm University, Stockholm, Sweden.

References

[1] Chow, J., Kopp, R. J., Portney, P. R. Energy resources and global development. *Science*, 2003. 302: pp. 1528–1531. doi: 10.1126/science.1091939

[2] Lewis, N. S., Nocera, D. G. Powering the planet: Chemical challenges in solar energy utilization. *Proc. Natl. Acad. Sci. U. S. A*, 2006. 103: pp. 15729–15735. doi: 10.1073/pnas.0603395103

[3] Gray, H. B. Powering the planet with solar fuel. *Nature Chem*, 2009. 1: pp. 7. doi: 10.1038/nchem.141

[4] Cho, A. Energy's tricky tradeoffs. *Science*, 2010. 329: pp. 786–787. doi: 10.1126/science.329.5993.786

[5] Han, Z., Eisenberg, R. Fuel from water: The photochemical generation of hydrogen from water. *Acc. Chem. Res*, 2014. 47: pp. 2537–2544. doi: 10.1021/ar5001605

[6] Pagliaro, M., Konstandopoulos, A. G., Ciriminna, R., Palmisano, G. Solar hydrogen: Fuel of the near future. *Energy Environ. Sci*, 2010. 3: pp. 279–287. doi: 10.1039/B923793N

[7] Meyer, T. J. Chemical approaches to artificial photosynthesis. *Acc. Chem. Res*, 1989. 22: pp. 163–170. doi: 10.1021/ar00161a001

[8] Suga, M., Akita, F., Hirata, K., Ueno, G., Murakami, H., Nakajima, Y., Shimizu, T., Yamashita, K., Yamamoto, M., Ago, H., Shen, J.-R. Native structure of photosystem II at 1.95 Å resolution viewed by femtosecond X-ray pulses. *Nature*, 2015. 517: pp. 99–103. doi: 10.1038/nature13991

[9] Wydrzynski, T. J., Satoh, K. (eds.). *Photosystem II: The Light-Driven Water Plastoquinone Oxidoreductase*. Dordrecht, The Netherlands: Springer. 2005. doi: 10.1007/1-4020-4254-X

[10] Barber, J., Tran, P. D. From natural to artificial photosynthesis. *J. R. Soc. Interface*, 2013. 10: pp. 20120984. doi: 10.1098/rsif.2012.0984

[11] Sun, L., Hammarström, L., Åkermark, B., Styring, S. Towards artificial photosynthesis: Ruthenium-manganese chemistry for energy production. *Chem. Soc. Rev*, 2001. 30: pp. 36–49. doi: 10.1039/A801490F

[12] Barber, J. Photosynthetic energy conversion: Natural and artificial. *Chem. Soc. Rev*, 2009. 38: pp. 185–196. doi: 10.1039/B802262N

[13] McDaniel, N. D., Bernhard, S. Solar fuels: Thermodynamics, candidates, tactics, and figures of merit. *Dalton Trans*, 2010. 39: pp. 10021–10030. doi: 10.1039/C0DT00454E

[14] Fujishima, A., Honda, K. Electrochemical photolysis of water at a semiconductor electrode. *Nature*, 1972. 238: pp. 37–38. doi: 10.1038/238037a0

[15] Swierk, J. R., Mallouk, T. E. Design and development of photoanodes for water-splitting dye-sensitized photoelectrochemical cells. *Chem. Soc. Rev*, 2013. 42: pp. 2357–2387. doi: 10.1039/c2cs35246j

[16] Knör, G. Recent progress in homogeneous multielectron transfer photocatalysis and artificial photosynthetic solar energy conversion. *Coord. Chem. Rev*, 2015. 304–305: pp. 102–108. doi: 10.1016/j.ccr.2014.09.013

[17] Kärkäs, M. D., Johnston, E. V., Verho, O., Åkermark, B. Artificial photosynthesis: From nanosecond electron transfer to catalytic water oxidation. *Acc. Chem. Res*, 2014. 47: pp. 100–111. doi: 10.1021/ar400076j

[18] Alstrum-Acevedo, J. H., Brennaman, M. K., Meyer, T. J. Chemical approaches to artificial photosynthesis. 2. *Inorg. Chem*, 2005. 44: pp. 6802–6827. doi: 10.1021/ic050904r

[19] Gust, D., Moore, T. A., Moore, A. L. Mimicking photosynthetic solar energy transduction. *Acc. Chem. Res*, 2001. 34: pp. 40–48. doi: DOI: 10.1021/ar9801301

[20] Knör, G. Artificial enzyme catalysis controlled and driven by light. *Chem. Eur. J*, 2009. 15: pp. 568–578. doi: 10.1002/chem.200801179

[21] Knör, G., Monkowius, U. Photosensitization and photocatalysis in bioinorganic, bioorganometallic and biomimetic systems. *Adv. Inorg. Chem*, 2011. 63: pp. 235–289. doi: 10.1016/B978-0-12-385904-4.00005-6

[22] Marcus, R. A., Sutin, N. Electron transfers in chemistry and biology. *Biochim. Biophys. Acta*, 1985. 811: pp. 265–322. doi: 10.1016/0304-4173(85)90014-X

[23] Gust, D., Moore, T. A., Moore, A. L. Molecular mimicry of photosynthetic energy and electron transfer. *Acc. Chem. Res*, 1993. 26: pp. 198–205. doi: DOI: 10.1021/ar00028a010

[24] Kalyanasundaram, K. Photophysics, photochemistry and solar energy conversion with tris(bipyridyl)ruthenium(II) and its analogues. *Coord. Chem. Rev*, 1982. 46: pp. 159–244. doi: 10.1016/0010-8545(82)85003-0

[25] Juris, A., Balzani, V., Barigelletti, F., Campagna, S., Belser, P., von Zelewsky, A. Ru(II) polypyridine complexes: photophysics, photochemistry, electrochemistry, and chemiluminescence. *Coord. Chem. Rev*, 1988. 84: pp. 85–277. doi: 10.1016/0010-8545(88)80032-8

[26] Campagna, S., Puntoriero, F., Nastasi, F., Bergamini, G., Balzani, V. Photochemistry and photophysics of coordination compounds: Ruthenium. *Top. Curr. Chem*, 2007. 280: pp. 117–214. doi: 10.1007/128_2007_133

[27] Gau, B. C., Chen, H., Zhang, Y., Gross, M. L. Sulfate radical anion as a new reagent for fast photochemical oxidation of proteins. *Anal. Chem*, 2010. 82: pp. 7821–7827. doi: 10.1021/ac101760y

[28] Bolletta, F., Juris, A., Maestri, M., Sandrini, D. Quantum yield of formation of the lowest excited state of $Ru(bpy)_3^{2+}$ and $Ru(phen)_3^{2+}$. *Inorg. Chim. Acta*, 1980. 44: pp. L175–L176. doi: 10.1016/S0020-1693(00)90993-9

[29] Kärkäs, M. D., Verho, O., Johnston, E. V., Åkermark, B. Artificial photosynthesis: Molecular systems for catalytic water oxidation. *Chem. Rev*, 2014. 114: pp. 11863–12001. doi: 10.1021/cr400572f

[30] Blakemore, J. D., Crabtree, R. H., Brudvig, G. W. Molecular catalysts for water oxidation. *Chem. Rev*, 2015. 115: pp. 12974–13005. doi: 10.1021/acs.chemrev.5b00122

[31] Sala, X., Maji, S., Bofill, R., García-Antón, J., Escriche, L., Llobet, A. Molecular water oxidation mechanisms followed by transition metals: State of the art. *Acc. Chem. Res*, 2014. 47: pp. 504–516. doi: 10.1021/ar400169p

[32] Das, B., Orthaber, A., Ott, S., Thapper, A. Water oxidation catalysed by a mononuclear Co^{II} polypyridine complex; possible reaction intermediates and the role of the chloride ligand. *Chem. Commun*, 2015. 51: pp. 13074–13077. doi: 10.1039/c5cc04148a

[33] Nakazono, T., Parent, A. R., Sakai, K. Cobalt porphyrins as homogeneous catalysts for water oxidation. *Chem. Commun*, 2013. 49: pp. 6325–6327. doi: 10.1039/c3cc43031f

[34] Leung, C.-F., Ng, S.-M., Ko, C.-C., Man, W.-L., Wu, J., Chen, L., Lau, T.-C. A cobalt(II) quaterpyridine complex as a visible light-driven catalyst for both water oxidation and reduction. *Energy Environ. Sci*, 2012. 5: pp. 7903–7907. doi: 10.1039/C2EE21840B

[35] Wang, H.-Y., Mijangos, E., Ott, S., Thapper, A. Water oxidation catalyzed by a dinuclear cobalt-polypyridine complex. *Angew. Chem. Int. Ed*, 2014. 53: pp. 14499–14502. doi: 10.1002/anie.201406540

[36] Barnett, S. M., Goldberg, K. I., Mayer, J. M. A soluble copper-bipyridine water-oxidation electrocatalyst. *Nature Chem*, 2012. 4: pp. 498–502. doi: 10.1038/nchem.1350

[37] Garrido-Barros, P., Funes-Ardoiz, I., Drouet, S., Benet-Buchholz, J., Maseras, F., Llobet, A. Redox non-innocent ligand controls water oxidation overpotential in a new family of mononuclear Cu-based efficient catalysts. *J. Am. Chem. Soc*, 2015. 137: pp. 6758–6761. doi: 10.1021/jacs.5b03977

[38] Su, X.-J., Gao, M., Jiao, L., Liao, R.-Z., Siegbahn, P. E. M., Cheng, J.-P., Zhang, M.-T. Electrocatalytic water oxidation by a dinuclear copper complex in a neutral aqueous solution. *Angew. Chem. Int. Ed*, 2015. 54: pp. 4909–4914. doi: 10.1002/anie.201411625

[39] Coggins, M. K., Zhang, M.-T., Vannucci, A. K., Dares, C. J., Meyer, T. J. Electrocatalytic water oxidation by a monomeric amidate-ligated Fe(III)-aqua complex. *J. Am. Chem. Soc*, 2014. 136: pp. 5531–5534. doi: 10.1021/ja412822u

[40] Najafpour, M. M., Moghaddam, A. N., Sedigh, D. J., Hołyńska, M. A dinuclear iron complex with a single oxo bridge as an efficient water-oxidizing catalyst in the presence of cerium(IV) ammonium nitrate: New findings and current controversies. *Catal. Sci. Technol*, 2014. 4: pp. 30–33. doi: 10.1039/C3CY00644A

[41] Wickramasinghe, L. D., Zhou, R., Zong, R., Vo, P., Gagnon, K. J., Thummel, R. P. Iron complexes of square planar tetradentate polypyridyl-type ligands as catalysts for water oxidation. *J. Am. Chem. Soc*, 2015. 137: pp. 13260–13263. doi: 10.1021/jacs.5b08856

[42] Codolà, Z., Gómez, L., Kleespies, S. T., Que, L. Jr., Costas, M., Lloret-Fillol, J. Evidence for an oxygen evolving iron-oxo-cerium intermediate in iron-catalysed water oxidation. *Nature Commun*, 2015. 6: 5865. doi: 10.1038/ncomms6865

[43] Limburg, J., Vrettos, J. S., Liable-Sands, L. M., Rheingold, A. L., Crabtree, R. H., Brudvig, G. W. A functional model for O–O bond formation by the O_2-evolving complex in photosystem II. *Science*, 1999. 283: pp. 1524–1527. doi: 10.1126/science.283.5407.1524

[44] Karlsson, E. A., Lee, B.-L., Åkermark, T., Johnston, E. V., Kärkäs, M. D., Sun, J., Hansson, Ö., Bäckvall, J.-E., Åkermark, B. Photosensitized water oxidation by use of a bioinspired manganese catalyst. *Angew. Chem. Int. Ed*, 2011. 50: pp. 11715–11718. doi: 10.1002/anie.201104355

[45] Liao, R.-Z., Kärkäs, M. D., Lee, B.-L., Åkermark, B., Siegbahn, P. E. M. Photosystem II like water oxidation mechanism in a bioinspired tetranuclear manganese complex. *Inorg. Chem*, 2015. 54: pp. 342–351. doi: 10.1021/ic5024983

[46] Lee, W.-T., Muñoz, S. B. III., Dickie, D. A., Smith, J. M. Ligand modification transforms a catalase mimic into a water oxidation catalyst. *Angew. Chem. Int. Ed*, 2014. 53: pp. 9856–9859. doi: 10.1002/anie.201402407

[47] Gao, Y., Åkermark, T., Liu, J., Sun, L., Åkermark, B. Nucleophilic attack of hydroxide on a Mn^V oxo vomplex: A model of the O–O bond formation in the oxygen evolving complex of photosystem II. *J. Am. Chem. Soc*, 2009. 131: pp. 8726–8727. doi: 10.1021/ja901139r

[48] Gersten, S. W., Samuels, G. J., Meyer, T. J. Catalytic oxidation of water by an oxo-bridged ruthenium dimer. *J. Am. Chem. Soc*, 1982. 104: pp. 4029–4030. doi: 10.1021/ja00378a053

[49] Gilbert, J. A., Eggleston, D. S., Murphy, W. R. Jr., Geselowitz, D. A., Gersten, S. W., Hodgson, D. J., Meyer, T. J. Structure and redox properties of the water-oxidation catalyst $[(bpy)_2(OH_2)RuORu(OH_2)(bpy)_2]^{4+}$. *J. Am. Chem. Soc*, 1985. 107: pp. 3855–3864. doi: 10.1021/ja00299a017

[50] Rotzinger, F. P., Munavalli, S., Comte, P., Hurst, J. K., Grätzel, M., Pern, F. J., Frank, A. J. A molecular water-oxidation catalyst derived from ruthenium diaqua bis(2,2′-bipyridyl-5,5′-dicarboxylic acid). *J. Am. Chem. Soc*, 1987. 109: pp. 6619–6626. doi: 10.1021/ja00256a010

[51] Xu, Y., Åkermark, T., Gyollai, V., Zou, D., Eriksson, L., Duan, L., Zhang, R., Åkermark, B., Sun, L. A new dinuclear ruthenium complex as an efficient water oxidation catalyst. *Inorg. Chem*, 2009. 48: pp. 2717–2719. doi: 10.1021/ic802052u

[52] Xu, Y., Duan, L., Tong, L., Åkermark, B., Sun, L. Visible light-driven water oxidation catalyzed by a highly efficient dinuclear ruthenium complex. *Chem. Commun*, 2010. 46: pp. 6506–6508. doi: 10.1039/C0CC01250E

[53] Xu, Y., Fischer, A., Duan, L., Tong, L., Gabrielsson, E., Åkermark, B., Sun, L. Chemical and light-driven oxidation of water catalyzed by an efficient dinuclear ruthenium complex. *Angew. Chem. Int. Ed*, 2010. 49: pp. 8934–8937. doi: 10.1002/anie.201004278

[54] Laine, T. M., Kärkäs, M. D., Liao, R.-Z., Åkermark, T., Lee, B.-L., Karlsson, E. A., Siegbahn, P. E. M., Åkermark, B. Efficient photochemical water oxidation by a dinuclear

molecular ruthenium complex. *Chem. Commun*, 2015. 51: pp. 1862–1865. doi: 10.1039/C4CC08606F

[55] Kärkäs, M. D., Johnston, E. V., Karlsson, E. A., Lee, B.-L., Åkermark, T., Shariatgorji, M., Ilag, L., Hansson, Ö., Bäckvall, J.-E., Åkermark, B. Light-induced water oxidation by a Ru complex containing a bio-inspired ligand. *Chem. Eur. J*, 2011. 17: pp. 7953–7959. doi: 10.1002/chem.201003702

[56] Laine, T. M., Kärkäs, M. D., Liao, R.-Z., Siegbahn, P. E. M., Åkermark, B. A dinuclear ruthenium-based water oxidation catalyst: Use of non-innocent ligand frameworks for promoting multi-electron reactions. *Chem. Eur. J*, 2015. 21: pp. 10039–10048. doi: 10.1002/chem.201406613

[57] Berardi, S., Francàs, L., Neudeck, S., Maji, S., Benet-Buchholz, J., Meyer, F., Llobet, A. Efficient light-driven water oxidation catalysis by dinuclear ruthenium complexes. *ChemSusChem*, 2015. 8: pp. 3688–3696. doi: 10.1002/cssc.201500798

[58] Sens, C., Romero, I., Rodríguez, M., Llobet, A., Parella, T., Benet-Buchholz, J. A new Ru complex capable of catalytically oxidizing water to molecular dioxygen. *J. Am. Chem. Soc*, 2004. 126: pp. 7798–7799. doi: 10.1021/ja0486824

[59] Bozoglian, F., Romain, S., Ertem, M. Z., Todorova, T. K., Sens, C., Mola, J., Rodríguez, M., Romero, I., Benet-Buchholz, J., Fontrodona, X., Cramer, C. J., Gagliardi, L., Llobet, A. The Ru-hbpp water oxidation catalyst. *J. Am. Chem. Soc*, 2009. 131: pp. 15176–15187. doi: 10.1021/ja9036127

[60] Lewandowska-Andralojc, A., Polyansky, D. E., Zong, R., Thummel, R. P., Fujita, E. Enabling light-driven water oxidation via a low-energy Ru^{IV}= O intermediate. *Phys. Chem. Chem. Phys*, 2013. 15: pp. 14058–14068. doi: 10.1039/C3CP52038B

[61] Polyansky, D. E., Muckerman, J. T., Rochford, J., Zong, R., Thummel, R. P., Fujita, E. Water oxidation by a mononuclear ruthenium catalyst: Characterization of the intermediates. *J. Am. Chem. Soc*, 2011. 133: pp. 14649–14665. doi: 10.1021/ja203249e

[62] Duan, L., Fischer, A., Xu, Y., Sun, L. Isolated seven-coordinate Ru(IV) dimer complex with $[HOHOH]^-$ bridging ligand as an intermediate for catalytic water oxidation. *J. Am. Chem. Soc*, 2009. 131: pp. 10397–10399. doi: 10.1021/ja9034686

[63] Duan, L., Xu, Y., Zhang, P., Wang, M., Sun, L. Visible light-driven water oxidation by a molecular ruthenium catalyst in homogeneous system. *Inorg. Chem*, 2010. 49: pp. 209–215. doi: 10.1021/ic9017486

[64] Wang, L., Duan, L., Tong, L., Sun, L. Visible light-driven water oxidation catalyzed by mononuclear ruthenium complexes. *J. Catal*, 2013. 306: pp. 129–132. doi: 10.1016/j.jcat.2013.06.023

[65] Duan, L., Xu, Y., Gorlov, M., Tong, L., Andersson, S., Sun, L. Chemical and photochemical water oxidation catalyzed by mononuclear ruthenium complexes with a

negatively charged tridentate ligand. *Chem. Eur. J*, 2010. 16: pp. 4659–4668. doi: 10.1002/chem.200902603

[66] Kärkäs, M. D., Åkermark, T., Johnston, E. V., Karim, S. R., Laine, T. M., Lee, B.-L., Åkermark, T., Privalov, T., Åkermark, B. Water oxidation by single-site ruthenium complexes: Using ligands as redox and proton transfer mediators. *Angew. Chem. Int. Ed*, 2012. 51: pp. 11589–11593. doi: 10.1002/anie.201205018

[67] Kärkäs, M. D., Liao, R.-Z., Laine, T. M., Åkermark, T., Ghanem, S., Siegbahn, P. E. M., Åkermark, B. Molecular ruthenium water oxidation catalysts carrying non-innocent ligands: Mechanistic insight through structure–activity relationships and quantum chemical calculations. *Catal. Sci. Technol*, In press.doi: 10.1039/C5CY01704A

[68] Yu, Z., Li, F., Sun, L. Recent advances in dye-sensitized photoelectrochemical cells for solar hydrogen production based on molecular components. *Energy Environ. Sci*, 2015. 8: pp. 760–775. doi: 10.1039/C4EE03565H

[69] Xue, L.-X., Meng, T.-T., Yang, W., Wang, K.-Z. Recent advances in ruthenium complex-based light-driven water oxidation catalysts. *J. Photochem. Photobiol. B: Biol*, 2015. 152: pp. 95–105. doi: 10.1016/j.jphotobiol.2015.07.005

[70] Karlsson, E. A., Lee, B.-L., Liao, R.-Z., Åkermark, T., Kärkäs, M. D., Becerril, V. S., Siegbahn, P. E. M., Zou, X., Abrahamsson, M., Åkermark, B. Synthesis and electron-transfer processes in a new family of ligands for coupled Ru–Mn_2 complexes. *ChemPlusChem*, 2014. 79: pp. 936–950. doi: 10.1002/cplu.201402006

[71] Li, F., Jiang, Y., Zhang, B., Huang, F., Gao, Y., Sun, L. Towards a solar fuel device: Light-driven water oxidation catalyzed by a supramolecular assembly. *Angew. Chem. Int. Ed*, 2012. 51: pp. 2417–2420. doi: 10.1002/anie.201108051

[72] Wang, L., Mirmohades, M., Brown, A., Duan, L., Li, F., Daniel, Q., Lomoth, R., Sun, L., Hammarström, L. Sensitizer-catalyst assemblies for water oxidation. *Inorg. Chem*, 2015. 54: pp. 2742–2751. doi: 10.1021/ic502915r

[73] Li, H., Li, F., Zhang, B., Zhou, X., Yu, F., Sun, L. Visible light-driven water oxidation promoted by host-guest interaction between photosensitizer and catalyst with a high quantum efficiency. *J. Am. Chem. Soc*, 2015. 137: pp. 4332–4335. doi: 10.1021/jacs.5b01924

[74] Frischmann, P. D., Mahata, K., Würthner, F. Powering the future of molecular artificial photosynthesis with light-harvesting metallosupramolecular dye assemblies. *Chem. Soc. Rev*, 2013. 42: pp. 1847–1870. doi: DOI: 10.1039/C2CS35223K

[75] Young, K. J., Martini, L. A., Milot, R. L., Snoeberger, R. C. III, Batista, V. S., Schmuttenmaer, C. A., Crabtree, R. H., Brudvig, G. W. Light-driven water oxidation for solar fuels. *Coord. Chem. Rev*, 2012. 256: pp. 2503–2520. doi: 10.1016/j.ccr.2012.03.031

[76] Sun, J., Zhong, D. K., Gamelin, D. R. Composite photoanodes for photoelectrochemical solar water splitting. *Energy Environ. Sci*, 2010. 3: pp. 1252–1261. doi: 10.1039/C0EE00030B

[77] Ghosh, P. K., Brunschwig, B. S., Chou, M., Creutz, C., Sutin, N. Thermal and light-induced reduction of the ruthenium complex cation $Ru(bpy)_3^{3+}$ in aqueous solution. *J. Am. Chem. Soc*, 1984. 106: pp. 4772–4783. doi: 10.1021/ja00329a022

[78] McNamara, W. R., Snoeberger, R. C. III, Li, G., Schleicher, J. M., Cady, C. W., Poyatos, M., Schmuttenmaer, C. A., Crabtree, R. H., Brudvig G. W., Batista, V. S. Acetylacetonate anchors for robust functionalization of TiO_2 nanoparticles with Mn(II)−terpyridine complexes. *J. Am. Chem. Soc*, 2008. 130: pp. 14329–14338. doi: 10.1021/ja805498w

[79] Zou, C., Wrighton, M. S. Synthesis of octamethylferrocene derivatives via reaction of (octamethylferrocenyl)methyl carbocation with nucleophiles and application to functionalization of surfaces. *J. Am. Chem. Soc*, 1990. 112: pp. 7578–7584. doi: 10.1021/ja00177a020

[80] McNamara, W. R., Milot, R. L., Song, H.-e., Snoeberger, R. C. III, Batista, V. S., Schmuttenmaer, C. A., Brudvig, G. W., Crabtree, R. H. Water-stable, hydroxamate anchors for functionalization of TiO_2 surfaces with ultrafast interfacial electron transfer. *Energy Environ. Sci*, 2010. 3: pp. 917–923. doi: 10.1039/C001065K

[81] Haller, I. Covalently attached organic monolayers on semiconductor surfaces. *J. Am. Chem. Soc.*, 1978. 100: pp. 8050–8055. doi: 10.1021/ja00494a003

[82] Gillaizeau-Gauthier, I., Odobel, F., Alebbi, M., Argazzi, R., Costa, E., Bignozzi, C. A., Qu, P., Meyer, G. J. Phosphonate-based bipyridine dyes for stable photovoltaic devices. *Inorg. Chem*, 2001. 40: pp. 6073–6079. doi: 10.1021/ic010192e

[83] Brown, D. G., Schauer, P. A., Borau-Garcia, J., Fancy, B. R., Berlinguette, C. P. Stabilization of ruthenium sensitizers to TiO_2 surfaces through cooperative anchoring groups. *J. Am. Chem. Soc*, 2013. 135: pp. 1692–1695. doi: 10.1021/ja310965h

[84] Bae, E., Choi, W., Park, J., Shin, H. S., Kim, S. B., Lee, J. S. Effects of surface anchoring groups (carboxylate vs phosphonate) in ruthenium-complex-sensitized TiO_2 on visible light reactivity in aqueous suspensions. *J. Phys. Chem. B*, 2004. 108: pp. 14093–14101. doi: 10.1021/jp047777p

[85] Park, H., Bae, E., Lee, J.-J., Park, J., Choi, W. Effect of the anchoring group in Ru-bipyridyl sensitizers on the photoelectrochemical behavior of dye-sensitized TiO_2 electrodes: Carboxylate versus phosphonate linkages. *J. Phys. Chem. B*, 2006. 110: pp. 8740–8749. doi: 10.1021/jp060397e

[86] Hanson, K., Brennaman, M. K., Luo, H., Glasson, C. R. K., Concepcion, J. J., Song, W., Meyer, T. J. Photostability of phosphonate-derivatized, RuII polypyridyl complexes on metal oxide surfaces. *ACS Appl. Mater. Interfaces*, 2012. 4: pp. 1462–1469. doi: 10.1021/am201717x

[87] Chen, Z., Concepcion, J. J., Hull, J. F., Hoertz, P. G., Meyer, T. J. Catalytic water oxidation on derivatized nanoITO. *Dalton Trans*, 2010. 39: pp. 6950–6952. doi: 10.1039/C0DT00362J

[88] Concepcion J. J., Jurss, J. W., Hoertz, P. G., Meyer, T. J. Catalytic and surface-electrocatalytic water oxidation by redox mediator-catalyst assemblies. *Angew. Chem. Int. Ed*, 2009. 48: pp. 9473–9476. doi: 10.1002/anie.200901279

[89] Norris, M. R., Concepcion, J. J., Fang, Z., Templeton, J. L., Meyer, T. J. Low-overpotential water oxidation by a surface-bound ruthenium-chromophore–ruthenium-catalyst assembly. *Angew. Chem. Int. Ed*, 2013. 52: pp. 13580–13583. doi: 10.1002/anie.201305951

[90] Ashford, D. L., Lapides, A. M., Vannucci, A. K., Hanson, K., Torelli, D. A., Harrison, D. P., Templeton, J. L., Meyer, T. J. Water oxidation by an electropolymerized catalyst on derivatized mesoporous metal oxide electrodes. *J. Am. Chem. Soc*, 2014. 136: pp. 6578–6581. doi: 10.1021/ja502464s

[91] Ashford, D. L., Song, W., Concepcion, J. J., Glasson, C. R. K., Brennaman, M. K., Norris, M. R., Fang, Z., Templeton, J. L., Meyer, T. J. Photoinduced electron transfer in a chromophore–catalyst assembly anchored to TiO_2. *J. Am. Chem. Soc*, 2012. 134: pp. 19189–19198. doi: 10.1021/ja3084362

[92] Song, W., Ito, A., Binstead, R. A., Hanson, K., Luo, H., Brennaman, M. K., Concepcion, J. J., Meyer, T. J. Accumulation of multiple oxidative equivalents at a single site by cross-surface electron transfer on TiO_2. *J. Am. Chem. Soc*, 2013. 135: pp. 11587–11594. doi: 10.1021/ja4032538

[93] Moore, G. F., Blakemore, J. D., Milot, R. L., Hull, J. F., Song, H.-e., Cai, L., Schmuttenmaer, C. A., Crabtree, R. H., Brudvig, G. W. A visible light water-splitting cell with a photoanode formed by codeposition of a high-potential porphyrin and an iridium water-oxidation catalyst. *Energy Environ. Sci*, 2011. 4: pp. 2389–2392. doi: 10.1039/C1EE01037A

[94] Glasson, C. R. K., Song, W., Ashford, D. L., Vannucci, A., Chen, Z., Concepcion, J. J., Holland, P. L., Meyer, T. J. Self-assembled bilayers on indium-tin oxide (SAB-ITO) electrodes: A design for chromophore-catalyst photoanodes. *Inorg. Chem*, 2012. 51: pp. 8637–8639. doi: 10.1021/ic300636w

[95] Gao, Y., Ding, X., Liu, J., Wang, L., Lu, Z., Li, L., Sun, L. Visible light driven water splitting in a molecular device with unprecedentedly high photocurrent density. *J. Am. Chem. Soc*, 2013. 135: pp. 4219–4222. doi: 10.1021/ja400402d

[96] Gao, Y., Zhang, L., Ding, X., Sun, L. Artificial photosynthesis – functional devices for light driven water splitting with photoactive anodes based on molecular catalysts. *Phys. Chem. Chem. Phys*, 2014. 16: pp. 12008–12013. doi: 10.1039/C3CP55204G

[97] Ding, X., Gao, Y., Zhang, L., Yu, Z., Liu, J., Sun, L. Visible light-driven water splitting in photoelectrochemical cells with supramolecular catalysts on photoanodes. *ACS Catal*, 2014. 4: pp. 2347–2350. doi: 10.1021/cs500518k

[98] Li, F., Fan, K., Wang, L., Daniel, Q., Duan, L., Sun, L. Immobilizing Ru(bda) catalyst on a photoanode via electrochemical polymerization for light-driven water splitting. *ACS Catal*, 2015. 5: pp. 3786–3790. doi: 10.1021/cs502115f

[99] Ashford, D. L., Sherman, B. D., Binstead, R. A., Templeton, J. L., Meyer, T. J. Electro-assembly of a chromophore-catalyst bilayer for water oxidation and photocatalytic water splitting. *Angew. Chem. Int. Ed*, 2015. 54: pp. 4778–4781. doi: 10.1002/anie.201410944

[100] Ding, X., Gao, Y., Ye, L., Zhang, L., Sun, L. Assembling supramolecular dye-sensitized photoelectrochemical cells for water splitting. *ChemSusChem*, 2015. 8: pp. 3992–3995. doi: 10.1002/cssc.201500313

Edited by Mohammad Mahdi Najafpour

Using the energy from sunlight, photosynthesis usually converts carbon dioxide into organic compounds, which are important for all living creatures. Photosynthesis is one of the most important reactions on Earth, and it is a scientific field that is intrinsically interdisciplinary, and many research groups have considered photosynthesis. The aim of this book is to provide new progresses on applied aspects of photosynthesis, and different research groups collected their voluble results from study of this interesting process. All sections have been written by experts in their fields, and book chapters present different and new subjects on photosynthesis.

ISBN 978-953-51-5427-3

Photo by MADDRAT / DollarPhotoClub

IntechOpen